

Copyright  
by  
Samuel Reid Long  
2012

**The Dissertation Committee for Samuel Reid Long  
Certifies that this is the approved version of the following dissertation:**

**Studies of Multicomponent Assemblies**

**Committee:**

---

Eric V. Anslyn, Co-Supervisor

---

Brent L. Iverson, Co-Supervisor

---

Hung-wen Liu

---

G. Barrie Kitto

---

Christian P. Whitman

---

Louis A. Waldman



**Studies of Multicomponent Assemblies**

**by**

**Samuel Reid Long, B.S.Ch.; B.A.**

**Dissertation**

Presented to the Faculty of the Graduate School of

The University of Texas at Austin

in Partial Fulfillment

of the Requirements

for the Degree of

**Doctor of Philosophy**

**The University of Texas at Austin**

**December 2012**

## **Dedication**

To Mom, Dad, John and Lucky for all your love, laughter and support

## Acknowledgements

As with any work of this length, there are numerous people who have played an important role in its creation. First, I must give thanks to God for all of the blessing that have been bestowed on me these past almost thirty years. Next, my parents require special thanks for all the love, support, and encourage that they have given me during my graduate career. More than any other, they helped to ensure my academic success and to them I will be eternally indebted. My brother has also been a key influence in my life and his encouragement and love should be duly noted.

Next, I should thank my wonderful boss and mentor, Dr. Eric V. Anslyn for his leadership, guidance, and support. I have been truly blessed to work with him on the projects discussed in this dissertation. Without a doubt, there is no better person to work for and I know that I would not have completed this work without him. Dr. Brent L. Iverson, also, deserves special acknowledgement as he has played a key role in my early graduate education and should be credited as the person who made me fall in love with organic chemistry. My life would be profoundly different (and much less enjoyable) if he had not taken a stand and helped to ensure that I could take his second semester organic chemistry class. I would be remiss if I did not mention Dr. J.J. Lagowski who took me in as a freshman and let me do research in his lab. Those first years doing research set me on this path and kicked off this journey. For that, I will always be grateful.

Additionally, my coworkers in the Anslyn group have been instrumental in my development as a scientist and as a person. I will always treasure all of the wonderful memories of all our discussions in the office or the random nature of some of our

conversations. The reason that I made it through his PhD was because the work environment you created made me want to come to work every day. I must give a special shout out to my office mates for the some part of the last three years, Michelle, Katharine, Alex, Justin, Diana, Pedro, Leo, Jeff, Brette, and Igor, because our office has a little too much fun but it is definitely worth it. Dr. Lei You also needs mentioning for his help with the dynamic covalent bond assembly. A few previous Anslyn group members also need special recognition. Drs. Diana Leung and Amanda Hargrove for helping with my early scientific development and putting up with my endless questions. Drs. J. Chance Rainwater and Macro Bonnizzoni should be mentioned for all of the help on the dendrimer projects. Finally, I would like to thank Drs. Amanda Hargrove and Leo Joyce along with Ms. Brette Chapin for being my early morning support group whose presence allowed me to work early mornings in the lab.

Additionally, I have been fortunate to serve as the TA for the Anslyn research stream in the FRI program. Through this program, I have gotten to meet so many of the up and coming research superstars at UT and I will always treasure the small role I played in their development. The program has richly rewarded me and made me a better person.

Finally, I am deeply indebted to my numerous friends from outside the lab who provided me with an outlet for my other interests and pursuits. Of these, I must first mention my constant companion for the past four years, Lucky Alexander Long, my black lab “puppy” whose smiling face and constant enthusiasm reminded me that there is more too life than a set of reactions. When I came home and was greeted with his smiling face, it made me forget how terribly my chemistry had gone and put a smile on his face.

Of the two legged human species friends, I must acknowledge all of the people in the Graduate Student Assembly and its offices for allowing me to be a part of the fold. You do amazing work for so many which is often not recognized. Daniel, Manny, and Michael keep up the good work.

The staff of the Chemistry and Biochemistry graduate office has been especially helpful for the last five years of this journey. Penny Kile should receive an award because until her retirement she had to put up with all of us and still could maintain a laugh and a smile; a feat that only a goddess could achieve. I wish all of them the best of luck in their future pursuits.

The members of the Friar Society have been a constant source of support and encouragement. There are too many people to mention them all by name but I will mention some of the key players who have enriched my UT experience and my life. Many of these people, I hope will be life long friends and colleagues because together we can make the world a better place. Those key players are Dave Player, Brette Garner, John Adkins, Terry Tottenham, Natalie Butler, Erica Brody, David Forinash, Michael Daehne, Mariana Fanous, Shannon Allport, Rachel Meyerson, Frankie Shulkin, Kathy Tally, Brent Chaney, Andrew Solomon, Cal and Claire Chaney, Peggy Liddle, Andrew Townsell, John Woods and Muneezeh Kabir.

My roommates over these last few years have formed how I am and must be mentioned. Thank you to my undergraduate roommates, Daniel Kievlan (and by extension, his [now] amazing wife, Tricia), Jason Sussman, James Riddlesperger and Brian Roberts. Finally, for the last four years, I have had two amazing housemates, Andy Yin and David Wogan. They have always been there for me and I hope I can always be there for them.

Finally, there are three very special individuals who have left an indelible mark on my life. Now, I could not even think of my life or where I would be without them.

First, Cecilia López who has taught me to always smile and that no matter how crazy things get that we will make it through. She has been a constant ray of optimum and the one to keep me grounded. She is the true model of a selfless leader.

Next, I would like to give my thanks to John F. Brady. John has retaught me how to have fun and to enjoy life to its fullest. I cannot think of anyone else who has done more to break me out of my shell. He has been my lifeline when I need to talk to someone these past few years and has opened his home for numerous events including our weekly Game of Thrones watching party. He has encouraged me to explore my passions and provided sage advice whenever it has been needed. His friendship has made me a better person and a more caring friend for which I will be eternally grateful.

Finally, but in no way, least, I must mention Stephen L. Myers. Stephen is my conscious and my rock. He is one of the few people I know with whom I cannot speak for weeks or months yet we can pick up like we just spoke hours ago. He has inspired me to continue on through the tough times and been there to celebrate the triumphs. He has always reminded me that all things and actions, great and small, have a purpose and in the end if we keep faith will become something great. I can never replay his kindness, time and faith but I will certainly try.

# **Studies of Multicomponent Assemblies**

Samuel Reid Long, Ph.D.

The University of Texas at Austin, 2012

Co-Supervisors: Eric V. Anslyn and Brent L. Iverson

This dissertation is divided into three major sections (one on dendrimers, one on tripodal metal ligands and one on a research oriented chemistry curricula) with a primary focus on different types of multicomponent assemblies. In the first chapter, a system is described that used a multicomponent assembly of AT-PAMAM dendrimers and an indicator, carboxyfluorescein, to detect and identify various polyanions at a low micromolar concentration. The system was able to successfully differentiate twelve anions, many of biological interest, including three tricarboxylates. The tricarboxylates were differentiated based primarily on the regiochemistry of the anionic groups.

In the second chapter, further studies with AT-PAMAM dendrimers were carried out to provide some understanding of the thermodynamic origins of binding. Utilizing isothermal titration calorimetry, the binding of the dendrimers to large polyanionic dendrons with increasing numbers of charges was studied. Through these studies, the thermodynamic values of the binding events were obtained allowing us to explore the properties of the dendrimers. The cooperativity of the system was measured, and primarily negative cooperativity determined by the entropic contributions was uncovered. As the dendrimers increased in size, the thermodynamic origins of binding were determined to a greater extent by the entropy of binding.

In the third chapter, a novel dynamic ligand system for metal binding is described. In the presence of a metal salt, a heterocyclic aldehyde and a secondary amine with two heterocyclic arms reversibly condense to form a hemiaminal with a tripodal metal binding site. This chapter describes studies on the metal binding ability, the variety of metals that will lead to this formation, the effects of anions and the range of aldehydes that can be used are described. Furthermore, the system's reversibility was explored. Finally, the use of a bistriazole secondary amine was explored. The modular nature of triazole formation could lead to the introduction of additional functionalities.

The fourth chapter discusses how the novel ligand system could be used to study the enantiomeric excess (*ee*) of chiral thiols. Based upon the system's ability to form a stable hemiaminal thioether, a CD signal could be generated that is proportional to the amount of a particular enantiomer in solution. Using this system, a calibration curve relating CD signal and *ee* can be generated giving the *ee* of an unknown solution.

In the final chapter, a look at the Freshman Research Initiative will be carried out with a focus on the ability to teach basic skills in an introductory laboratory through research. Four different skills or techniques will be explored through three different FRI streams,<sup>x</sup> and how they teach the four skills. Finally, analysis of the success of the program, particularly students' success in the next laboratory course in the sequence, is discussed, and a model for adopting this type of teaching at other universities is given.



## Table of Contents

|  |      |
|--|------|
| List of Tables .....   | xvii |
| List of Figures .....  | xix  |
| List of Schemes and Equations .....  | xxix |
| Chapter 1: Dendrimer Based Anion Detection Using PAMAM Dendrimer .....                 | 1    |
| 1.1 Introduction.....  | 1    |
| 1.1.1 Goals of Studies and Scientific Question.....                                    | 1    |
| 1.1.2 Origins of Dendrimers .....  | 1    |
| 1.1.3 General PAMAM Dendrimer Characteristics.....                                     | 3    |
| 1.1.4 General Indicator Binding to PAMAM Dendrimers .....                              | 6    |
| 1.1.5 Binding of Carboxyfluorescein to the PAMAM Dendrimers.....                       | 8    |
| 1.1.6 ITC Studies of Carboxyfluorescein Binding.....                                   | 10   |
| 1.1.7 Target Selection .....   | 14   |
| 1.1.8 General Anion Recognition Previous Work .....                                    | 14   |
| 1.1.9 Biologic Anion Detection .....   | 16   |
| 1.1.9.1 Highlights of Nucleotide Triphosphate Detection .....                          | 16   |
| 1.1.9.2 Supramolecular Detection of Nicotinamide Adenine<br>Dinucleotide .....         | 17   |
| 1.1.9.3 Supramolecular Detection of Flavin Adenine Dinucleotide<br>.....               | 18   |
| 1.1.10 Differential Array Sensing Approach .....                                       | 20   |
| 1.2 Results and Discussions .....  | 21   |
| 1.2.1 Tricarboxylate Sequestration at Low Carboxyfluorescein<br>Concentrations .....   | 21   |
| 1.2.2 Tetracarboxylate Sequestration at Low Carboxyfluorescein<br>Concentrations ..... | 24   |
| 1.2.3 Analysis of Ratio of Carboxyfluorescein to Dendrimer .....                       | 25   |
| 1.2.4 Anion Titrations in Carboxyfluorescein Dendrimer System at Lower<br>Ratio .....  | 26   |

|  |  |    |
|--|--|----|
| 1.2.4.1  | Titration of 1,3,5-benzenetricarboxylate into Carboxyfluorescein Dendrimer Systems .....                 | 26 |
| 1.2.4.2  | Titration of Adenine Triphosphate into Carboxyfluorescein Dendrimer Systems .....                        | 29 |
| 1.2.4.3  | Titration of Nicotinamide Adenine Dinucleotide Phosphate into Carboxyfluorescein Dendrimer Systems ..... | 30 |
| 1.2.4.4  | Titration of Flavin Adenine Dinucleotide into Carboxyfluorescein Dendrimer Systems .....                 | 33 |
| 1.2.4.5  | Titration of Thiamine Pyrophosphate into Carboxyfluorescein Dendrimer Systems .....                      | 34 |
| 1.2.4.6  | Titration of Folic Acid into Carboxyfluorescein Dendrimer Systems .....                                  | 36 |
| 1.3  | Anion Pattering .....  | 38 |
| 1.3.1  | Generation of Array and Chemometric Analysis.....  | 38 |
| 1.3.2  | Regioisomer of Tricarboxylatebenzene Analysis .....  | 42 |
| 1.4  | Conclusions.....   | 44 |
| 1.5  | Future Directions .....  | 44 |
| 1.6  | Experimental Methods .....   | 45 |
| 1.7  | References.....  | 47 |
| Chapter 2: Studies on the Cooperativity of Binding in Polycationic PAMAM Dendrimers and Polyanionic Species..... |  |    |
| 2.1  | Introduction.....  | 55 |
| 2.1.1  | Scientific Question and Goal .....   | 55 |
| 2.1.2  | Background into Cooperativity .....  | 55 |
| 2.1.3  | Nomenclature .....   | 57 |
| 2.1.4  | Mathematical Representation of Cooperativity .....   | 58 |
| 2.1.5  | Real World Studies of Cooperativity .....  | 60 |
| 2.1.6  | Anslyn Group Cooperativity Studies .....   | 61 |
| 2.1.7  | Effects of Solvent on Cooperativity.....   | 64 |
| 2.2  | Study Design .....   | 64 |
| 2.2.1  | Biological Relevance .....   | 65 |

|  |     |
|--|-----|
| 2.2.2 Previous Work Using Dendrimers for Modeling Biological Systems   | 66  |
| 2.2.3 First Anionic Dendron Synthesis Attempt  | 66  |
| 2.2.4 2 <sup>nd</sup> Generation Anionic Dendron Synthesis Attempt   | 70  |
| 2.2.5 ITC Setup  | 74  |
| 2.3 Results  | 75  |
| 2.3.1 Dendron Models   | 75  |
| 2.3.2 Interactions of the Dendrons with G3 Dendrimers  | 76  |
| 2.3.4 Interaction of the Dendrons with G4 Dendrimer  | 81  |
| 2.3.5 General Concerns About Isotherm Fitting  | 85  |
| 2.3.6 The 2 <sup>nd</sup> Peak in the Isotherm   | 86  |
| 2.3.7 Interaction of the Dendrons with G5 Dendrimer  | 87  |
| 2.3.8 Interactions of the Dendron with G6 Dendrimer  | 90  |
| 2.3.9 Interactions of the Dendron with G7 Dendrimer  | 94  |
| 2.3.10 Overall Dendron – Dendrimer Binding Interaction Characteristics   | 98  |
| 2.3.11 Entropy-Enthalpy Compensation   | 99  |
| 2.3.12 General Lessons From our Analysis   | 101 |
| 2.4 Conclusions  | 102 |
| 2.5 Future Work  | 102 |
| 2.6 Experimental Methods   | 103 |
| 2.7 References   | 106 |
| Chapter 3 – Synthesis and Studies of a Dynamic Multicomponent Assembly with Reversible Covalent Bond Formation Driven by the Coordination of a Metal Ion | 111 |
| 3.1 Introduction   | 111 |
| 3.1.1 Goals and Scientific Question  | 111 |
| 3.2.1 Reversible Covalent Bond Formation   | 111 |
| 3.1.2.1 Disulfide Bond Formation   | 111 |
| 3.1.1.2 Boronic Ester Formation  | 114 |
| 3.1.1.3 Imine Bond Formation   | 117 |

|   |     |
|---|-----|
| 3.1.2 Hemiaminal Bond Formation .....   | 121 |
| 3.1.3 Tripodal Ligand Systems .....   | 122 |
| 3.2 Results and Discussion .....  | 124 |
| 3.2.1 Assembly of Pyridine 2-Carboxyaldehyde and Dipicolylamine                       | 124 |
| 3.2.2 Study on the Effects of Metal Counterions and Water Scavenging<br>Efforts ..... | 125 |
| 3.2.3 Measuring the Extent of Assembly Formation .....                                | 127 |
| 3.2.4 Metal Ligand Studies with ITC.....  | 129 |
| 3.2.5 Structural Analysis of the Multicomponent Assembly Complex                      | 130 |
| 3.2.6 Reversibility of the Multicomponent Assembly .....                              | 131 |
| 3.3 Component Exchange in Pyridine Assembly .....                                     | 134 |
| 3.3.1 Pyridine Assembly Aldehyde Exchange and Screening .....                         | 134 |
| 3.3.2 Exchange of Aldehyde in the Assembly .....                                      | 136 |
| 3.3.3 Concentration and Time to Equilibrium .....                                     | 138 |
| 3.3.4 Solvent Effects on Assembly .....   | 139 |
| 3.3.5 Counterion Screening.....   | 139 |
| 3.3.6 Pyridine Assembly Conclusions .....   | 141 |
| 3.3.7 Future Directions .....   | 142 |
| 3.4 Triazole Based Assembly .....   | 142 |
| 3.4.1 Background on Click Chemistry .....   | 142 |
| 3.4.2 Model System Design .....   | 143 |
| 3.4.3 Interactions with Pyridine-2-Carboxyaldehyde .....                              | 144 |
| 3.4.4 Screening of Various Heterocyclic Aldehydes .....                               | 147 |
| 3.4.5 Aldehyde Exchange .....   | 149 |
| 3.4.6 Screening of Metal Exchange .....   | 151 |
| 3.5 Conclusions.....  | 152 |
| 3.6 Experimental Methods .....  | 153 |
| 3.7 References.....   | 154 |

|  |     |
|--|-----|
| Chapter 4 – Progress Towards the Development of a Sensing System for Chiral Thiols .....   | 159 |
| 4.1 Introduction .....   | 159 |
| 4.1.1 – Goals and Scientific Questions .....   | 159 |
| 4.1.2 – Chirality in Biological Systems .....  | 159 |
| 4.1.3 – Naming Systems of Chiral Compounds.....  | 160 |
| 4.1.4 Importance of Chirality .....  | 162 |
| 4.1.5 – Need for High Throughput Detection Methods for Chirality   | 163 |
| 4.1.6 – Optical Methodologies in Chirality Detection .....   | 165 |
| 4.1.7 – Supramolecular Chirality Determination .....   | 166 |
| 4.1.8 Chirality Determination Using Tripodal Ligand Systems .....  | 168 |
| 4.1.9 – Anslyn Group Work on Alcohol <i>ee</i> Determination .....   | 169 |
| 4.1.10 Importance of Thiols.....   | 171 |
| 4.1.11 Previous Work on <i>ee</i> Determination of Chiral Thiols .....   | 172 |
| 4.2 – Synthesis of Chiral Thiols.....  | 174 |
| 4.2.1 Representative Chiral Thiols.....  | 174 |
| 4.2.2 Synthesis of Chiral Thiols.....  | 174 |
| 4.2.3 Difficulties with Chiral Thiol Synthesis .....   | 175 |
| 4.2.4 Current Status of Thiol Synthesis .....  | 177 |
| 4.3 Assembly Studies with Chiral Thiols .....  | 177 |
| 4.3.1 Studies with a Model Chiral Thiol.....   | 177 |
| 4.3.2 <sup>1</sup> H NMR Analysis of Assembly Formation .....  | 178 |
| 4.3.3 Studies of the Equivalents of Thiol Needed to Reach Signal Saturation .....  | 179 |
| 4.3.4 Comparison of Secondary Amines Between Dipicolylamine and Bis(triazole)amine through <sup>1</sup> H NMR and CD Spectroscopy .... | 181 |
| 4.4 <i>ee</i> Measurements.....  | 183 |
| 4.4.1 Measurement of <i>ee</i> .....   | 183 |
| 4.4.2 <i>ee</i> Calibration Curve of 2-Octanethiol.....  | 183 |
| 4.5 Conclusions.....   | 183 |
| 4.6 Future Work.....   | 184 |

|  |     |
|--|-----|
| 4.7 Experimental Methods .....   | 184 |
| 4.8 References – .....   | 186 |
| Chapter 5: Teaching Through Research: Revolutionizing the Freshman Experience<br>..... | 190 |
| 5.1 Introduction – .....   | 190 |
| 5.1.1 Overview of Study – .....  | 190 |
| 5.1.1 Introduction on the Teaching of Science – .....                                  | 190 |
| 5.2 FRI Summary – .....  | 193 |
| 5.3 Stream Summaries – .....   | 197 |
| 5.3.1 Supramolecular Stream .....  | 197 |
| 5.3.2 Nanomaterials for Chemical Catalysis Stream .....                                | 199 |
| 5.3.3 Mitochondrial Gene Expression Stream .....                                       | 201 |
| 5.4 Fundamental Laboratory Skills .....  | 203 |
| 5.5 Solutions and Dilutions – .....  | 204 |
| 5.6 Synthesis – .....  | 207 |
| 5.7 Separations and Purifications – .....  | 211 |
| 5.8 UV-Vis Spectroscopy – .....  | 214 |
| 5.9 The FRI Model and its Success in Student Academic Performance – .....              | 222 |
| 5.9 Expanding a Research Oriented Model to Other Universities – .....                  | 227 |
| 5.9 Conclusions .....  | 229 |
| 5.10 References – .....  | 230 |
| Appendix 1: Isothermal Titration Calorimetry Traces .....                              | 232 |
| A.1 Dendrimer Cooperativity ITC Traces .....   | 232 |
| A1.2 Metal Ligand ITC Traces .....   | 242 |
| Bibliography .....   | 248 |
| Vita .....   | 266 |

## List of Tables

|  |    |
|--|----|
| Table 1.1 – Select Molecular Properties of Amine Terminated Dendrimers <sup>7</sup> .....          | 5  |
| Table 1.2 – ITC Data for the Titration of CF into G3-G6 PAMAM Dendrimer ...                        | 12 |
| Table 1.3 – Ratio of Carboxyfluorescein to Dendrimer Used for Anion Titrations                     | 26 |
| Table 1.4 - Anions with total charge versus position on the F1 axis of the LDA chart<br>.....      | 42 |
| Table 2.1 – G3 Dendron Binding Thermodynamic Values for 1 <sup>st</sup> Binding Event.             | 77 |
| Table 2.2 – G3 Dendron Binding Cooperativity Values for 1 <sup>st</sup> Binding Event .....        | 78 |
| Table 2.3 – G3 Dendron Binding Thermodynamic Parameters for 2 <sup>nd</sup> Binding Site           | 79 |
| Table 2.4 - G3 Dendron Binding Cooperativity Values for 2 <sup>nd</sup> Binding Event.....         | 80 |
| Table 2.5 – G4 Dendron Binding Thermodynamic Parameters for 1 <sup>st</sup> Binding Site           | 81 |
| Table 2.6 – G4 Dendron Binding Cooperativity Values for 1 <sup>st</sup> Binding Site.....          | 83 |
| Table 2.7 - G4 Dendron Binding Thermodynamic Parameters for 2 <sup>nd</sup> Binding Site           | 84 |
| Table 2.8 – G4 Dendron Binding Cooperativity Values for 2 <sup>nd</sup> Binding Site .....         | 85 |
| Table 2.9 – G5 Dendron Binding Thermodynamic Parameters for 1 <sup>st</sup> Binding Site           | 88 |
| Table 2.9 – G5 Dendron Binding Cooperativity Values for 1 <sup>st</sup> Binding Site .....         | 89 |
| Table 2.10 – G5 Dendron Binding Thermodynamic Parameters for 2 <sup>nd</sup> Binding Site<br>..... | 90 |
| Table 2.11 – G5 Dendron Binding Cooperativity Values for 2 <sup>nd</sup> Binding Site .....        | 90 |
| Table 2.12 – G6 Dendron Binding Thermodynamic Parameters for 1 <sup>st</sup> Binding Site<br>..... | 91 |
| Table 2.13 – G6 Dendron Binding Cooperativity Values for 1 <sup>st</sup> Binding Site .....        | 92 |
| Table 2.14 – G6 Dendron Binding Thermodynamic Parameters for 2 <sup>nd</sup> Binding Site<br>..... | 93 |

|  |     |
|--|-----|
| Table 2.15 – G6 Dendron Binding Cooperativity Values for 2 <sup>nd</sup> Binding Site .....  | 94  |
| Table 2.16 – G7 Dendron Binding Thermodynamic Parameters for 1 <sup>st</sup> Binding Site<br>.....   | 95  |
| Table 2.17 – G7 Dendron Binding Cooperativity Values for 1 <sup>st</sup> Binding Site .....  | 96  |
| Table 2.18 – G7 Dendron Binding Thermodynamic Parameters for 2 <sup>nd</sup> Binding Site<br>.....   | 97  |
| Table 2.19 – G7 Binding Cooperativity Values for 2 <sup>nd</sup> Binding Site .....  | 98  |
| Table 3.1 – Summary of metal and molecular sieves ability to drive assembly<br>formation .....   | 126 |
| Table 3.2 – ITC binding constants for different metals with dipicolylamine and<br>tripicolylamine and the difference between the two ligands .....   | 130 |
| Table 3.3 – Equilibrium constant for the different heterocyclic aldehydes .....  | 136 |
| Table 3.4 – Equilibrium constant for the binding of heterocyclic aldehydes to the<br>bis(triazole)amine .....  | 148 |
| Table 3.5 – ITC binding constants for the bis(triazole)amine (3.33) and<br>tripicolylamine and the difference between those two binding affinities<br>.....  | 151 |
| Table 5.1 - Data comparing performance of students in organic chemistry labs, who<br>either received the alternate freshman chemistry lab experience provided<br>through the FRI program, or who were natural science majors who did<br>not participate in FRI and received the regular freshman chemistry lab<br>training ..... | 226 |



## List of Figures

|   |    |
|---|----|
| Figure 1.1 – Major Classifications of Parts of a Dendrimer .....  | 2  |
| Figure 1.2 – Chemical Examples of Two Major Dendrimer Classifications.....  | 3  |
| Figure 1.3 – Chemical Structure of Generation 2 PAMAM Dendrimer.....  | 4  |
| Figure 1.4 – Binding Isotherms for Pyrocatechol Violet, Pyrogallol Red, and<br>Fluorescein with G3-G7 PAMAM Dendrimers.....       | 7  |
| Figure 1.5 – Comparison of the Binding of Fluorescein and 5(6)-Carboxyfluorescein<br>to G5 PAMAM Dendrimer .....                  | 7  |
| Figure 1.6 – Titration of CF into G4-G7 PAMAM Dendrimers .....  | 8  |
| Figure 1.7 – Fluorescence Anisotropy Graph for the Titration of CF into PAMAM<br>Dendrimer .....                                  | 9  |
| Figure 1.8 – Raw ITC Isotherm and the Process ITC Isotherm for the Titration of CF<br>into G4 PAMAM Dendrimer .....               | 11 |
| Figure 1.9 – Results of Anzenbacher system for high resolution small molecule anion<br>detection (Copyright ACS Publishing) ..... | 15 |
| Figure 1.10 – Structure of Adenine Triphosphate, a Model Nucleotide Triphosphate<br>.....   | 16 |
| Figure 1.11 – Structure of Nicotinamide Adenine Dinucleotide and Nicotinamide<br>Adenine Dinucleotide Phosphate .....             | 17 |
| Figure 1.12 – Structure of Flavin Adenine Dinucleotide.....   | 18 |
| Figure 1.13 – Graphical Representation of Differential Sensing versus Lock and Key<br>Sensing Models .....                        | 20 |
| Figure 1.14 – Structure of Carboxyfluorescein.....  | 21 |
| Figure 1.15 – Trimesic Acid (1.9) and Pyromellitic Acid (1.10).....   | 23 |

|  |    |
|--|----|
| Figure 1.16 – Titration of Trimesic Acid into Dendrimer Carboxyfluorescein<br>Complex .....  | 23 |
| Figure 1.17 – Titration of Pyromellitic Acid into Carboxyfluorescein Dendrimer<br>Complex .....  | 24 |
| Figure 1.18 – Change in Fluorescence Intensity Titration Isotherm of 1,3,5-<br>Benzenetricarboxylate into the CF-Dendrimer System .....                          | 27 |
| Figure 1.19 - Fluorescence Polarization Titration Isotherm of 1,3,5-<br>Benzenetricarboxylate into the CF-Dendrimer System .....                                 | 28 |
| Figure 1.20 - Change in Fluorescence Intensity Titration Isotherm of Adenine<br>Triphosphate into the CF-Dendrimer System .....                                  | 29 |
| Figure 1.21 - Fluorescence Polarization Titration Isotherm of Adenine Triphosphate<br>into the CF-Dendrimer System .....   | 30 |
| Figure 1.22 - Change in Fluorescence Intensity Titration Isotherm of Nicotinamide<br>Adenine Dinucleotide Phosphate (NADP) into the CF-Dendrimer<br>System ..... | 31 |
| Figure 1.23 - Fluorescence Polarization Titration Isotherm of Nicotinamide Adenine<br>Dinucleotide Phosphate (NADP) into the CF-Dendrimer System ...             | 31 |
| Figure 1.24 – Overlap of Fluorescence Intensity Titration Isotherms for ATP and<br>NADP into CF-Dendrimer Complex .....  | 32 |
| Figure 1.25 – Overlap of Fluorescence Polarization Titration Isotherms for ATP and<br>NADP into CF-Dendrimer Complex .....                                       | 32 |
| Figure 1.26 - Change in Fluorescence Intensity Titration Isotherm of Flavin Adenine<br>Dinucleotide (FAD) into the CF-Dendrimer System .....                     | 33 |
| Figure 1.27 - Fluorescence Polarization Titration Isotherm of Flavin Adenine<br>Dinucleotide (FAD) into the CF-Dendrimer System .....                            | 33 |

|  |    |
|--|----|
| Figure 1.28 - Change in Fluorescence Intensity Titration Isotherm of Thiamine<br>Pyrophosphate (TPP) into the CF-Dendrimer System.....   | 35 |
| Figure 1.29 - Fluorescence Polarization Titration Isotherm of Thiamine<br>Pyrophosphate (TPP) into the CF-Dendrimer System.....  | 35 |
| Figure 1.30 - Change in Fluorescence Intensity Titration Isotherm of Folic Acid into<br>the CF-Dendrimer System .....  | 37 |
| Figure 1.31 - Fluorescence Polarization Titration Isotherm of Folic Acid into the CF-<br>Dendrimer System .....  | 37 |
| Figure 1.32 – LDA Plot of All Anions Used in Carboxyfluorescein-Dendrimer<br>System.....   | 39 |
| Figure 1.33 – PCA Plot of All Anions Used in Carboxyfluorescein-Dendrimer<br>System with Generations 4-7 Dendrimer.....  | 39 |
| Figure 1.34 – LDA Plot of All Anions Used in Carboxyfluorescein-Dendrimer<br>System Which Displaced CF .....   | 41 |
| Figure 1.35 – LDA Plot of All Tricarboxylates Used in Carboxyfluorescein-<br>Dendrimer System .....  | 43 |
| Figure 2.1 – Hosts used in Anslyn group cooperativity studies with small<br>carboxylates .....   | 56 |
| Figure 2.2 – Improper tethering of connected binding units leads to weakened<br>connectivity. When properly aligned, the ligands can interact with both<br>of the binding pockets..... | 59 |
| Figure 2.3 – Hosts and guests used by Hughes in the system that displayed positive<br>cooperativity in water. ....   | 63 |
| Figure 2.4 – First anionic repeating unit for the dendron target synthesis .....   | 66 |
| Figure 2.5 – Comparison of First and Second Generation Anionic Para Dendrons   | 70 |

|   |     |
|---|-----|
| Figure 2.6 – Different Target Regioisomer Dendrons .....  | 72  |
| Figure 2.7 – Ortho Dendron and Byproducts.....  | 74  |
| Figure 2.8 – Dendrimer Dendron System Enthalpy Entropy Compensation Graph<br>with a corresponding trend line.....   | 100 |
| Figure 2.9 – Plot of Cooperativity values for enthalpy against the cooperativity value<br>for entropy for all of the dendron-dendrimer pairs. ....  | 101 |
| Figure 3.1 – Components and the catenanes formed by the exchange of disulfide<br>bonds in the Sanders system. A wide variety of size structures were<br>synthesized from the library of complex. .... | 113 |
| Figure 3.2 – Boronic acid capsule used by the James group to bind alkylamines   | 114 |
| Figure 3.3 – Seminal sugar receptor developed by James and Shinkai .....  | 115 |
| Figure 3.4 – Anslyn group boronic acid based chiral diol eIDA overview where the<br>presence of the diol displaces an indicator to lead to an optical signal  | 116 |
| Figure 3.5 – Anslyn group boronic acid receptor that reversibly binds tannins and<br>tannic acid from the aging of Scotch whisky.....   | 116 |
| Figure 3.6 – Pieces used by Lehn to create an imine and hydrazone helical polymer<br>.....  | 118 |
| Figure 3.7 – Representative model of Cooper’s cages and the different aldehyde and<br>amines used in that complexes formation .....   | 119 |
| Figure 3.8 – Leigh’s molecular track where the hydrazone hydrolyzes and then reacts<br>with the next aldehyde on the chain. The disulfide then breaks to reform<br>with the next thiol. ....          | 120 |
| Figure 3.9 – James and Anslyn system for determining <i>ee</i> of chiral amines through the<br>formation of an imine bond.....  | 121 |

|   |     |
|---|-----|
| Figure 3.10 – Anslyn group tripodal ligand system that measures glucose oxidase activity in buffer and serum. ....                                    | 124 |
| Figure 3.11 – Schematic representation of the proposed tripodal ligand system with pyridine-2-carboxaldehyde, dipicolylamine, and zinc triflate ..... | 125 |
| Figure 3.12 – Crystal structure of the tripyridine system .....   | 130 |
| Figure 3.13 – <sup>1</sup> H NMR spectra of tripyridine assembly at various temperatures from -40°C at bottom to 75°C at the top .....                | 132 |
| Figure 3.14 – <sup>1</sup> H NMR spectra of mixture when a second higher equilibrium constant aldehyde is added to the mixture. ....                  | 137 |
| Figure 3.15 – Plot of the ratio of assembly to aldehyde against the total concentration of the aldehyde showing the equilibrium each day .....        | 138 |
| Figure 3.16 – Effects of the addition of anions to the thiazole assembly .....  | 140 |
| Figure 3.17 – Effects of the addition of anions into 5-bromopyridine assembly   | 141 |
| Figure 3.18 – Model Click Reaction .....  | 142 |
| Figure 3.19 – Schematic representation of bis(triazole)amine assembly reaction  | 144 |
| Figure 3.20 – Model <sup>1</sup> H NMR of the triazole assembly .....   | 145 |
| Figure 3.21 – Zoomed in <sup>1</sup> H NMR from 3.5 to 6.2 ppm showing the six non-equivalent protons .....   | 146 |
| Figure 3.22 – <sup>1</sup> H NMR spectra of aldehyde exchange from quinolone aldehyde assembly to the pyridine aldehyde assembly .....                | 150 |
| Figure 4.1 – A Pair of Amino Acids Showing Both Enantiomers .....   | 160 |
| Figure 4.2 – Representation of Both Stereoisomers of 1,2-Methylcyclohexane Which Shows Cis versus Trans Relationship .....                            | 161 |
| Figure 4.3 – Representation of Two Idealized Molecules Showing R and S Using the Cahn, Ingold, Prelog System (Fourth Group is Behind Central Atom)    | 161 |

|  |     |
|--|-----|
| Figure 4.4 – Structure of the Antinausea Medication, Thalidomide.....  | 163 |
| Figure 4.5 – Schematic Showing the Bottleneck in Asymmetric Catalyst<br>Development .....  | 164 |
| Figure 4.6 – James and Anslyn Supramolecular Assembly for Chiral Amine <i>ee</i><br>Determination .....  | 166 |
| Figure 4.7 – Wolf dialdehyde which forms a rigid imine based structure that can be<br>used for <i>ee</i> determination.....  | 167 |
| Figure 4.8 – Boronic acid based receptor for <i>ee</i> determination of chiral diols using<br>eIDA.....  | 167 |
| Figure 4.9 – Canary bisquinolylamine system from modified amino acids .....  | 168 |
| Figure 4.10 – Anslyn modified heterocyclic copper complex which can be used to<br>determine the <i>ee</i> of chiral carboxylates .....   | 169 |
| Figure 4.11 – Dynamic Tripodal Assembly Used for Alcohol <i>ee</i> Determination   | 170 |
| Figure 4.12 – Anslyn system which condenses on a chiral alcohol to give a<br>hemiaminal ether and leads to a CD signal that can be used to quantify<br>the <i>ee</i> of a solution ..... | 171 |
| Figure 4.13 – Structure of Two Drugs Containing Chiral Sulfur Atoms From Which<br>Chiral Thiols are Synthetically Important.....   | 172 |
| Figure 4.16 – Seven Initial Chiral Alcohols for Conversion to Chiral Thiols .....  | 174 |
| Figure 4.17 – Synthetic Scheme for Thiol Synthesis.....  | 175 |
| Figure 4.18 – The Model Chiral Thiol - $\beta$ -D-thiogluocse tetraacetate .....   | 178 |
| Figure 4.19 - $^1\text{H}$ NMR spectral overlay from 3.5 to 6.4 ppm of the assembly with no<br>thiol (on top) and the assembly with 5 equivalents of thiol (bottom).                     | 179 |
| Figure 4.20 – Graph of CD spectra as a Function of Thiol Equivalents.....  | 180 |
| Figure 4.21 – CD Signal at 269 nm as a Function of Thiol Equivalence .....   | 181 |

|   |     |
|---|-----|
| Figure 4.22 - <sup>1</sup> H NMR Spectral Overlay of the Two Secondary Amine Ligands with Thiols .....  | 182 |
| Figure 5.1 – Representation of the three major classifications of universities and how they relate to research and teaching .....   | 192 |
| Figure 5.2 – Research Group, Teaching Laboratory and FRI Research Stream Laboratory Traditional Personnel Arrangement .....   | 194 |
| Figure 5.3 – Course Overview and Timeline for Students in the FRI program...  | 196 |
| Figure 5.4 – Graphical Representation of the Supramolecular Sensors Stream’s Research .....   | 198 |
| Figure 5.5 – Graphical Representation of the Nanomaterials for Chemical Catalyst Stream’s Research.....   | 200 |
| Figure 5.6 – Graphical Representation of the Mitochondrial Gene Expression Stream’s Research.....   | 202 |
| Figure 5.7 – Nanomaterials Stream Synthetic Scheme for the Production of DEN’s and Use as a Catalyst in Model Reduction Reaction .....  | 210 |
| Figure 5.8 – Schematic of Purifications Used by the Mitochondrial Gene Expression Stream. At the Top, a Graphical Representation of the Antibody Which Binds the TAP portion of the Target Protein is Given. At the Bottom, the Binding of the Antibody to the TAP Tag on a Target Protein is Illustrated. .... | 213 |

|  |     |
|--|-----|
| Figure 5.9 – Schematic Showing UV-Vis Spectroscopic Uses by Nanomaterials Stream to Characterize Their Synthesized DEN and the Catalytic Reaction. At the Top, The UV-Vis Spectrum of the Stages of DEN Synthesis is Illustrated. At the Bottom, a Reaction Scheme is Shown for the Catalytic Reaction of the DEN with a UV-Vis Spectra of the Reaction with Increasing Time. ....                           | 217 |
| Figure 5.10 – Graphical Representation of UV-Vis Spectroscopy Use in the Mitochondrial Gene Expression Stream .....  | 218 |
| Figure 5.11 – UV-Vis Spectroscopy Techniques Employed by the Supramolecular Sensors Stream. At the Top, a Schematic Representation of the Sensing Ensemble is Shown. At the Bottom Left, an Example Displacement Isotherm is Shown for the Addition of Tannin to the Sensing Ensemble. Finally, on the Bottom Right, an Idealized Representation of the Array When Exposed to Different Wines is Shown ..... | 220 |
| Figure 5.12 – On the Left, the Graph Illustrates the Retention Rates of Students in FRI Compared to a Control Group. On the Right, the Graph Shows Retention Rates of Students in Different Ethnic Groups Between FRI Students and the Control Group.....  | 223 |
| Figure 5.13 – Graphs showing the cumulative grade distributions of students in organic chemistry labs over a five year period, who either received the alternate freshman chemistry lab experience provided through the FRI program (FRI-CH), or who were natural science majors who did not participate in FRI and received the regular freshman chemistry lab training (CNS not FRI). ....                 | 225 |
| Figure A1.1 – G3 Benzyl Trace .....  | 232 |



|                                      |     |
|--------------------------------------|-----|
| Figure A1.2 – G3 Meta Trace .....    | 232 |
| Figure A1.3 – G3 Para Trace .....    | 233 |
| Figure A1.4 – G3 Tris Trace .....    | 233 |
| Figure A1.5 – G4 Benzyl Trace .....  | 234 |
| Figure A1.6 – G4 Meta Trace .....    | 234 |
| Figure A1.7 – G4 Para Trace .....    | 235 |
| Figure A1.8 – G4 Tris Trace .....    | 235 |
| Figure A1.9 – G5 Benzyl Trace .....  | 236 |
| Figure A1.10 – G5 Meta Trace .....   | 236 |
| Figure A1.11 – G5 Para Trace .....   | 237 |
| Figure A1.12 – G5 Tris Trace .....   | 237 |
| Figure A1.13 – G6 Benzyl Trace ..... | 238 |
| Figure A1.14 – G6 Meta Trace .....   | 238 |
| Figure A1.15 – G6 Para Trace .....   | 239 |
| Figure A1.16 – G6 Tris Trace .....   | 239 |
| Figure A1.17 – G7 Benzyl Trace ..... | 240 |
| Figure A1.18 – G7 Meta Trace .....   | 240 |
| Figure A1.19 – G7 Para Trace .....   | 241 |
| Figure A1.20 – G7 Tris Trace .....   | 241 |
| Figure A1.21 – Co DPA Trace .....    | 242 |
| Figure A1.22 – Co TPA Trace .....    | 242 |
| Figure A1.23 – Co DBTA Trace .....   | 243 |
| Figure A1.24 – Cu DPA Trace .....    | 243 |
| Figure A1.25 – Cu TPA Trace .....    | 244 |
| Figure A1.26 – Cu DBTA Trace .....   | 244 |

|                                    |     |
|------------------------------------|-----|
| Figure A1.27 – Ni DPA Trace .....  | 245 |
| Figure A1.28 – Ni TPA Trace .....  | 245 |
| Figure A1.29 – Ni DBTA Trace ..... | 246 |
| Figure A1.30 – Zn DPA Trace.....   | 246 |
| Figure A1.31 – Zn TPA Trace .....  | 247 |
| Figure A1.32 – Zn DBTA Trace.....  | 247 |

## List of Schemes and Equations

|   |     |
|---|-----|
| Scheme 1.1 – Equilibrium of the CF Binding to PAMAM Dendrimers .....  | 22  |
| Scheme 1.2 - The indicator displacement assay (IDA). D = dendrimer, A = anion,<br>CF = 5(6)-carboxyfluorescein .....  | 22  |
| Equation 2.1 – Jenck’s Mathematical representation of cooperativity .....   | 58  |
| Scheme 2.1 – First Anionic Dendron Synthesis .....  | 68  |
| Scheme 2.2 –Benzyl Halide Starting Material and Azide Synthesis .....   | 69  |
| Scheme 2.3 – 2 <sup>nd</sup> Generation Anionic Dendron Synthesis.....  | 73  |
| Equation 3.1 – First formulation of the equilibrium constant (K) where ZnC is the<br>final complex, 2-PA is pyridine-2-carboxaldehyde and Zn-DPA is<br>the complex of zinc to dipicolylamine..... | 132 |
| Equation 3.2 – A simplification of the previous equation based upon the mass balance<br>of the overall reaction equation.....   | 133 |
| Equation 3.3 – Mass balance equation for the total aldehyde concentration in solution<br>.....  | 133 |
| Equation 3.4 – Ratio of <sup>1</sup> H NMR peaks for the complex with the aldehyde .....  | 133 |
| Equation 3.5 – Final equilibrium constant equation combining all previous equations<br>.....  | 133 |
| Equation 4.1 – Equation for calculating enantiomeric excess ( <i>ee</i> ) .....   | 164 |

# **Chapter 1: Dendrimer Based Anion Detection Using PAMAM Dendrimer**

## **1.1 INTRODUCTION**

### **1.1.1 Goals of Studies and Scientific Question**

In this study, a signaling methodology for a potential multicomponent assembly sensing ensemble is explored. The methodology explores the ability to see signal modulation in the presence of anions and its ability to generate a characteristic signal based upon the presence of that anion. Furthermore, any signal modulation is exploited to identify and differentiate numerous different anions or anionic groups through optical and chemometric methods. The overarching scientific question for the study is summarized as can dendrimer bound indicators be utilized as a signaling method for the presence of target compounds.

### **1.1.2 Origins of Dendrimers**

Developed in the late 70's and early 80's, dendrimers are highly branched polymer like structures that contain a final number of repeating units.<sup>1-3</sup> Unlike traditional polymers, dendrimers branch out from a central point growing out in three dimensions to create trees of different reactive moieties. The name dendrimers arises from the molecules' tree like structure, where the Greek word, dendron means tree. The first dendrimers were developed via divergent synthesis methods, in which one starts from the core of the dendrimers and builds the molecule out towards the ends of the branches.<sup>1</sup> In contrast, convergent synthesis, pioneered by Jean Fréchet, begins by making individual pieces and then joining those pieces together to form the final macromolecule.<sup>4</sup>

A dendrimer contains three major areas: the core, the inner shell and the outer shell. The core is the central molecule from which each of the branches, or

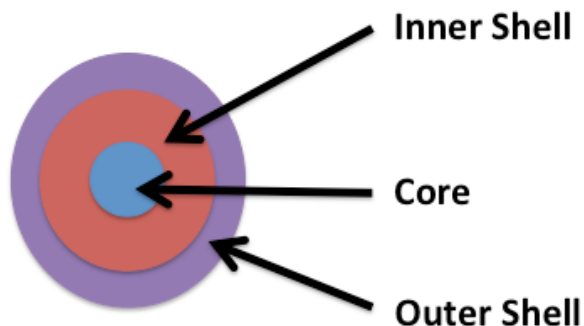
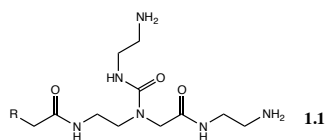


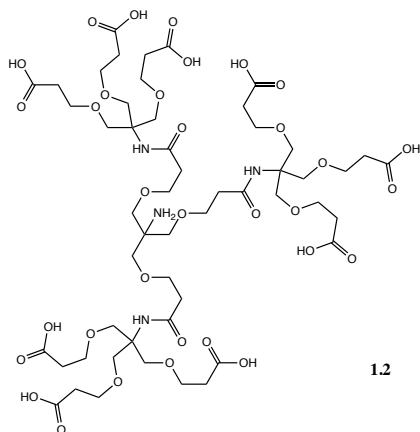
Figure 1.1 – Major Classifications of Parts of a Dendrimer

dendrons, extends. The inner shell is the portion of the dendron not fully exposed to the solvent between the core and the outer solvent exposed ends of the branches. In aqueous solutions, the inner shell can contain pockets of solvent free environment. The outer shell contains the termini of all of the branches and provides a large number of typically uniform functional groups on the surface. The surface of a dendrimer displays monodisperse functional groups that contain a highly symmetric tertiary structure. Furthermore, dendrimers, unlike polymeric counterparts, are soluble in various solvents including water, which makes them useful scaffolds for biological applications. These facts and properties have led to the explosions of interest in dendrimers in the past 20 years.<sup>5</sup>

While there are many different types of dendrimers, dendrimers generally fall into two classifications named for two of the early pioneers of dendrimer synthesis. A Fréchet type dendrimer branches out from the core at each iteration into two additional arms making the total number of groups grow as a power of 2.<sup>4</sup>



**Frechet Style Dendrimer**



**Newkome Style Dendrimer**

Figure 1.2 – Chemical Examples of Two Major Dendrimer Classifications

The other major dendrimer classification is a Newkome type dendrimer, in which each successive branch divides out into three separate units making the final number of surface groups grow as a power of 3.<sup>6</sup> The size of a dendrimer is measured in generations where a generation is the addition of a single repeating unit to every branch. G0, or generation 0, dendrimers contain only the central core whereas G1 adds one additional set of repeating units and this process continues for each successive generation.

### 1.1.3 General PAMAM Dendrimer Characteristics

In the studies that are reported here, commercially available poly(amido)amine dendrimers or PAMAM dendrimers for short, were utilized.<sup>7</sup> PAMAM dendrimers are synthesized via the condensation of methyl acrylate and ethylenediamine and the final surface typically contains primary amines, which in water should be protonated at neutral pH. PAMAM dendrimers are among the best studied and most commonly utilized

dendrimers owing to the fact that they possess, their high water solubility and the ease with which they can be obtained. While amine terminated dendrimers are most common, PAMAM dendrimers can have several functional groups on the terminal ends, hydroxyl groups and carboxylates.<sup>7</sup> These functional groups give the dendrimer different properties overall and allow the reactivity of the dendrimer to be tuned to many varied applications.

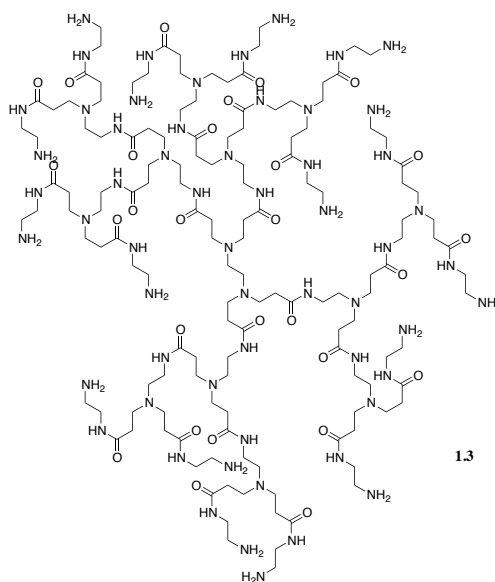


Figure 1.3 – Chemical Structure of Generation 2 PAMAM Dendrimer

PAMAM dendrimers have been utilized for many different applications over the last 20 years. Among the most common uses, dendrimers have been explored as gene and drug delivery devices.<sup>8,9,10</sup> The polycationic nature of the primary amine allows the dendrimer to bind to DNA, making it an ideal gene delivery device and such applications have been explored. Furthermore, the inner core of the dendrimer can accommodate hydrophobic molecules, particularly ones with a negative charge that can have electrostatic interactions with the dendrimer. While many people have used this fact

about dendrimers to carry a drug payload, others, including our group, have explored this same phenomenon for the development of an optical signaling methodology.<sup>11,12,13</sup>

Before moving on to the development of a signaling methodology, there remain a few characteristics of PAMAM dendrimers that are important to highlight. First of all, as was briefly mentioned before, the number of surface groups for Fréchet dendrimers increases by multiples of 2 as the generation increases. For comparison, Table 1 shows some of the properties of generation 3 – generation 7 PAMAM dendrimers that will be used for all of the studies reported, both in this chapter and the next chapter. As can be seen in the table, the number of surface groups increases from 32 groups on the smallest generation to 512 groups for the largest dendrimer. Our studies will focus on the amino terminated dendrimers, so that at its fully protonated form, the dendrimer contains as many as 512 charges making the dendrimer strongly cationic in nature. Furthermore,

| Gen. | M <sub>w</sub> | Diameter | Surface NH <sub>2</sub> | # of Charges (pH 7.4) |
|------|----------------|----------|-------------------------|-----------------------|
| G4   | 14.2 kDa       | 45 Å     | 64                      | 10                    |
| G5   | 28.8 kDa       | 54 Å     | 128                     | 21                    |
| G6   | 58.0 kDa       | 67 Å     | 256                     | 42                    |
| G7   | 116.5 kDa      | 81 Å     | 512                     | 85                    |

Table 1.1 – Select Molecular Properties of Amine Terminated Dendrimers<sup>7</sup>

unlike the smaller starting components, the dendrimer exhibits a range of pKa's, from approximately 6.6 to 7.2 for the inner amines to 9 to 10 for the surface amines since the protonation of one amine effects the protonation of its neighbors making the actual pKa's of an particular amine vary with its microenvironment despite the high degree of symmetry within the molecule.<sup>14</sup> Using this principle, the table shows an estimated protonation of the dendrimer at physiological pH of 7.4. As can be seen from these values, the protonation is roughly half of the terminal amines at this pH.



Furthermore, the weight roughly doubles as the generation increases and the size increases per increase in generation by about 9 Å. Furthermore, the increases in generation make the dendrimer act more spherical in nature and possess a more uniform outer shell. In addition to creating a spherical shell, the dendrimer also forms pockets within the structure that can encapsulate other molecules.<sup>15</sup>

#### **1.1.4 General Indicator Binding to PAMAM Dendrimers**

To this end, a previous member of the Anslyn group explored the binding of numerous anionic indicators to different generations of PAMAM dendrimers. Studies were carried out using many different generations (Generation 3-7) of dendrimers to study the effects of the increasing size and positive charge upon the binding of anionic indicators. The binding of indicators, such as pyrocatechol violet, shows a bathochromic shift in the UV-Vis spectra when the concentration of dendrimer is increased. The change in the absorbance maxima corresponds to a deprotonation of pyrocatechol violet upon the binding of the indicator to the dendrimer.

Plotting the change in absorbance versus the equivalent of AT-PAMAM dendrimer added, a binding isotherm was obtained which could be used to extrapolate an approximate binding stoichiometry for each indicator. Based upon these spectra, it can be seen that the spectra for a single indicator bound to a dendrimer has little difference depending on the generation of the dendrimer to which it is bound. As might be expected, higher generations of dendrimers bind to an exponentially increasing number of indicators, thereby mirroring the exponential growth of the dendritic surface area as well as the increasing interior pockets that can bind the indicators.

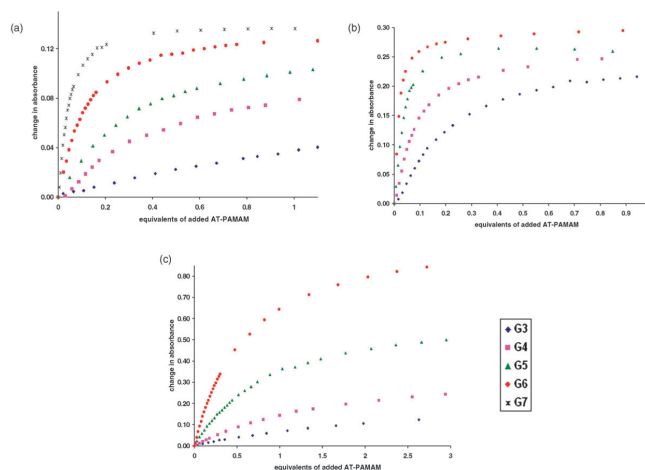


Figure 1.4 – Binding Isotherms for Pyrocatechol Violet, Pyrogallol Red, and Fluorescein with G3-G7 PAMAM Dendrimers

Comparing the binding curves of 5-carboxyfluorescein and fluorescein reveals a difference due to the larger anionic character of 5-carboxyfluorescein, which leads to a stronger binding to the AT-PAMAM dendrimer. This fact supports the concept of a primarily electrostatic driving force for binding to the dendrimer. Further evidence in support of this hypothesis is illustrated by the lack of significant binding of the indicator to hydroxy-terminated (HT)-PAMAM dendrimers.

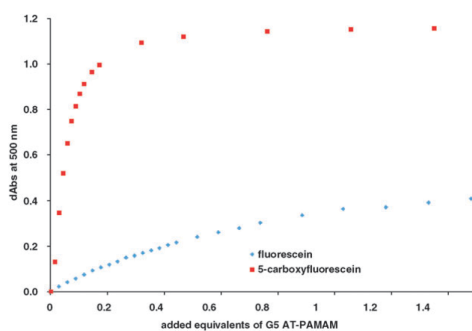


Figure 1.5 – Comparison of the Binding of Fluorescein and 5(6)-Carboxyfluorescein to G5 PAMAM Dendrimer

In this study, these previous results show that multiple anionic indicators are taken up within the dendritic scaffolding of AT-PAMAM dendrimers, primarily via electrostatic attractions. The binding of these indicators causes a shift in the UV-Vis spectra and can be used to determine a ratio of indicators bound to the dendrimer. Furthermore, the amount of indicator taken up exponentially increases with increases in the dendritic scaffolding as well as the charge density on the indicator. While this phenomenon can be used in a signaling methodology for a detection system, the dynamic nature of binding and the reason that the signal is modulated upon binding was explored first.

### 1.1.5 Binding of Carboxyfluorescein to the PAMAM Dendrimers

In further studies, the binding of 5(6)-carboxyfluorescein (CF) to varying different generations of AT-PAMAM dendrimers was explored. When studying the binding of this indicator, the isotherm shows a distinctive pattern with a steep decrease in fluorescence intensity before a small dip in the fluorescence with a slight restoration of fluorescence intensity before the fluorescence intensity levels out.

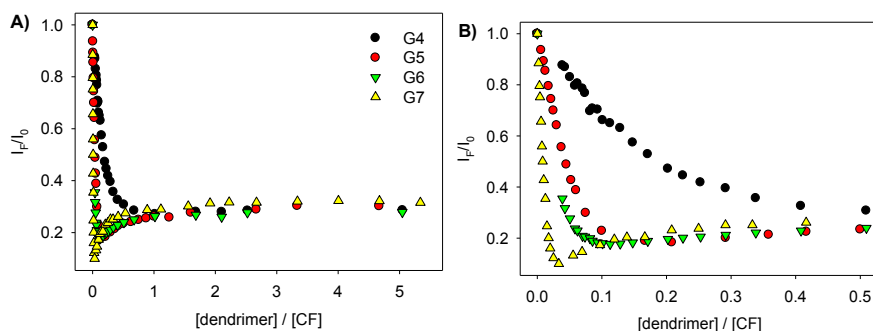


Figure 1.6 – Titration of CF into G4-G7 PAMAM Dendrimers

Furthermore, the fluorescence anisotropy<sup>16</sup> of the system was investigated. As the fluorophore becomes bound to the dendrimer, the anisotropy increases as the rotation of the dendrimer slows the tumbling of the fluorophore until it reaches a specific value for each generation of dendrimer. A similar pattern was observed for the fluorescence anisotropy, where the initial change is very small until a critical point is reached. After this initial phase is complete, the anisotropy increases rapidly until it reaches the maximum value for the generation of dendrimer, which represents the fluorophores tumbling when completely bound to a dendrimer. This optical signal was proposed as a potential signaling methodology.

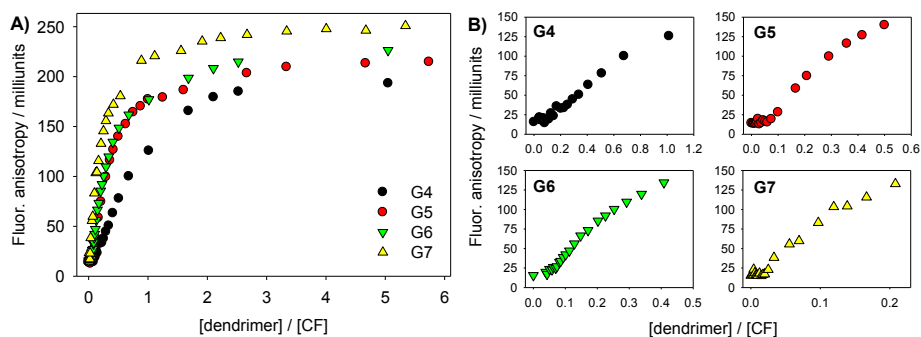


Figure 1.7 – Fluorescence Anisotropy Graph for the Titration of CF into PAMAM Dendrimer

This phenomenon was explored in more detail through detailed titrations that collected numerous data points in the lower concentration region of the unusual dip in the titration curve. The early points show the binding of the fluorophore with a fluorescence is turned off by interaction with the dendrimer's amines through PET as well as self quenching due to being held in close proximity. These effects lead to a rapid decrease in the fluorescence intensity signal at relatively low concentrations of dendrimer. The plots

are consistent with both of these phenomenon. The fluorescence intensity decreases as would be expect but furthermore, the anisotropy does not immediate begin to increase because the bound fluorophores are quenched and thus the anisotropy does not change at low concentrations.

As the concentration of dendrimer is increased, the indicator redistributes from multiple fluorophores on a single dendrimer to ultimately single fluorophores in a dendrimer and thus the self-quenching is eliminated, leading to a restoration of the fluorescence intensity. Also, the anisotropy begins to increase as the fluorophore self-quenching drops, giving a signal which shows the fluorophore bound to the dendrimer.

#### **1.1.6 ITC Studies of Carboxyfluorescein Binding**

In an effort to further study these binding events, a series of isothermal titration calorimetry (ITC) titrations with 5(6)-carboxyfluorescein and four different generations of AT-PAMAM dendrimers were performed. Isothermal titration calorimetry works by injecting the same amount of ligands into a solution at a fixed temperature. The instrument then measures the amount of heat evolved as a fixed amount of ligand binds the host. The molar concentration of ligand is plotted against the total amount of heat evolved. A line is determined that best fits the graph and this line is used to determine the stoichiometry of binding, the binding constant, the amount of enthalpy contribution of the binding and the amount of entropy contribution to the binding. Using the data obtained, the generations of dendrimer and their binding properties can be compared and trends in the fluorophore binding can be evaluated.

Given the high stoichiometry binding of 5(6)-carboxyfluorescein to the AT-PAMAM dendrimers, we found ITC to be an ideal way to delve more deeply into the multiple binding interactions. Using ITC, we were able to obtain binding isotherms for

the different generations of dendrimer. In this manner, we studied the binding of CF to G3-G6 AT-PAMAM dendrimers. The G7 AT-PAMAM dendrimer was not included in this study because we were unable to obtain solutions concentrated enough to give adequate signals with the dendrimer-CF pair.

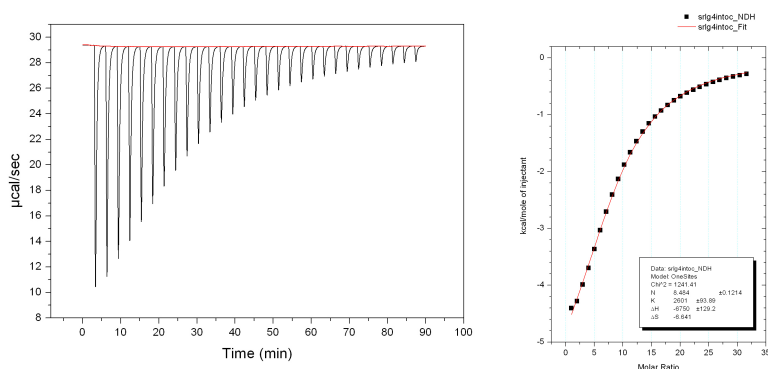


Figure 1.8 – Raw ITC Isotherm and the Process ITC Isotherm for the Titration of CF into G4 PAMAM Dendrimer

Given previous reports,<sup>17</sup> the dilution of a large cationic dendrimer during ITC measurements can give large artifacts in the ITC spectra due to its own dilution and thus a constant concentration of dendrimer was used in each experiment. Hence, CF and dendrimer was used as the titrant solution. The titrations gave a consistent exponential increase in the amount of CF bound as expected due to the exponential increase in both size and charge on the larger generations of dendrimers. As shown in Table 1.2, the equivalents of CF bound increases from  $2.4 \pm 0.1$  for generation 3 to  $50.2 \pm 0.3$  for generation 6. These amounts of CF

| Generation | n          | Binding Constant (M <sup>-1</sup> ) | Enthalpy (cal/mol) | Entropy (e.u.) |
|------------|------------|-------------------------------------|--------------------|----------------|
| G3         | 2.4 ± 0.1  | 3100 ± 100                          | - 6700 ± 300       | - 6.03         |
| G4         | 8.5 ± 0.1  | 2600 ± 90                           | - 6800 ± 100       | - 6.64         |
| G5         | 21.8 ± 0.2 | 2300 ± 100                          | - 6100 ± 100       | - 4.64         |
| G6         | 50.2 ± 0.3 | 2020 ± 70                           | - 5870 ± 50        | - 4.23         |

Table 1.2 – ITC Data for the Titration of CF into G3-G6 PAMAM Dendrimer

are much larger than the values attained through traditional optical techniques, such as through the analysis of the fluorescence intensity, anisotropy and absorbance measurements. This observation makes good logical sense when one realizes that the ITC measures all binding events, while these other techniques require some form of optical signal modulation. All binding events, no matter how weak, will release heat but not all binding events result in changes in the optical properties of the dye making the event optically silent.

The ITC results show that the binding constant for CF decreases as dendrimer generation increases going from 3100 ± 100 for generation 3 to 2020 ± 70 for generation 6. This phenomenon supports the hypothesis that the interaction is electrostatically driven but also suggests that more than electrostatics play a role particularly in the binding of CF to the higher generations of dendrimers. If electrostatic interactions were the only mode of binding for the CF then we would be expected to become larger as the generations increases because the total charge of the dendrimer increases. The larger generations of dendrimers have a higher charge density, but the decrease in binding constant is likely due the need for the dendrimer to release counter ions held more tightly or deeper in the dendrimer's cavities in order to bind the larger numbers of anionic CF molecules as more CF molecules are bound to the dendrimer.

Finally, given that the thermodynamic values are very similar for each of the dendrimer generations further supports that the dendrimers bind CF using similar binding modes. As can be seen in the table, the  $\Delta H$  values are all very similar at approximately -6000 kJ/mol but the values are slightly weaker for the larger generations. Furthermore, the  $\Delta S$  values between -6.6 to -4.2 eu. The  $\Delta H$  values support a strong electrostatic binding interaction with higher generations.

The negative entropy values are supportive of the idea that multiple indicators are binding to form one larger complex thus increasing the order of the system, but the values are smaller than might be expected as the binding is countered by release of counter anions into solution. Additionally, the release of the hydration sphere around the fluorophores as they bind provides favorable entropic contributions. Furthermore, the entropy is also tempered by the formation of a more rigid structure preventing molecular motions within the dendrimer. The rigid complex is formed as the fluorophore locks the dendritic arms together through electrostatic interactions as well as through hydrophobic effects.

Overall, the ITC results appear to be consistent with the data obtained from fluorescence and allowed estimation of the binding stoichiometry of the CF to the larger AT-PAMAM dendrimers. We were also able to obtain a binding constant for this larger fluorophore-dendrimer assembly in water with similar results for the enthalpy and entropy in all four systems, supporting a single binding mode for the fluorophores. The binding of other anionic structures to the polycationic dendrimers will be explored later in this dissertation.



### **1.1.7 Target Selection**

Given the cationic nature of the dendrimers, the most obvious feature of the dendrimer is its charged nature, which makes the system an ideal scaffold for the detection of anions. While there are numerous different potential anionic targets, biological relevant anions were chosen as the ideal target analyte because of their importance and relative ubiquitous nature, as well as the lack of systems that can distinguish between them.

Many biological processes rely on cofactors which contain anionic moieties, particularly phosphates and carboxylates, in order to carry out their desired biological function.<sup>18</sup> Some cofactors, such as NAD and NADP, serve as oxidation/reduction electron donors for key biological process such as the generation of ATP and the degradation of nutrients. Levels of these cofactors, as well as the regulation of the production of these cofactors, are important for studying and understanding many disease states.<sup>19</sup>

### **1.1.8 General Anion Recognition Previous Work**

Numerous other groups have studied anion sensing with particular focus on small ions rather than larger and more complex anionic structures that make up cofactors.<sup>20</sup> Many groups have developed molecules that are selective for an anionic group such as a halide, a carboxylate, or a cyanide. For example, the Gunnlaugsson group has developed several anion receptors based upon a urea-amide linkage.<sup>21-23</sup> While these structures are sensitive to anions, they also possess high specificity for a particular class of anion such as aliphatic carboxylates or phosphates. Additionally, the Sessler group has developed several molecules that are highly selective for phosphate, a common biological anionic group.<sup>24-27</sup> Some of these molecules recognize phosphate or pyrophosphate but they have not been expanded to study biological targets. Others, such as the Saha<sup>28</sup>, Beer<sup>29</sup>, Steed<sup>30</sup>,

Gale<sup>20</sup> and Fabbrizzi<sup>31</sup> groups, have developed selective anion receptors for particular ions such as particular halide or a carboxylate, but these receptors were not studied with complicated biological anionic moieties.

While these systems have a particular ion class as a target, and several sensor systems have been developed that can pattern different types of anions or particular mixtures of anions.<sup>32</sup> An array of calix[4]pyrroles developed by the Anzenbacher group was able to identify anions and found the calix[4]pyrroles the group tested were particularly sensitive

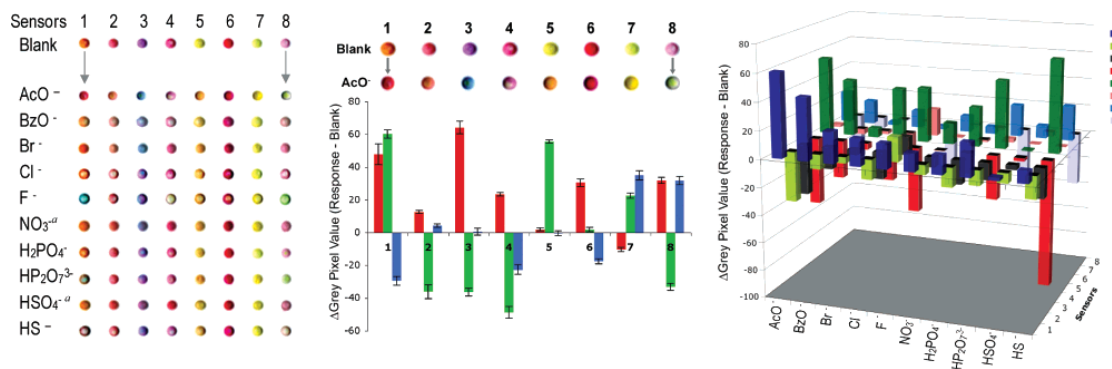


Figure 1.9 – Results of Anzenbacher system for high resolution small molecule anion detection (Copyright ACS Publishing)

to fluoride ions.<sup>33</sup> To further extend this system, their group used the system to analyze both type of the ion and the ion concentration. Finally, the Anzenbacher group patterned a variety of different toothpastes based upon the presence and amount of fluoride ion they contain. In another example, Anzenbacher used only two receptors to study zinc and identify the counteranion based upon the turning on and off of fluorescence and FRET in two indicators.<sup>34</sup>

### 1.1.9 Biologic Anion Detection

Furthermore, some of the individual biological anions we propose to detect have been screened and identified individually through various supramolecular methodologies. Among the best studied of biological anions are the nucleotide triphosphates (NTP) for which numerous different methods of detections have been developed.<sup>35-37</sup> The Anslyn lab has developed a few detection methods for the differentiation of NTP's as well.<sup>38</sup> While many different methodologies exist, they have been extensively reviewed and only a few important parts of that extensive work will be discussed here.<sup>39</sup> For more extensive information, please consult the extensive review about phosphate binding given in reference 39.

#### 1.1.9.1 Highlights of Nucleotide Triphosphate Detection

First, the most popular phosphate sensor is one developed by the Hamachi group. This group developed a ratiometric sensor based upon the acridine moiety with a dipicolylamine side chain.<sup>40</sup> The zinc coordinated chemosensor bound the phosphate tail of a NTP which induced a charge transfer between the bound metal

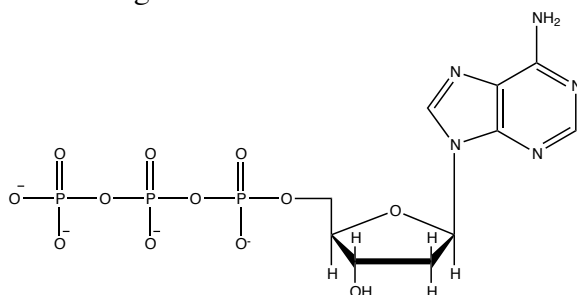


Figure 1.10 – Structure of Adenine Triphosphate, a Model Nucleotide Triphosphate

and the acridine ring leading to a dual emission shift allowing for selective detection of the NTP. This system was further used to study the hydrolysis of the nucleotide group from UDP-Gal to form free UDP as an application for the chemosensor.<sup>35,41</sup> In 2007, the

Wolfbeis group used a europium tetracycline complex to detect NTP based upon modulation of the europium luminescence.<sup>37</sup> This group used the system to monitor the formation of ATP byproducts as a result of enzymatic processes. Additionally, our group has shown that a trisaminobenzene scaffold with peptidic arms can be used to detect and differentiate ATP from either other NTP's, including GTP or the less charged AMP in aqueous media.<sup>38</sup> The peptidic arms were varied to generate a pool of receptors with similar but distinct interactions in the arms that impart the nucleotide differentiation enhancing the NTP binding to the trisaminobenzene core. Using multivariate data analysis, such as principle component analysis (PCA), these analytes were differentiated.

### 1.1.9.2 Supramolecular Detection of Nicotinamide Adenine Dinucleotide

There are a number of supramolecular detection protocols that extend beyond the common NTP and expand to other common cofactors; these methods are far less common than those for NTP. Only a handful of supramolecular methods have been developed for the detection of NAD or NADP and their reduced counterparts. In 1997 and 1998, the Lehn and then Bianchi group reported receptors for NAD and NADP based upon a polyammonium macrocycle.<sup>42,43</sup>

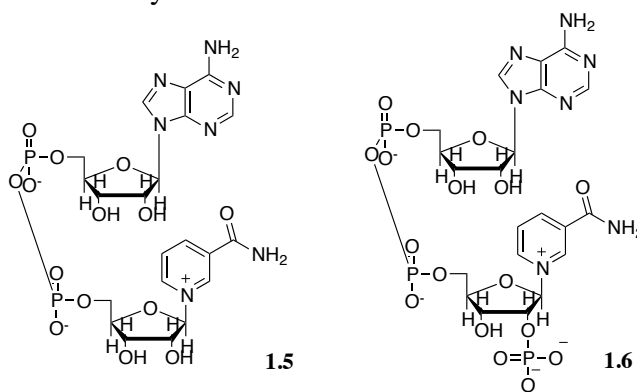


Figure 1.11 – Structure of Nicotinamide Adenine Dinucleotide and Nicotinamide Adenine Dinucleotide Phosphate

The Lehn group added an acridine group that through  $\pi$ - $\pi$  stacking interactions binds the base of the nucleotide with reported binding constants on the order of  $10^7$  to  $10^8$ .<sup>42</sup> Bianchi used the protonated azacrown ether to bind the anionic phosphate group and used the redox potential of the nicotinamide to detect the NAD group.<sup>43</sup> Previously, Schmidtchen had reported the chemosensor that represents the state of the art, a macrocyclic anion binding unit which binds NAD and NADP selectively as early as 1981.<sup>44</sup> More recently in 2005, the Klärner group reported a bisphosphonate clip that binds NAD in water with a binding constant of  $9100 \text{ M}^{-1}$ , but this clip had poor differentiation between other N-alkylpyridinium salts.<sup>45</sup>

### 1.1.9.3 Supramolecular Detection of Flavin Adenine Dinucleotide

Several different methods for supramolecular sensing of flavin adenine dinucleotide (FAD) have been developed owing to its own optical properties. In the early 90's, the Yano group reported several flavin receptors, which mimicked the hydrogen bonding isoalloxazine ring. Unfortunately, these receptors only worked in organic solvents, and thus will not be further elaborated in this dissertation as it is incompatible with biological sensing.<sup>46</sup> The Kunitake group, as a part of their work in

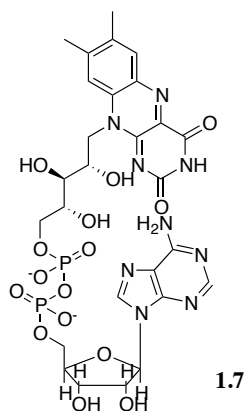


Figure 1.12 – Structure of Flavin Adenine Dinucleotide

the field of monolayer recognition, developed a mix of monolayer headgroups, which form hydrogen bond donors to the isoalloxazine ring, the phosphate backbone and the adenine headgroup of FAD.<sup>47</sup> Their studies showed that FAD bound the monolayer at concentrations as low as  $10^{-7}$  M. More recently, Rotello has reported a hydrogen bond partner for FAD based upon a pyridine ring that can selectively recognize FAD.<sup>48</sup> While Rotello obtained recognition of the FAD core isoalloxazine ring, his group was more interested in studying the effects of hydrogen bonding on the redox potential of the ring rather than detection of FAD.<sup>49-51</sup> König and Desvergne reported a phenothiazine and zinc-cyclen complex that forms a dyad with the flavin ring at high pH.<sup>52</sup> While this system works in water, it only forms the complex at high pH (pH > 9) when the flavin ring is deprotonated, making it unsuited to working at physiological conditions. In 2001, the Burke group developed an RNA aptamer that shows selective modulation for FAD over AMP and FMN.<sup>53</sup> The aptamer showed affinity for FAD on the order of 50  $\mu$ M, but lacked specificity for FAD over either FADH<sub>2</sub>. Finally, the Hong group developed a zinc coordinated dipicolylamine receptor that bound FAD.<sup>54</sup> By using the natural fluorescence of FAD, they were able to identify the binding of FAD over PP<sub>i</sub>, which actually binds tighter to the receptor than FAD. The receptor was used in count human eosinophils using fluorescence-activated cell sorting. Unfortunately, the receptor binding to NTP was not reported and thus we do not know what effect the competitive binding of NTP would have on the fluorescence.

While differentiation of multiple types of anions can be affected using instrumental methods such as high performance liquid chromatography (HPLC), gas chromatography (GC) or capillary electrophoresis (CE), these techniques often require high concentration of samples, tedious sample preparation and require expensive

instrumentation.<sup>55-61</sup> Furthermore, these techniques cannot be used to study biological systems in real time or for in vivo analysis.

### 1.1.10 Differential Array Sensing Approach

In recent years, the Anslyn group, along with others, has used arrays of supramolecular based small molecule receptors that allow for the differentiation of similar analytes in complex media.<sup>62-64</sup> An array of receptors are used with targeted interactions or binding for a particular class of analytes or functional groups. The receptors often may be either highly selective for a single analyte, but more commonly have general affinity for most of the target analytes. These receptors have different reactivity for the different targets, and each of the receptors give a characteristic signal based upon its affinity for the particular target. The characteristic pattern of each of the analytes is thus generated. Using the patterns generated coupled with chemometric techniques, our group has been able to successfully identify analytes in solution as well as the identity of complex solutions.<sup>65-69</sup>

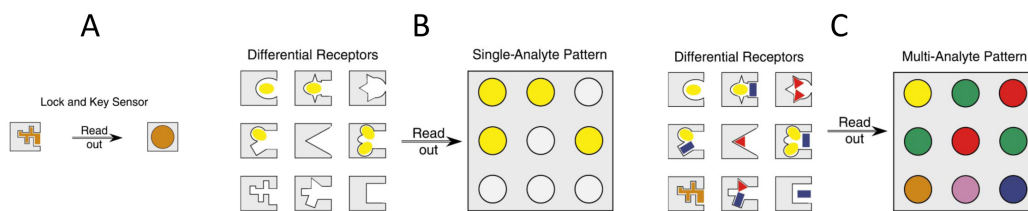


Figure 1.13 – Graphical Representation of Differential Sensing versus Lock and Key Sensing Models

Additionally, the Anslyn group has studied the use of large macromolecular structures, such as bovine serum albumin (BSA) as a scaffold for the development of an

array of supramolecular receptors, providing the impetus to our attempts to pattern biological anions.<sup>68,69</sup>

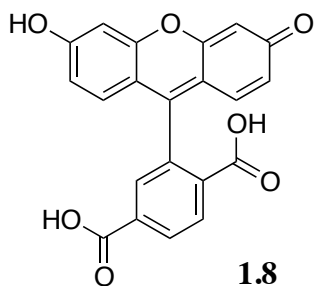


Figure 1.14 – Structure of Carboxyfluorescein

In this study, we report the use of four generations of amino-terminated PAMAM dendrimers and the fluorescence indicator 5(6)-carboxyfluorescein (CF) to differentiate biologically relevant anions and other polyanions in an aqueous solution. Using UV/vis, fluorescence and fluorescence anisotropy measurements, coupled with chemometrics, we were able to differentiate nine unique types of biologically relevant anions. Furthermore, we were also able to use the dendrimer system to differentiate three different tricarboxylates based solely upon the regioisomerization of the charges.

## 1.2 RESULTS AND DISCUSSIONS

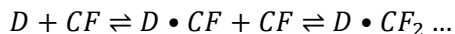
### 1.2.1 Tricarboxylate Sequestration at Low Carboxyfluorescein Concentrations

While the polycationic dendrimer makes a great host for the sequestration of anionic structures, there is no a priori method by which an optical signal can be modulated upon the binding of target anions. While it has been shown that fluorescein can be covalently attached to the terminal amines, the modification of dendrimers is a complicated process and often leads to incomplete modification.<sup>70</sup> Furthermore, the

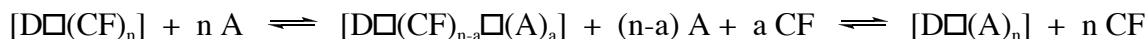


modification limits the information that can be obtained from the fluorophore which might signal anion binding.

But given our previous reports that dendrimers sequester a large number of anionic indicators, particularly the anionic CF fluorescence indicator, we explored in Section 1.1.5. Based upon this reported phenomena, the system shows potential as a possible indicator displacement assay signaling methodology.<sup>12,13</sup> In an indicator displacement assay, the CF shows a different optical signal between the bound CF indicator and the CF free in solution (Scheme 1). In order to probe this signaling methodology, two small anions were used to probe the ability of the CF to be displaced from dendrimers as a potential signal. The displacement that leads to an optical signal is shown in Scheme 2



Scheme 1.1 – Equilibrium of the CF Binding to PAMAM Dendrimers



Scheme 1.2 - The indicator displacement assay (IDA). D = dendrimer, A = anion,  
CF = 5(6)-carboxyfluorescein

In this first study, tri- and tetracarboxylates were used to probe the ability of the CF indicator to be displaced with these anions. The target anions, trimesic and pyromellitic acid, were used because they have low UV/Vis absorbance, no fluorescence, as well as are commercially available. To test this strategy for

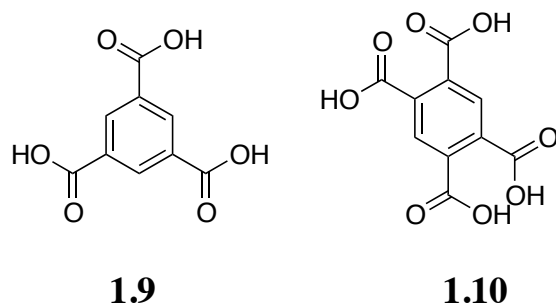


Figure 1.15 – Trimesic Acid (1.9) and Pyromellic Acid (1.10)

signalling, a fixed ratio of CF to dendrimer corresponding to the point that the anisotropy was at 90 percent of its maximum was used in the set. At these ratios, the dendrimer to CF indicator ratio contained only 1 to 2 CF per dendrimer, and thus each dendrimer contained many charges which can be still be paired with the anionic analytes in question. As shown in the figure, the tricarboxylate, 1,3,5-benzenetricarboxylate (trimesic acid), was titrated into a fixed ratio of dendrimer and the CF indicator. Many equivalents had to added before the signal was modulated. As can be seen in the figure, the titration of the anion into the solution finally caused an increase in the fluorescence intensity as well as a decrease in anisotropy toward the anisotropy of the free CF indicator, showing that displacement was occurring.

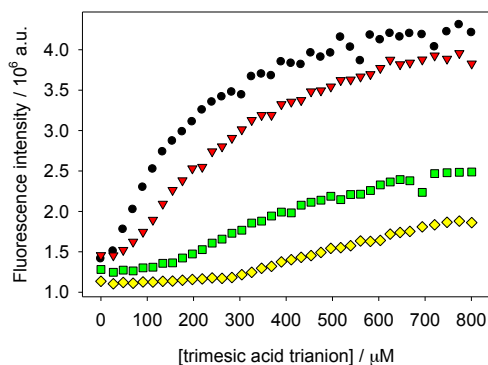


Figure 1.16 – Titration of Trimesic Acid into Dendrimer Carboxyfluorescein Complex

### 1.2.2 Tetracarboxylate Sequestration at Low Carboxyfluorescein Concentrations

A similar titration was carried out with pyromellitic acid, 1,2,4,5-benzenetetracarboxylate, using the same ratio of CF indicator to dendrimer as the trimesic acid. The pyromellitic acid more quickly showed restoration of the fluorescence intensity than trimesic acid, likely due to the higher charge density of the four charges versus three found in trimesic acid. In addition to the restoration of fluorescence intensity, fluorescence anisotropy also decreased in all generation to the approximate anisotropy of free CF indicator. This change is different than the previous anion in which only G3 and G4 returned to the anisotropy of free CF indicator but G6 and G7 did not completely return to the levels of free indicators even after the addition of 800  $\mu\text{M}$  of the target anion. Additionally, the fluorescence intensity of the titration with pyromellitic acid reached a higher intensity at lower equivalents of the targeted anion than the trianion. These changes in the isotherms indicate that the tetraanionic pyromellitic acid shows a higher binding affinity than the trianionic trimesic acid for the polycationic dendrimer.

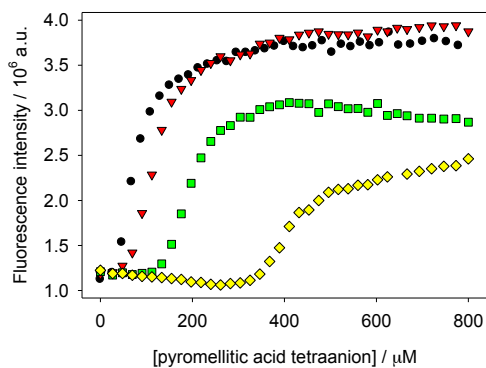


Figure 1.17 – Titration of Pyromellitic Acid into Carboxyfluorescein Dendrimer Complex

But while the pyromellitic acid shows higher binding, the higher generations of dendrimers at high concentrations of anion experienced solubility problems because

aggregates were formed. This problem limits the ability of the pyromellic acid for further use in the optimization of indicator displacement assay for the analysis of other anion analysis. While these carboxylates serve as a useful proof of principle that anions can generate an optical signal that can be detected, the dendrimer to CF indicator ratios proved less than optimal for sensitive detection of the target anions because at least a concentration of 100  $\mu\text{M}$  was needed to begin to modulate the optical signal from the dendrimer bound CF indicator. In order to explore anions at a more reasonable concentration, on the order of those found in biological systems, the ratio of CF to dendrimer was optimized.

### 1.2.3 Analysis of Ratio of Carboxyfluorescein to Dendrimer

In order to improve the sensitivity of the assay, we changed the ratio of CF per dendrimer to new ratios based upon the CF binding isotherm. As can be seen in the table, the lower ratios allow for the indicator to be more readily displaced from the dendrimer because the cationic charges on the dendrimer are saturated with indicator. As such, the complex is closer to charge neutrality and sensitive to the anionic nature of the target analyte. Instead of choosing the point at which the anisotropy signal was 90% saturated, the point in which the fluorescence intensity stopped significantly decreasing was chosen. At this point, the uptake of the CF indicator to the dendrimer no longer causes a signal modulation, thus we anticipated that the presence of an added anion would cause displacement of the indicator allowing the fluorescence to turn back on and decrease the anisotropy of the CF indicator. At these lower concentrations, a smaller concentration of the target analyte should be needed to cause a signal modulation at these ratios of dendrimer to indicator, and this is observed in our anion titrations.

| Generation | Ratio (Low Sensitivity) | Ratio (High Sensitivity) |
|------------|-------------------------|--------------------------|
|------------|-------------------------|--------------------------|

|                          |              |             |
|--------------------------|--------------|-------------|
| <b>G3-NH<sub>2</sub></b> | N/A          | 1 CF : 1 D  |
| <b>G4-NH<sub>2</sub></b> | 2.5 CF : 1 D | 2 CF : 1 D  |
| <b>G5-NH<sub>2</sub></b> | 1.9 CF : 1 D | 3 CF : 1 D  |
| <b>G6-NH<sub>2</sub></b> | 2.1 CF : 1 D | 5 CF : 1 D  |
| <b>G7-NH<sub>2</sub></b> | 1.6 CF : 1 D | 10 CF : 1 D |

Table 1.3 – Ratio of Carboxyfluorescein to Dendrimer Used for Anion Titrations

#### **1.2.4 Anion Titrations in Carboxyfluorescein Dendrimer System at Lower Ratio**

The lower analyte concentrations would be more applicable to biological systems and thus give the system much more utility. Furthermore, the lower concentration makes the system more sensitive to smaller changes in anion concentration giving the system a lower dynamic range than the previous ratio. In order to explore the displacement ability of the lower indicator and dendrimer ratio, we choose to explore the displacement by titrating several different anions (ATP, FAD, NAD and thiamine pyrophosphate [TPP]) with two different anion types: anionic phosphates and trimesic acid with carboxylates. The phosphate group is prevalent in biological systems, and many of the common cofactors and biological molecules contain this functional group, making the anionic group a target of interest for study and differentiation. Many of the common phosphate anions have very similar structures making them to difficult to differentiate using supramolecular techniques based upon ionic and hydrogen bonding partners. Supramolecular techniques have a strong advantage for biological systems because they allow for in vivo analysis, often without modification to the surrounding environmental matrix, unlike most instrumental based methodologies.

##### ***1.2.4.1 Titration of 1,3,5-benzenetricarboxylate into Carboxyfluorescein Dendrimer Systems***

For our study at the lower concentrations of anion, we first used the 1,3,5-benzenetricarboxylate to displace the CF indicator from the dendrimer. In all

generations, a similar pattern of displacement to the higher ratio of indicator to dendrimer was observed during the titration. The displacement occurred with smaller amounts of anion including what appears to be complete displacement of the indicator at the end of the titration. The displacement with smaller amounts of anions, and at lower anion concentrations makes the lower ratio of CF indicator and dendrimer a more sensitive assay than the previous attempt. As can be seen in Figures 1.18 and 1.19, both the fluorescence intensity and the fluorescence anisotropy provide valid and useful information about the intensity of binding between the dendrimer and the target anionic analyte, including an ability to generate relative binding affinity.

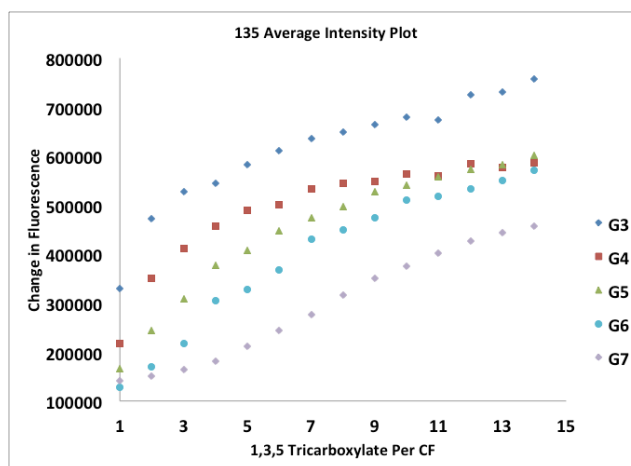


Figure 1.18 – Change in Fluorescence Intensity Titration Isotherm of 1,3,5-Benzenetricarboxylate into the CF-Dendrimer System

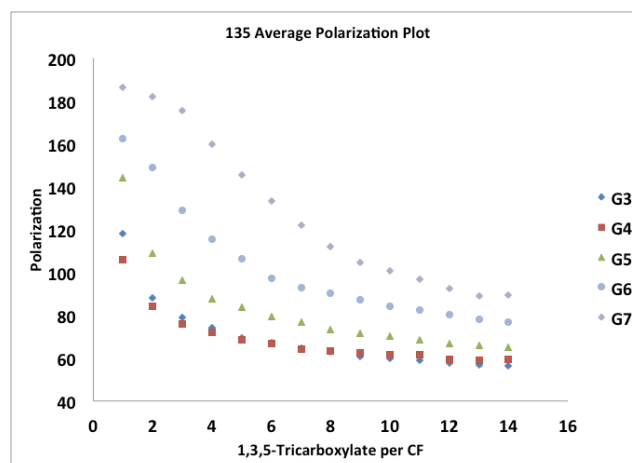


Figure 1.19 - Fluorescence Polarization Titration Isotherm of 1,3,5-Benzenetricarboxylate into the CF-Dendrimer System

While only one of these spectra could be used in our efforts to differentiate multiple biologically relevant anions, the plots support the idea that using both spectra rather than duplicating the same information can provide useful information in the discrimination of the target anions. While the intensity plots show a quick return of fluorescence, the polarization plots do not follow a simple increase, and each generation does not begin near the same point leading to differing changes in fluorescence polarization. In this study, we will continue to explore the use of both signals as a way to enhance our potential differentiation.

While we have proven that the 1,3,5-benzenetricarboxylate can displace the CF indicator from the dendrimers giving an optical signal change in both fluorescence and fluorescence anisotropy, we decided to test the system with our biologically relevant anions. Before patterning, we tested if these anions could also displace CF, but at different levels leading to potential differentiation. Furthermore, we hoped to see different proportions of displacement of CF depending on the generation of dendrimers in addition to the type of anion. So we conducted similar studies on five biological anions

that contain multiple anionic groups. The selected anions also contain many of the same head groups that might hamper differentiation in our assay, including: ATP, NADP, FAD, and TPP. Furthermore, the titrations were also carried out using folic acid (FA), which is a biological anion that contains anionic carboxylates rather than phosphates.

#### ***1.2.4.2 Titration of Adenine Triphosphate into Carboxyfluorescein Dendrimer Systems***

In our ATP study, we were able to see displacement of the indicator similar to that with the tricarboxylate, yet restoration of fluorescence occurred with fewer equivalents giving us hope that we would be able to pattern the anions of interest. The increased displacement of the CF indicator by ATP is likely due to increased local charge density in the phosphate tail of ATP from that of the carboxylate. While the charge density is high in the tail, the phosphate may also form a better array of hydrogen bonding and salt bridge partners with the amines of the dendrimers than the indicator, thus leading to

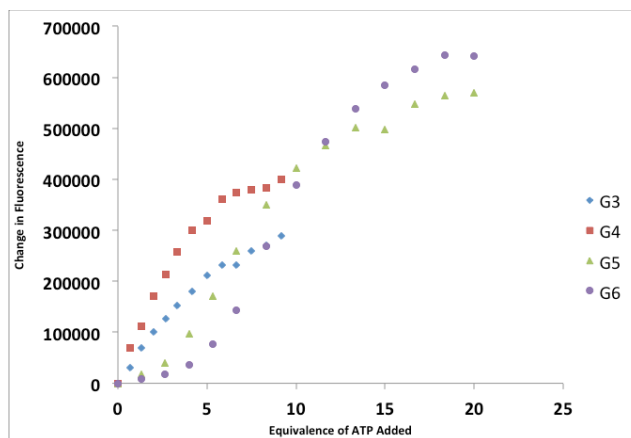


Figure 1.20 - Change in Fluorescence Intensity Titration Isotherm of Adenine Triphosphate into the CF-Dendrimer System



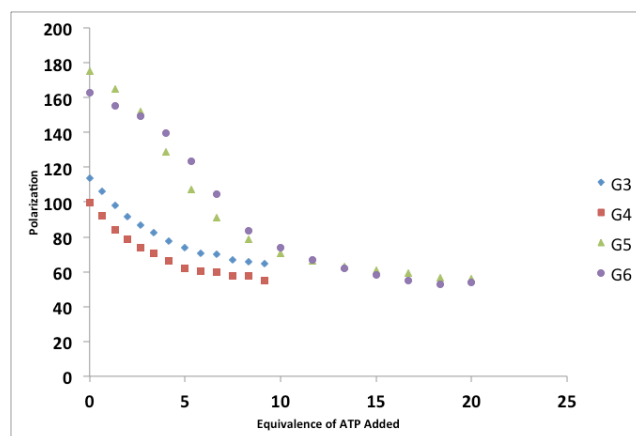


Figure 1.21 - Fluorescence Polarization Titration Isotherm of Adenine Triphosphate into the CF-Dendrimer System

increased displacement. Additionally, the polarization data showed some interesting trends in the larger generations. While G3 and G4 showed simple displacement curves, the larger generations G5-G7 showed a more sigmoidal displacement curve and started at a significantly higher initial polarization. The differences in the fluorescence intensity and fluorescence polarization will provide additional data for the differentiation of multiple anions. The studies with ATP proved that biological anions could displace CF, giving us evidence that the target anions can be patterned in water.

#### ***1.2.4.3 Titration of Nicotinamide Adenine Dinucleotide Phosphate into Carboxyfluorescein Dendrimer Systems***

If we want to be able to pattern the targeted anions, each needs to have different binding affinity and/or binding interactions, and thus we studied the binding curves for NADP to see if the anion gave a different binding isotherm than ATP. As can be seen in the Figures 1.22 and 1.23, the NADP binding isotherms from the fluorescence intensity and

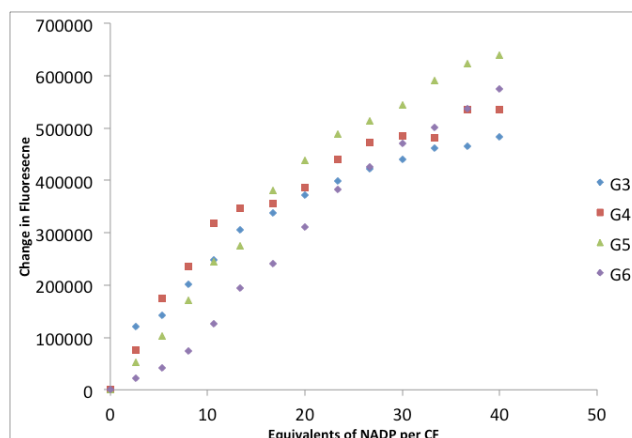


Figure 1.22 - Change in Fluorescence Intensity Titration Isotherm of Nicotinamide Adenine Dinucleotide Phosphate (NADP) into the CF-Dendrimer System

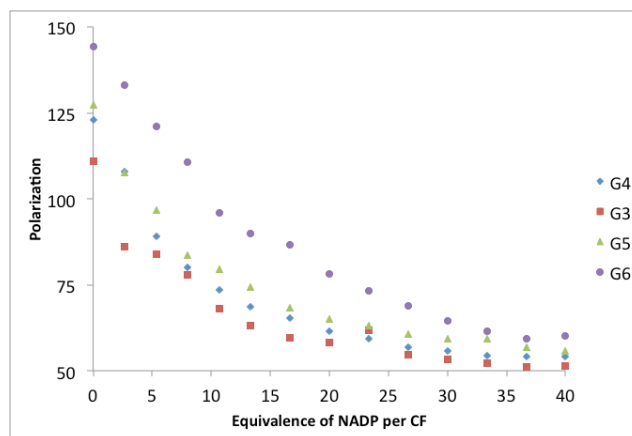


Figure 1.23 - Fluorescence Polarization Titration Isotherm of Nicotinamide Adenine Dinucleotide Phosphate (NADP) into the CF-Dendrimer System

the fluorescence polarization data are clearly different from those of ATP. In the graph, the G5 and G6 curves for NADP are significantly different from those generations with ATP. Furthermore, they require significantly more equivalents of anions to lead to the same level of indicator displacement as ATP. In the isotherm, a much more pronounced sigmoidal shape for the larger generations of dendrimers in both intensity and polarization data was observed. As can be seen by analyzing Figures 1.24 and 1.25, which overlays the two binding curves, there are substantial

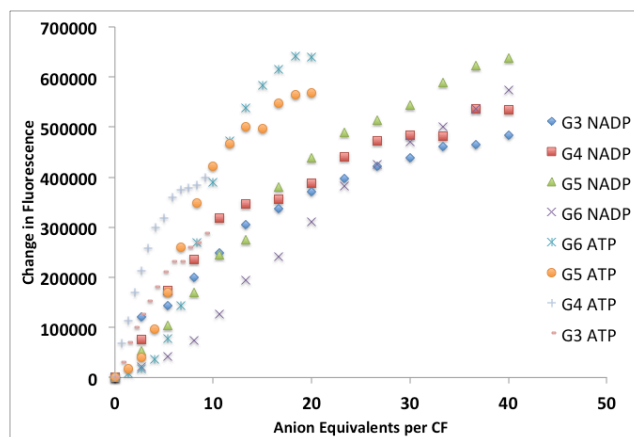


Figure 1.24 – Overlap of Fluorescence Intensity Titration Isotherms for ATP and NADP into CF-Dendrimer Complex

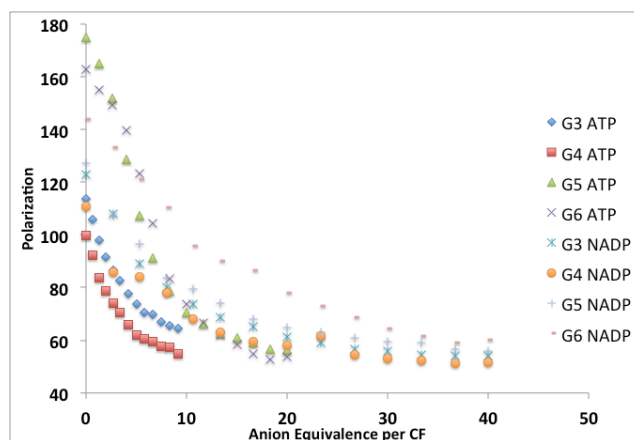


Figure 1.25 – Overlap of Fluorescence Polarization Titration Isotherms for ATP and NADP into CF-Dendrimer Complex

and significant differences in the isotherm giving evidence that the dendrimer systems and chemometrics will be able to differentiate our target anions.

#### 1.2.4.4 Titration of Flavin Adenine Dinucleotide into Carboxyfluorescein Dendrimer Systems

Flavin adenine dinucleotide (FAD) was also titrated into the dendrimer-CF complex. The titration of this anion showed a brief decrease in fluorescence intensity before an increase in fluorescence. In each generation, the

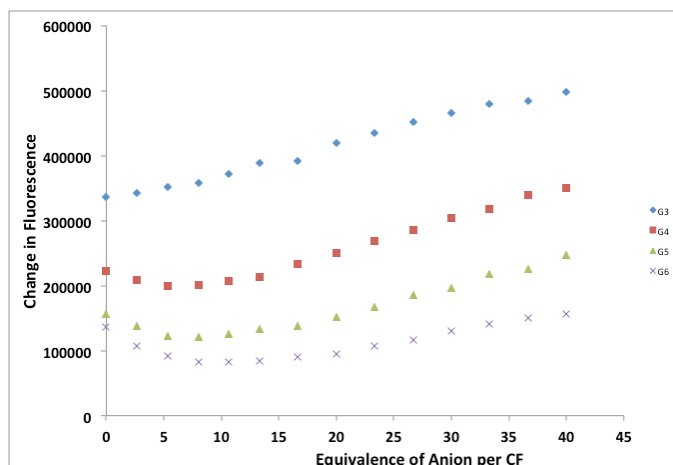


Figure 1.26 - Change in Fluorescence Intensity Titration Isotherm of Flavin Adenine Dinucleotide (FAD) into the CF-Dendrimer System

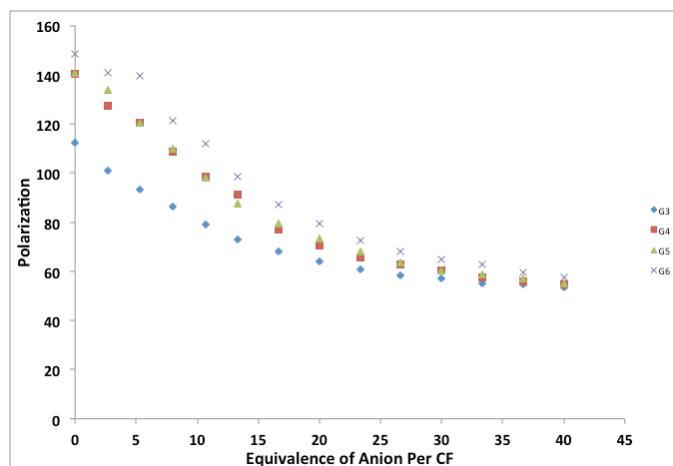


Figure 1.27 - Fluorescence Polarization Titration Isotherm of Flavin Adenine Dinucleotide (FAD) into the CF-Dendrimer System

titration did not show full return of the fluorescence, but the sigmoidal pattern of the intensity is different from the titrations shown by the other anions. The initial decrease in fluorescence is likely due to quenching from the anion with the CF on the dendrimer. Furthermore, the absorbance of this anion shows a linear increase at approximately 500 nm with the absorbance of the anion contributing to this increase. Having an absorbance spectra in the visible region are not characteristic of the other anions making this anion, which absorbs near 500 nm, unique in the set tested. Additionally, the polarization of the CF in the titration shows a more traditional displacement curve with the G4 and G5 showing almost identical displacement isotherms. The G6 displacement isotherm displays some sigmoidal shape. The four generations show unique starting points for the polarization, which gives the FAD anion a unique pattern supporting the idea that the anions will be distinguishable via chemometric techniques.

#### ***1.2.4.5 Titration of Thiamine Pyrophosphate into Carboxyfluorescein Dendrimer Systems***

The next anion titrated into the system was thiamine pyrophosphate (TPP). This anion has a unique characteristic that the thiazolium ring is both cationic and able to generate a ylide complex through the deprotonation of the ring to form an anionic carbon at relatively low pH. Despite the pyrophosphate chain, the thiazolium ring limits the anionic character of this anion. In the titration of this anion, the fluorescence

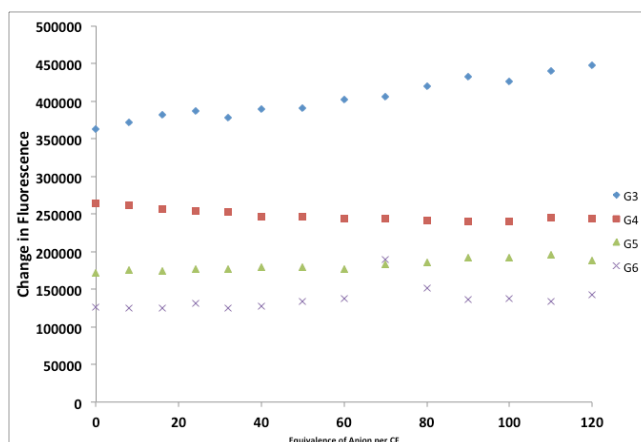


Figure 1.28 - Change in Fluorescence Intensity Titration Isotherm of Thiamine Pyrophosphate (TPP) into the CF-Dendrimer System

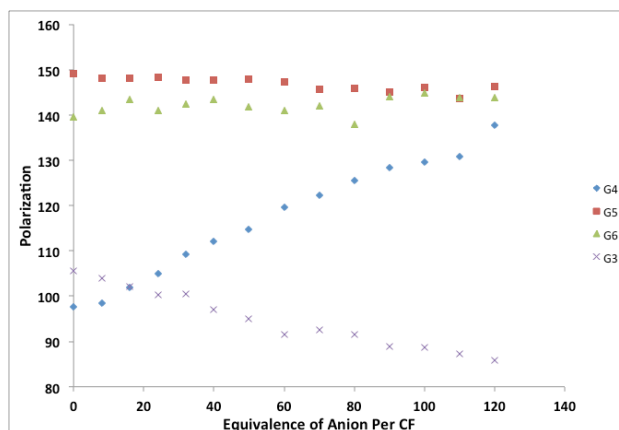


Figure 1.29 - Fluorescence Polarization Titration Isotherm of Thiamine Pyrophosphate (TPP) into the CF-Dendrimer System

intensity and the anisotropy shows little change even with over 120 equivalents of anion introduced. The charge density was not sufficient to lead to the displacement of the anionic indicator. The smaller generations show a change of approximately 30% in the anisotropy values after the addition of 120 equivalents of anion, but the larger generations show effectively no change in the polarization. Furthermore, the G4 polarization showed a unique isotherm in which the polarization increased. The increase with this generation

is unprecedented with the various anions studied and could be an outlier. But given that we were only looking to see if there was a unique pattern, the plot was not reproduced. While the titration could be an outlier, it is also possible that with this particular system the TPP drives the CF to bind more tightly to the dendrimer. Overall, the lack of significant change in the signals supports the idea that the anion shows a binding weaker than CF giving only small signal modulation. Because this anion only binds weakly to the dendrimer, the isotherms obtained are distinct from those obtained with the other anions and showed a small amount of binding, and the anion was left in the screening.

#### ***1.2.4.6 Titration of Folic Acid into Carboxyfluorescein Dendrimer Systems***

The folic acid anion was the final titration of an anion performed using the CF and dendrimer system. Unlike the other biological anions, this anion contains only carboxylates rather than phosphates. The titrations of the anion showed increases in fluorescence when the anion is added into the solution. While G3 and G4 dendrimers showed increases in fluorescence intensity at low equivalents of anions the larger generations of dendrimer G5 and G6 again showed a brief decrease in fluorescence before starting to increase. In this case, the

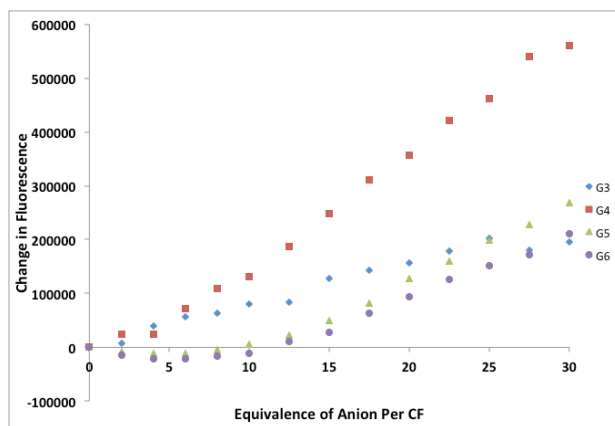


Figure 1.30 - Change in Fluorescence Intensity Titration Isotherm of Folic Acid into the CF-Dendrimer System

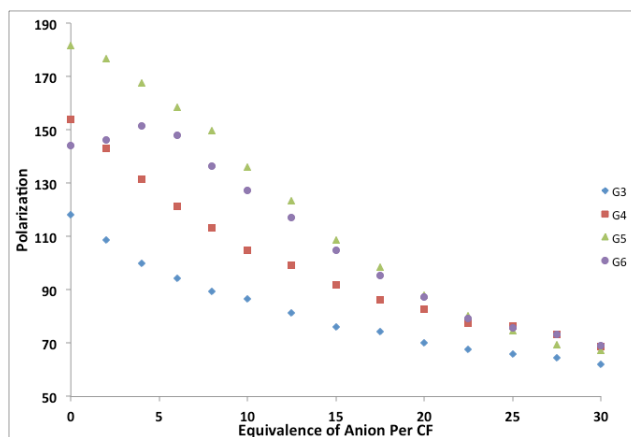


Figure 1.31 - Fluorescence Polarization Titration Isotherm of Folic Acid into the CF-Dendrimer System

binding of folic acid leads to the quenching of the fluorophore as the indicator can likely interact through the  $\pi$ - $\pi$  stacking of the fluorophore and the anion at the lower anion ratios. Additionally, the amines in folic acid can cause additional PET quenching. Furthermore, the polarization shows a marked decrease with each generation reaching approximately the same polarization value. Again, these values are distinct from those obtained with the other anions and make the differentiation of the target anions appear



probable. Upon reviewing all of our anion titration isotherms for all five generations, we believe that multiple dendrimers be used for our intended purposes.

### **1.3 ANION PATTERNING**

#### **1.3.1 Generation of Array and Chemometric Analysis**

Each of the patterning studies was carried out with five different generations of dendrimers. The exact procedure of the studies is described in the experimental methods sections later in this chapter. Patterning with each generation of dendrimer was carried out on its own individual plate to prevent misclassification based upon generation rather than anion identity. In each plate, the displacement of the CF indicator from the dendrimer to the following nine biologic anions (Adenine Triphosphate, Adenine Diphosphate, Adenine Monophosphate, Thiamine Pyrophosphate, Flavin Adenine Dinucleotide, Folic Acid, Nicotinamide Adenine Dinucleotide reduced and oxidized forms, and Nicotinamide Adenine Dinucleotide Phosphate reduced and oxidized form) and three carboxylate anions (1,3,5-Benzenetricarboxylate, 1,3,4-Benzenetricarboxylate, and 1,2,3-Benzenetricarboxylate) were measured. Each plate contained a unique ratio of CF indicator and dendrimer based upon the generation along with a fixed amount of each anion. The plates were read on a 96 well plate reader giving a fluorescence intensity and polarization reading as well as a UV/Vis spectrum from 460-510 nm. The intensity, polarization and UV/Vis absorbance at 495 nm were entered into XLStat and used to produce a linear discriminate assay (LDA) and principle component analysis (PCA) plot. As can be seen, each of the anions is separated, but

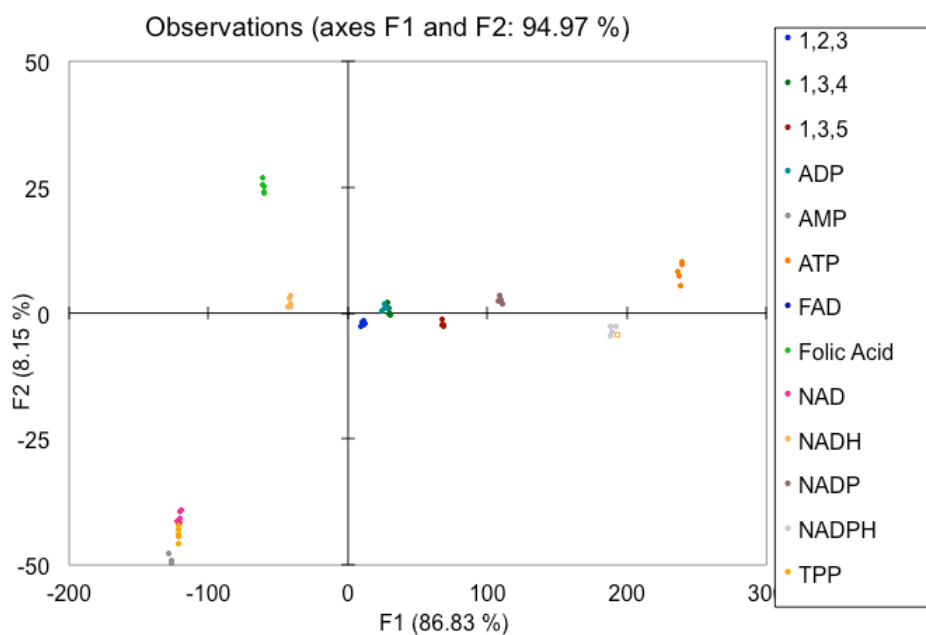


Figure 1.32 – LDA Plot of All Anions Used in Carboxyfluorescein-Dendrimer System

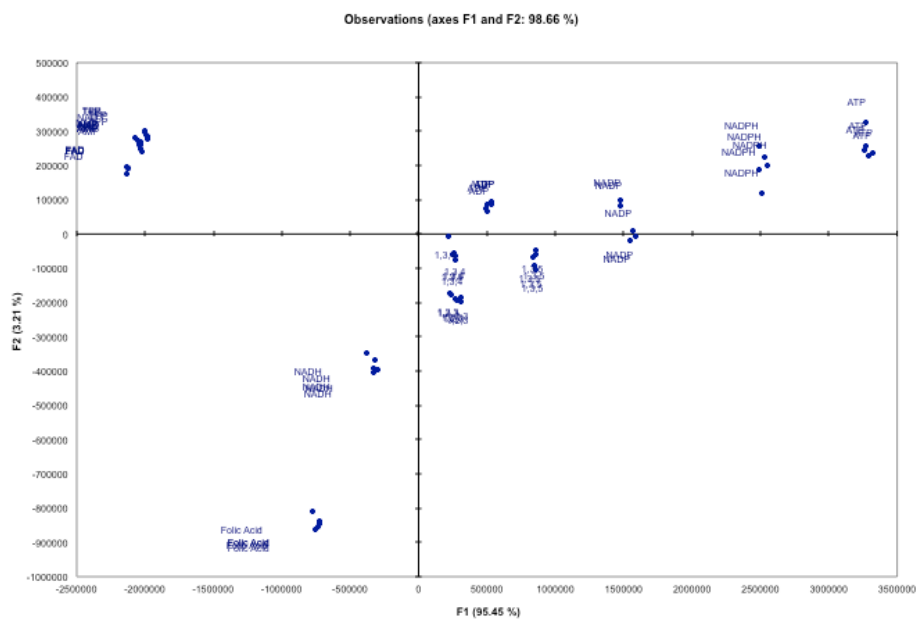


Figure 1.33 – PCA Plot of All Anions Used in Carboxyfluorescein-Dendrimer System with Generations 4-7 Dendrimer

some of the weaker binders cluster very close together. Additionally, the anions themselves are relatively tightly clustered together. The jack knife analysis showed a 100 % classification of each anion when running the validation analysis. The jack knife analysis is a leave one out analysis, that tests the ability of the plot to identify an unknown analyte. While the LDA plot of those weak binding analytes show tight clustering, the jack knife analysis shows they can be cleanly differentiated from one another. Furthermore, the FAD anion was clearly differentiated, but that is likely due to the increased absorbance of the FAD anion in the same region as the CF indicator. Furthermore, the PCA plot that was generated was very similar to the LDA plot but did not cluster or show as much differentiation along the F2 axis as the LDA plot. For all future plots, we limited our analysis to using the LDA technique as it gave tighter clustering. An additional

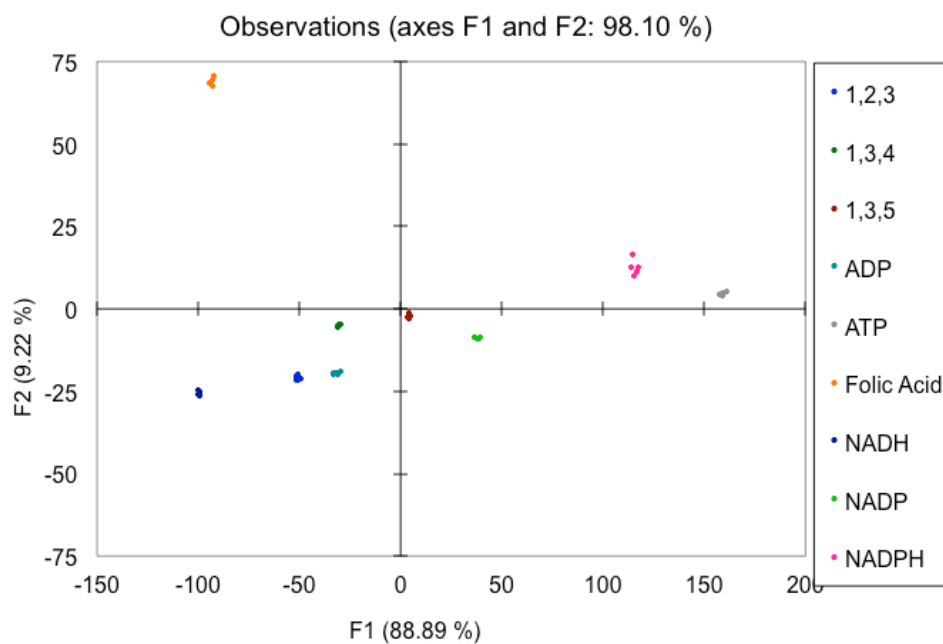


Figure 1.34 – LDA Plot of All Anions Used in Carboxyfluorescein-Dendrimer System Which Displaced CF

LDA plot was generated which excluded the weak binders and FAD to allow for the maximum amount of differentiation of those anions that bind the dendrimers, but even the plot with all anions showed 100% discrimination. The additional plot was only generated to test the ability to statistically increase the differentiation between the anions.

The F1 axis in the plot describes the factor that represents the primary variance between all of the anions appears to be directly related to the binding ability of the anion to the cationic dendrimers. While there is some correlation with

| Anion   | Net Charge | Location on LDA (L to R) |
|---|------------|--------------------------|
| Flavin Adenine Dinucleotide                           | 2          | 1                        |
| Adenosine Monophosphate                               | 2          | 2                        |
| Thiamine Pyrophosphate                                | 2          | 3                        |
| Nicotinamide Adenine Dinucleotide, Oxidized           | 1          | 4                        |
| Folic Acid  | 2          | 5                        |
| Nicotinamide Adenine Dinucleotide, Reduced            | 2          | 6                        |
| 1,2,3-Benzenetricarboxylate                           | 3          | 7                        |
| Adenosine Diphosphate                                 | 3          | 8                        |
| 1,3,4-Benzenetricarboxylate                           | 3          | 9                        |
| 1,3,5-Benzenetricarboxylate                           | 3          | 10                       |
| Nicotinamide Adenine Dinucleotide Phosphate, Oxidized | 3          | 11                       |
| Nicotinamide Adenine Dinucleotide Phosphate, Reduced  | 4          | 12                       |
| Adenosine Triphosphate                                | 4          | 13                       |

Table 1.4 - Anions with total charge versus position on the F1 axis of the LDA chart

the number of charges on each anionic molecule, this factor axis is not always related specifically to the number of charges. As can be seen in the table, the total number of charges is mostly related to the location of the anion on the F1 axis. As such, the locations of anions are important in the patterning, but the different generations of dendrimers themselves do not seem to have much cross reactive ability other than total number of charges that they carry. The larger generations of dendrimers (G5-G7) do seem to have different reactivity than the smaller generations of dendrimers (G3-G4). The larger generations have a more ordered structure that with a stronger and more defined secondary structure, and thus can have other types of interactions other than electrostatic interactions, like hydrophobic interactions. These small differences most likely account for some of the differentiation along the F2 axis, but it is difficult to assign the specific origins of the F2 axis.

### 1.3.2 Regioisomer of Tricarboxylatebenzene Analysis

The carboxylate derivatives are a case where charge alone cannot be the primary mode of differentiation. Using the patterning plates, the three possible regioisomers of a

tricarboxylatebenzene, a 1,3,5, a 1,2,3 and a 1,2,4 regioisomer, were studied with the fluorophore dendrimer system. Each of these isomers contain the exact same number of charges and vary only in the location of the charges, making them an interesting study for determining if the dendrimers can differentiate anions based upon regiochemistry. As can be seen in the figure, each of

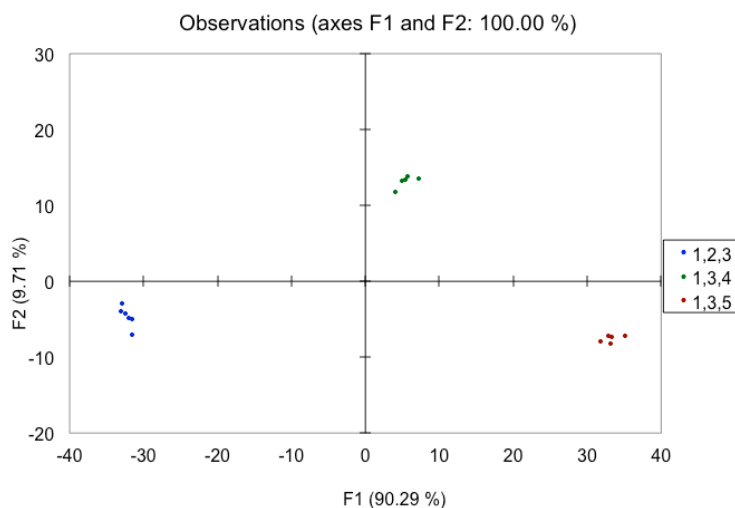


Figure 1.35 – LDA Plot of All Tricarboxylates Used in Carboxyfluorescein-Dendrimer System

these regioisomers are clearly discriminated from the other leading to the idea that the location and order of anion placement are both important to binding. The location of the anions in some of the tricarboxylates likely forms tighter salt bridges or hydrogen bond networks with the dendrimer leading to increased displacement of the CF indicator from the dendrimer. Based upon the raw data, the all meta arrangement of the 1,3,5 regioisomer appears to form the best contacts with the amines on the dendrimer. These studies prove that more than anionic character helps to differentiate the cofactors and

organic anions, thus supporting the idea that the F2 axis shows the location of the charges and not just the number of charges.

#### **1.4 CONCLUSIONS**

Our results show that the different anions in aqueous solution can be discriminated at a fixed concentration with only 50  $\mu\text{M}$  of the target anion using a set of dendrimer and carboxyfluorescein systems. While the primary differentiating factor was the number of charges, there was some differentiation based upon the location and regioisomerization of those charges. The biological anions and a set of organic triacids were clearly differentiated based upon the regioisomers of the triacids using this CF-dendrimer complex.

In this chapter, a system using a commercially available indicator CF and scaffold G3-G7 AT-PAMAM dendrimers is described that gives separation among several biologically relevant anions in water at micromolar concentration and at physiological pH. In addition to the biological anions, the system is able to differentiate the regioisomers of a commercially available organic trianion. The system has sensitivity for anions into the low micromolar level with full differentiation of all anions independent of the other anions. In this report, we have shown that using the polycationic generations of dendrimers' differentiation is obtainable based upon both charge density and regioisomer, and this chapter highlights a system created completely from commercially available receptors that work in biological-like conditions.

#### **1.5 FUTURE DIRECTIONS**

While the system shows complete discrimination among the major anion cofactors used, a larger screening of biologic anions should be undertaken to determine if a larger sample can be distinguished. Particular emphasis should be placed on the

differentiation of nucleobases. Since the primary interactions are through electrostatics, this differentiation is unlikely but should be undertaken. The differentiation could be improved by adding other binding moieties through other complementary functionalities to the dendrimer. Furthermore, tests with mixtures of different anions would be an interesting test of the system's potential real world applications. Finally, the dendrimer-indicator system could be expanded through the use of different anionic indicators or other additives that could help to further enhance the differentiation of the anions.

## **1.6 EXPERIMENTAL METHODS**

The G3-G7 PAMAM dendrimers (MeOH solutions) and 5(6)-carboxyfluorescein were purchased from Sigma-Aldrich and used as received. 4-(2-hydroxyethyl)-1-piperazineethanesulfonic acid (HEPES) was purchased from Fisher Scientific and used to create the buffer solution without further purification. All biological anions were purchased from Chem-Impex International except for folic acid, which was purchased from Sigma Aldrich. Pyromellitic acid and 1,3,5-benzenetricarboxylate was purchased from Sigma Aldrich, while 1,2,3-benzenetricarboxylate and 1,3,4-benzenetricarboxylate were purchased from AK Scientific. A 50 mM HEPES buffer was prepared using millipure water from a Siemens purification system, and the pH was adjusted to 7.4 using aqueous solutions of NaOH and HCl. While the purity of the water should contain only trace amounts of metal ions which do not effect the charge on the cofactors, the millipure water was not tested for the presence of metal cations. The buffer was then degassed via sonication and filtered through filter paper to remove particulates. All solutions were made using this buffer.

All spectroscopic readings was carried out using a BioTek Synergy 2 Multi-mode Microplate reader. 96-well plates with black plate and an optically clear plastic bottom



purchased from Fisher Scientific were used to allow for simultaneous UV/Vis and fluorescence detection. Each plate contained a 2  $\mu\text{M}$  CF solution without dendrimer which was used to reference the instrument and to measure plate to plate reproducibility. The fluorescence was referenced to the 2  $\mu\text{M}$  CF as high wells making them the maximum intensity recorded in each fluorescence read. Each well was repeated in at least triplicate on the same plate to reduce random error.

Before studying the interaction with anions, the PAMAM dendrimers were titrated into a constant concentration of the CF indicator. In previous work, a maximum loading value of CF to the dendrimer has been obtained. The inflection point obtained where the addition of more dendrimer to CF no longer caused a decrease in the fluorescence intensity was used for all anion displacement and patterning studies.

Using a set ratio of dendrimer to CF, shown in the table, different anions were titrated into the solution to test the signal modulation of the CF based upon the addition of the target anions. The introduction of anions caused the fluorescence intensity of CF to increase and the fluorescence anisotropy to decrease until both measurements approximated free CF in solution or reached a level in which it was believed that full displacement would not occur.

Furthermore, fluorescence anisotropy was probed as a method which could alone be used to identify the target anions. Again, the fixed ratio of dendrimer to CF was used and the anions introduced in increasing aliquots. Modulation of the anisotropy signal as well as a change in fluorescence intensity were observed and plotted against the concentration of the anion.

In the patterning studies, a set amount (50  $\mu\text{M}$ ) of each anion was placed in a well with the predetermined ratio of dendrimer and CF indicator with five different replicates of each set of anions. Each generation of dendrimer was used on its own plate to prevent

plate-to-plate variations within a generation from being detected when conducting the chemometric techniques.

The chemometric calculations were conducted in Microsoft Excel 2007 with Alladinsoft's XLSTAT software.

## 1.7 REFERENCES

- (1) Buhleier, E.; Wehner, W.; Vogtle, F. "Cascade" and 'Nonskid-Chain-Like; Synthesis of Molecular Cavity Topologies. *Synthesis* **1978**, 155–58.
- (2) Newkome, G. R.; Yao, Z.; Baker, G. R.; Gupta, V. K. Micelles. Part 1. Cascade molecules: a new approach to micelles. A [27]-arborol. *The Journal of Organic Chemistry* **1985**, *50*, 2003–2004.
- (3) Tomalia, D. A.; Baker, H.; Dewald, J.; Hall, M.; Kallos, G.; Martin, S.; Roeck, J.; Ryder, J.; Smith, P. A New Class of Polymers: Starburst-Dendritic Macromolecules. *Polymer Journal* **1985**, *17*, 117–132.
- (4) Hawker, C. J.; Frechet, J. M. J. Preparation of polymers with controlled molecular architecture. A new convergent approach to dendritic macromolecules. *Journal of the American Chemical Society* **1990**, *112*, 7638–7647.
- (5) Frechet, J. M.; Tomalia, D. A. *Dendrimer and other Dendritic Polymers*; Wiley, 2001.
- (6) Newkome, G. R.; Kotta, K. K.; Moorefield, C. N. Convenient Synthesis of 1 → 3 C-Branched Dendrons. *The Journal of Organic Chemistry* **2005**, *70*, 4893–4896
- (7) Inc, D. Dendritech <http://www.dendritech.com/pamam.html> (accessed Nov 9, 2012).
- (8) Challa, T.; Goud, B. A.; Baskar, S.; Chandra Mouli, G.; Jukuri, R. DENDRIMERS: A NOVEL POLYMER FOR DRUG DELIVERY. *International Journal of Pharmaceutical Sciences Review & Research* **2011**, *9*, 88–99.
- (9) Sun, M.; Fan, A.; Wang, Z.; Zhao, Y. Dendrimer-mediated drug delivery to the skin. *Soft Matter* **2012**, *8*, 4301–4305.

- (10) Mullen, D. G.; Fang, M.; Desai, A.; Baker, J. R.; Orr, B. G.; Banaszak Holl, M. M. A Quantitative Assessment of Nanoparticle–Ligand Distributions: Implications for Targeted Drug and Imaging Delivery in Dendrimer Conjugates. *ACS Nano* **2010**, *4*, 657–670
- (11) Willerich, I.; Ritter, H.; Gröhn, F. Structure and Thermodynamics of Ionic Dendrimer–Dye Assemblies. *The Journal of Physical Chemistry B* **2009**, *113*, 3339–3354 ST – Structure and Thermodynamics of Io.
- (12) Bonizzoni, M.; Long, S. R.; Rainwater, C.; Anslyn, E. V. PAMAM dendrimer-induced aggregation of 5(6)-carboxyfluorescein. *The Journal of organic chemistry* **2012**, *77*, 1258–1266.
- (13) Rainwater, J. C.; Anslyn, E. V. Amino-terminated PAMAM dendrimers electrostatically uptake numerous anionic indicators. *Chem. Commun. (Cambridge, U. K.)* **2010**, *46*, 2904–2906
- (14) Niu, Y.; Sun, L.; Crooks, R. M. Determination of the Intrinsic Proton Binding Constants for Poly(amidoamine) Dendrimers via Potentiometric pH Titration. *Macromolecules* **2003**, *36*, 5725–5731.
- (15) Zeng, F.; Zimmerman, S. C. Dendrimers in Supramolecular Chemistry: From Molecular Recognition to Self-Assembly. *Chemical Reviews* **1997**, *97*, 1681–1712.
- (16) Gradinaru, C. C.; Marushchak, D. O.; Samim, M.; Krull, U. J. Fluorescence anisotropy: from single molecules to live cells. *Analyst* **2010**, *135*, 452–459.
- (17) Yang, W.; Li, Y.; Cheng, Y.; Wu, Q.; Wen, L.; Xu, T. Evaluation of phenylbutazone and poly(amidoamine) dendrimers interactions by a combination of solubility, 2D-NOESY NMR, and isothermal titration calorimetry studies. *Journal of Pharmaceutical Sciences* **2009**, *98*, 1075–1085.
- (18) Voet, D.; Voet, J. G.; Pratt, C. 2006 *Fundamentals of biochemistry : life at the molecular level*; Wiley: Hoboken, N.J. ET - 2nd, 2006.
- (19) Channon, K. Tetrahydrobiopterin: Regulator of Endothelial Nitric Oxide Synthase in Vascular Disease. *Trends in Cardiovascular Medicine* **2004**, *14*, 323–327.

- (20) Bates, G. W.; Triyanti; Light, M. E.; Albrecht, M.; Gale, P. A. 2,7-Functionalized Indoles as Receptors for Anions. *J. Org. Chem.* **2007**, *72*, 8921–8927 ST – 2,7-Functionalized Indoles as Receptors for Anions.
- (21) Ali, H. D. P.; Kruger, P. E.; Gunnlaugsson, T. Colorimetric “naked-eye” and fluorescent sensors for anions based on amidourea functionalised 1,8-naphthalimide structures: anion recognition via either deprotonation or hydrogen bonding in DMSO. *New Journal of Chemistry* **2008**, *32*, 1153–1161
- (22) dos Santos, C. M. G.; McCabe, T.; Watson, G. W.; Kruger, P. E.; Gunnlaugsson, T. The Recognition and Sensing of Anions through , "Positive Allosteric Effects," Using Simple Urea-Amide Receptors. *The Journal of Organic Chemistry* **2008**, *73*, 9235–9244
- (23) Veale, E. B.; Gunnlaugsson, T. Bidirectional Photoinduced Electron-Transfer Quenching Is Observed in 4-Amino-1,8-naphthalimide-Based Fluorescent Anion Sensors. *The Journal of Organic Chemistry* **2008**, *73*, 8073–8076
- (24) Sessler, J. L.; Cho, D.-G.; Lynch, V. Diindolylquinoxalines: An Effective Indole-Based Receptors for Phosphate Anion. *Journal of the American Chemical Society* **2006**, *128*, 16518–16519
- (25) Gong, H.-Y.; Rambo, B. M.; Karnas, E.; Lynch, V. M.; Keller, K. M.; Sessler, J. L. Environmentally Responsive Threading, Dethreading, and Fixation of Anion-Induced Pseudorotaxanes. *Journal of the American Chemical Society* **2011**, *133*, 1526–1533
- (26) Yoo, J.; Kim, M.-S.; Hong, S.-J.; Sessler, J. L.; Lee, C.-H. Selective Sensing of Anions with Calix[4]pyrroles Strapped with Chromogenic Dipyrrolylquinoxalines. *The Journal of Organic Chemistry* **2008**, *74*, 1065–1069
- (27) Lee, M. H.; Cao, Q.-Y.; Kim, S. K.; Sessler, J. L.; Kim, J. S. Anion Responsive TTF-Appended Calix[4]arenes. Synthesis and Study of Two Different Conformers. *The Journal of Organic Chemistry* **2010**, *76*, 870–874
- (28) Guha, S.; Saha, S. Fluoride Ion Sensing by an Anion- $\pi$  Interaction. *Journal of the American Chemical Society* **2010**, *132*, 17674–17677
- (29) Cormode, D. P.; Evans, A. J.; Davis, J. J.; Beer, P. D. Amplification of anion sensing by disulfide functionalized ferrocene and ferrocene-calixarene

- receptors adsorbed onto gold surfaces. *Dalton Transactions* **2010**, *39*, 6532–6541
- (30) Swinburne, A. N.; Paterson, M. J.; Beeby, A.; Steed, J. W. Fluorescent “Twist-on” Sensing by Induced-Fit Anion Stabilisation of a Planar Chromophore. *Chemistry – A European Journal* **2010**, *16*, 2714–2718
- (31) Amendola, V.; Fabbri, L.; Mosca, L. Anion recognition by hydrogen bonding: urea-based receptors. *Chemical Society Reviews* **2010**, *39*, 3889–3915.
- (32) Schiller, A.; Vilozy, B.; Wessling, R. A.; Singaram, B. Recognition of phospho sugars and nucleotides with an array of boronic acid appended bipyridinium salts. *Analytica Chimica Acta* **2008**, *627*, 203–211.
- (33) Palacios, M. A.; Nishiyabu, R.; Marquez, M.; Anzenbacher, P. Supramolecular Chemistry Approach to the Design of a High-Resolution Sensor Array for Multianion Detection in Water. *Journal of the American Chemical Society* **2007**, *129*, 7538–7544
- (34) Wang, Z.; Palacios, M. A.; Zyryanov, G.; Anzenbacher, P. Harnessing a Ratiometric Fluorescence Output from a Sensor Array. *Chemistry – A European Journal* **2008**, *14*, 8540–8546
- (35) Ojida, A.; Nanaka, H.; Miyahara, Y.; Tamaru, S.; Sada, K.; Hamachi, I. Bis(Dpa-ZnII) appended xanthone: excitation ratiometric chemosensor for phosphate anions. *Angew. Chem., Int. Ed.* **2006**, *45*, 5518–5521
- (36) Cano, M.; Rodríguez, L.; Lima, J. C.; Pina, F.; Dalla Cort, A.; Pasquini, C.; Schiaffino, L. Specific Supramolecular Interactions between Zn<sup>2+</sup>-Salophen Complexes and Biologically Relevant Anions. *Inorganic Chemistry* **2009**, *48*, 6229–6235.
- (37) Schaeferling, M.; Wolfbeis, O. S. Europium tetracycline as a luminescent probe for nucleoside phosphates and its application to the determination of kinase activity. *Chem.–Eur. J.* **2007**, *13*, 4342–4349
- (38) McCleskey, S. C.; Griffin, M. J.; Schneider, S. E.; McDevitt, J. T.; Anslyn, E. V. Differential Receptors Create Patterns Diagnostic for ATP and GTP. *Journal of the American Chemical Society* **2003**, *125*, 1114–1115

- (39) Hargrove, A. E.; Nieto, S.; Zhang, T.; Sessler, J. L.; Anslyn, E. V. Artificial Receptors for the Recognition of Phosphorylated Molecules. *Chemical Reviews* **2011**, *111*, 6603–6782
- (40) Ojida, A.; Mito-oka, Y.; Sada, K.; Hamachi, I. Molecular Recognition and Fluorescence Sensing of Monophosphorylated Peptides in Aqueous Solution by Bis(zinc(II)-dipicolylamine)-Based Artificial Receptors. *Journal of the American Chemical Society* **2004**, *126*, 2454–2463
- (41) Ojida, A.; Miyahara, Y.; Wongkongkatep, J.; Tamaru, S.; Sada, K.; Hamachi, I. Design of dual-emission chemosensors for ratiometric detection of ATP derivatives. *Chem.-Asian J.* **2006**, *1*, 555–563
- (42) Fenniri, H.; Hosseini, M. W.; Lehn, J.-M. Molecular Recognition of NADP(H) and ATP by Macrocyclic Polyamines Bearing Acridine Groups. *Helvetica Chimica Acta* **1997**, *80*, 786–803
- (43) Domenech, A.; Garcia-Espana, E.; Ramirez, J.; Celda, B.; Carmen Martinez, M.; Monleon, D.; Tejero, R.; Bencini, A.; Bianchi, A. A thermodynamic, electrochemical and molecular dynamics study on NAD and NADP recognition by 1,4,7,10,13,16,19-heptaazacycloheptacosane ([21]aneN7) [dagger]. *Journal of the Chemical Society, Perkin Transactions 2* **1999**, 23–32
- (44) Schmidtchen, F. P. Macrocyclic quaternary ammonium salts. II. Formation of inclusion complexes with anions in solution. *Chem. Ber.* **1981**, *114*, 597–607
- (45) Fokkens, M.; Jasper, C.; Schrader, T.; Koziol, F.; Ochsenfeld, C.; Polkowska, J.; Lobert, M.; Kahlert, B.; Klarner, F.-G. Selective complexation of N-alkylpyridinium salts: binding of NAD<sup>+</sup> in water. *Chemistry* **2005**, *11*, 477–94
- (46) Yano, Y.; Tamura, N.; Mitsui, K.; Nabeshima, T. A flavin receptor. Effect of 2,6-diaminopyridine derivatives on the reduction of benzodipteridine (oxidation-active flavin model). *Chem. Lett.* **1989**, 1655–8
- (47) Ariga, K.; Kamino, A.; Koyano, H.; Kunitake, T. Recognition of aqueous flavin mononucleotide on the surface of binary monolayers of guanidinium and melamine amphiphiles. *Journal of Materials Chemistry* **1997**, *7*, 1155–1161
- (48) Breinlinger, E. C.; Keenan, C. J.; Rotello, V. M. Modulation of Flavin Recognition and Redox Properties through Donor Atom Interactions. *Journal of the American Chemical Society* **1998**, *120*, 8606–8609

- (49) Deans, R.; Niemz, A.; Breinlinger, E. C.; Rotello, V. M. Electrochemical Control of Recognition Processes. A Three-Component Molecular Switch. *Journal of the American Chemical Society* **1997**, *119*, 10863–10864
- (50) Boal, A. K.; Rotello, V. M. Redox-Modulated Recognition of Flavin by Functionalized Gold Nanoparticles. *Journal of the American Chemical Society* **1999**, *121*, 4914–4915
- (51) Breinlinger, E. C.; Rotello, V. M. Model Systems for Flavoenzyme Activity. Modulation of Flavin Redox Potentials through  $\pi$ -Stacking Interactions. *Journal of the American Chemical Society* **1997**, *119*, 1165–1166
- (52) König, B.; Pelka, M.; Zieg, H.; Ritter, T.; Bouas-Laurent, H.; Bonneau, R.; Desvergne, J.-P. Photoinduced Electron Transfer in a Phenothiazine-Riboflavin Dyad Assembled by Zinc-Imide Coordination in Water. *Journal of the American Chemical Society* **1999**, *121*, 1681–1687
- (53) Roychowdhury-Saha, M.; Lato, S. M.; Shank, E. D.; Burke, D. H. Flavin Recognition by an RNA Aptamer Targeted toward FAD. *Biochemistry* **2002**, *41*, 2492–2499
- (54) Rhee, H.-W.; Choi, H.-Y.; Han, K.; Hong, J.-I. Selective Fluorescent Detection of Flavin Adenine Dinucleotide in Human Eosinophils by Using Bis(Zn<sup>2+</sup>-Dipicolylamine) Complex. *Journal of the American Chemical Society* **2007**, *129*, 4524–4525
- (55) Giannattasio, S.; Gagliardi, S.; Samaja, M.; Marra, E. Simultaneous determination of purine nucleotides, their metabolites and Beta-nicotinamide adenine dinucleotide in cerebellar granule cells by ion-pair high performance liquid chromatography. *Brain Res. Protoc.* **2003**, *10*, 168–174
- (56) Britz-McKibbin, P.; Markuszewski, M. J.; Iyanagi, T.; Matsuda, K.; Nishioka, T.; Terabe, S. Picomolar analysis of flavins in biological samples by dynamic pH junction-sweeping capillary electrophoresis with laser-induced fluorescence detection. *Analytical Biochemistry* **2003**, *313*, 89–96
- (57) Mohler, R. E.; Tu, B. P.; Dombek, K. M.; Hoggard, J. C.; Young, E. T.; Synovec, R. E. Identification and evaluation of cycling yeast metabolites in two-dimensional comprehensive gas chromatography-time-of-flight-mass spectrometry data. *J. Chromatogr., A* **2008**, *1186*, 401–411

- (58) Cordell, R. L.; Hill, S. J.; Ortori, C. A.; Barrett, D. A. Quantitative profiling of nucleotides and related phosphate-containing metabolites in cultured mammalian cells by liquid chromatography tandem electrospray mass spectrometry. *J. Chromatogr., B: Anal. Technol. Biomed. Life Sci.* **2008**, *871*, 115–124
- (59) Yang, S.; Sadilek, M.; Lidstrom, M. E. Streamlined pentafluorophenylpropyl column liquid chromatography-tandem quadrupole mass spectrometry and global <sup>13</sup>C-labeled internal standards improve performance for quantitative metabolomics in bacteria. *J. Chromatogr., A* **2010**, *1217*, 7401–7410
- (60) Pabst, M.; Grass, J.; Fischl, R.; Leonard, R.; Jin, C.; Hinterkorn, G.; Borth, N.; Altmann, F. Nucleotide and Nucleotide Sugar Analysis by Liquid Chromatography-Electrospray Ionization-Mass Spectrometry on Surface-Conditioned Porous Graphitic Carbon. *Anal. Chem. (Washington, DC, U. S.)* **2010**, *82*, 9782–9788.
- (61) Bolin, C.; Cardozo-Pelaez, F. Assessing biomarkers of oxidative stress: Analysis of guanosine and oxidized guanosine nucleotide triphosphates by high performance liquid chromatography with electrochemical detection. *J. Chromatogr., B: Anal. Technol. Biomed. Life Sci.* **2007**, *856*, 121–130
- (62) Edwards, N. Y.; Sager, T. W.; McDevitt, J. T.; Anslyn, E. V. Boronic Acid Based Peptidic Receptors for Pattern-Based Saccharide Sensing in Neutral Aqueous Media, an Application in Real-Life Samples. *Journal of the American Chemical Society* **2007**, *129*, 13575–13583
- (63) Wiskur, S. L.; Anslyn, E. V. Using a Synthetic Receptor to Create an Optical-Sensing Ensemble for a Class of Analytes: A Colorimetric Assay for the Aging of Scotch. *Journal of the American Chemical Society* **2001**, *123*, 10109–10110
- (64) Zhang, T.; Edwards, N. Y.; Bonizzoni, M.; Anslyn, E. V. The Use of Differential Receptors to Pattern Peptide Phosphorylation. *J. Am. Chem. Soc.* **2009**, *131*, 11976–11984
- (65) Umali, A. P.; Anslyn, E. V. A general approach to differential sensing using synthetic molecular receptors. *Curr. Opin. Chem. Biol.* **2010**, *14*, 685–692 ST – A general approach to differential sensing using synthetic molecular receptors.
- (66) Gallagher, L. T.; Heo, J. S.; Lopez, M. A.; Ray, B. M.; Xiao, J.; Umali, A. P.; Zhang, A.; Dharmarajan, S.; Heymann, H.; Anslyn, E. V. Pattern-based discrimination



of organic acids and red wine varieties by arrays of synthetic receptors. *Supramolecular Chemistry* **2012**, *24*, 143–148

- (67) Umali, A. P.; LeBoeuf, S. E.; Newberry, R. W.; Kim, S.; Tran, L.; Rome, W. A.; Tian, T.; Taing, D.; Hong, J.; Kwan, M.; Heymann, H.; Anslyn, E. V. Discrimination of flavonoids and red wine varieties by arrays of differential peptidic sensors. *Chemical Science* **2011**, *2*, 439–445
- (68) Kubarych, C. J.; Adams, M. M.; Anslyn, E. V. Serum Albumins as Differential Receptors for the Discrimination of Fatty Acids and Oils. *Org. Lett.* **2010**, *12*, 4780–4783
- (69) Adams, M. M.; Anslyn, E. V. Differential Sensing Using Proteins: Exploiting the Cross-Reactivity of Serum Albumin To Pattern Individual Terpenes and Terpenes in Perfume. *J. Am. Chem. Soc.* **2009**, *131*, 17068–17069
- (70) Saovapakhiran, A.; D'Emanuele, A.; Attwood, D.; Penny, J. Surface Modification of PAMAM Dendrimers Modulates the Mechanism of Cellular Internalization. *Bioconjugate Chemistry* **2009**, *20*, 693–701.

## **Chapter 2: Studies on the Cooperativity of Binding in Polycationic PAMAM Dendrimers and Polyanionic Species**

### **2.1 INTRODUCTION**

#### **2.1.1 Scientific Question and Goal**

In this work, the thermodynamic properties of binding between polyanionic groups and PAMAM dendrimers are explored. In an attempt to study the properties of the dendrimers, numerous polyanions with increasing amounts of negative charges were synthesized and the binding of those dendrons with several different generations of PAMAM dendrimer. The thermodynamic parameters between the generations are compared and analyzed to determine if the large amounts of contacts joined together will lead to positive cooperativity. The study overall explores if the joining of several complimentary ionic groups joined together when binding to the larger multivalent dendrimer surface will lead to positive cooperativity.

#### **2.1.2 Background into Cooperativity**

Biological systems make use of many weak interactions between different functional groups to form a variable wealth of structures with numerous distinct functions based upon the structure dictated by those weak interactions.<sup>1</sup> Each of these interactions between the functional groups amounts to little in terms of binding interactions taken individually, but the sum of the numerous interactions lead to the functional structure that often has a high association constant for a particular ligand.<sup>2</sup> Numerous supramolecular systems also make use of multiple associations to drive the assembly of functional materials and sensors.<sup>3</sup> For example, Krische and coworkers reported a functional material that makes use of numerous hydrogen bond donor and acceptor interactions to

create a novel 2D architecture in nonpolar solvents.<sup>4</sup> Our own group has used reversible covalent bonds and electrostatic complementarity to recognize target organic acids in a water methanol mixture.<sup>5</sup>

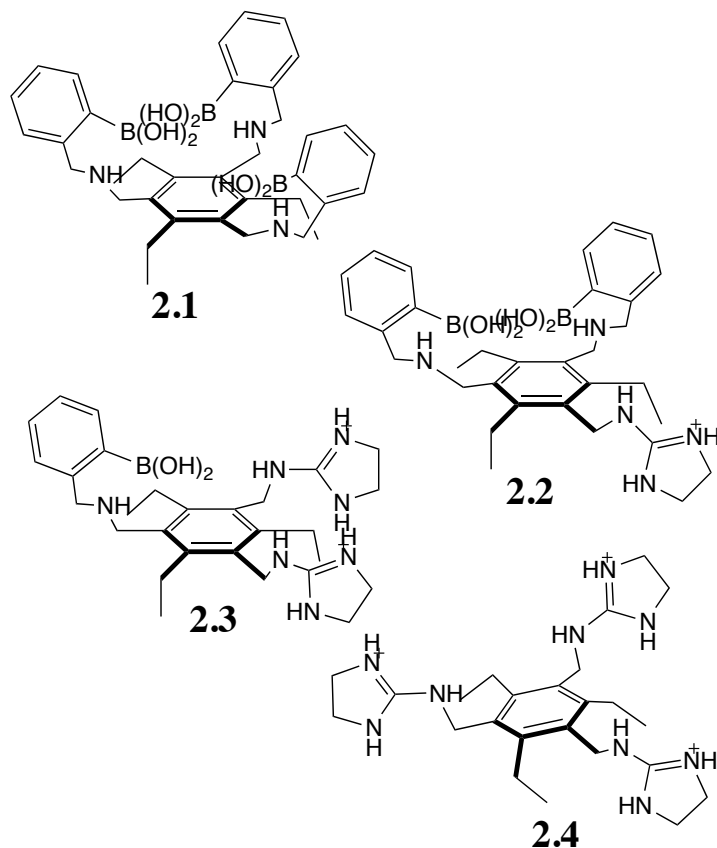


Figure 2.1 – Hosts used in Anslyn group cooperativity studies with small carboxylates

Unfortunately, with increasing amounts of water in the solvent and in pure aqueous systems, hydrogen bonds and other polar contacts must compete with 55 M water in order to find the perfect binding complement weakening binding interactions that require polar contacts. In addition to finding the ideal binding partner, these polar contacts are often thermodynamically less favorable in a polar solvent. In order to overcome these weaker interactions, nature uses the sum of multiple interactions tied

together to create the functional structure.<sup>6</sup> The sum of multiple binding interactions that have been covalently linked is known generally as cooperativity.

Qualitatively, cooperativity can be illustrated through the binding of oxygen to hemoglobin.<sup>7</sup> The biological protein binds four oxygen molecules per protein and each oxygen molecule binds more easily and with a higher binding constant than the previous oxygen molecule. This phenomenon results from structural modifications that occur as the first oxygen molecule binds so that the second molecule binds more strongly allowing oxygen to be bound at lower concentrations. Without this phenomenon, aerobic respiration would be hampered and life would be fundamentally different.<sup>8</sup> While qualitative descriptions of cooperativity are intuitively easy to understand in biological systems, the concept can become more instinctively difficult as the systems become more complicated. In a system with numerous polycationic and polyanionic interactions, the system's behavior is not as easy to predict, and thus a quantitative system is needed to develop a better understanding of the cooperativity of a system.

### **2.1.3 Nomenclature**

Cooperativity as a phenomenon is the additive effect of multiple binding interactions added together leading to an enhancement in the binding constant.<sup>9</sup> But before we develop a qualitative model of cooperativity, we should describe some of the terminology surrounding this phenomenon. Cooperativity is known by many names depending on the area of science and the types of ligands and host. In inorganic chemistry, cooperativity is known as the chelate effect and is used to describe the effects of additional ligand contacts to a metal center.<sup>10</sup> In biological systems, the term avidity and multivalency effects are also fundamentally the same phenomenon as cooperativity. For the rest of this chapter, the term cooperativity will be used over these other terms.

### 2.1.4 Mathematical Representation of Cooperativity

In the 1980s, Jencks developed a mathematical equation to represent the additional binding strength obtained by cooperative binding (Equation 2.1).<sup>9</sup>

$$\Delta G_S = \Delta G_A + \Delta G_B - \Delta G_{AB}$$

Equation 2.1 – Jenck’s Mathematical representation of cooperativity

Additionally, Jencks provided a rigid definition for positive and negative cooperativity, which is still used today. In a system that displays positive cooperativity, the binding energies of the tethered ligands sums to greater than the binding energy of each of the ligands when taken independently. According to Jencks and his mathematical equation,  $\Delta G_S$  is positive. In a system that displays negative cooperativity, the converse is true.  $\Delta G_S$  is negative and the binding energy of the system is less than the binding energy of each of the individual components.

In order to utilize Equation 1, the  $\Delta G_A$  and the  $\Delta G_B$  must first be defined and calculated with some level of accuracy. While in some cases the  $\Delta G_A$  and  $\Delta G_B$  can be efficiently measured, the binding energies are not always straightforward to calculate. In synthetic systems, each binding motif can be sequentially removed to obtain the  $\Delta G_A$  and  $\Delta G_B$  energies for each of these binding units. In biological systems, the microenvironment around the binding moiety often plays a large role in determining the binding strength making the measurements of  $\Delta G_A$  and  $\Delta G_B$  difficult.

The Anslyn group has used modifications to the original Jenck’s equation to look at the specific thermodynamic driving force of the binding through the  $\Delta H_S$  and  $-T\Delta S_S$  terms.<sup>11</sup> Using these more granular terms, the enthalpic and entropic contributions to binding can be quantified and the thermodynamic origin of the cooperativity in binding can be determined. Because positive cooperativity is defined as having a positive  $\Delta G_{AB}$

of connection, the term  $-T\Delta S_s$  was used so that positive values would correspond to entropy values which support positive cooperativity.

Furthermore, Bundle and coworkers reported that the entropy of binding could be modeled based upon the type of connectivity giving some insight into the cooperativity that could be computationally determined.<sup>12</sup> Their work reported four types of binding topologies: indifferent, linear, circular, and radial. Each of these topologies is an idealized form and good for modeling, but most ligand systems are a combination of these topologies. While the model works well, the calculations are no substitute for measuring the thermodynamic values of the binding interaction and this model only has limited utility.

While we can expect to see higher binding affinity due to the multimodal binding, additional considerations must be made to obtain the optimal binding. Tethered binding units must have an optimal length in order to obtain ideal binding energies.<sup>13</sup>

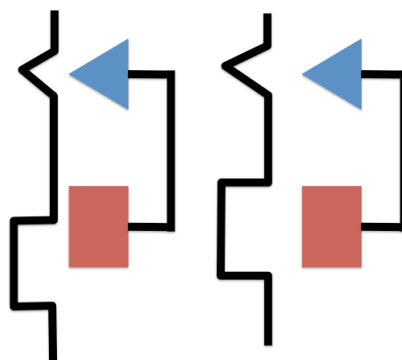


Figure 2.2 – Improper tethering of connected binding units leads to weakened connectivity. When properly aligned, the ligands can interact with both of the binding pockets.

When a tether is of an inappropriate length, the binding energy pays an enthalpic penalty, weakening the overall binding affinity of the tethered ligand to the host.<sup>14</sup>

Additionally, the tethered ligands lose some of the translational energy that each of the independent ligands possessed, giving weaker entropic contributions to the free energy of binding. These two phenomena, together, make systems that display true Jenck's positive cooperativity rare, particularly for aqueous systems.<sup>11</sup>

### **2.1.5 Real World Studies of Cooperativity**

While the mathematical description and the qualitative assessment of cooperativity provide a basis for which to understand the concept, the idea can be best conceptualized in terms of its application to a real world example. The two most widely studied systems for which the cooperativity of binding is measured are lectin-carbohydrate interactions and the binding of antibiotics, particularly vancomycin, to bacterial cell walls. Each study has shown how the individual interactions lead to the enhanced and specific binding of the analyte to the receptor. As shown by Westwell and Williams, small changes in the cell wall or to the antibiotic can lead to marked decreases in the affinity of the ligand for its natural target.<sup>15</sup> Similarly, changes in ligand design that combine multiple repeating units, Whitesides was able to obtain a  $K_d$  value of  $10^{-17}$ , while single vancomycin units show  $K_d$  values on the order of  $10^{-6}$ .<sup>16</sup> Furthermore, the identity of the linker can lead to changes in the binding parameters. Flexible linkers lead to a decreased binding affinity because they must adopt the proper conformation in order to interact with ligand.

When looking at protein-carbohydrate interactions, lectins make use of the so-called glycoside cluster effect where several sugar molecules located in close proximity to each other are enveloped by numerous areas of hydrogen bonding and metal coordination in the lectin to facilitate recognition.<sup>1,17</sup> The close proximity of both the hydrogen bonding side groups and the numerous glycosides lead to valency effects that

enhance the binding of the carbohydrates to these protein receptors. The level of specificity in these multivalent systems is extraordinary.<sup>1</sup> The changing of a single hydroxyl group can lead to a change in affinity of the analyte by several orders of magnitude. The study of these interactions and their origins has significant ramifications as the interactions form the basis for cell-to-cell recognition.

### 2.1.6 Anslyn Group Cooperativity Studies

The Anslyn group<sup>5,11,18,19</sup>, along with others,<sup>20,21</sup> has expanded the study of cooperativity to the study of artificial receptors for analyte binding. In 2002, studies were carried out on the thermodynamic origins of the binding of citrate to a *tris*-guanidinium based receptor. The receptor at low concentrations of one of the analytes tended to form higher order aggregates that are driven by entropy through solvent expulsion from around the ligand with only minor contributions from electrostatic interactions. Further studies using a tripodal amine ligand chelating a copper atom were carried out using a variety of anionic ligands to determine the effects of increasing numbers of anionic groups. Using anions (acetate, glutarate, tricarballate, and 1,2,3,4-butanetetracarboxylate), an entropically driven negative cooperativity was observed. The entropy difference between binding A-B and the binding of A and B separately is likely driven by solvent and counterion release into the bulk solution.<sup>18</sup> The study also highlighted some of the weaknesses of the Jenck's methodology that the type of the thermodynamic properties of the individual components can be ambiguous and difficult to ascertain. In this system, the values for  $\Delta G_A$ ,  $\Delta H_A$ , and  $\Delta S_A$  cannot always be simply assumed to be the same interaction since the system involves two types of molecular recognition events: ion pairing and metal coordination.<sup>11</sup> These effects are influenced by the microenvironment and thus the values of each ligand can be different when joined together. Using good



experimental design that understands these difficulties, a straightforward analysis using the Jenck's equation can be carried out in a system with multiple types of binding interactions.

In another study by the Anslyn group, the origins of binding between carboxylates,  $\alpha$ -hydroxycarboxylates, and diols to a benzene scaffold with varying numbers of boronic acids and guanidinium groups was explored using ITC and UV-Vis spectroscopy.<sup>5</sup> The studies showed that the binding with these receptors was exothermic and often entropically-driven but that the addition of boronic acids produced changes in the enthalpy as well. Furthermore, these receptors were used to analyze the phenomenon known as enthalpy-entropy compensation. If the measured entropy and enthalpy of a series of receptors is plotted against each other, the corresponding graph will traditionally show a straight line since more favorable enthalpic interactions tend to decrease the amount of entropy released as the molecules interact.<sup>22</sup> More specifically, as the ligand and host bind more tightly leading to an increase in enthalpy, the complex becomes more rigid and loses a lot of the residual motion, which weakens the entropic driving force. As the slope of the line approaches one, the tradeoff between entropy and enthalpy becomes more complete. The enthalpy-entropy compensation theory is also routinely critiqued.<sup>23,24,25</sup> Many of the theory's detractors claim that the effect is simply a trivial treatment of the data, or that the effect is a logical fallout of the way the data is experimentally obtained particularly when calculated from NMR data.<sup>26</sup>

In a final study of the thermodynamic driving forces between a synthetic host and anionic ligands from the Anslyn group, a system that displays positive cooperativity in water was identified.<sup>11</sup> Utilizing a host which contains both a metal chelation site and two guanidinium groups, positive cooperativity was observed as anionic ligands with increasing numbers of carboxylates were used.

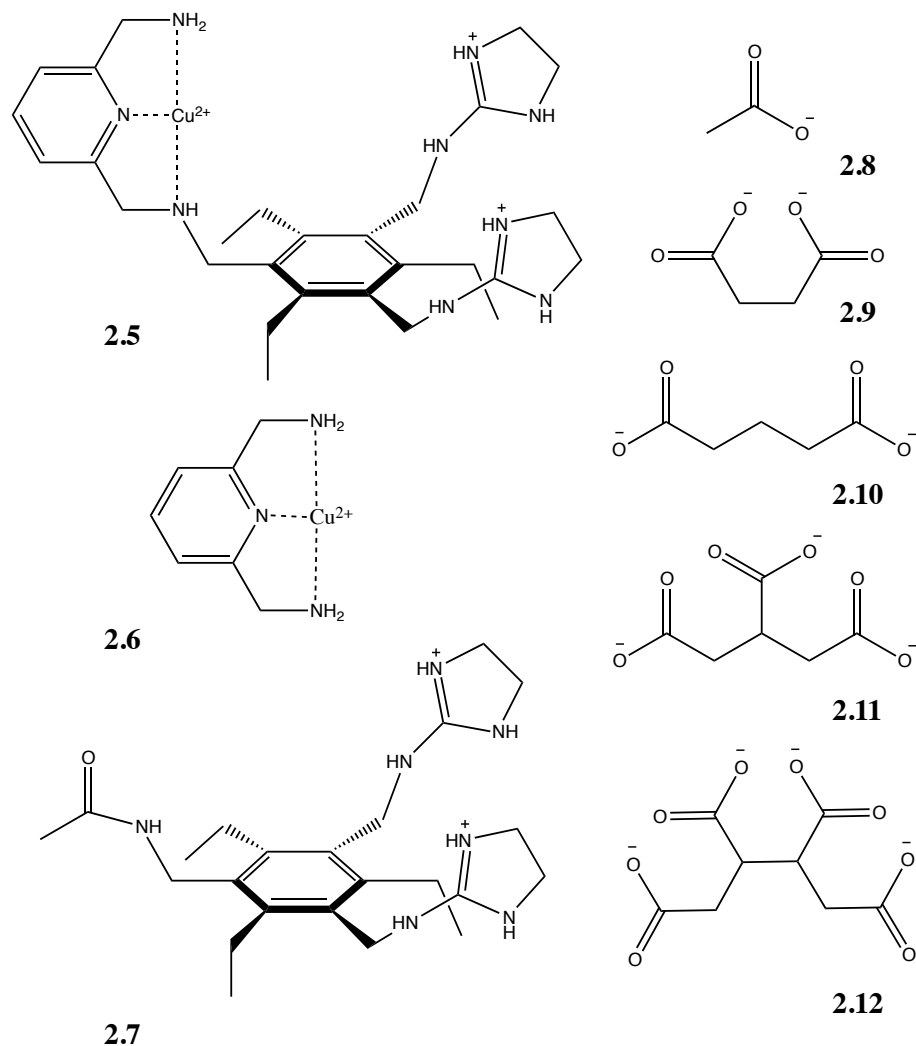


Figure 2.3 – Hosts and guests used by Hughes in the system that displayed positive cooperativity in water.

The source of the positive cooperativity is enthalpic in nature and is likely driven by the electrostatic destabilization when a metal is chelated in close proximity to two positively charged guanidinium groups. The binding of the target analytes relieves this destabilization effects. From each of these studies by our group, we draw our inspiration for the studies described in this chapter.

### **2.1.7 Effects of Solvent on Cooperativity**

Previous work looking at cooperativity has shown that water based systems have a great dependence on solvent.<sup>19,20,27,28</sup> The interaction of the polar water molecule with the host and guest as well as its ability to hydrogen bond with itself play an important role in determining the cooperativity of the system.<sup>20,27</sup> Often, systems carried out in water show complete compensation for entropy and enthalpy because the most important interactions are the water molecules with themselves, the host and the guest rather than the interactions of the host and guest to each.<sup>28</sup> In one of the Anslyn group studies previously mentioned, the driving force was postulated to be the effects of tethering the carboxylates together decreased the favorable solvation sphere around the ligand.<sup>19</sup> These solvent mediated reactions often generate larger signals that engulf the signal from the host and guest interaction between those two molecules. Thus, the effects of the solvent rather than host and guest interactions in most cases drive the signals and the cooperativity.

## **2.2 STUDY DESIGN**

Each of these previous studies relied on the binding of a polyanionic guest to a polycationic host. Our current studies build off of that work, but take it to a macroscopic level with exponentially increasing amounts of charges rather than increasing by a single charge. Utilizing commercially available dendrimers described in the previous chapter of this dissertation, we aim to explore the binding of large polyanionic structures to these large macromolecules with numerous charges along the exterior surface of the macromolecule. Through a systematic study, the properties of the dendrimers can be explored and some information about the thermodynamics of binding can be obtained. By increasing the generation of the dendrimer used, we can exponentially increase the number of surface functional groups and thus the charge. In order to understand how

these polycations interact with anions, we designed a series of anionic guests or dendrons that bear from 3 to 9 carboxylates.

### **2.2.1 Biological Relevance**

In these studies, we want to develop a better understanding of these polyion interactions because of their ubiquitous nature in biological systems. The most common example of a biological interaction driven by such polyion binding would be the condensation of DNA onto histones, which allows for the tight binding of the DNA and modulates gene regulation and protection.<sup>29</sup> Histones are proteins which bear numerous lysine and arginine residues to give them a polycationic structure. The cations of the histone bind to the negatively charged phosphate backbone of DNA making the DNA unavailable for transcription and translation. This unavailability limits the production of the proteins encoded by the DNA thus regulating cellular processes. Much like histones, dendrimers are macromolecules containing numerous amines, which are protonated at physiological pH.<sup>30</sup> As such, dendrimers have become a common mimic for histones in biological studies because they are commercially available and ease to handle.

Several studies of the binding of DNA to dendrimers have been carried out.<sup>31-36</sup> Some of these studies have analyzed the binding thermodynamics, but these studies have lacked a comprehensive nature that can further help to understand the cooperative nature of the binding and the effects of charge. Comprehensive studies have been carried out with a single generation of dendrimer and studies have been carried out that explore multiple generations of a dendrimer, but only focus on a single piece of DNA rather than exploring different lengths and differing secondary and tertiary structures.

### 2.2.2 Previous Work Using Dendrimers for Modeling Biological Systems

In order to provide a context for the current work, the two of the most comprehensive studies of DNA binding to dendrimers will be briefly highlighted. In a study by Jensen, the enthalpy of binding for short siDNA was measured with G1, G4 and G7 dendrimers.<sup>37</sup> Unfortunately, the ITC was reported without entropy and was only recorded with a single DNA strain limiting the effectiveness of the study towards measuring binding parameters and understanding how the thermodynamic parameters change with the amount of charge. Previously, Jensen has done a more exhaustive study of the binding with different ratios of G7 dendrimer and a small strand of siDNA. In these binding studies, different complexes were formed as more DNA was added to the solution moving from an exothermic binding to an endothermic dendriplex aggregate. While both of these studies lay important groundwork, neither is an exhaustive study that would help to elucidate the thermodynamic driving forces of the DNA complex.

### 2.2.3 First Anionic Dendron Synthesis Attempt

In order to interrogate the binding thermodynamics of the PAMAM dendrimers with polyanions, a series of polyanions were developed. A benzene scaffold was designed that contains numerous carboxylate groups and another handle from which the scaffold can be joined together.

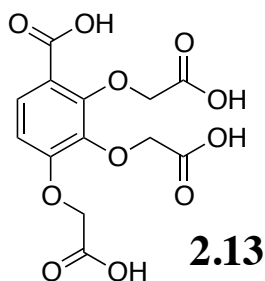
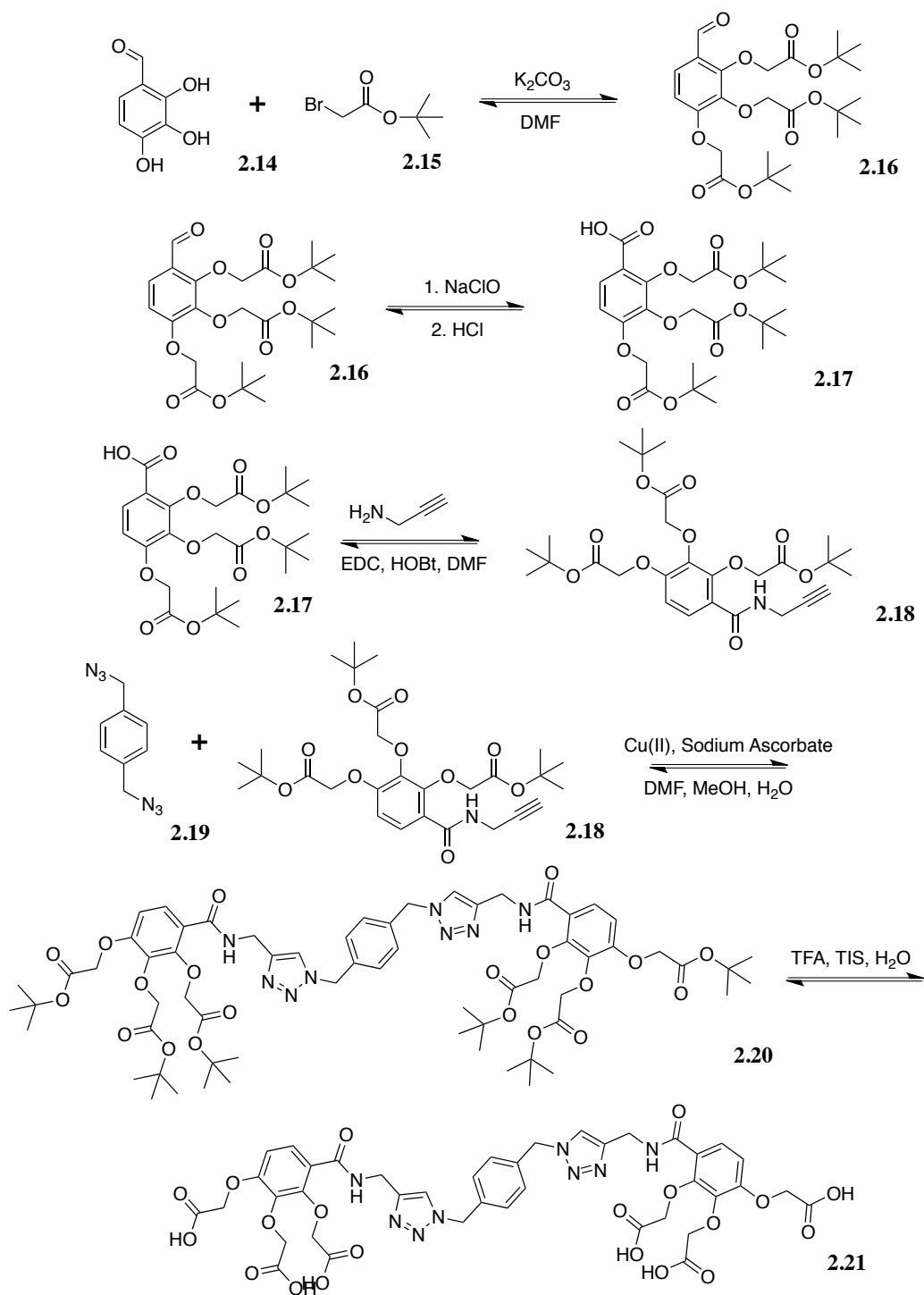


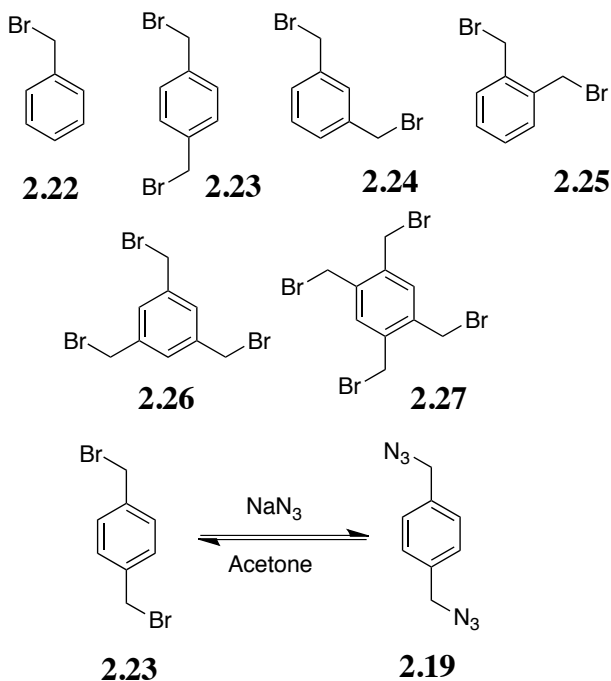
Figure 2.4 – First anionic repeating unit for the dendron target synthesis

The first scaffold (**2.13**) was designed by a previous group member to create such a structure with three carboxylates and a benzylic acid that can be used to functionalize the unit with other groups including short peptides chains. Using this tricarboxylate scaffold, a number of different length dendrons were designed to incorporate many units of the scaffold leading to increased numbers of charges.



Scheme 2.1 – First Anionic Dendron Synthesis

The synthetic scheme for these dendrons is shown in Scheme 1. The three phenol groups of the starting material were alkylated with *t*-butylbromoacetate in DMF with potassium carbonate. After the alkylation, the aldehyde was oxidized using sodium hypochlorite and then acidified with concentrated HCl in a 2-day process to give the target carboxylate group in good yield. The entire process took over three days to complete and could be synthesized on a gram scale. The carboxylate group was reacted using standard amide bond formation conditions with propargylamine to form the amide bond. Unfortunately, these conditions lead to a low yield of the desired amide with the bulky side groups likely hampering the formation of the desired product and the reaction mixture was difficult to effectively separate. In parallel with these reactions, a group of benzylic halides (shown in Scheme 2) were reacted with sodium azide in acetone to make the organic azides in high yield.



Scheme 2.2 –Benzyl Halide Starting Material and Azide Synthesis





Each molecule contains the same number of freely rotatable  $sp^3$  carbons and each repeating unit contains three negative carboxylate charges. The new molecule, on the other hand, has fewer total bonds between the core and the anionic groups and the groups on the original molecule contain more rigid linkers that prevent rotation compared to the new molecule, which imparts more of an ability to rotate its charges to form favorable interactions with the branches of the dendrimers. In general, the two molecules appear to be similar enough that the study would not likely be affected by using the newly designed molecule. Since the trizma-based molecule synthesis only required three linear steps as opposed to five linear steps for the original molecule, the trizma-based molecule was synthesized and used for all further studies. Originally, five different regioisomers of the triazole dendron core were to be synthesized.

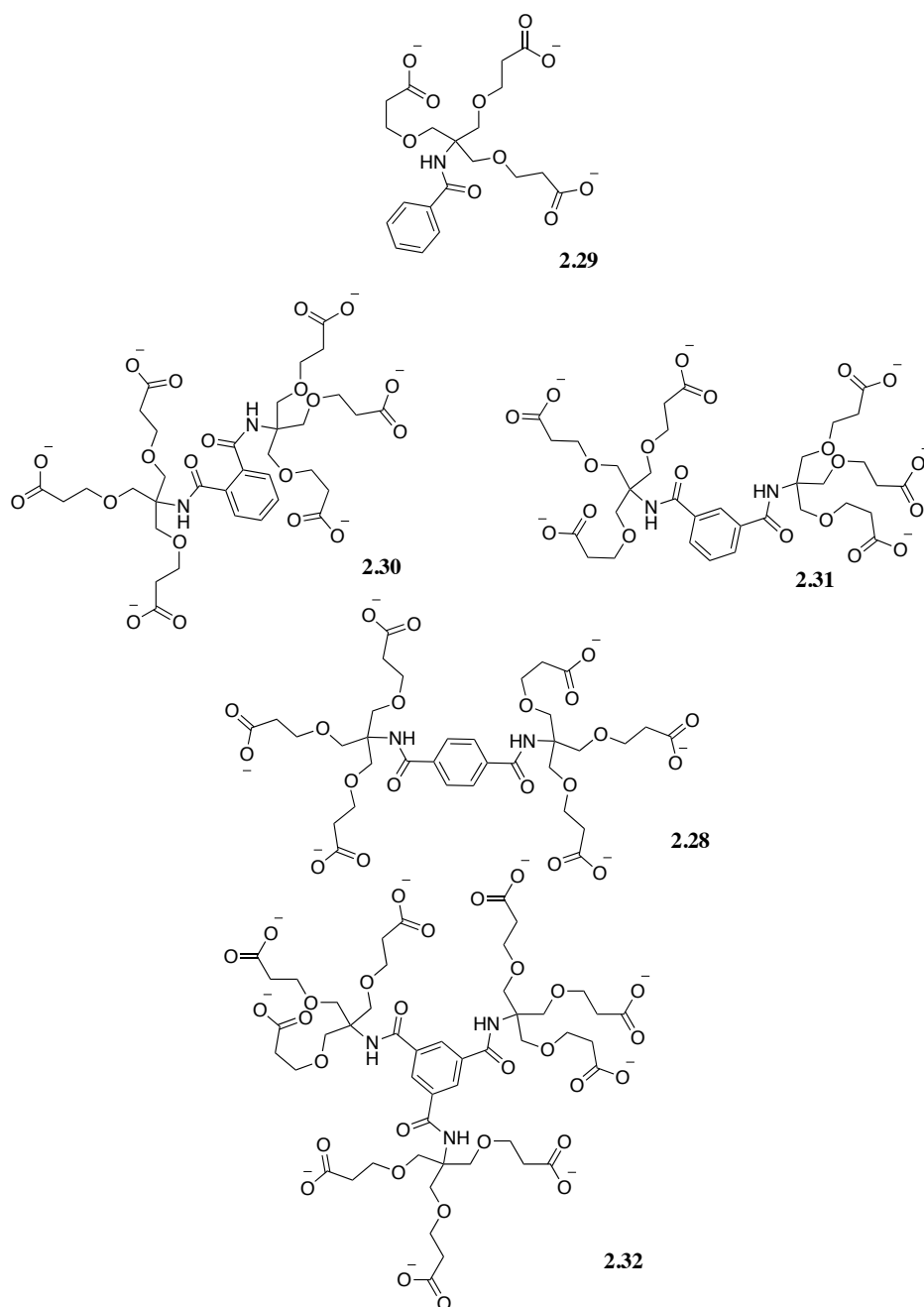
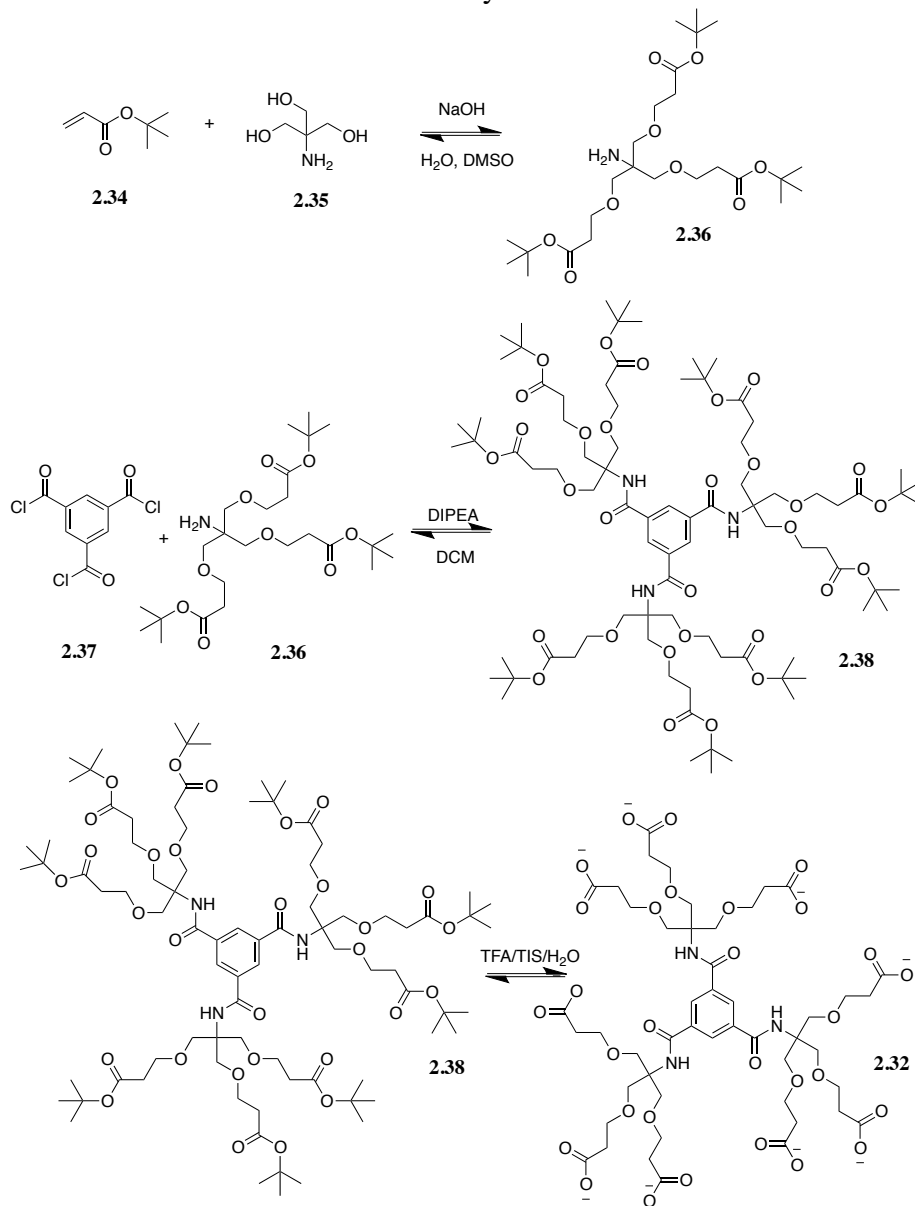


Figure 2.6 – Different Target Regioisomer Dendrons

Of those original five regioisomers, four were synthesized using the trizma dendron. The tetra derivative was considered but the acid chloride is not commercially available and

the derivative would likely have proven to be difficult to effectively synthesize in high yield, and thus it was eliminated from the study.



Scheme 2.3 – 2<sup>nd</sup> Generation Anionic Dendron Synthesis

Furthermore, using the acid chloride as a building block for the core of the dendron made the synthesis of the ortho derivative difficult.

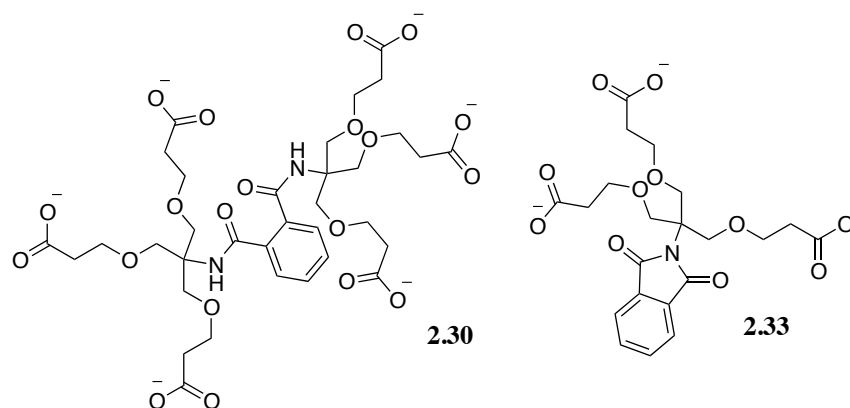


Figure 2.7 – Ortho Dendron and Byproducts

After the addition of the first trizma group, the second acid chloride cyclizes onto the amide nitrogen to form a phthalamide derivative rather than the desired product. Each of these products was purified using reverse phase C18 silica chromatography giving the desired product in high yield and purity.

After the trizma derivatives were synthesized, the t-Butyl groups were cleaved using a traditional acid cleavage cocktail of trifluoroacetic acid (9.5 mL), triisopropylsilane (0.25 mL), and water (2.25 mL). A larger percentage of water relative to the normal peptide resin cleavage cocktail was used to prevent the formation of anhydrides as the tButyl groups on the carboxylates were cleaved. Each of these cleaved products was purified via reverse-phase chromatography and then the resultant oil was dissolved in buffer to make stock solutions.

### 2.2.5 ITC Setup

To make the stock solutions, an aqueous 50 mM pH 7.4 HEPES buffer was used for these studies. In our previous studies of dendrimers using ITC, we had used a much higher concentration of buffer to prevent pH changes with the large polyelectrolytes. For these studies, we wanted to lower the ionic strength of the solutions to help achieve

effective binding. Furthermore, studies have shown that dendrimers can undergo changes in their tertiary structures at higher ionic strength that make them less than ideal for studying binding interactions. But given the number of pH sensitive groups in both the dendrons and the dendrimers themselves, the 50 mM buffer proved ineffective at controlling the pH of the solution, and the pH of the stock solutions of the dendrons were manually adjusted using 1M HCl and 1M NaOH solutions to within  $\pm 0.05$  of the starting buffer pH. At these pH's, the movement of protons should be limited and the primary interactions of binding should be between the dendrimer and the dendrons.

The individual solutions were made containing dendrimer, and each of the individual trizma dendrons with titrant solutions containing both dendrimer and dendron, while the cuvette solution contained only dendrimer. Using a fixed concentration of dendrimer prevents peaks due to the dilution of the large polycationic macromolecule and makes the resultant signals easier to interpret. Each of these solutions was analyzed by ITC. As was mentioned before, the ITC allows for the determination of binding thermodynamic values through the measurement of heat released during the binding event. Through a mathematical fitting of the data obtained, a binding constant (a value corresponding to the stoichiometry of binding),  $\Delta H$  and  $\Delta S$  values are obtained.

## **2.3 RESULTS**

### **2.3.1 Dendron Models**

In order to measure the cooperativity of binding, the thermodynamic values of binding need to be determined for each of the components of the larger binding molecules. In this situation, the binding event is the addition of more than one of the individual trizma units. As such, we can assume the benzyl unit to represent the binding energetics of a single unit, and we use this value as the basic anion unit. Using this

assumption that the benzyl dendron (2.29) is a single binding unit, we can assume that the binding energy of the meta and the para units should be the addition of two of the benzyl groups, and the tris should be the addition of three benzyl groups or the addition of a meta or para and a benzyl group.

### **2.3.2 Interactions of the Dendrons with G3 Dendrimers**

When looking at the G3 dendrimer with the different dendrons, we can explore the relationship between the increasing numbers of charges as well as the locations of these charges. When looking at the first binding events, the number of anionic groups – the  $n$  value – decreased by approximately 0.5 dendrons for the benzyl to the para to the tris derivatives. This trend is broken in the meta derivative which binds two units during the first binding event likely due to the small size of the G3 dendrimer and to the orientation of the meta trizma groups, which are not able to allow all the anionic groups to coordinate to the dendrimer. When looking at the affinity constants ( $K$  values) for each of the derivatives with this dendrimer, the values increase as the number of charges increase, but the dendrons with two and three trizma groups all show similar equilibrium constants. When we use the cooperativity equations discussed earlier for  $K$  and  $\Delta G$  values we obtain negative cooperativity for each of the dendrons with the G3 dendrimer. Seeing negative cooperativity for this system is not surprising since positive cooperativity is rare in aqueous systems without the relief of some other form of strain present in the system before binding.

| All values in cal/mol | n   | K     | $\Delta H$ | $\Delta S$ | $\Delta G$ |
|-----------------------|-----|-------|------------|------------|------------|
| <b>Benzyl</b>         | 1.6 | 8700  | -2000      | 11         | -5400      |
| <b>Meta</b>           | 1.9 | 45000 | -2900      | 12         | -6400      |
| <b>Para</b>           | 1.0 | 45000 | -3400      | 10         | -6400      |
| <b>Tris</b>           | 0.5 | 53000 | -7100      | -2         | -6500      |

Table 2.1 – G3 Dendron Binding Thermodynamic Values for 1<sup>st</sup> Binding Event

When we look at the  $\Delta H$  and  $\Delta S$  values for the system, we notice a more distinct and interesting pattern in this first binding event. First, let's explore the trends in the  $\Delta H$  values and the associated cooperativity within this thermodynamic parameter. As can be seen in the chart (Table 1), the  $\Delta H$  values increase as the number of charges increase but with a small increase for the meta derivative which supports the interpretation that the meta does not bind to the dendrimer generation as well as the para derivative. All of the cooperativity values for the meta and para derivatives show negative enthalpic cooperativity, but the tris shows positive enthalpic cooperativity. The orientation of the three charged groups likely encapsulates the dendrimer to form more ideal salt bridges around the dendrimer than the meta or para derivatives. The interaction also likely releases strain in the dendrimer from the dendrimer folding in on itself to form hydrogen bonds amongst its functional groups but can now form these interactions with the dendrons.



| All values in cal/mol  | K     | $\Delta H$ | $\Delta S$ | $\Delta G$ |
|------------------------|-------|------------|------------|------------|
| Meta - Benzyl + Benzyl | -4400 | -1200      | -3200      | -4400      |
| Para - Benzyl + Benzyl | -4400 | -700       | -3700      | -4400      |
| Tris - Benzyl x3       | -9700 | 940        | -11000     | -9700      |
| Tris - Benzyl + Meta   | -5300 | 2200       | -7500      | -5300      |
| Tris - Benzyl + Para   | -5300 | 1700       | -7000      | -5300      |

Table 2.2 – G3 Dendron Binding Cooperativity Values for 1<sup>st</sup> Binding Event

When we look at the  $\Delta S$  values the smaller groups (benzyl, meta and para) show favorable entropy values while the tris groups shows negative entropy values likely due to the interaction of the large groups restricting the movements of the dendron and dendrimer and to an assembly of the two molecules into a single complex. Each of these  $\Delta S$  values when measured in the cooperativity equations mentioned earlier show negative cooperativity with the tris groups showing a large negative cooperativity due to the complex and to the formation of a more rigid structure in that system. This negative entropic cooperativity drives the overall cooperativity for the system.

While the first binding event measured is likely the major binding event, the secondary binding events are likely nonspecific interactions based upon charge interactions between the two molecules. This phenomenon appears to be true of the benzyl, meta and para dendrons (2.29,2.31,2.32) but not necessarily true for the tris derivative. The meta and para dendrons in these weak interactions only have K values on the order of  $10^2$  or less and are driven by enthalpy and will be entropically unfavorable. The enthalpy contributions derive from interaction of the

complementary charges, while the entropy arises from creating a more rigid complex as the two molecules interact that is not overcome by the release of bound water and counterions as those molecules were likely displaced in the first set of binding interactions. In the benzyl case, the binding arises mainly from entropic considerations with only a weak enthalpy contribution. The process for this binding is likely different from the meta and para derivative. In the benzyl dendron (**2.29**), one potential explanation lies in the fact that the benzyl group could bury itself into the dendrimer inner core giving rise to a little bit of enthalpic contribution from hydrophobic interactions. Furthermore, the smaller charge density of the benzyl dendron (**2.29**) is not as strongly attracted to the G3 dendrimer. The large entropic component arises from the release of the hydration shell around the benzyl ring as it intercalates into the dendrimer shell. This process is entropy driven because the process releases water into the bulk solution as well as the water molecules trapped inside the dendrimer shell.

| All values in cal/mol | K   | $\Delta H$ | $\Delta S$ | $\Delta G$ |
|-----------------------|-----|------------|------------|------------|
| <b>Benzyl</b>         | 260 | -430       | 10         | -3300      |
| <b>Meta</b>           | 350 | -4500      | -3         | -3500      |
| <b>Para</b>           | 21  | -4400      | -9         | -1800      |
| <b>Tris</b>           | 19  | -42000     | -140       | -1800      |

Table 2.3 – G3 Dendron Binding Thermodynamic Parameters for 2<sup>nd</sup> Binding Site

On the other hand, the second binding event for the tris dendron is very distinct. The interaction only involves a single molecule with a small K value, but with a very strong enthalpic contribution and negative entropy value. The

interaction's enthalpic contribution likely arises from complementary electrostatic interactions, while the entropy results from the formation of a more rigid complex and the reduction of the number of molecules in solution. This entropy contribution is much larger than the previously measured entropy for the first binding event. One possible explanation for this large enthalpic contribution with an equally strong entropic contribution is that the second tris molecule binds the dendrimer almost entirely or even entirely encapsulating it, creating a rigid cage, which is entropically disfavored but has a strong enthalpic component from the overlap of the charges. In this case, the relatively small size of the G3 dendrimer makes this potential complex possible. Overall, the cooperativity in the tris system binding is negative, but that cooperativity is driven by the negative cooperativity of  $\Delta S$  and positive  $\Delta H$  cooperativity.

| All values in cal/mol  | K     | $\Delta H$ | $\Delta S$ | $\Delta G$ |
|------------------------|-------|------------|------------|------------|
| Meta - Benzyl + Benzyl | -3100 | 3600       | -6700      | -3100      |
| Para - Benzyl + Benzyl | -4800 | 3500       | -8300      | -4800      |
| Tris - Benzyl x3       | -8100 | 41000      | -49000     | -8100      |
| Tris - Benzyl + Meta   | -5000 | 37000      | -42000     | -5000      |
| Tris - Benzyl + Para   | -3300 | 37000      | -41000     | -3300      |

Table 2.4 - G3 Dendron Binding Cooperativity Values for 2<sup>nd</sup> Binding Event

Overall, the G3 dendrimer complex system shows that the cooperativity of the anionic binding is overall negative. In some cases, the  $\Delta H$  cooperativity is positive or slightly negative but the entropic cooperativity is always negative and

dominates the cooperativity terms effectively setting the nature of the overall cooperativity.

### 2.3.4 Interaction of the Dendrons with G4 Dendrimer

As the dendrimers increase in size, the fitting for the dendron binding becomes more complicated but the G4 dendrimer also seems to fit mainly to the same two sites binding model, a linear fitting algorithm used by the instrument. Again, a similar analysis of the binding of the four anionic structures to the G4 dendrimer was carried out.

Exploring the binding to the G4 dendrimer, the  $n$  value of the binding isotherm decreases as the number of charge increases. This fact follows the pattern we would expect although the larger anions need fewer charges to complete the saturation of this first binding mode. As the larger dendrons increase in size, the dendrimer itself may be covered by the dendron and prevent other dendrons from binding tightly.

| All values in cal/mol | K      | $\Delta H$ | $\Delta S$ | $\Delta G$ |
|-----------------------|--------|------------|------------|------------|
| <b>Benzyl</b>         | 10000  | -2700      | 9.3        | -5500      |
| <b>Meta</b>           | 98000  | -6300      | 1.9        | -6800      |
| <b>Para</b>           | 120000 | -9600      | -8.8       | -7000      |
| <b>Tris</b>           | 130000 | -7300      | -0.90      | -7000      |

Table 2.5 – G4 Dendron Binding Thermodynamic Parameters for 1<sup>st</sup> Binding Site

After exploring the binding stoichiometry, we explored the changes in the K value as the dendrons increase in total charge. Again, this dendrimer set shows a

systematic increase in the first set of binding events. The first binding event with benzyl-based dendron (2.29) occurs with an association constant of almost  $10^4$ , and the binding constant increases to approximately  $10^5$  with the larger dendrons and the tris derivative, which shows the highest binding affinity. The likely source of this change in binding affinity is that the fully charged arms of the tris dendron (2.33) do not bind to the dendrimer as might be anticipated, and the changes in entropy of binding support this idea. The entropy decreases as the dendrons become larger because the larger dendrons make more contacts with the dendrimers thus forms a more rigid complex structure. However, the relative number of change in entropy between the meta and the tris does not correlate to the changes seen between the benzyl dendron (2.29) and the meta dendron (2.31). The para dendron (2.32) actually shows the largest change in the entropy of any dendron despite having a slightly stronger enthalpic contribution. One explanation of this dendron's more significant change in entropy is that the para dendron (2.32) forms a barbell like structure, a structure that would be highly entropically disfavored while being more enthalpically favorable. The charged arms of the dendrons could be interacting with the full dendrimer charge causing a stronger enthalpic measurement, which could explain the thermodynamic parameters observed.

Comparing the enthalpic contributions, the benzyl, meta and tris all appear to increase in  $\Delta H$  value but the changes are relatively small, particularly in the larger dendrons with the para showing the largest increase, for which a possible explanation was given earlier. These similar enthalpic measurements indicate a similar binding mode, which is driven by the complimentary electrostatic interactions of the dendron anions to the cationic dendrimer.

When comparing the cooperativity of the binding in the G4 dendrimer with the various dendrons, similar trends were seen to the ones noted in the cooperativity of the first binding event in the G3 dendrimer. Overall, the system displays negative cooperativity, which is driven by negative entropic cooperativity. The cooperativity in the  $\Delta H$  values shows positive cooperativity for meta and para and only slightly negative cooperativity in the tris dendron (2.33). The para dendron (2.32) shows greater positive enthalpic cooperativity than the other systems due to the higher enthalpic contributions in the binding of the dendron. Again, these systems appear to follow much of the same trends as the G3 dendrimer.

| All values in cal/mol         | K     | $\Delta H$ | $\Delta S$ | $\Delta G$ |
|-------------------------------|-------|------------|------------|------------|
| <b>Meta - Benzyl + Benzyl</b> | -4100 | 900        | -5000      | -4100      |
| <b>Para - Benzyl + Benzyl</b> | -4000 | 4200       | -8200      | -4000      |
| <b>Tris - Benzyl x3</b>       | -9400 | -800       | -8600      | -9400      |
| <b>Tris - Benzyl + Meta</b>   | -5300 | -1700      | -3600      | -5300      |
| <b>Tris - Benzyl + Para</b>   | -5400 | -5000      | -420       | -5400      |

Table 2.6 – G4 Dendron Binding Cooperativity Values for 1<sup>st</sup> Binding Site

When we transition to looking at the second binding event with the dendron, a similar pattern can be observed as the first binding event. The benzyl dendron

(2.29) shows smaller  $K$ ,  $\Delta H$  and  $\Delta G$  values with a similar  $\Delta S$  value to the other three complexes formed. The para dendron (2.32) shows higher values than the other dendron pairs, which is mainly driven by higher entropy and slightly favorable entropy contributions. These measurements support the earlier hypothesis of the initial formation of a dumbbell-like structure. The initial binding of the para dendron (2.32) between the two dendrimers leads to a structure that already has paid an entropic price to form and the binding of additional dendrons then becomes more entropically favorable as the additional binding releases water and counterions, making it more entropically favorable compared to the initial binding. Furthermore, the enthalpic contributions are greater than the other dendrons because the net charge on each dendrimer is higher than when both arms of the dendrons bind to a single dendrimer leading to a stronger electrostatic attraction and thus higher enthalpic contributions in the binding.

| All values in cal/mol | K     | $\Delta H$ | $\Delta S$ | $\Delta G$ |
|-----------------------|-------|------------|------------|------------|
| <b>Benzyl</b>         | 920   | -750       | 11         | -4000      |
| <b>Meta</b>           | 26000 | -1900      | 14         | -6000      |
| <b>Para</b>           | 33000 | -2900      | 11         | -6200      |
| <b>Tris</b>           | 25000 | -1700      | 15         | -6000      |

Table 2.7 - G4 Dendron Binding Thermodynamic Parameters for 2<sup>nd</sup> Binding Site

The values for the cooperativity are also similar to those in the first binding mode. The cooperativity is negative overall for each case, but less so than the first binding event. The binding is dominated by very negative entropy with a small positive enthalpic cooperativity for the smaller meta and para dendrons (2.31-2.32). This binding mode

appears to be more significant in terms of the number of anions bound than the second binding mode seen in the G3 dendrimer. Because of the larger size of the host dendrimer, the dendrons have a larger surface area upon which they can interact and form complexes, and thus more surface for anions to bind. The larger dendrimer allows for more modes of interaction rather than simply non-specific electrostatic attraction between the two molecules.

| All values in cal/mol  | K     | $\Delta H$ | $\Delta S$ | $\Delta G$ |
|------------------------|-------|------------|------------|------------|
| Meta - Benzyl + Benzyl | -2100 | 410        | -2500      | -2100      |
| Para - Benzyl + Benzyl | -1900 | 1400       | -3300      | -1900      |
| Tris - Benzyl x3       | -6100 | -600       | -5500      | -6100      |
| Tris - Benzyl + Meta   | -4100 | -1000      | -3000      | -4100      |
| Tris - Benzyl + Para   | -4200 | -2000      | -2200      | -4200      |

Table 2.8 – G4 Dendron Binding Cooperativity Values for 2<sup>nd</sup> Binding Site

### 2.3.5 General Concerns About Isotherm Fitting

While the above analysis of the dendrimer systems makes intuitive sense, the study would be remiss if it was not highlighted that the modeling upon which these values are determined is somewhat simplified. By only taking into account two major modes of interaction, we condense disparate events into a general class, and create an average of multiple events. In the case of the tris derivative, taking the simplified approach led to a worse fit than the curve fit with a higher order binding equation, but allowed for a more logical interpretation of the data. The actual case, when analyzed with more modes of binding, may be more exacting in its interpretation but cannot be



generalized to the same overall trend as was seen in the simplified case, and thus we choose to utilize the simplified model instead.

If the higher order model is used, the first binding event shows slightly different interactions than the first binding event in the generalized binding model as this first binding event would help to organize the dendrimer to bind the anions after those first anions bind with a lower entropic penalty. However, this step-wise approach is lumped together in the simplified model. As such the models provide some insight, but their quantitative power is limited.

### **2.3.6 The 2<sup>nd</sup> Peak in the Isotherm**

Another point of interest that limits our analysis of these complexes is the formation of a second peak in the tris dendron (2.33) titration. With the G4 dendrimer, the titration isotherm showed a second peak after the completion of the initial binding event. This peak was also exothermic, and its origins are distinct from the initial anion binding. A likely explanation is that the dendron, due to its highly branched structures forms some initial complex that can rearrange to form a more ideal structure, likely from the movement of one or more arms. These molecular flexing motions lead to the formation of a thermodynamic sink that is slightly different from the kinetic structure that is measured initially. These second peaks are impossible to fit to a traditional binding model used by the ITC software for determining binding parameters. Thus, our analysis in which we make this approximation on those isotherms becomes more suspect and thus less quantitative. The analysis, though, is still good for estimating trends in the dendron binding.

While this methodology simplifies the binding modes of the components, this method serves as a useful approximation. In the larger generations of dendrimer and with

the tris trizma dendron (2.33), the binding isotherms are more complicated and thus harder to fit to a simple binding approximation. In the approximations, an effort was made to fit them to as small a number of binding modes as possible. Using the sequential binding model of curve fitting, each of the titrations was fit despite the more complicated nature of the binding isotherm. While this model treats each of the different binding models as having an  $n$  value of 1, the model does a good job of qualitatively explaining the data and its relative trends in the binding events. Furthermore, even without the stoichiometry data obtained from the single or double binding site models, the calculations of the cooperativity of binding can still be carried out by utilizing the calculated thermodynamic values for the binding of the dendrons. While this analysis might not provide definitive quantitative proof of the cooperativity factor in binding these polyanions, it will provide us with some evidence of the magnitude and type of cooperativity displayed by the larger stoichiometry and generation complexes. Some of these titrations were modeled on a two-site binding model and others on a multimodal binding site model, but the general trends follow no matter what model was used.

### **2.3.7 Interaction of the Dendrons with G5 Dendrimer**

The generation 5 dendrimer titrations show a larger and more complex curvature in the isotherm than the previous dendrimers. These curvatures make the isotherms more difficult to fit, but the isotherms could generally be fit well to a two binding site model. The general trends identified via the earlier generations appear to hold true for this generation as well, but are not as consistent and routine in their variance as the trends in the smaller generations. The majority of the anionic dendrons show relative increasing affinity constants except for the tris derivative, which does not appear to have as high a binding constant as the smaller generations despite its higher amount of total charge. The

higher charge density of the larger complex manifests itself as a much higher enthalpy value for those binding events. As was seen in the earlier classes, the enthalpy values seem to increase as the amount of charge increases from the benzyl to the tris derivative, with the meta and para dendrons (2.31-2.32) being relatively close in their enthalpy values. While the enthalpy values show a logical increase, the entropy measurements appear to have a less consistent trend, but a general pattern can still be observed. The benzyl dendron (2.29) is entropically favorable, while the meta and para are less favorable, and the binding of the tris dendron is extremely entropically disfavored. The

| All values in cal/mol | K      | $\Delta H$ | $\Delta S$ | $\Delta G$ |
|-----------------------|--------|------------|------------|------------|
| <b>Benzyl</b>         | 14000  | -4000      | 5.7        | -5700      |
| <b>Meta</b>           | 61000  | -8200      | -5.5       | -6500      |
| <b>Para</b>           | 110000 | -6700      | 0.9        | -6900      |
| <b>Tris</b>           | 13000  | -26000     | -68        | -5600      |

Table 2.9 – G5 Dendron Binding Thermodynamic Parameters for 1<sup>st</sup> Binding Site

trend begins to breakdown with meta and para dendrons (2.31-2.32) where the meta is more unfavorable than the para anion, but they are generally similar in their entropic penalty. While there are potentially several explanations for this phenomenon, one explanation is that the meta derivative simply forms tighter ion pairs, and thus leads to a more rigid complex that is more entropically disfavored. Furthermore, the tighter interactions lead to a more entropically favorable complex observed in the data.

Furthermore, the trends in the cooperativity are similar to those shown in the earlier generations. The overall cooperativity of the system is highly negative and becomes more so as the anions become larger. While the overall cooperativity in the

generation 5 dendrimers is negative, the enthalpic cooperativity is positive except for the case of the para derivative which is slightly negative. The cooperativity in the entropic component is highly negative and drives the overall cooperativity of the system. This trend is the same as the two previous generations.

| All values in cal/mol         | K      | $\Delta H$ | $\Delta S$ | $\Delta G$ |
|-------------------------------|--------|------------|------------|------------|
| <b>Meta - Benzyl + Benzyl</b> | -4800  | 280        | -5052.31   | -4800      |
| <b>Para - Benzyl + Benzyl</b> | -4400  | -1200      | -3200      | -4400      |
| <b>Tris - Benzyl x3</b>       | -11000 | 14000      | -25000     | -11000     |
| <b>Tris - Benzyl + Meta</b>   | -6600  | 14000      | -20000     | -6600      |
| <b>Tris - Benzyl + Para</b>   | -7000  | 15000      | -22000     | -7000      |

Table 2.9 – G5 Dendron Binding Cooperativity Values for 1<sup>st</sup> Binding Site

After the first major binding event, the second binding event modeled in this system's isotherms appears to show general and nonspecific attraction of the anionic dendrons. The stoichiometry of the binding events often gives n values of over 100 anions to a single dendrimer. As such, the thermodynamic parameters are unable to provide much insight into the system. The affinity constants tend to be much smaller for the first binding event by at least one or two orders of magnitude. The entropy is still generally unfavorable with the majority of the binding event driven by enthalpy through nonspecific charge complementarity.

| All values in cal/mol | K    | $\Delta H$ | $\Delta S$ | $\Delta G$ |
|-----------------------|------|------------|------------|------------|
| <b>Benzyl</b>         | 190  | -2600      | 1.7        | -3100      |
| <b>Meta</b>           | 5800 | -18000     | -43        | -5100      |
| <b>Para</b>           | 3800 | -3000      | 6.2        | -4900      |
| <b>Tris</b>           | 4400 | -35000     | -100       | -5000      |

Table 2.10 – G5 Dendron Binding Thermodynamic Parameters for 2<sup>nd</sup> Binding Site

The cooperativity in the second binding mode is much like the first binding event with overall negative cooperativity. This net cooperativity is a result of positive enthalpic cooperativity and negative cooperativity relative to the entropic contribution. The entropic contribution drives the overall cooperativity of the system, but is generally less negatively cooperative than the first binding event.

| All values in cal/mol         | K     | $\Delta H$ | $\Delta S$ | $\Delta G$ |
|-------------------------------|-------|------------|------------|------------|
| <b>Meta - Benzyl + Benzyl</b> | -1100 | 13000      | -14000     | -1100      |
| <b>Para - Benzyl + Benzyl</b> | -1300 | -2200      | 850        | -1300      |
| <b>Tris - Benzyl x3</b>       | -4300 | 27000      | -32000     | -4300      |
| <b>Tris - Benzyl + Meta</b>   | -3300 | 15000      | -18000     | -3300      |
| <b>Tris - Benzyl + Para</b>   | -3000 | 30000      | -33000     | -3000      |

Table 2.11 – G5 Dendron Binding Cooperativity Values for 2<sup>nd</sup> Binding Site

### 2.3.8 Interactions of the Dendron with G6 Dendrimer

While the generation 5 dendrimer showed only slight curvature of the isotherms, the generation 6 dendrimer takes a distinctive shaped second peak in the isotherm.

Again, these dendrimers were modeled using similar models including the two binding site model, as well as the multiple binding site model with three and four binding events. In general, when able to be fit, the anionic binding to the G6 dendrimer was modeled with the two binding site model. Additionally, the tris dendron showed a significant secondary peak, that was discussed in terms of the G5 dendrimer earlier, making that particular isotherm difficult to fit. In order to fit the isotherm, the secondary peak was ignored as best as the fitting algorithms would allow.

| All values in cal/mol | K       | $\Delta H$ | $\Delta S$ | $\Delta G$ |
|-----------------------|---------|------------|------------|------------|
| <b>Benzyl</b>         | 11000   | -4300      | 4.2        | -5500      |
| <b>Meta</b>           | 4400000 | -6000      | 10         | -9100      |
| <b>Para</b>           | 23000   | -8100      | -7.1       | -6000      |
| <b>Tris</b>           | 230000  | -16000     | -29        | -7300      |

Table 2.12 – G6 Dendron Binding Thermodynamic Parameters for 1<sup>st</sup> Binding Site

When comparing the trends in the G6 dendrimer, we see several interesting phenomena. The affinity constants of the anionic dendrons increase as the number of charges increases with the exception of the meta derivative which shows a binding affinity that is much greater than any of the other dendrons. The large difference in the affinity constant is driven by a higher entropy contribution. The anionic structure likely binds with the dendrimer without a concomitant loss of flexibility as it binds. Similarly, the enthalpic contributions increased linearly as the total number of charges increases on the dendron. With the G6 dendrimer and its larger size, the anionic dendron arms can interact with the cationic surface of the dendrimer no matter their orientation leading to strong enthalpy. As such, the  $\Delta H$  values increase almost doubling from the benzyl to the

para and finally to the tris. The  $\Delta H$  value of the meta does not quite double from the benzyl dendron (2.29) but the smaller increase is compensated by the concurrent increase in the  $\Delta S$ . When the changes in entropy are compared, an inverse but similar trend is observed. The entropy becomes increasingly unfavorable as the dendrons increase in size with the tris dendron (2.33) being highly entropically unfavorable. The meta is also an outlier from the overall entropy trend of the other dendrons as the meta is more favorable by a significant amount than any of the other dendrons studied.

The cooperativity of the system shows a similar trend as the generations of dendrimers. This generation shows a highly negative cooperativity overall. The overall cooperativity is driven by the entropy component that also shows highly negative cooperativity. The enthalpy contributions indicate either positive, or are very slightly negative cooperativity compared to the meta dendron (2.31) which showed slightly less cooperativity than the other dendrons.

| All values in cal/mol  | K     | $\Delta H$ | $\Delta S$ | $\Delta G$ |
|------------------------|-------|------------|------------|------------|
| Meta - Benzyl + Benzyl | -2000 | -2500      | 550        | -2000      |
| Para - Benzyl + Benzyl | -5100 | -470       | -4600      | -5100      |
| Tris - Benzyl x3       | -9300 | 3100       | -12000     | -9300      |
| Tris - Benzyl + Meta   | -7300 | 5600       | -13000     | -7300      |
| Tris - Benzyl + Para   | -4200 | 3500       | -7700      | -4200      |

Table 2.13 – G6 Dendron Binding Cooperativity Values for 1<sup>st</sup> Binding Site

The second binding event for these dendrimers also shows weak binding with a small affinity constant of approximately  $10^4$  with a weak enthalpic and stronger entropic contribution to the binding. Additionally, the stoichiometric values of these second

binding events showed the binding of more anionic dendrons than could physically fit around the dendrimer. As such, these values should be considered highly suspect, and only the general trend is explored rather than a specific value.

| All values in cal/mol | K     | $\Delta H$ | $\Delta S$ | $\Delta G$ |
|-----------------------|-------|------------|------------|------------|
| <b>Benzyl</b>         | 72    | -1600      | 3.1        | -2500      |
| <b>Meta</b>           | 11000 | -1600      | 8.3        | -5500      |
| <b>Para</b>           | 22000 | -9800      | -13        | -5900      |
| <b>Tris</b>           | 42000 | -1400      | 17         | -6300      |

Table 2.14 – G6 Dendron Binding Thermodynamic Parameters for 2<sup>nd</sup> Binding Site

As was observed in the first binding event, an outlier within the trend was observed. In the second set of binding events, the para dendron (**2.32**) showed a more favorable enthalpy and unfavorable entropy while the other dendrons show only a weak  $\Delta H$  contribution to the binding with a favorable  $\Delta S$  contribution, which drives the binding. The relative  $\Delta H$  values are all similar but the  $\Delta S$  becomes more favorable as the size of the dendron increases, corresponding to the release of water and other anions from the dendrimer surface.

Finally, the overall cooperativity of this system shows that the only dendron-dendrimer system with positive cooperativity is the meta and para dendron (**2.31-2.32**) combinations. Given the highly varied nature of the anionic dendron binding and the fitting algorithms, these positive cooperativity measurements



| All values in cal/mol  | K     | $\Delta H$ | $\Delta S$ | $\Delta G$ |
|------------------------|-------|------------|------------|------------|
| Meta - Benzyl + Benzyl | 480   | -1600      | 630        | 480        |
| Para - Benzyl + Benzyl | 870   | 6600       | -5700      | 870        |
| Tris - Benzyl x3       | -1300 | -3400      | 2100       | -1300      |
| Tris - Benzyl + Meta   | -1800 | -1800      | 1500       | -1800      |
| Tris - Benzyl + Para   | -2200 | -10000     | 7900       | -2200      |

Table 2.15 – G6 Dendron Binding Cooperativity Values for 2<sup>nd</sup> Binding Site

should be treated with extreme caution. The tris dendron (**2.33**) with the G6 dendrimer showed the traditional negative cooperativity of the other systems. Furthermore, the majority of the cooperativity in this system arises from the positive entropy contributions with a slightly negative contribution from the enthalpy opposite from all the other dendrimer dendron pairs. The cooperativity values for the second binding site with the G6 dendrimer tend to be much closer to zero than the other combinations, but, given the weaker fit of the isotherms, these calculations should not be taken as definitive proof of positive cooperativity.

### 2.3.9 Interactions of the Dendron with G7 Dendrimer

The final set of ligands was analyzed with the G7 dendrimer. This generation shows a similar pattern of increasing binding affinity with the para derivative being an outlier from the general trend, even though this dendron is still a stronger binder than the benzyl derivatives. The enthalpic components show a strong contribution to the binding affinity with entropic contributions being unfavorable. Again, the meta dendron (**2.31**) shows a slightly different trend than the others with a slightly less favorable enthalpy, but

the meta's entropy is much more favorable than the other regioisomers. This relationship is similar to the trend that was observed with the G6 dendrimer where the enthalpy was less than for the other regioisomer with favorable entropy in comparison. These two systems show that the meta derivative has similar binding interactions for the two generations. The dendron-dendrimer system also highlights that the meta dendron (**2.31**) has a unique binding mode compared to the other regioisomers. The entropy values were much greater and extremely favorable compared to all of the other generations of dendrimer. The larger size of the G7 dendrimer coupled with the binding of the anions does not lead to as substantially restricted rotational motions, while the binding frees additional counterions and the water shell around the dendrimer. With the large dendrimer size, the solvent shell around the dendrimer itself likely becomes highly ordered, and the binding of the anions releases that ordered hydration shell increasing the overall entropy of the system upon the anion binding. This phenomenon causes the entropy component to dominate the binding interactions for this generation.

| All values in cal/mol | K     | $\Delta H$ | $\Delta S$ | $\Delta G$ |
|-----------------------|-------|------------|------------|------------|
| <b>Benzyl</b>         | 3700  | -75000     | -240       | -4900      |
| <b>Meta</b>           | 28000 | -8700      | -9         | -6100      |
| <b>Para</b>           | 11000 | -62000     | -190       | -5500      |
| <b>Tris</b>           | 44000 | -33000     | -91        | -6300      |

Table 2.16 – G7 Dendron Binding Thermodynamic Parameters for 1<sup>st</sup> Binding Site

Unlike the other dendrimer systems, the cooperativity seems to be driven by the enthalpic and not the entropic contributions. In this case, the system displays negative enthalpic contribution as the values of  $\Delta H$  are similar for all of the generations of

dendrimers. A likely explanation for these similar enthalpic values arises from the large size of the generation 7 dendrimer. The size of the dendrimer is large enough and contains so many functional groups that it models a solid sphere of charge, and thus the orientation of the anionic groups no longer matters as much. The positive entropy cooperativity arises from more favorable entropic contributions, but the overall cooperativity still remains negative. The absolute value of the cooperativity term was similar compared to all of the other systems despite the larger values of entropy and enthalpy. The binding mode of this generation shows the largest increase in the values of the thermodynamic parameters, but the trends as the generations increase show only a small increase in the thermodynamic values.

| All values in cal/mol  | K     | $\Delta H$ | $\Delta S$ | $\Delta G$ |
|------------------------|-------|------------|------------|------------|
| Meta - Benzyl + Benzyl | -3700 | -140000    | 140000     | -3700      |
| Para - Benzyl + Benzyl | -4200 | -89000     | 84000      | -4200      |
| Tris - Benzyl x3       | -8300 | -192830    | 180000     | -8300      |
| Tris - Benzyl + Meta   | -4600 | -51000     | 46000      | -4600      |
| Tris - Benzyl + Para   | -4000 | -100000    | 100000     | -4000      |

Table 2.17 – G7 Dendron Binding Cooperativity Values for 1<sup>st</sup> Binding Site

Finally, when we examine the values of the second binding event of the G7 dendrimers, these binding events show decreased affinity constants compared to the first binding constant. In this binding event, we see weaker enthalpic contributions as well as weaker entropy than the first binding model. In this case, the para showed a lower affinity constant than the other systems and had a positive enthalpic penalty but was driven by the strongly favorable entropy. This generation of dendrimer contains 512

terminal amines making the dendrimer highly charged. The fact that the dendrimer is so highly charged makes the enthalpic binding of the second para dendrons (2.32) unusual. This dendron's positive enthalpic measurements are the only positive enthalpic measurements of any of the dendron binding events. Given this reversal, this feature is likely not driven by the electrostatic complementarity but by another phenomenon, like hydrophobic attraction of the benzyl core of the dendron to the dendrimer's inner shell. Furthermore, the large enthalpic values for the other dendrons lead to the hypothesis that the charge density of the system is still high despite the first binding events leaving the dendrimer still highly charged enough to allow strong electrostatic attraction. The entropy for the systems are still unfavorable, meaning the system is likely losing some amount of flexibility upon the dendron binding. All of the systems show favorable binding despite the different interaction modes between the dendrons.

| All values in cal/mol | K     | $\Delta H$ | $\Delta S$ | $\Delta G$ |
|-----------------------|-------|------------|------------|------------|
| <b>Benzyl</b>         | 2100  | -18000     | -46        | -4500      |
| <b>Meta</b>           | 21000 | -43000     | -120       | -5900      |
| <b>Para</b>           | 9200  | 17000      | 74         | -5400      |
| <b>Tris</b>           | 26000 | -23000     | -55        | -6000      |

Table 2.18 – G7 Dendron Binding Thermodynamic Parameters for 2<sup>nd</sup> Binding Site

Finally, we can look at the cooperativity of this second binding event for the G7 dendrimer and the origins of its driving forces. Again, the overall cooperativity of the system showed negative cooperativity, but the driving force was different from that of the other dendrimers. In the G7 dendrimer, negative cooperativity arises from negative enthalpic cooperativity that has been tempered by a positive entropic cooperativity.

Unlike the other generations, G7 is much larger, and thus the molecular motions and the solvent sphere around the dendrimer play a larger role in the binding interactions than the electrostatic complementarity. The previous generations show a positive or slightly negative cooperativity of enthalpy, with negative cooperativity of entropy making the electrostatic complementarity of the dendrimer and dendron the most important contribution to the binding event.

| All values in cal/mol  | K     | $\Delta H$ | $\Delta S$ | $\Delta G$ |
|------------------------|-------|------------|------------|------------|
| Meta - Benzyl + Benzyl | -3200 | 6720       | -9877.69   | -3200      |
| Para - Benzyl + Benzyl | -3600 | -53000     | 49000      | -3600      |
| Tris - Benzyl x3       | -7500 | -32000     | 25000      | -7500      |
| Tris - Benzyl + Meta   | -4400 | -39000     | 34000      | -4400      |
| Tris - Benzyl + Para   | -3900 | 21000      | -25000     | -3900      |

Table 2.19 – G7 Binding Cooperativity Values for 2<sup>nd</sup> Binding Site

### 2.3.10 Overall Dendron – Dendrimer Binding Interaction Characteristics

When we look at how each of the different generations' binding parameters change with a specific dendron, a few notable characteristic can be observed. Comparing the benzyl dendron (2.29), the values of enthalpy increase as the dendrimer generation increases, likely due to stronger electrostatic attraction of the larger dendrimers as those generations have a larger number of total charges per dendrimer. Furthermore, the entropy values become increasingly unfavorable as the generation increases. In the larger generations, the binding of the dendron leads to a more rigid anion upon binding, preventing the rotation in both the dendron and dendrimer, thus losing its rotational freedom in its outer branches. Furthermore, the G7 entropy value decreases significantly

compared to the other generations. In this case, the outer solvent shell of the dendrimer must become more highly ordered as the dendron binds. This increase in order can be rationalized since the cationic surface is being quenched with an anionic dendron that then presents a hydrophobic face (i.e. the dendrimer's benzyl core) to the solvent creating a more ordered solvent shell.

When exploring trends between the other anionic dendrons, no overall patterns can be observed between the different generations. The lack of an overall pattern is likely due to the multiple types of interactions that occur between the different generations' size, total number of functional groups, and total number of charges. Furthermore, as the dendrimers increase in size, the dendrons have more surface area to interact with, and the binding can occur through multiple different modes. Thus, the lack of singular binding contacts makes the interactions more difficult to interpret based upon the type of dendron and prevents the development of a single trend of cooperativity.

### **2.3.11 Entropy-Enthalpy Compensation**

We also explored the entropy-enthalpy compensation of the overall system. If entropy (as  $-T\Delta S$ ) is plotted against enthalpy, the resultant graph shows a straight line. The points made up of each dendrimer and dendron complex shows a strong linear correlation with an  $R^2$  value of higher than 0.998 with only one point appearing to be somewhat of an outlier from the other systems. The outlier point is the meta system with the G6 dendrimer. This combination also showed the highest affinity constant by more than an order of magnitude, which

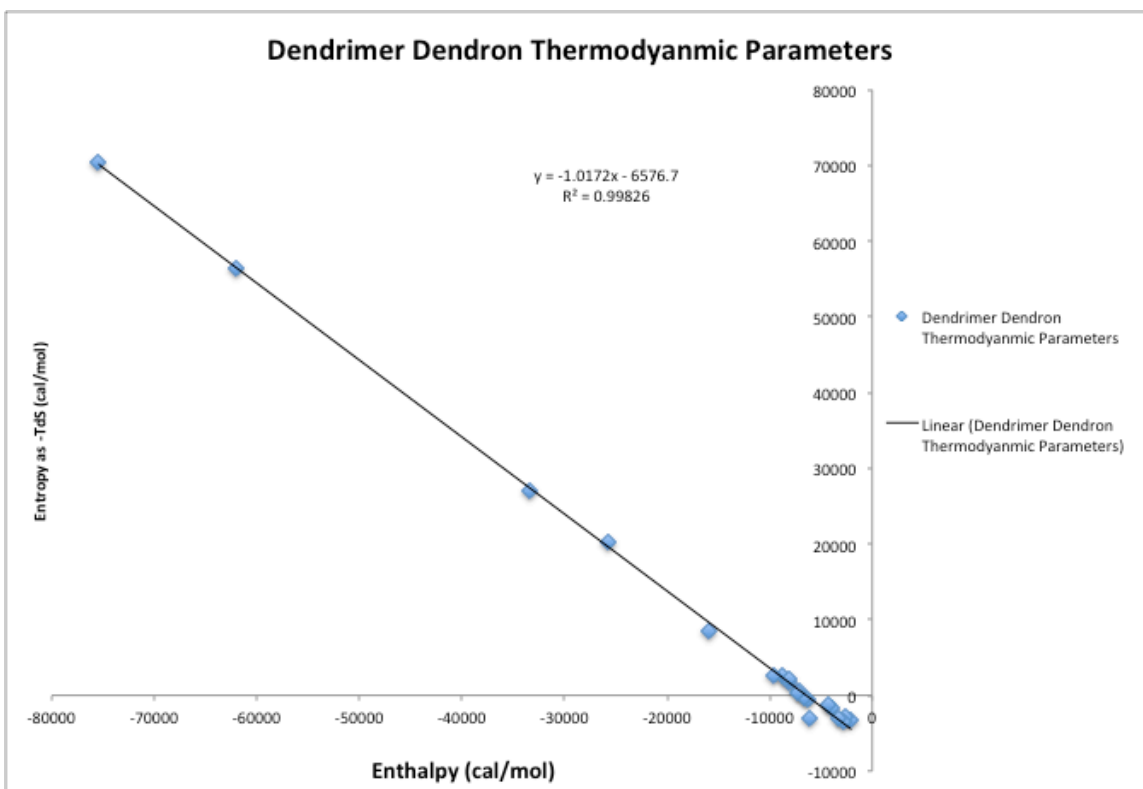


Figure 2.8 – Dendrimer Dendron System Enthalpy Entropy Compensation Graph with a corresponding trend line.

probably explains why the system is an outlier. Additionally, the majority of the systems are grouped together, but both the larger systems with the G7 dendrimer of the other generations and the tris dendron (2.33) appear earlier on the trend line further to the left of where the majority of the systems are found. Each of these systems have much larger values of each of their thermodynamic parameters but still maintain a similar type of compensation. Furthermore, the slope of the line is approximately one meaning that the tradeoff between enthalpy and entropy completely offset each other.

Furthermore, the values of the cooperativity obtained for each of the systems which gives a linear line, too. The system gain shows complete offset of entropy to compensate for enthalpic gains. Because of this fact, the overall Gibbs free energy of the

systems show similar values of approximately 6 kcal/mol for each system with the average difference for any pair of dendrimer and dendron of approximately 2 kcal/mol. The plot of the cooperativity values is shown in Figure 2.9.

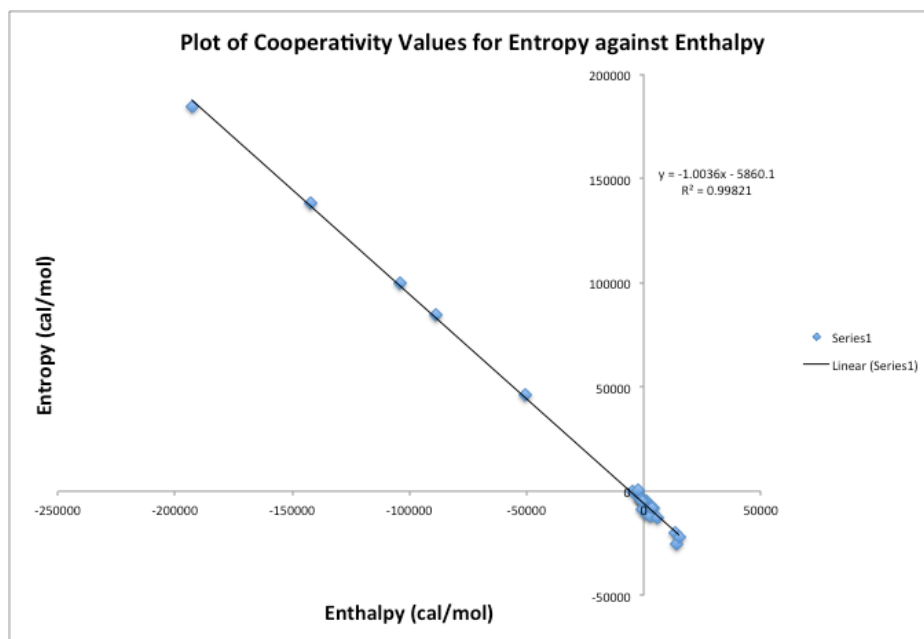


Figure 2.9 – Plot of Cooperativity values for enthalpy against the cooperativity value for entropy for all of the dendron-dendrimer pairs.

### 2.3.12 General Lessons From our Analysis

While this report highlights a large amount of data, a few general lessons among the data can be learned. First, all of the dendrimer-dendron systems experience negative cooperativity. The origins of this cooperativity vary and provide us with an important lesson. The driving force for the cooperativity among the smaller generations of dendrimers is primarily entropic in nature. In these cases, both the dendrimer and dendrons form stronger bonds with less residual motion in each molecule. These complexes also tend to form stronger bonds making the enthalpic contribution relatively thermoneutral.



Some of the intermediate dendrimers can form aggregates or higher order structures, particularly with the para dendron (2.32). These aggregates lead to thermodynamic parameters distinct from the trends observed with the other regioisomers of the dendron. These structures also hamper the development of generation to generation trends.

Finally, as the dendrimers grow in size, the negative cooperativity of the assembly process tends to shift from being driven by entropic contributions to enthalpic ones. The larger dendrimers form less rigid complexes retaining some of their inherent molecular motions, and the larger generations have a more organized structure and hydration sphere which is broken up when the dendron binds.

## **2.4 CONCLUSIONS**

Finally, after analysis of the system, a few overarching conclusions can be reached. The system appears overall to exhibit negative cooperativity in all generations and with all dendrons. Furthermore, the smaller generations show either positive or slightly negative enthalpic cooperativity but negative entropy, which dominates the overall cooperativity. The largest generation shows an opposite trend where the overall cooperativity remains negative, but the cooperativity is driven by positive entropy cooperativity tempered by negative enthalpy cooperativity. These trends tend to be somewhat generalizable, but the large generations, multiple binding modes, and the multiple interactions, make these systems difficult to analyze beyond broad classifications and general trends.

## **2.5 FUTURE WORK**

Further studies could provide more definitive and quantifiable analysis of the cooperativity. In order to develop more quantitative models, similar dendrons with

anionic groups could be synthesized to study if they show similar patterns. Furthermore, the use of different dendrimers that bear anionic surface groups should be studied to identify if the system behaves differently based upon interactions with the opposite charges. Finally, the use of DNA instead of carboxylate-based anionic dendrons would allow for a more direct comparison of the dendrimers to the DNA binding proteins histones. These studies would be used to augment the studies outlined in this chapter and provide a more detailed and complete understanding of the multivalent binding of polyanionic groups to cationic dendrimers and the origins of cooperativity in these systems.

## **2.6 EXPERIMENTAL METHODS**

All chemicals except triethylamine were purchased from Aldrich and used as received. Triethylamine was purchased from Fisher Scientific and dried over molecular sieves. All solvents used were purified using a VAC solvent purification system. The trizma dendron piece was synthesized and purified according to literature procedures. All NMR spectra were collected using chloroform-d from Cambridge Isotope Labs and spectra were recorded using a 400 MHz Varian NMR with a robotic arm through The UT Austin NMR facility. All mass spectra were obtained through electrospray ionization mass spectrometry at the UT Austin Mass Spectrometry facility. Both high and low resolution spectra were obtained for the compounds with low resolution being obtained through a Agilent liquid chromatography mass spectrometry instrument after a 4 minute gradient.

All tButyl protected dendrons were synthesized using a similar procedure based upon the same literature procedure that was used to make the dendron. In a solution of dry THF, 1.1 equivalents per acid chloride of tButyl protected trizma dendron piece were

added with 1.1 equivalents per acid chloride of triethylamine to the solution. With moderate stirring, the corresponding acid chloride was added to the solution and allowed to stir for about 2 hours. After dilution of the reaction with DCM, the solution was washed with 1 M HCl, brine, and then distilled water. The resultant solvent was removed under reduced pressure to leave a clear oily substance. The substance was purified using a CombiFlash instrument using a reverse phase C18 column using an acetonitrile/water gradient. The instrument used a gradient with a 1 minute hold at 100% water, a 5 minute ramp to 50% acetonitrile/50% water with a 3 minute hold at that ratio, a 5 minute ramp to 80% acetonitrile/20% water with a 3 minute hold at that ratio followed by a 5 minute ramp until 100% acetonitrile with a 5 minute hold and finally a 1 minute return to 100% water.

Benzyl derivative – <sup>1</sup>H NMR – 7.65 (2H, benzyl, d), 7.52 (1H, benzyl, t), 7.43 (2H, benzyl, t), 6.75 (1H, NH, s), 3.85 (6H, CH<sub>2</sub>, s), 3.75 (6H, CH<sub>2</sub>, t), 2.61 (6H, CH<sub>2</sub>, t), 1.09 (9H, -CH<sub>3</sub>, s) Mass Spectra – M+H<sup>+</sup> 610.35

Meta derivative – <sup>1</sup>H NMR – 8.18 (1H, benzyl, t), 7.87 (2H, benzyl, dd), 7.43 (1H, benzyl, t), 6.66 (2H, NH, s), 3.83 (12H, CH<sub>2</sub>, s), 3.68 (12H, CH<sub>2</sub>, t), 2.46 (12H, CH<sub>2</sub>, t), 1.40 (18H, -CH<sub>3</sub>, s) Mass Spectra – M+H<sup>+</sup> 1141.66

Para derivative – <sup>1</sup>H NMR – 7.81 (4H, benzyl, s), 6.66 (2H, NH, s), 3.84 (12H, CH<sub>2</sub>, s), 3.68 (12H, CH<sub>2</sub>, t), 2.45 (12H, CH<sub>2</sub>, t), 1.56 (18H, -CH<sub>3</sub>, s) Mass Spectra – M+H<sup>+</sup> 1141.66

Tris derivative – <sup>1</sup>H NMR – 8.14 (3H, benzyl, s), 6.66 (2H, NH, s), 3.66 (18H, CH<sub>2</sub>, s), 3.32 (18H, CH<sub>2</sub>, t), 2.46 (18H, CH<sub>2</sub>, t), 1.45 (27H, -CH<sub>3</sub>, s) Mass Spectra – M+H<sup>+</sup> 1672.96

After the dendrons with the tButyl groups were synthesized, the tButyl groups were cleaved to generate the free acids. Using 9.5 mL of trifluoroacetic acid, 0.25 mL triisopropylsilane, and 2.75 mL of water, the tButyl groups were cleaved. After the addition of the solution, the resultant mixture was stirred overnight. The resultant solution was removed under reduced pressure to leave a sticky residue. The resultant mixture was purified using a CombiFlash C18 reverse phase column with a water/acetonitrile gradient. The purification gradient started with 1 minute of 0% water, a ramp to 30% acetonitrile over five minutes, hold at 30% acetonitrile for 3 minutes, ramp to 50% acetonitrile over five minutes, hold at 50% acetonitrile for 3 minutes and then ramp to 100% acetonitrile over seven minutes, hold at 100% acetonitrile for three minutes before a 1 minute return to 100% water. The compound was a gel like solid.

Benzyl derivative – Yield 54.5% –  $^1\text{H}$  NMR (400 MHz, DMSO- $d_6$ ) – 7.70 (2H, benzyl, d), 7.48 (1H, benzyl, t), 7.40 (2H, benzyl, t), 3.66 (6H,  $\text{CH}_2$ , s), 3.57 (6H,  $\text{CH}_2$ , t), 2.41 (6H,  $\text{CH}_2$ , t)  $^{13}\text{C}$  NMR (100 MHz, DMSO- $d_6$ ) 173.08, 167.09, 135.62, 131.45, 128.62, 127.65, 68.47, 67.13, 60.61, 35.04 Mass Spectra –  $\text{M}+\text{H}^+$  442.16

Meta derivative – Yield 82.4% –  $^1\text{H}$  NMR (400 MHz, DMSO- $d_6$ ) – 8.02 (1H, benzyl, t), 7.81 (2H, benzyl, dd), 7.47 (1H, benzyl, t), 3.66 (12H,  $\text{CH}_2$ , s), 3.57 (12H,  $\text{CH}_2$ , t), 2.40 (12H,  $\text{CH}_2$ , t), 1.40 (18H,  $-\text{CH}_3$ , s)  $^{13}\text{C}$  NMR (100 MHz, DMSO- $d_6$ ) 173.05, 166.77, 135.56, 130.20, 128.58, 126.96, 68.37, 67.13, 60.82, 35.01 Mass Spectra –  $\text{M}+\text{H}^+$  805.28

Para derivative – Yield 85.2% –  $^1\text{H}$  NMR (400 MHz, DMSO- $d_6$ ) – 7.75 (4H, benzyl, s), 6.66 (2H, NH, s), 3.66 (12H,  $\text{CH}_2$ , s), 3.57 (12H,  $\text{CH}_2$ , t), 2.40 (12H,  $\text{CH}_2$ , t)  $^{13}\text{C}$  NMR (100 MHz, DMSO- $d_6$ ) 173.09, 166.51, 137.67, 127.60, 68.38, 67.14, 60.77, 35.04 Mass Spectra –  $\text{M}+\text{H}^+$  805.28

Tris derivative – Yield 36.0% –  $^1\text{H}$  NMR (400 MHz, DMSO- $d_6$ ) – 8.14 (3H, benzyl, s), 3.67 (18H,  $\text{CH}_2$ , s), 3.58 (18H,  $\text{CH}_2$ , t), 2.41 (18H,  $\text{CH}_2$ , t) Mass Spectra –  $\text{M}+\text{H}^+$  1672.96

ITC spectra were collected using a VP-ITC manufactured by MicroCal. For these studies, the anion was titrated into a buffered solution of dendrimer. Each solution was prepared in a 50 mM HEPES buffer at pH 7.4 and the resultant pH of the solution was measured. Since both of the macromolecules contain numerous acidic or basic groups, the solutions often exceeded the buffering capacity and the pH was manually adjusted with dilute HCl or NaOH until the pH was within 0.1 unit of the starting buffer pH. In order to prevent signals from the dilution of dendrimers, the macromolecule was included in both solutions. The dendrimer was included at various concentrations depending on the size starting with 100  $\mu\text{M}$  for G3 and finally with 10  $\mu\text{M}$  for the G7. Using 5  $\mu\text{L}$  injections, 60 sequential injects were carried out with a 3 minute spacing between injections and 300 rpm stirring of the syringe. The integral of the amount of heat released upon binding was plotted the molar ratio of the ligand to the macromolecules. The resultant graph was fitted to a line of best fit from which  $n$ ,  $K_{\text{eq}}$ ,  $\Delta\text{H}$  and  $\Delta\text{S}$  can be obtained. Most of the dendrimer titrations were fitted to a two binding site model which treats the binding of the anionic dendrons as if they have two unique binding modes. Larger anionic dendrons and larger generations of dendrimers were fit with a sequential binding site model. All thermodynamic parameters obtained from the ITC traces have an average error of 20%.

## 2.7 REFERENCES

- (1) Lundquist, J. J.; Toone, E. J. The Cluster Glycoside Effect. *Chemical Reviews* **2002**, *102*, 555–578

- (2) H. Williams, D.; S. Westwell, M. Aspects of weak interactions. *Chemical Society Reviews* **1998**, *27*, 57–64
- (3) Cram, D. J. The design of molecular hosts, guests, and their complexes. *Science* **1988**, *240*, 760–767
- (4) Archer, E. A.; Krische, M. J. Duplex Oligomers Defined via Covalent Casting of a One-Dimensional Hydrogen-Bonding Motif. *Journal of the American Chemical Society* **2002**, *124*, 5074–5083
- (5) Wiskur, S. L.; Lavigne, J. J.; Metzger, A.; Tobey, S. L.; Lynch, V.; Anslyn, E. V Thermodynamic Analysis of Receptors Based on Guanidinium/Boronic Acid Groups for the Complexation of Carboxylates,  $\alpha$ -Hydroxycarboxylates, and Diols: Driving Force for Binding and Cooperativity. *Chemistry – A European Journal* **2004**, *10*, 3792–3804
- (6) Mammen, M.; Choi, S.-K.; Whitesides, G. M. Polyvalent Interactions in Biological Systems: Implications for Design and Use of Multivalent Ligands and Inhibitors. *Angewandte Chemie International Edition* **1998**, *37*, 2754–2794
- (7) Johnson, C. R.; Ownby, D. W.; Gill, S. J.; Peters, K. S. Oxygen binding constants and stepwise enthalpies for human and bovine hemoglobin at pH 7.6. *Biochemistry* **1992**, *31*, 10074–10082.
- (8) Philo, J. S.; Lary, J. W. Kinetic investigations of the quaternary enhancement effect and alpha/beta differences in binding the last oxygen to hemoglobin tetramers and dimers. *Journal of Biological Chemistry* **1990**, *265*, 139–143.
- (9) Jencks, W. P. On the attribution and additivity of binding energies. *Proceedings of the National Academy of Sciences* **1981**, *78*, 4046–4050
- (10) Christensen, T.; Gooden, D. M.; Kung, J. E.; Toone, E. J. Additivity and the Physical Basis of Multivalency Effects: A Thermodynamic Investigation of the Calcium EDTA Interaction. *Journal of the American Chemical Society* **2003**, *125*, 7357–7366
- (11) Hughes, A. D.; Anslyn, E. V A cationic host displaying positive cooperativity in water. *Proceedings of the National Academy of Sciences* **2007**, *104*, 6538–6543
- (12) Kitov, P. I.; Bundle, D. R. On the Nature of the Multivalency Effect: A Thermodynamic Model. *Journal of the American Chemical Society* **2003**, *125*, 16271–16284
- (13) Breslow, R.; Greenspoon, N.; Guo, T.; Zarzycki, R. Very strong binding of appropriate substrates by cyclodextrin dimers. *Journal of the American Chemical Society* **1989**, *111*, 8296–8297
- (14) Chekmeneva, E.; Hunter, C. A.; Packer, M. J.; Turega, S. M. Evidence for Partially Bound States in Cooperative Molecular Recognition Interfaces. *Journal of the American Chemical Society* **2008**, *130*, 17718–17725

- (15) Searle, M. S.; Westwell, M. S.; Williams, D. H. Application of a generalised enthalpy-entropy relationship to binding co-operativity and weak associations in solution. *Journal of the Chemical Society, Perkin Transactions 2* **1995**, 141–151
- (16) Rao, J.; Lahiri, J.; Weis, R. M.; Whitesides, G. M. Design, Synthesis, and Characterization of a High-Affinity Trivalent System Derived from Vancomycin and l-Lys-d-Ala-d-Ala. *Journal of the American Chemical Society* **2000**, *122*, 2698–2710
- (17) Lee, Y. C.; Lee, R. T. Carbohydrate-Protein Interactions: Basis of Glycobiology. *Accounts of Chemical Research* **1995**, *28*, 321–327
- (18) Rekharsky, M.; Inoue, Y.; Tobey, S.; Metzger, A.; Anslyn, E. Ion-Pairing Molecular Recognition in Water: Aggregation at Low Concentrations That Is Entropy-Driven. *Journal of the American Chemical Society* **2002**, *124*, 14959–14967
- (19) Tobey, S. L.; Anslyn, E. V Studies into the Thermodynamic Origin of Negative Cooperativity in Ion-Pairing Molecular Recognition. *Journal of the American Chemical Society* **2003**, *125*, 10963–10970
- (20) Linton, B. R.; Goodman, M. S.; Fan, E.; Van Arman, S. A.; Hamilton, A. D. Thermodynamic Aspects of Dicarboxylate Recognition by Simple Artificial Receptors. *The Journal of Organic Chemistry* **2001**, *66*, 7313–7319
- (21) Badjić, J. D.; Nelson, A.; Cantrill, S. J.; Turnbull, W. B.; Stoddart, J. F. Multivalency and Cooperativity in Supramolecular Chemistry. *Accounts of Chemical Research* **2005**, *38*, 723–732
- (22) Yang, R. C. K.; Huang, J. T. B.; Chien, S.-C.; Huang, R.; Jeng, K.-C. G.; Chen, Y.-C.; Liao, M.; Wu, J.-R.; Hung, W.-K.; Hung, C.-C.; Chen, Y.-L.; Waring, M. J.; Sheh, L. Energetic studies on DNA-peptide interaction in relation to the enthalpy-entropy compensation paradox. *Organic & Biomolecular Chemistry* **2013**.
- (23) Starikov, E.; Nordén, B. Entropy-enthalpy compensation may be a useful interpretation tool for complex systems like protein-DNA complexes: An appeal to experimentalists. *Applied Physics Letters* **2012**.
- (24) Sharp, K. Entropy—enthalpy compensation: Fact or artifact? *Protein Science* **2001**, *10*, 661–667.
- (25) Cornish-Bowden, A. Enthalpy-entropy compensation: a phantom phenomenon. *Journal of Biosciences* **2002**, *27*, 121–26.
- (26) Liu, L.; Guo, Q.-X. Isokinetic Relationship, Isoequilibrium Relationship, and Enthalpy–Entropy Compensation. *Chemical Reviews* **2001**, *101*, 673–696.

- (27) Gelb, R. I.; Lee, B. T.; Zompa, L. J. Hexacyclen complexes of inorganic anions. 2. Bonding forces, structures, and selectivity. *Journal of the American Chemical Society* **1985**, *107*, 909–916.
- (28) Nasief, N. N.; Tan, H.; Kong, J.; Hangauer, D. Water Mediated Ligand Functional Group Cooperativity: The Contribution of a Methyl Group to Binding Affinity is Enhanced by a COO<sup>-</sup> Group Through Changes in the Structure and Thermodynamics of the Hydration Waters of Ligand–Thermolysin Complexes. *Journal of Medicinal Chemistry* **2012**, *55*, 8283–8302.
- (29) Routh, A.; Sandin, S.; Rhodes, D. Nucleosome repeat length and linker histone stoichiometry determine chromatin fiber structure. *Proceedings of the National Academy of Sciences* **2008**, *105*, 8872–8877
- (30) Korolev, N.; Allahverdi, A.; Lyubartsev, A. P.; Nordenskiöld, L. The polyelectrolyte properties of chromatin. *Soft Matter* **2012**, *8*, 9322–9333.
- (31) Fant, K.; Esbjorner, E. K.; Lincoln, P.; Norden, B. DNA Condensation by PAMAM Dendrimers: Self-Assembly Characteristics and Effect on Transcription†. *Biochemistry* **2008**, *47*, 1732–1740
- (32) Pavan, G. M.; Danani, A.; Pricl, S.; Smith, D. K. Modeling the Multivalent Recognition between Dendritic Molecules and DNA: Understanding How Ligand “Sacrifice” and Screening Can Enhance Binding. *Journal of the American Chemical Society* **2009**, *131*, 9686–9694
- (33) Pavan, G. M.; Albertazzi, L.; Danani, A. Ability to Adapt: Different Generations of PAMAM Dendrimers Show Different Behaviors in Binding siRNA. *The Journal of Physical Chemistry B* **2010**, *114*, 2667–2675
- (34) Örberg, M.-L.; Schillén, K.; Nylander, T. Dynamic Light Scattering and Fluorescence Study of the Interaction between Double-Stranded DNA and Poly(amido amine) Dendrimers. *Biomacromolecules* **2007**, *8*, 1557–1563
- (35) Braun, C. S.; Vetro, J. A.; Tomalia, D. A.; Koe, G. S.; Koe, J. G.; Russell Middaugh, C. Structure/function relationships of polyamidoamine/DNA dendrimers as gene delivery vehicles. *Journal of Pharmaceutical Sciences* **2005**, *94*, 423–436
- (36) Coles, D. J.; Yang, S.; Minchin, R. F.; Toth, I. The characterization of a novel dendritic system for gene delivery by isothermal titration calorimetry. *Peptide Science* **2008**, *90*, 651–654
- (37) Jensen, L. B.; Pavan, G. M.; Kasimova, M. R.; Rutherford, S.; Danani, A.; Nielsen, H. M.; Foged, C. Elucidating the molecular mechanism of PAMAM–siRNA dendriplex self-assembly: Effect of dendrimer charge density. *International Journal of Pharmaceutics* **2011**, *416*, 410–418.



- (38) Newkome, G. R.; Kotta, K. K.; Moorefield, C. N. Convenient Synthesis of 1 → 3 C-Branched Dendrons. *The Journal of Organic Chemistry* **2005**, *70*, 4893–4896

## **Chapter 3 – Synthesis and Studies of a Dynamic Multicomponent Assembly with Reversible Covalent Bond Formation Driven by the Coordination of a Metal Ion**

### **3.1 INTRODUCTION**

#### **3.1.1 Goals and Scientific Question**

In this study, the formation of a metal chelating complex through the formation of a reversible covalent bond is explored. The ability to use different pieces to form the multicomponent assembly is shown. Furthermore, the thermodynamic origins of the assembly process were explored and the ability to use different types of heterocycles including the ability to use triazoles. In summary, the goal of the project is to study the ability of different heterocyclic aldehydes and heterocyclic amines to form a tripodal metal chelating complex in the presence of a metal ion.

#### **3.2.1 Reversible Covalent Bond Formation**

One of the hallmarks of chemical intuition that students are exposed to early in their scientific studies is that covalent bonds are strong and not easily broken under ambient conditions. Unfortunately or fortunately, depending on the perspective, this idea is not actually correct. There are numerous examples where covalent bonds can be readily exchangeable at ambient conditions.<sup>1-25</sup>

##### ***3.1.2.1 Disulfide Bond Formation***

The most common covalent bond exchange seen at such conditions is the exchange of disulfide bonds. In biological systems, protein disulfide bonds can shuffle, leading to conformation changes in the protein and causing the protein to have new properties or structures.<sup>1,2</sup> This biological shifting of protein components leads to the

regulation of the protein's function and controls the biological process associated with the protein in question.<sup>3</sup>

The formation of reversible disulfide bonds has also been employed in organic chemistry to create a template-driven dynamic system of catenanes by the Sanders group.<sup>4-7</sup> Using different templating molecules, variable ratios of the catenane mixtures can be obtained based upon the ability to template the resultant structures, and their interactions with the  $\pi$ -donor or  $\pi$ -acceptor components, and how the templating molecules stabilizes those components. Because the molecules can template to and thus recognize molecules in solution, the catenane can be evolved to detect a specific molecule using the evolved

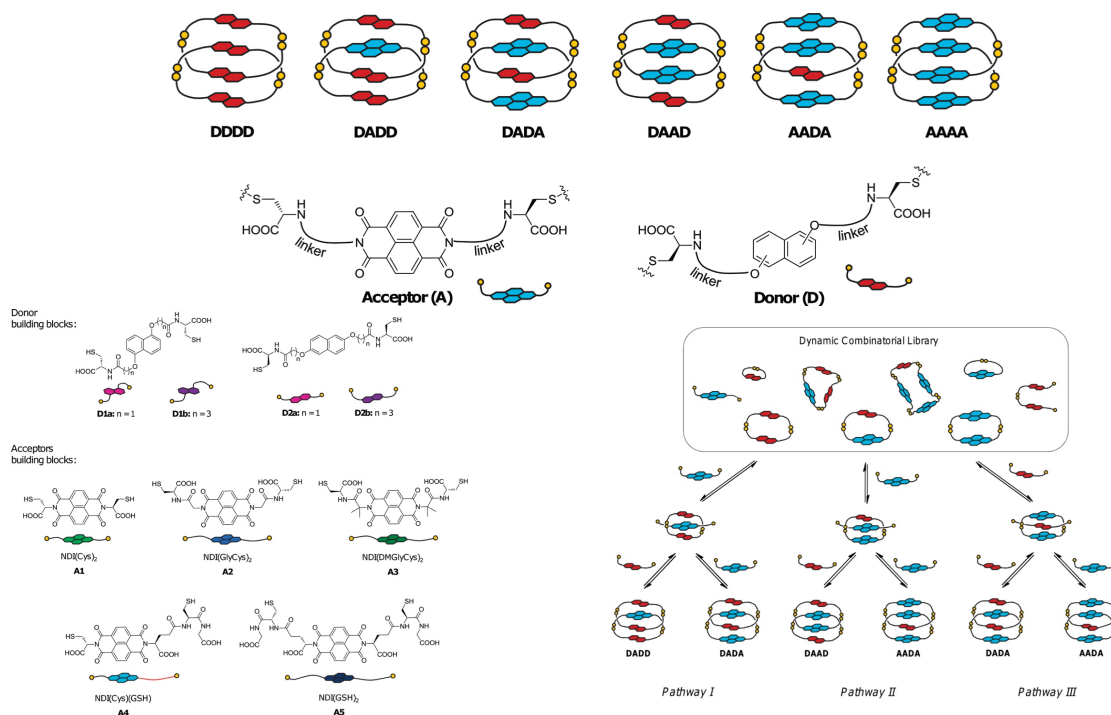


Figure 3.1 – Components and the catenanes formed by the exchange of disulfide bonds in the Sanders system. A wide variety of size structures were synthesized from the library of complex.

catentane as a receptor for that molecule.

Furthermore, disulfide bonds have been explored for use in dynamic combinatorial chemistry for the formation of molecular cages. These cages were templated by aliphatic polyamines, with larger amines leading to the preferential formation of tetrameric and higher order cages that could not be synthesized with the templating polyamine alone. Being able to direct the synthesis to evolve a ligand is a highly sought after ability in supramolecular receptor development.

But disulfide linkages are not without their limitations. A pair of thiols must be present in order to form the linkage, and few common organic molecules have a thiol group, requiring the synthetic modification and design of components for the assembly. Furthermore, the thiols are reactive on their own and will form homodimeric disulfide

bonds in the presence of air, which makes them difficult to work with and store. Finally, even in the systems highlighted, multiple different products were formed *in situ* with the targeted complex only predominating at about 60 or 70% yields.<sup>4</sup>

### 3.1.1.2 Boronic Ester Formation

Boronic acids can react reversibly with diols, catechols, and  $\alpha$ -hydroxyacids to form a boronate ester, even in aqueous systems, making this functional group another commonly exploited covalent bond forming reaction.<sup>8,9</sup> The formation of this ester leads to two new reversible covalent linkages between the two hydroxyl groups of the diol and the boron. This functional group has been utilized in numerous cases to form reversible supramolecular complexes and architectures.

The boronic acid functional group has been exploited by the James and Kubo groups to create molecular capsules for organic cations using a bisboronic acid receptor.<sup>10</sup>

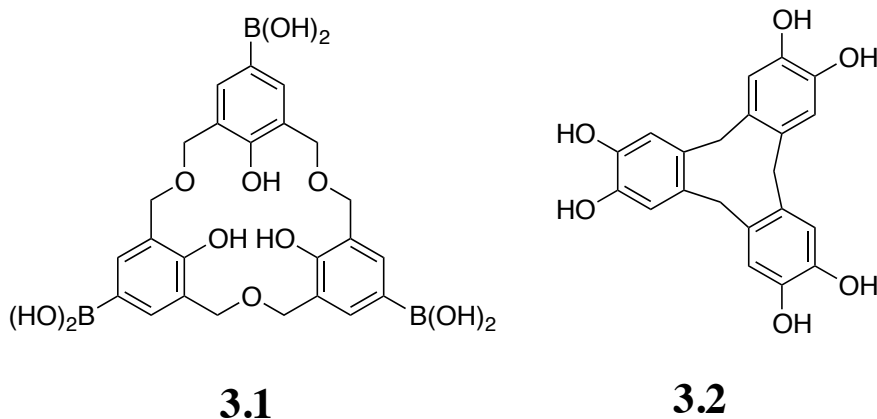
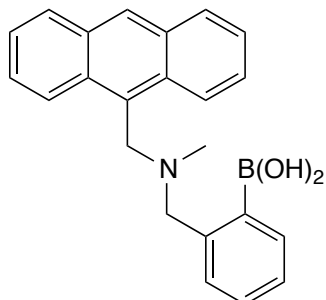


Figure 3.2 – Boronic acid capsule used by the James group to bind alkylamines

In methanol/acetonitrile solutions, a bisphenyl boronic acid ring-like structure binds to a polycatechol ring-like structure to form a cage which can encapsulated charged nitrogens. Furthermore, boronic acids have been used by the James group, our own group and others

to bind numerous different types of saccharides.<sup>8,9,11</sup> In a seminal example, James and Shinkai developed an anthracene derivatized with an ortho-aminomethylphenyl boronic



### 3.3

Figure 3.3 – Seminal sugar receptor developed by James and Shinkai

acid.<sup>11</sup> Upon binding of the sugar, the PET quenching of that amine was decreased, resulting in increased fluorescence. This signal modulation allowed for the detection of sugars in aqueous media. Since this hallmark design, the boronic acid has found wide adoption in other supramolecular structures and receptors.

Our own group has used this moiety to recognize these same functional groups in solution for sensing purposes. Using a boronic acid based receptor, our group has studied the chirality of diols and  $\alpha$ -hydroxyacids by developing systems that can determine the *ee* of the target molecule in solution.<sup>12-14</sup> One of these systems will be explored later in this

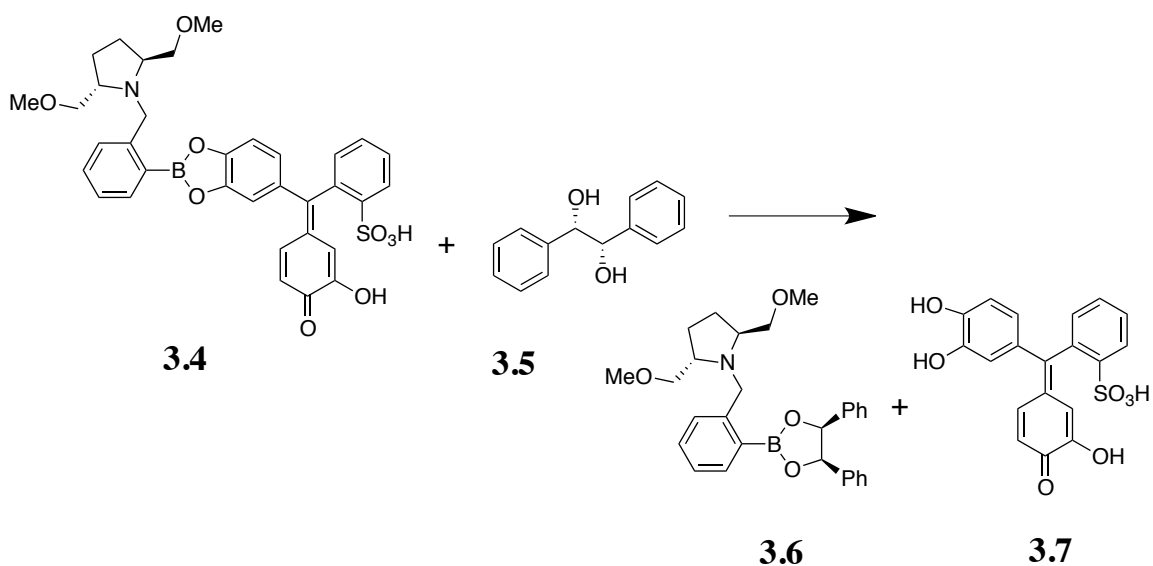


Figure 3.4 – Anslyn group boronic acid based chiral diol eIDA overview where the presence of the diol displaces an indicator to lead to an optical signal

dissertation, as it provides a good background for our current work in the detection of *ee* in chiral thiols. But beyond the determination of chirality, boronic acids have been used by the Anslyn group for the differentiation of polyols, such as

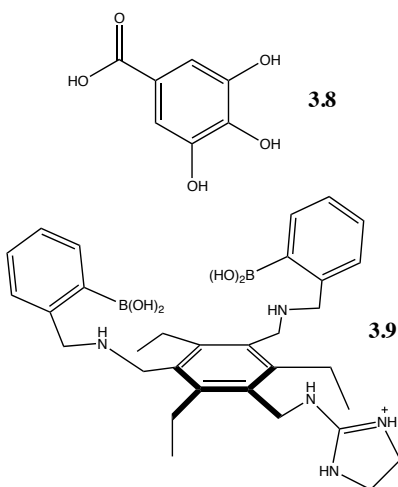


Figure 3.5 – Anslyn group boronic acid receptor that reversibly binds tannins and tannic acid from the aging of Scotch whisky.

tannins found in Scotch whisky, sugars, sugar derivatives, as well as polycarboxylates.<sup>8,9,14-16</sup> In each of these studies, the binding of the boronic acid formed a reversible covalent bond to the target analyte, often in protic media, illustrating another example of the formation of a covalent bond that is dynamic and readily reversible at ambient conditions.

While boronic acids are widely used, they too are not without their disadvantages. First of all, boronic acids often require additional synthesis as the functional group is not a ubiquitous, naturally occurring functional group. Furthermore, boronic acids can be difficult to purify using standard organic chromatographic techniques, such as silica, as they will bind to the media. Finally, the boronic acid primarily pairs with polyols – as cis diols – and  $\alpha$ -hydroxyacids making them only useful with select compounds.

### ***3.1.1.3 Imine Bond Formation***

Finally, the last reversible covalent bond that I want to highlight in this chapter is the formation of imine bonds. Imine bonds, along with structurally similar hydrazones, are amongst the most common reversible covalent bonds that supramolecular chemists use to create a new macromolecule or receptor.<sup>17</sup> In order to form a structure or architecture, only a primary amine and an aldehyde are needed. The amine condenses on an aldehyde to form an imine, or Schiff base, with the concomitant elimination of water. This newly created functional group is readily reversible, particularly if care is not taken to eliminate the water from the reaction.

The construction of several higher-order molecular architectures has been carried out through the formation these types of bonds. In one illustrative example, the Lehn group constructed a molecular strand that twisted upon itself to form a helix based upon the joining of the molecular pieces, through imine and hydrazone bond formation.<sup>18</sup> In



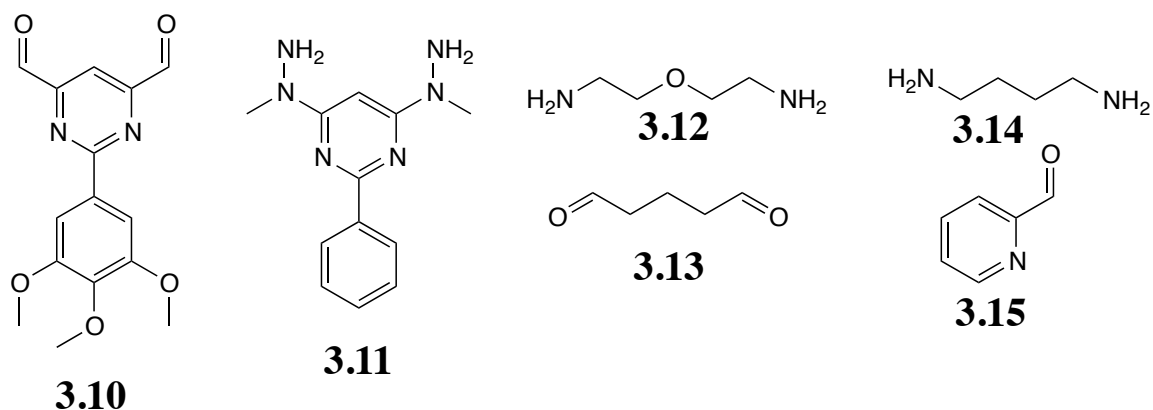


Figure 3.6 – Pieces used by Lehn to create an imine and hydrazone helical polymer

this complex, addition of certain pairs of components over others drove the formation of the molecular strand, while other pairs of components prevented strand elongation and helix formation. By choosing the components and the mixtures to optimize the formation of the helix, the Lehn group was able to greatly amplify the formation of the desired molecular strand, cutting the rate of formation by almost 80%.

Additionally, recent reports by the Mastalerz group and others have shown that 2-to-3 ratio of specific amines and aldehydes can be used to create reversible molecular cages or carcerands.<sup>19,20</sup> When mixing a bis- or tris-aldehyde with a tris- or bis-amine, respectively, a porous molecular cage can be obtained that can absorb small molecules as well as gases for storage.

Furthermore, Cooper published a similar report where a tris-aldehyde and various diamines was able to create a cage like structure that bound numerous small molecules within in its cage structure.<sup>21</sup> Furthermore, the structure could also form catenates or trefoil knots under certain conditions.

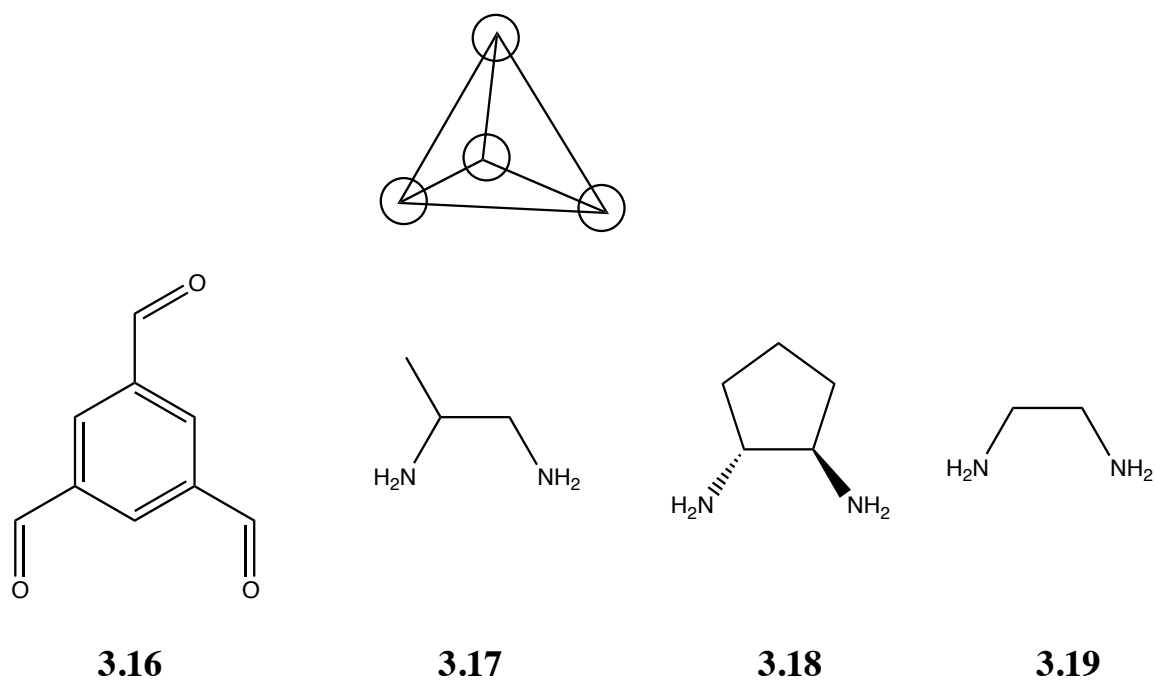
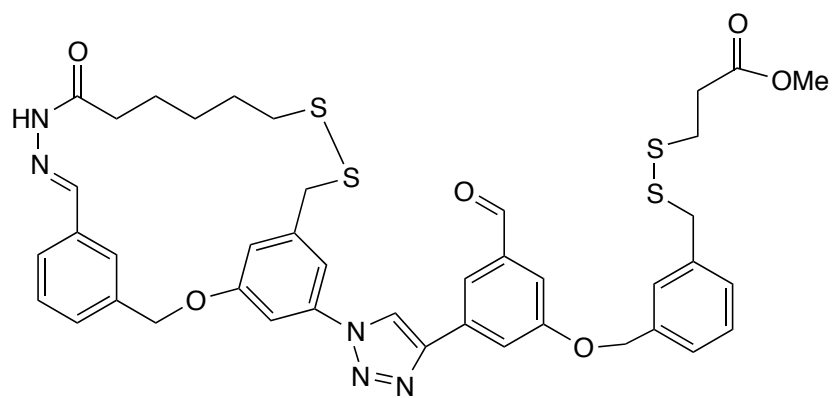


Figure 3.7 – Representative model of Cooper’s cages and the different aldehyde and amines used in that complexes formation

Despite its frequent use in the formation of molecular architectures, imine bonds have also been exploited to accomplish other goals. The Leigh group has used the formation of hydrazone bonds to allow a molecular to move along a reactive “track” of functional groups.<sup>22</sup> The goal of this structure with its hydrazine bond is to design a system for which a external trigger causes the molecule to process. While the molecule



### 3.20

Figure 3.8 – Leigh’s molecular track where the hydrazone hydrolyzes and then reacts with the next aldehyde on the chain. The disulfide then breaks to reform with the next thiol.

moves along the track, the structure ultimately releases some form of biological cargo like a medicine in a targeted location. Our group has used imine bond formation chemistry to enhance the metal chelation of a pyridine ligand, or to generate a nitrogen ortho to a boronic acid, thus generating a CD signal allowing for the measurement of the *ee* of the amine molecules.<sup>23,24</sup>

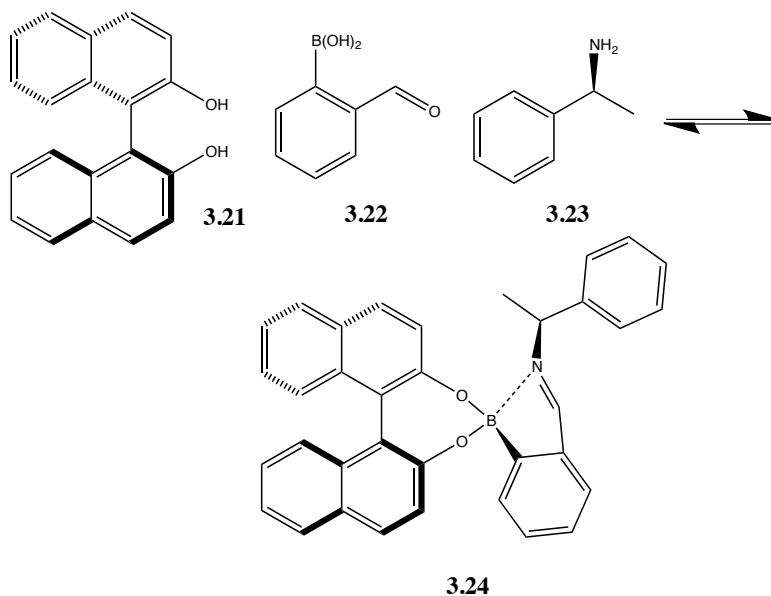


Figure 3.9 – James and Anslyn system for determining *ee* of chiral amines through the formation of an imine bond.

While imines and hydrazones are widely used for the formation of reversible bonds, they have a few disadvantages. The imine bond, and the hydrazone to a lesser degree, is often not very stable in aqueous conditions. Without the rigid exclusion of water, the imine and, sometimes, hydrazone often will not form.<sup>25</sup> Furthermore, their formation is limited in many cases to only aldehydes and primary amines. Although ketones will work, they tend to be significantly slower than the analogous aldehyde, while steric bulk and the formation of quaternary ammonium ions often prevents secondary amines from condensing to form imines.

### 3.1.2 Hemiaminal Bond Formation

While each of these systems has potential applications in the field of supramolecular chemistry, this chapter will highlight the development of a relatively new form of dynamic covalent bond, the hemiaminal. In a hemiaminal, an aldehyde undergoes nucleophilic attack with a secondary amine, stopping at the hemiaminal

intermediate. Normally, with a primary amine, the system undergoes dehydration to form an imine, but with a secondary amine, the loss of water will form a charged iminium ion. The iminium is relatively unstable making the hemiaminal an intermediate on the way to the formation of an unfavored product. In this chapter, we will discuss a new methodology that drives the formation of the hemiaminal because of the formation of a thermodynamic sink when the functionality is formed.

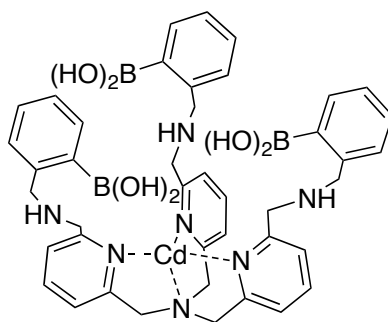
Using metal chelation and the augmentation of the avidity of the ligand system that chelates the metal only when the functionality is formed, a hemiaminal can be formed and isolated at ambient conditions. Using a heterocyclic aldehyde and a secondary amine with two heterocyclic arms, a tripodal ligand system that chelates a metal ion could be generated along with a new carbon-nitrogen bond. This newly formed bond is reversible under ambient conditions and forms an equilibrium mixture of free aldehyde and amine along with the formed complex. In the initial studies, a pyridine was chosen as the model heterocyclic arm but the use of other heterocycles, such as triazoles, as the arms of the secondary amine will be explored as the studies progress. Furthermore, numerous different metals and aldehydes will be explored to increase the potential diversity of this system. This chapter will highlight the details of this new synthetic receptor.<sup>26</sup>

### **3.1.3 Tripodal Ligand Systems**

Using dipicolylamine and pyridine-2-carboxaldehyde as the model reagents, a metal mediated hemiaminal structure forms with a metal chelating tripyridineamine structure. This moiety is a common metal binding unit that has found use as a ligand system for a variety of metal based chemical catalysts.<sup>27,28</sup>

The most common catalytic reaction to use a tripyridine ligand around a metal center is atom transfer radical polymerization (ATRP), which uses these ligand systems to modulate the reactivity of a copper(I) ion center, thus controlling the reaction speed and efficiency.<sup>28-30</sup> Modification of the ligand system can lead to profound changes in the reactivity of the metal center and thus efficiency of the polymerization process. The ability to dynamically construct the ligand could greatly enhance the ability to fine tune polymer synthesis as well as control the length and composition of the formed polymer. The tripyridine ligand system has also been used as a catalyst for click reactions as well as for sensing purposes.

The Anslyn group used a tripyridine ligand system that coordinates to a cadmium ion which had been modified with three boronic acid units, as a method to detect glucose and glucose oxidase activity.<sup>27</sup> The binding of gluconic acid to the receptor caused the displacement of the indicator, pyrocatechol violet, from the binding cavity and thus changed its optical properties. Measuring the change in absorbance of the free indicator as a function of changes in concentration of gluconic acid, a byproduct of glucose oxidase function, the amount of starting glucose could be determined.



### 3.24

Figure 3.10 – Anslyn group tripodal ligand system that measures glucose oxidase activity in buffer and serum.

Each of these two examples was designed to highlight the versatility of the ligand system and the benefits of modifications to these ligand structures. A dynamic and reversible system could be highly prized in these situations. In this chapter, we describe the development of such a system that interacts with a wide variety of heterocyclic aldehydes with numerous different metals and two different secondary amines with heterocyclic arms. Furthermore, studies were carried out to measure the dynamic exchange ability of the system as well as the effect of different anions on the extent to which the system assembles.

## 3.2 RESULTS AND DISCUSSION

### 3.2.1 Assembly of Pyridine 2-Carboxyaldehyde and Dipicolylamine

When pyridine-2-carboxyaldehyde was added to a solution of dipicolylamine in acetonitrile, no reaction of the aldehyde with the secondary amine was observed. In order to enhance the electrophilicity of the aldehyde, a metal ion Lewis acid that could bind to the aldehyde was selected. In addition to increasing the electrophilicity of the aldehyde,

the lewis acidic metal ion can also be chelated between the formed tripodal pyridines, leading to the development of a greater thermodynamic sink than the

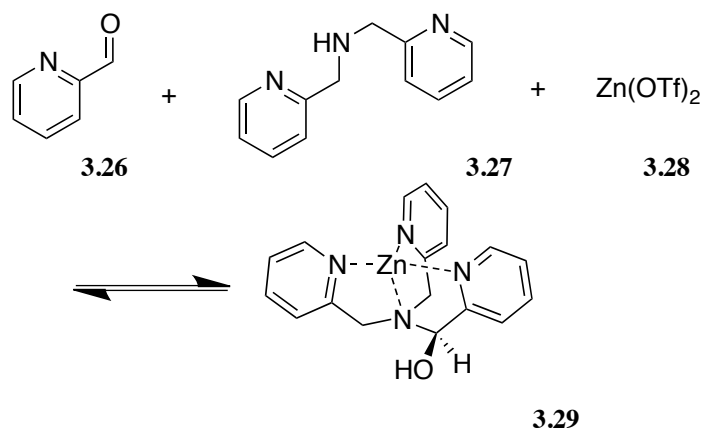


Figure 3.11 – Schematic representation of the proposed tripodal ligand system with pyridine-2-carboxaldehyde, dipicolylamine, and zinc triflate

formation of just the hemiaminal. The formation of a stronger metal chelating moiety on the molecule drives the formation of the complex between these two molecules. When comparing the formation of this complex to the amount of starting material, a careful balance must be created between the amines ability to chelate the metal ion and its ability to activate the carbonyl. The equilibrium constant without zinc is very small and undetectable via  $^1\text{H NMR}$  giving an equilibrium constant of less than  $1 \text{ M}^{-1}$ . When zinc is added to the system, the equilibrium constant of the assembly is calculated to be over  $6600 \text{ M}^{-1}$ , a huge increase driven simply by metal chelation.

### 3.2.2 Study on the Effects of Metal Counterions and Water Scavenging Efforts

After the discovery that zinc drives the assembly of dipicolylamine and pyridine-2-carboxyaldehyde, a series of metals were screened to determine what effect the metal ion and the coordinating ability of the counter anion would have on the extent of the



tripodal ligand structure formation. Using two noncoordinating counter anions, perchlorates and triflates, the corresponding zinc salts were studied to determine if they had different extents of complex formation. When comparing zinc triflate and zinc perchlorate, the triflate showed slightly higher complex formation as a percent of assembly as a function of total aldehyde with roughly a 10% greater extent of assembly. While both counterions are relatively noncoordinating and thus should cause assembly to the same degree, perchlorates are traditionally stored as hydrates that can interfere with the assembly process. Furthermore, the softer triflic anion leads to a more Lewis acidic zinc ion.

| <b>Metal Salt</b>                                      | <b>MS Added</b> | <b>Complex%<br/>(via NMR)</b> |
|--|-----------------|-------------------------------|
| <b>Zn(OTf)<sub>2</sub></b>                             | No              | >90%                          |
| <b>Zn(OTf)<sub>2</sub></b>                             | Yes             | >90%                          |
| <b>Zn(ClO<sub>4</sub>)<sub>2</sub>•6H<sub>2</sub>O</b> | No              | 83%                           |
| <b>Zn(ClO<sub>4</sub>)<sub>2</sub>•6H<sub>2</sub>O</b> | Yes             | 85%                           |
| <b>Fe(OTf)<sub>2</sub></b>                             | No              | ~39%                          |
| <b>Co(ClO<sub>4</sub>)<sub>2</sub>•6H<sub>2</sub>O</b> | No              | N/A                           |
| <b>Ni(ClO<sub>4</sub>)<sub>2</sub>•6H<sub>2</sub>O</b> | No              | N/A                           |
| <b>Cu(OTf)<sub>2</sub></b>                             | No              | N/A                           |
| <b>Eu(OTf)<sub>3</sub></b>                             | No              | trace                         |

Table 3.1 – Summary of metal and molecular sieves ability to drive assembly formation

In addition, the use of molecular sieves to remove water was explored, and the presence of sieves seemed to change the percentage of assembly. When measuring the extent of assembly formation, the presence of molecular sieves appeared to increase the extent of tripodal assembly formation by a few percentage points. Unfortunately, the removal of water from perchlorate salts is difficult to achieve using only molecular sieves and potentially dangerous by other methods. Because of the larger extent of complex formation even without molecular sieves, the triflate salt was used for all future studies unless otherwise mentioned.

### **3.2.3 Measuring the Extent of Assembly Formation**

$^1\text{H}$  NMR was used to measure the formation of the complex. The formation of the complex should lead to the decrease of the aldehyde resonance around 10.0 ppm and the formation of a new set of peaks between 3.6 and 6.0 ppm which corresponds to the hemiaminal structure. While this measurement technique provides a fast and effective way to measure a binding constant, only a few metal ions are diamagnetic and this technique is limited in the measurement of equilibria using other metals. To this end, our analysis turned to using mass spectroscopy to determine the formation of the assembly complex with other metals.

When studying the assembly of the complex with a variety of metals, zinc remained the metal which lead to the greatest extent of assembly. Additionally, cobalt(II) and nickel(II) showed some extent of assembly but not to the same levels as zinc. Finally, studies were carried out with iron(II) as well as copper(II) and europium(III) triflate salts but each of these metal complexes formed to a much lower extent or only formed a trace amount of the desired complex as shown in the table of the complexes (Table 3.1).

If you explore the origins of this effect, three major competing factors seem to be at work in the assembly process. The first of these factors is the ability of the metal ion to act as a Lewis acid and increase the electrophilicity of the aldehyde. Each of the metal ions has a different Lewis acidity and therefore ability to activate the pyridine-2-carboxyaldehyde. Lewis acidity tends to be complicated to explain and is often context dependent. Studies of Lewis acidity generally show that transition metals like zinc and copper tend to be very Lewis acidic while other transition metals, such as nickel and cobalt, tend to be less Lewis acidic. Furthermore, the type of anion is important because softer anions tend to create a more Lewis acidic metal cation, as was mentioned earlier. The triflate anion is much softer than perchlorate, which also explains why zinc triflate tends to lead to a larger extend of complex formation.

Secondly, the geometry of the metal ion plays an important role in the extent of complex formation. Zinc and copper ions tend to form trigonal bipyramidal geometry, while cobalt, nickel, and iron ions tend to form octahedral complexes. Since the ligand system forms a trigonal bipyramidal chelation sphere, metals that adopt that geometry would be expected to favorably drive the assembly process.

Finally, the next important component is the relative stability of the tripicolylamine ligand over the dipicolylamine ligand. As one might expect, the tris-substituted ligand should be more energetically stable than the di-substituted ligand because of the additional pyridine to coordinate to the metal center. Previous studies had been carried out with various metal ions and determined the binding energies between different nitrogenous ligands and different valency.<sup>31,32</sup> These studies also measured the Gibbs free energy ( $\Delta G$ ) and enthalpy values ( $\Delta H$ ), but the measurements were taken in water and the assembly process is carried out in acetonitrile, making the values only a first approximation.

### 3.2.4 Metal Ligand Studies with ITC

ITC titrations were carried out in order to measure the differences in  $\Delta G$  for the binding of the different metals to the dipicolylamine and the tripicolylamine ligands. In each of the titrations, metal ions were placed in the cell and the nitrogenous ligand was titrated into the solution with moderate stirring. The change in heat released as the ligand coordinated to the metal ion was observed.

We obtained similar results to those reported in the work in water and through our mass spectral analysis, the biggest thermodynamic sink would come from the nickel and zinc ions. Each of these two metals showed an improvement of binding affinity of approximately an order of magnitude in acetonitrile from the dipicolylamine complex to the tripicolylamine complex. As might be expected the driving force of these complexations is an enthalpic contribution with a negative entropic contribution driven by the formation of a rigid complex around the metal center. Cobalt and copper ions showed a roughly equal contribution between the two ligands with the dipicolylamine showing a slightly higher binding constant. These observations are similar but not identical to those reported in the literature. Based upon the literature, we would have expected cobalt and zinc to show similar affinities with a significant difference between the two ligand systems. Nickel should be even more favorable than either of these metals based upon differences between the two ligand systems. Based upon the binding constants, the ITC traces should only be used for qualitative interpretations because the binding is stronger than can be measured quantitatively.

|               | DPA    | TPA   | Difference |
|---------------|--------|-------|------------|
| <b>Zinc</b>   | 3.70E7 | 6.3E8 | 5.6E8      |
| <b>Cobalt</b> | 4.5E8  | 6.1E7 | -3.9E8     |
| <b>Nickel</b> | 1.7E7  | 5.6E8 | 5.4E8      |
| <b>Copper</b> | 5.4E8  | 5.1E7 | -4.9E8     |

Table 3.2 – ITC binding constants for different metals with dipicolylamine and tripicolylamine and the difference between the two ligands

### 3.2.5 Structural Analysis of the Multicomponent Assembly Complex

Using an equimolar ratio of 2-pyridinecarboxaldehyde, dipicolylamine, and zinc perchlorate in acetonitrile, an X-ray quality crystal was grown through the slow diffusion of diethyl ether into the solvent. The perchlorate salt was used instead of the triflate because the complex formed with this anion more readily crystallized out of solution. The X-ray structure is shown in figure 3.6. As expected, the zinc atom adopts a trigonal

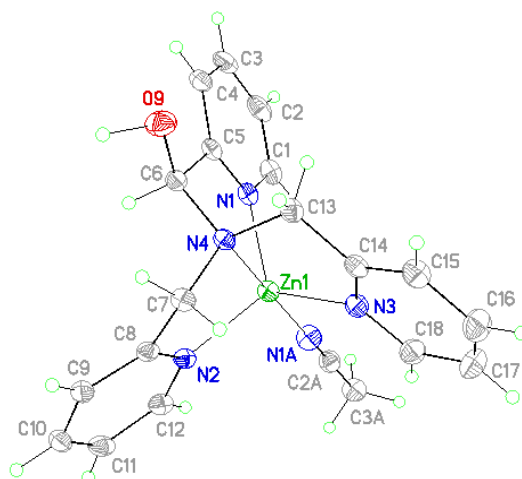


Figure 3.12 – Crystal structure of the tripyridine system

bipyramidal geometry with the three pyridine molecules forming the base of the pyramid. The apical nitrogen is located below the zinc atom and an acetonitrile molecule was resolved in the crystal to be bound to the top coordination site of the metal. Each of the bond lengths from the zinc ion to the pyridine rings are approximately the same (2.04, 2.04 and 2.07 Å) with the bond to the apical nitrogen being slightly larger (2.20 Å) than the pyridine bonds or the solvent bond (2.07 Å). Furthermore, an analysis of the bond angles between the apical nitrogen and the pyridine nitrogen atoms are all approximately 80° indicating that there is little distortion between the pyridine rings. The X-ray structure corresponds closely with the structure that we had predicted to exist in solution. Given the close relationship between the two structures, we are confident in our assignment of the NMR spectra.

### **3.2.6 Reversibility of the Multicomponent Assembly**

While we have shown that the aldehyde will add to the secondary amine through NMR, mass spectrometry, and X-ray crystal diffraction, the question remains if the components are in dynamic equilibrium at ambient conditions. One of the hallmarks of a truly reversible covalent bond forming reaction is an equilibrium of the components. In the first test of equilibrium, a solid crystal of the assembly was taken and then redissolved into acetonitrile. When the NMR spectrum was recorded, an aldehyde peak, was observed which precludes a static system.

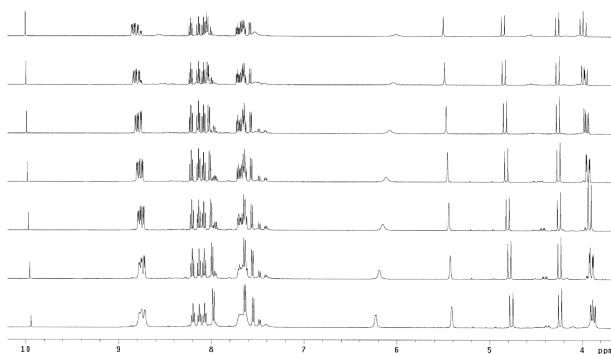


Figure 3.13 –  $^1\text{H}$  NMR spectra of tripyridine assembly at various temperatures from -40°C at bottom to 75°C at the top

Furthermore, the amount of aldehyde present increased with time as the temperature of the system was raised, illustrating the formation of a dynamic equilibrium of the assembly. Conversely, as the temperature was lowered, the formation of the complex increased.

While the dynamic nature of the assembly was demonstrated through these experiments, a way to quantitate the binding of the aldehyde to the assembly needed to be developed. In the mechanism for the complex formation, there are multiple potential equilibria between the metal ions and the different nitrogenous ligands. The zinc ion can bind to the 2-pyridinecarboxyaldehyde or the dipicolylamine, but given that the dipicolylamine has two coordinating nitrogen atoms, we can assume that the zinc will almost exclusively be bound to the dipicolylamine. Using that assumption, we can create an equilibrium equation as a function of aldehyde concentration.

$$K = \frac{[\text{ZnC}]}{\{[2\text{-PA}][\text{Zn-DPA}]\}}$$

Equation 3.1 – First formulation of the equilibrium constant (K) where ZnC is the final complex, 2-PA is pyridine-2-carboxaldehyde and Zn-DPA is the complex of zinc to dipicolylamine.

Furthermore, because the components are all added in equimolar ratios, we can assume that the concentration of aldehyde is equal to the concentration of the zinc-dipicolylamine via the mass balance equations. But even then, we are not able to identify the concentration of the zinc complex independently using equation 3.1.

$$K = [\text{ZnC}]/[\text{2-PA}]^2 \text{ (Eq. 2)}$$

Equation 3.2 – A simplification of the previous equation based upon the mass balance of the overall reaction equation.

As such, we need to substitute equation 3.2 so that the  $[\text{ZnC}]$  is related to a measurable quantity. Given that the ratio of aldehyde to complex can be easily obtained from the  $^1\text{H}$  NMR integrations, this ratio can be incorporated into the equilibrium equation. Using the equations below, the equilibrium constant ( $K$ ) can be calculated for any given mixture of complex and aldehyde.

$$[\text{2-PA}] + [\text{ZnC}] = [\text{2-PA}]_{\text{total}} \text{ (Eq. 3)}$$

Equation 3.3 – Mass balance equation for the total aldehyde concentration in solution

$$R = [\text{ZnC}]/[\text{2-PA}] \text{ (Eq. 4)}$$

Equation 3.4 – Ratio of  $^1\text{H}$  NMR peaks for the complex with the aldehyde

$$K = R(1 + R)/[\text{2-PA}]_{\text{total}} \text{ (Eq. 5)}$$

Equation 3.5 – Final equilibrium constant equation combining all previous equations



By measuring the K value of each of the aldehydes, we have a quantitative way to compare their extent of assembly. With this quantitative tool in hand, the scope of the assembly was explored through the exchange of various components.

### **3.3 COMPONENT EXCHANGE IN PYRIDINE ASSEMBLY**

#### **3.3.1 Pyridine Assembly Aldehyde Exchange and Screening**

Given that the system is dynamic, a screening of different heterocyclic aldehydes was carried out. Various substituted pyridines as well as other heterocycles, such as quinoline and imidazole, were used. The extent of assembly formation should be driven by the properties of the aldehyde. In terms of steric considerations, the interactions of the 3 position of the heterocyclic ring from the aldehyde with the groups on the tertiary center formed in the final structure when the structure is formed hampers the amount of assembly formed when the heterocycle is substituted there. Furthermore, groups at the 6 position affect the ability of the nitrogen to chelate to the metal and thus weaken the assembly's equilibrium constant for aldehydes substituted at that position.

Next, the electrophilicity of the aldehyde plays an important role in the extent of assembly. Some of the heterocycles, such as quinoline and the pyridine rings with electron withdrawing groups, do not activate the aldehyde when coordinated to the metal as well and thus are not as susceptible to nucleophilic attack even after the Lewis acid activation. These aldehydes tend to form the assembly to a significantly lower extent.

Finally, the metal chelation ability of the heterocycle is the last important factor to rationalizing the extent of assembly formation. This factor can be divided into two equally important components: the Lewis basicity of the nitrogen and its orientation in the complex. The stronger the Lewis basicity of the nitrogen atom, the stronger the complex will be at providing a thermodynamic sink to drive formation of the complex.

But the Lewis base strength is also modulated by the orientation of the nitrogen. If after condensation, the orbital overlap between the nitrogen and the metal is not as favorable as with other complexes, then the complex will have a weaker thermodynamic driving force. For example, the imidazole ring is traditionally considered strongly Lewis basic but the five membered ring strains the angles between the nitrogen and the metal center, making the complex chelate the metal less strongly.

To this end, we explored the complex formation with nine different heterocyclic aldehydes. The equilibrium constants obtained with each of these aldehydes is shown in Table 3.2. From the equilibrium constants measured, several of the factors mentioned earlier can be seen at work. The triazole has a small equilibrium constant because the nitrogen atom is not as Lewis basic as the pyridine. Furthermore, the dibromopyridine has a much smaller equilibrium constant than the monobromopyridine, which is smaller than the equilibrium constant of the pyridine derivative. The bromine atom is electron withdrawing and thus destabilizes the activation of the aldehyde and makes the pyridine less electron rich and thus a weaker Lewis base. When a second bromine is added, these effects are amplified and the halide in the third position on the ring adds steric clashing between the bromine and the tertiary center from the aldehyde. Steric arguments can be made for quinoline and isoquinoline based upon the second fused ring and are illustrated in their smaller equilibrium constants. Finally, the thiazole and the imidazole are both not able to activate the aldehyde as well as the pyridine making the nucleophilic attack of the amine less favorable and thus leads to less assembly formation.

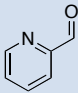
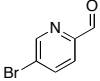
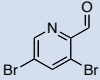
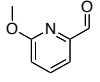
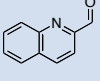
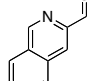
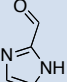
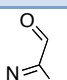
| Aldehyde  | Eq. Constant (M <sup>-1</sup> ) |
|---|---------------------------------|
|    | 6600                            |
|    | 230                             |
|    | 30                              |
|    | 70                              |
|    | 45                              |
|   | 220                             |
|  | 900                             |
|  | 320                             |

Table 3.3 – Equilibrium constant for the different heterocyclic aldehydes

### 3.3.2 Exchange of Aldehyde in the Assembly

With a truly dynamic system, the addition of an aldehyde that forms a complex with a higher equilibrium constant should bias the system to preferentially form that assembly to a greater extent. In order to study this process, an equilibrium with an

aldehyde that has a relatively low binding constant was formed. Then, a second aldehyde, which has a higher equilibrium constant, was added and the complexes that were formed were analyzed. Using thiazole-2-carboxaldehyde as the starting heterocyclic aldehyde, equilibrium of the assembly complex was established. When pyridine-2-carboxaldehyde was added to the solution, the equilibrium was perturbed and the NMR spectrum showed the formation of the complex from pyridine-2-carboxaldehyde preferentially. A similar phenomenon was observed using another aldehyde, 3-bromopyridine-2-carboxaldehyde, when the pyridine aldehyde was added to the solution. Given that both aldehydes have similar equilibrium constants, the extent of the formation of the pyridine-2-carboxaldehyde was similar. Furthermore, when the concentration of

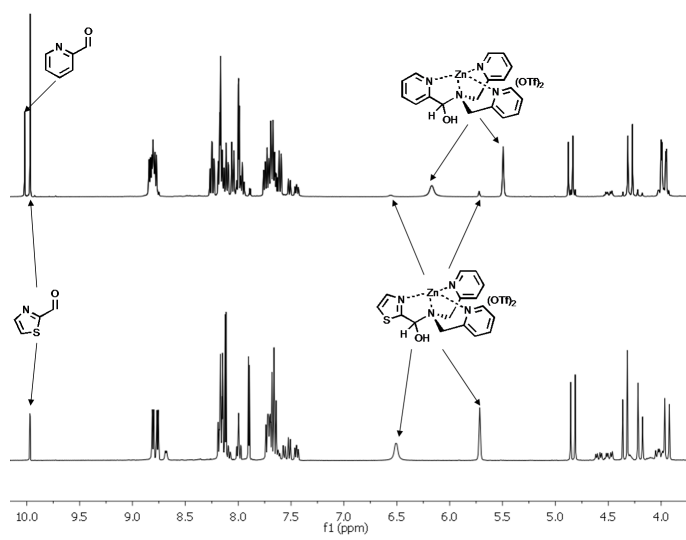


Figure 3.14 –  $^1\text{H}$  NMR spectra of mixture when a second higher equilibrium constant aldehyde is added to the mixture.

the assembly of the mixture was decreased to 10 mM, a similar exchange process was observed but took more time to come to equilibrium. The fact that it took longer to come to equilibrium at the lower concentration could not be explained given that the system was under thermodynamic control. The effects of concentration and the speed to which equilibrium is reached were thus explored.

### 3.3.3 Concentration and Time to Equilibrium

Given that we observed changes in the time required to reach equilibrium, a formal study of the effects of concentration was explored. A study of the time needed to reach equilibrium was measured for each of six different concentrations. When the time to equilibrium was plotted against the ratio of the integration of the complex over the integration of the aldehyde in the  $^1\text{H}$  NMR, the trend shows that as concentration increases, the ratio of the integrals, and thus assembly, also increases. Furthermore, as the

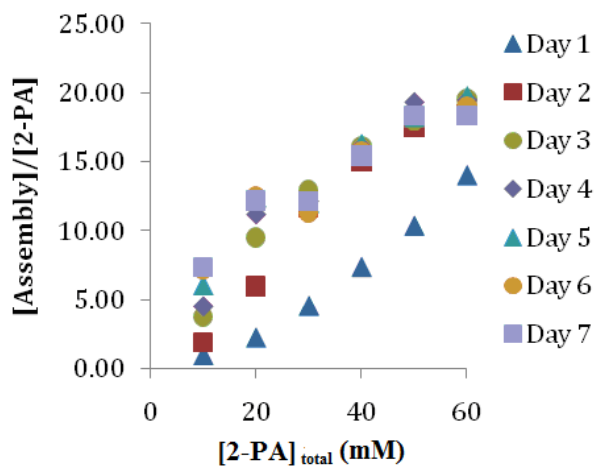


Figure 3.15 – Plot of the ratio of assembly to aldehyde against the total concentration of the aldehyde showing the equilibrium each day.

concentration increased, the time to reach equilibrium was shortened. When the concentration was higher than 30 mM, the equilibrium was reached within two days, the equilibrium was reached after four days for 20 mM and only after seven days for the 10 mM. The dependence of the equilibrium constant on the concentration simply arises from the overall concentration of the components being higher and thus leading to greater molecular collisions which lead to the condensation.

### **3.3.4 Solvent Effects on Assembly**

When studying the assembly process, most of the studies were carried out in acetonitrile, but we wanted to explore whether the complex would assemble in more polar solvents such as methanol and water. Studies with different solvents – dimethyl sulfoxide, methanol and water – all showed some extent of assembly formation but the acetonitrile lead to the most assembly. The more polar solvents lead to a lower thermodynamic sink from the metal chelation than in acetonitrile causing a weaker driving force for the assembly of the three components. The polar solvents better solvate the metal ion, making the energy released when the tripyridine ligand system binds significantly lower.

### **3.3.5 Counterion Screening**

Given that the anion of the zinc salt led to a different extent of complex formation and the crystal structure showed a vacant coordination site at the top of the complex, we decided to explore the addition of tetrabutylammonium salts that could potentially coordinate to that vacant site and hopefully drive assembly formation. In this study, five different anions were used – chloride, bromide, iodide, acetate and hexafluorophosphate – and two additional anions – sulfate and phosphate – were explored but led to precipitation of either the metal ion or the complex and thus were excluded from further

studies. Some of the anions should coordinate to the top of the complex and lead to further enhancement of the binding of complex, but the anions could also modulate the Lewis acidity of the metal and lower the activation of the aldehyde. Studying the effects of the anion with both the pyridine, 5-bromopyridine, and thiazole-2-carboxyaldehyde, most of the halides showed an increase in the extent of assembly. Within the halides, chloride showed the greatest extent of complex formation followed by bromide and then iodide. The halide ions have a greater charge localization relative to the acetate or hexafluorophosphate and thus leads to the formation of a strong bond and stronger complex which the thermodynamic sink and further drives the tripyridine ligand formation

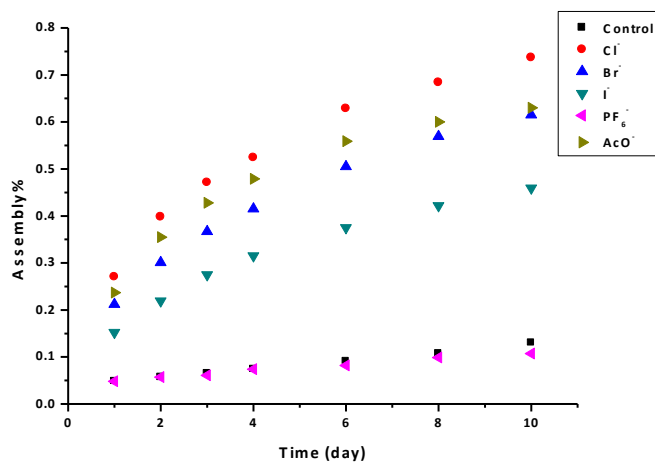


Figure 3.16 – Effects of the addition of anions to the thiazole assembly

for the thiazole-2-carboxyaldehyde. The acetate also showed some increase in percentage of assembly. The percentage did not increase as much due to the modulation of the Lewis acidity of the metal center. In the 5-bromopyridine-2-carboxyaldehyde case, the halides showed some assembly modulation,

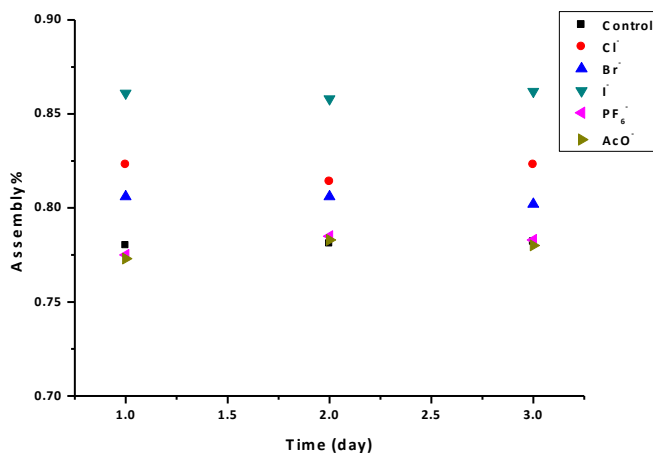


Figure 3.17 – Effects of the addition of anions into 5-bromopyridine assembly

but the acetate did not modulate the extent of assembly formation. In all cases, the hexafluorophosphate anion showed little to no modulation of the amount of assembly formed. These anion modulations likely come from binding in the apical position to form a stronger complex with changes in the Lewis acidity of the metal center only moderately affecting the extent of assembly. Finally, with pyridine-2-carboxyaldehyde, little modulation of the extent of assembly formation was observed. The assembly was exclusively formed meaning the anion had little effect to increased the amount of assembly formed by coordinating ion.

### 3.3.6 Pyridine Assembly Conclusions

Using a secondary amine, dipicolylamine, and pyridine-2-carboxyaldehyde in the presence of zinc triflate a tripodal ligand assembly was formed. The system is dynamic with each component being exchangeable. Given the dynamic nature of the tripodal ligand, we believe that it can be used to generate a variety of different heterocyclic



structures that could be used for a number of different purposes such as chirality determination.

### 3.3.7 Future Directions

In order to further expand the stability of this assembly, several new pyridine derivatives that modulate the reactivity of the aldehyde without compromising the Lewis basicity of the nitrogen should be explored. Furthermore, the expansion of the secondary amine portion of the assembly could modulate the reactivity of the complex and likely promote the formation of the assembly or lead to the addition of other functionalities.

## 3.4 TRIAZOLE BASED ASSEMBLY

### 3.4.1 Background on Click Chemistry

While we have shown a system which is highly dynamic with the potential for a large number of different components that can be incorporated; one of the weaker portions of the exchange system is the limited number of potential secondary amines with two heterocyclic arms. In order to greatly expand the potential applications of the system, modifying those arms using click chemistry was proposed and studied.

One of the most versatile and easiest ways to introduce heterocycles into a molecule is through the use of Huisgen 1,4-cycloaddition, or the colloquially called “click”, reaction. Click chemistry has grown extensively in popularity since the

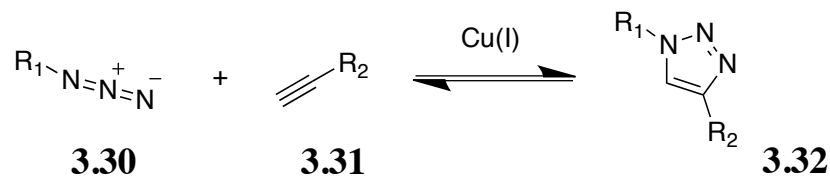


Figure 3.18 – Model Click Reaction

development of a Cu(I) catalyzed route to the resultant triazole in the early 2000's by Sharpless and Meldal through simultaneous independent reports.<sup>33,34,35</sup> The methodology is rapid, high yielding, and the products are synthesized from starting materials that are either commercially available or within one synthetic step and orthogonal to other functional groups in molecules.<sup>36</sup> The resultant triazole produces a heterocyclic nitrogen that has been previously shown to chelate a variety of different metals. Furthermore, by using the modified secondary amine core generated through click chemistry, the R groups attached to the starting azide can carry secondary functionality. These modified azides can impart the assembly with additional characteristics that are not present in the simple pyridine complex or would require extensive synthetic effort to introduce. The additional components give a system constructed from a bis-triazole a greater range of potential functionalities and expands the number of applications for this dynamic assembly. Furthermore, a wide variety of different azides are commercially available or readily easy to be synthesized in one or two steps and thus a large library of bis-triazoles can be quickly and easily generated. This library of complexes makes the use of the assembly easier and expands the potential for its use in an array of differential receptors where targeting functionalities can be rapidly introduced.

### **3.4.2 Model System Design**

In order to test if such a system would still function in the dynamic covalent bond assembly to make the tripodal metal ligand, a simple bis-triazole was designed and synthesized. As a proof of concept molecule, the bis-triazole made from the condensation of benzyl azide and dipropargylamine was chosen. The resultant complex has been reported and was relatively easy to synthesize and purify.<sup>37</sup> Furthermore, the target model system had many advantages including: synthesized from commercially

available starting materials, could demonstrated the ability of the assembly to be functionalized at the 1-position of the ring, contained only phenyl groups that should not prevent the compounds solubility in acetonitrile, or had exogenous functionalities to the complex. Assemblies using this secondary amine with triazole arms were carried out and shown to have similar properties to those reported in the assembly with dipicolylamine.

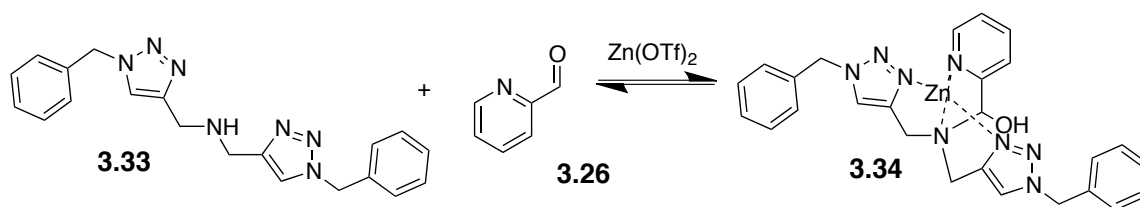


Figure 3.19 – Schematic representation of bis(triazole)amine assembly reaction

### 3.4.3 Interactions with Pyridine-2-Carboxaldehyde

After the addition of the aldehyde, metal and bis-triazole (3.33) components, the formation of new peaks in the  $^1\text{H}$  NMR spectrum are believed to correspond to the complex. The corresponding peak distribution and multiplets were similar to those seen in the complex formed with dipicolylamine, providing evidence that the bis(triazole)amine is acting in the formation of a metal chelating tripodal ligand structure. The six new sets of peaks from 3.5 to 6.1 ppm were observed and

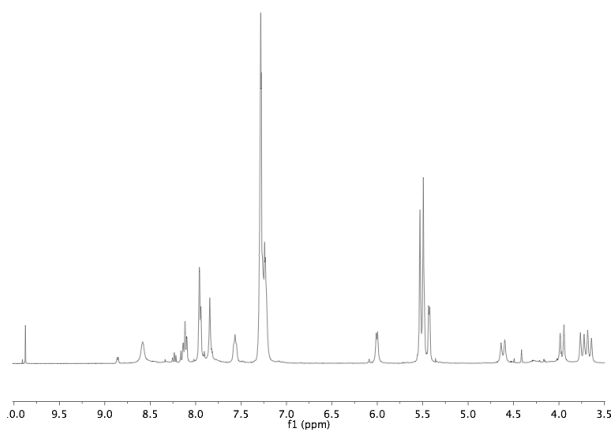


Figure 3.20 – Model  $^1\text{H}$  NMR of the triazole assembly

appeared to correspond to the formation of a complex where the six protons adjacent to the apical nitrogen are no longer identical. In order for the six protons to become nonequivalent, the resultant structure must be rigid. Four of the peaks from 3.5 to 4.8 ppm are tightly clustered and similar in structure and chemical shift suggesting the peaks correspond to the protons on the methylenes on the bis(triazole)amine which are each exposed to a slightly different chemical environment. The remaining two peaks correspond to the formation of the hemiaminal with one peak at approximately 5.4 ppm for the proton on the methylene, and one peak at approximately 6.1 ppm for the proton on the hydroxyl formed from the oxygen of the aldehyde.

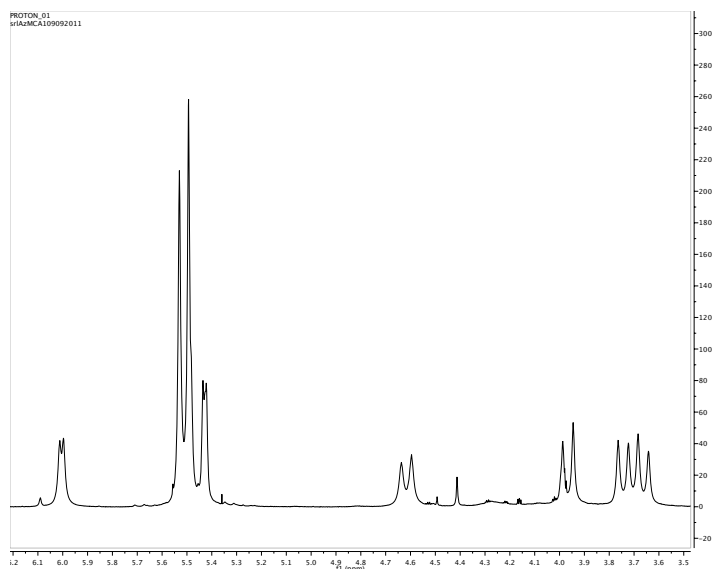


Figure 3.21 – Zoomed in <sup>1</sup>H NMR from 3.5 to 6.2 ppm showing the six non-equivalent protons.

Equilibrium constants between the aldehyde with one equivalent of bistriazole and zinc were calculated and measured using the integrals in <sup>1</sup>H NMR spectra. By comparing the integrals between the aldehyde and one of the six peaks from the rigid methylene, a ratio between the two components in solution was obtained. Using the concentration of the solution and the ratio of two components in solution, an equilibrium constant was calculated using the formula (Equation 3.5) discussed earlier in this chapter.

Furthermore, the complex formation appeared to occur rapidly, within approximately an hour after the components were combined. In the NMR studies, the composition of the solution changed relatively little after the first few hours leading to the assumption that the system had reached equilibrium. Our previous assemblies required almost 24 hours to come to equilibrium, making the triazole system much more accessible for use in a rapid dynamic combinatorial system.

### 3.4.4 Screening of Various Heterocyclic Aldehydes

Our previous study showed that a variety of aldehydes bound to the secondary amine leading to complex formation. In an attempt to explore the scope of this new secondary amine, its ability to bind to a variety of heterocyclic aldehydes was also measured. Each of the aldehydes shows a distinctive equilibrium constant that was different from the one measured when binding to the dipicolylamine as the secondary amine. Each of the aldehydes showed a similar equilibrium constant to the one measured with dipicolylamine. The pyridine-2-carboxyaldehyde showed the greatest extent of assembly formation, but had a lower absolute equilibrium constant than the dipicolylamine assembly did. Furthermore, the 5-bromopyridine, imidazole, and thiazole-2-carboxyaldehyde formed the next group of aldehydes if ranked in order of the system's equilibrium constants. These ligands all had greater equilibrium constants with the bis(triazole)amine ligand, except for the imidazole-2-carboxyaldehyde which remained close in equilibrium constant. The bis(triazole)amine ligand is a weaker metal chelator than the dipicolylamine which leads to more zinc being able to coordinate to the aldehyde and activate it to nucleophilic attack. Furthermore, the methoxypyridine-2-carboxyaldehyde shows a moderate assembly

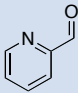
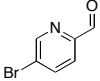
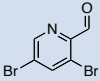
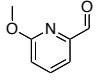
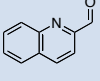
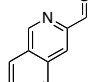
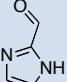
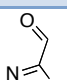
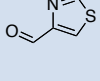
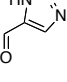
| Aldehyde  | Eq. Constant (M <sup>-1</sup> ) |
|---|---------------------------------|
|    | 1516                            |
|    | 608                             |
|    | 29.9                            |
|    | 519                             |
|    | 317                             |
|   | 136                             |
|  | 664                             |
|  | 706                             |
|  | 189                             |
|  | 67                              |

Table 3.4 – Equilibrium constant for the binding of heterocyclic aldehydes to the bis(triazole)amine

constant likely due to the electron donating ability of the methoxy group, making it a more Lewis basic heterocycle than the pyridine. Because the pyridine is more basic, the complex forms a larger thermodynamic sink and drives greater assembly formation but has a lower equilibrium constant than pyridine due to the aldehyde being less electrophilic. Quinoline-2-carboxaldehyde also showed a moderate assembly constant with the bis(triazole)amine ligand. The quinoline is a strong metal chelator and thus drives the formation of the assembly, but the larger aromatic system also reduces the electrophilicity of the aldehyde and introduces some steric interactions when the assembly is formed. Triazole, 4-thiazole, 3,5-dibromopyridine and isoquinoline all showed only slight assembly formation with the secondary amine. The 4-thiazole derivative and the triazole cannot as easily stabilize the electrophilically activated aldehyde. The dibromopyridine is likely also unable to activate the aldehyde as well, but also has some steric interactions as was discussed for the dipicolylamine system. Finally, the isoquinoline ligand is a weaker Lewis base and the assembly formed is not as thermodynamically favorable. The smaller sink leads to a weaker driving force and causes less extent of formation.

### **3.4.5 Aldehyde Exchange**

A second aldehyde was introduced to the assembly after the system had reached equilibrium to determine the dynamic nature of



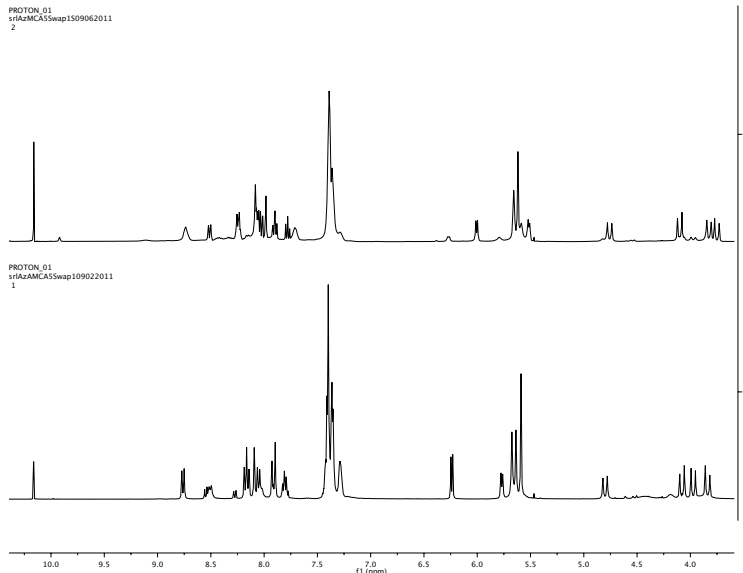


Figure 3.22 –  $^1\text{H}$  NMR spectra of aldehyde exchange from quinolone aldehyde assembly to the pyridine aldehyde assembly

the assembly. In the first study, an assembly with thiazole-2-carboxyaldehyde was allowed to reach equilibrium. When an equivalent of pyridine-2-carboxyaldehyde was introduced to the system, the assembly began to reverse and preferentially form the assembly with the pyridine aldehyde. As can be seen in the figure, the assembly shows a significant change between the two aldehydes where even the six peaks corresponding to the methylene bridges have slightly shifted in their resonances. As might be expected, the process shows the preferential formation of the assembly that has the highest association constant.

A second assembly with a quinoline aldehyde was carried out and allowed to reach an equilibrium mixture. After the system had reached equilibrium, a second equivalent of pyridine-2-carboxyaldehyde was added and a new equilibrium was reached. When comparing the NMR spectrum of the new equilibrium mixture to the previous spectra, the system showed almost exclusive formation of the pyridine complex. The

dramatic change in the assembly is due to the large change in the equilibrium constant of the aldehydes as can be seen in the previous figure. The dramatic changes in assembly shows that the complex is dynamic, reversible and an equilibrium mixture of complexes that can be driven to a particular complex based upon changes in the solution and component composition.

### 3.4.6 Screening of Metal Exchange

Because a triazole as a ligand has different metal chelation properties than the pyridine, we wanted to further explore the use of different metals to catalyze the formation of the tripodal assembly. The use of the copper(II) and iron(II) showed little assembly formation while other metals like cobalt and zinc each showed greater assembly formation. These metals do the best job of activating the aldehyde while still forming a tripodal ligand that is thermodynamically favorable to serve as an energetic sink. Each of these studies was carried out in the presence of zinc because the zinc should help to activate the aldehyde regardless of the metal binding energy to the tripodal assembly. Finally, we decided to pursue studies of the changes in metal binding based upon the valency of the heterocycles using ITC.

|               | DBTA (3.33) | TPA   | Difference |
|---------------|-------------|-------|------------|
| <b>Zinc</b>   | 6.0E7       | 6.3E8 | 5.7E8      |
| <b>Cobalt</b> | 4.3E6       | 6.1E7 | 1.8E7      |
| <b>Nickel</b> | 2.6E9       | 5.6E8 | -2.0E9     |
| <b>Copper</b> | 2.3E7       | 5.1E7 | 2.8E7      |

Table 3.5 – ITC binding constants for the bis(triazole)amine (3.33) and tripicolylamine and the difference between those two binding affinities

A similar analysis was carried out using our bis(triazole)amine ligand. In each case, similar results were observed. The zinc and cobalt ions showed an increased affinity between the triazole ligand and the tripyridine ligand by approximately an order of magnitude. The nickel ion showed stronger binding by approximately an order of magnitude to the triazole system than to the tripyridine ligand. In such a case, the metal ion would provide only a weak driving force for the assembly of the hemiaminal complex. Finally, the copper ion shows a very similar binding affinity for the two ligand complexes with no discernable difference, making the formation of the ligand structure contribute little to the overall stability of the complex. These binding constants of the metal ions correlates well with the observed binding in the mass spectral analysis where cobalt and zinc showed significant assembly formation while the other metals only showed trace assembly formation.

### **3.5 CONCLUSIONS**

This chapter highlights work towards a multicomponent assembly that forms a metal chelating complex. The complex formation is dynamic and can be formed using a variety of components and different metal ions. Numerous aldehydes were screened and an equilibrium constant was measured as a function of the ability of the complex to chelate the metal ion or the stability of the metal activated aldehyde. The effects of counterions that can coordinate in the apical position of the metal complex were also explored.

Additionally, a new secondary amine with heterocyclic arms based upon triazoles was synthesized. The new metal chelating core showed slightly lower equilibrium constants than the dipicolylamine core but took shorter amounts of time to reach

equilibrium and could be used to modularly construct additional recognition units or functionalities into the molecule.

Finally, studies of the binding of metal ions to tripodal ligand of structures were explored using ITC. Our results show that the addition of the extra metal chelating ability of the heterocycle for the aldehyde is one of the key elements in the driving force behind assembly formation.

### **3.6 EXPERIMENTAL METHODS**

The bis-triazole from dipropargylamine and benzyl azide was synthesized using literature procedures. All aldehydes, dipicolylamine and metal salts were purchased from commercial vendors and used as received. The assembly with either secondary amine with aldehyde in the presence of zinc were carried out in deuterated acetonitrile from Cambridge Isotope Laboratory. All NMR spectra were collected using a 400 MHz Varian NMR at The University of Texas at Austin NMR facility. The University of Texas at Austin X-Ray crystallography lab carried out the X-ray crystallographic studies and The University of Texas at Austin mass spectroscopy lab carried out all mass spectral studies.

Assemblies were formed by dissolving equal parts aldehyde, metal, and the bis(triazole)amine (**3.33**) in deuterated acetonitrile. To monitor the formation of the complex,  $^1\text{H}$  NMR spectra was taken and the formation of peaks corresponding to the hemiaminal and the disappearance of the aldehyde peak were used to identify the formation of complex.

Equilibrium constants were measured by finding the ratio of hemiaminal to aldehyde as had been reported. Exchange experiments were conducted with a mixture of the equilibrated complex and a second equivalent of an aldehyde. The  $^1\text{H}$  NMR spectrum was collected after 30 minutes and repeatedly collected every morning for five days.

Similar experiments were carried out for metal exchange using a second equivalent of an alternate metal, which was added to the equilibrated complex and the formation of new peaks in the mass spectra were observed.

Allowing the assembly to come to reach equilibrium, experiments on the effects of adding a secondary anion were carried out. After equilibrium had been reached, an equivalent of the corresponding tetrabutylammonium salt was added and the new  $^1\text{H}$  NMR spectra was recorded.

The ITC spectra of metal binding to nitrogenous ligands were studied using a VP-ITC, manufactured by MicroCal of Northhampton, MA. A 100  $\mu\text{M}$  metal solution was placed in the cell and 7  $\mu\text{L}$  of either a 600  $\mu\text{M}$  or 1.1 mM ligand solution was titrated into the metal solution. Approximately 43 injections were added to the solution and the heat evolved after each titration was measured. The resultant heat released was plotted against the molar ratio and the line fitted to determine the thermodynamic parameters of the binding event.

### **3.7 REFERENCES**

- (1) Collet, J.-F.; Depuydt, M.; Messens, J. How proteins form disulfide bonds. *Antioxidants & Redox Signaling* **2012**, *15*, 49+

- (2) Fass, D. Disulfide Bonding in Protein Biophysics. *Annual Review of Biophysics* **2012**, *41*, 63–79
- (3) Narayan, M. Disulfide bonds: protein folding and subcellular protein trafficking. *FEBS Journal* **2012**, *279*, 2272–2282
- (4) Au-Yeung, H. Y.; Pantoş, G. D.; Sanders, J. K. M. Dynamic combinatorial synthesis of a catenane based on donor–acceptor interactions in water. *Proceedings of the National Academy of Sciences* **2009**, *106*, 10466–10470
- (5) Au-Yeung, H. Y.; Cougnon, F. B. L.; Otto, S.; Pantos, G. D.; Sanders, J. K. M. Exploiting donor-acceptor interactions in aqueous dynamic combinatorial libraries: exploratory studies of simple systems. *Chemical Science* **2010**, *1*, 567–574
- (6) Corbett, P. T.; Sanders, J. K. M.; Otto, S. Competition between Receptors in Dynamic Combinatorial Libraries: Amplification of the Fittest? *Journal of the American Chemical Society* **2005**, *127*, 9390–9392
- (7) Au-Yeung, H. Y.; Pengo, P.; Pantos, G. D.; Otto, S.; Sanders, J. K. M. Templated amplification of a naphthalenediimide-based receptor from a donor-acceptor dynamic combinatorial library in water. *Chemical Communications* **2009**, 419–421
- (8) Zhang, T.; Anslyn, E. V A Colorimetric Boronic Acid Based Sensing Ensemble for Carboxy and Phospho Sugars. *Organic Letters* **2006**, *8*, 1649–1652
- (9) Edwards, N. Y.; Sager, T. W.; McDevitt, J. T.; Anslyn, E. V Boronic Acid Based Peptidic Receptors for Pattern-Based Saccharide Sensing in Neutral Aqueous Media, an Application in Real-Life Samples. *Journal of the American Chemical Society* **2007**, *129*, 13575–13583
- (10) Kataoka, K.; James, T. D.; Kubo, Y. Ion Pair-Driven Heterodimeric Capsule Based on Boronate Esterification: Construction and the Dynamic Behavior. *Journal of the American Chemical Society* **2007**, *129*, 15126–15127.
- (11) James, T. D.; Sandanayake, K. R. A. S.; Shinkai, S. Novel photoinduced electron-transfer sensor for saccharides based on the interaction of boronic acid and amine. *Journal of the Chemical Society, Chemical Communications* **1994**, 477–478

- (12) Shabbir, S. H.; Joyce, L. A.; Da Cruz, G. M.; Lynch, V. M.; Sorey, S.; Anslyn, E. V Pattern-Based Recognition for the Rapid Determination of Identity, Concentration, and Enantiomeric Excess of Subtly Different Threo Diols. *Journal of the American Chemical Society* **2009**, *131*, 13125–13131
- (13) Shabbir, S. H.; Regan, C. J.; Anslyn, E. V A general protocol for creating high-throughput screening assays for reaction yield and enantiomeric excess applied to hydrobenzoin. *Proceedings of the National Academy of Sciences* **2009**, *106*, 10487–10492.
- (14) Zhu, L.; Zhong, Z.; Anslyn, E. V Guidelines in Implementing Enantioselective Indicator-Displacement Assays for  $\alpha$ -Hydroxycarboxylates and Diols. *Journal of the American Chemical Society* **2005**, *127*, 4260–4269
- (15) Wiskur, S. L.; Anslyn, E. V Using a Synthetic Receptor to Create an Optical-Sensing Ensemble for a Class of Analytes: A Colorimetric Assay for the Aging of Scotch. *Journal of the American Chemical Society* **2001**, *123*, 10109–10110
- (16) Wiskur, S. L.; Lavigne, J. J.; Metzger, A.; Tobey, S. L.; Lynch, V.; Anslyn, E. V Thermodynamic Analysis of Receptors Based on Guanidinium/Boronic Acid Groups for the Complexation of Carboxylates,  $\alpha$ -Hydroxycarboxylates, and Diols: Driving Force for Binding and Cooperativity. *Chemistry – A European Journal* **2004**, *10*, 3792–3804
- (17) Belowich, M. E.; Stoddart, J. F. Dynamic imine chemistry. *Chemical Society Reviews* **2012**, *41*, 2003–2024.
- (18) Lao, L. L.; Schmitt, J.-L.; Lehn, J.-M. Evolution of a Constitutional Dynamic Library Driven by Self-Organisation of a Helically Folded Molecular Strand. *Chemistry – A European Journal* **2010**, *16*, 4903–4910
- (19) Mastalerz, M. Shape-Persistent Organic Cage Compounds by Dynamic Covalent Bond Formation. *Angewandte Chemie International Edition* **2010**, *49*, 5042–5053
- (20) Schneider, M. W.; Oppel, I. M.; Mastalerz, M. Exo-Functionalized Shape-Persistent [2+3] Cage Compounds: Influence of Molecular Rigidity on Formation and Permanent Porosity. *Chemistry – A European Journal* **2012**, *18*, 4156–4160

- (21) Hasell, T.; Wu, X.; JonesJames, T. A.; Bacsa, J.; Steiner, A.; Mitra, T.; Trewin, A.; Adams, D. J.; Cooper, A. I. Triply interlocked covalent organic cages. *Nat Chem* **2010**, *2*, 750–755
- (22) Von Delius, M.; Geertsema, E. M.; Leigh, D. A.; Tang, D.-T. D. Design, Synthesis, and Operation of Small Molecules That Walk along Tracks. *Journal of the American Chemical Society* **2010**, *132*, 16134–16145
- (23) Metola, P.; Anslyn, E. V; James, T. D.; Bull, S. D. Circular dichroism of multi-component assemblies for chiral amine recognition and rapid ee determination. *Chem. Sci.* **2012**, *3*, 156–161.
- (24) M. Dragna, J.; Pescitelli, G.; Tran, L.; Lynch, V. M.; Anslyn, E. V; Di Bari, L. In Situ Assembly of Octahedral Fe(II) Complexes for the Enantiomeric Excess Determination of Chiral Amines Using Circular Dichroism Spectroscopy. *Journal of the American Chemical Society* **2012**, *134*, 4398–4407
- (25) Rowan, S. J.; Cantrill, S. J.; Cousins, G. R. L.; Sanders, J. K. M.; Stoddart, J. F. Dynamic Covalent Chemistry. *Angewandte Chemie International Edition* **2002**, *41*, 898–952.
- (26) You, L.; Long, S. R.; Lynch, V. M.; Anslyn, E. V Dynamic Multicomponent Hemiaminal Assembly. *Chem.--Eur. J.* **2011**, *17*, 11017–11023, S11017/1–S11017/14.
- (27) Zhang, T.; Anslyn, E. V Using an Indicator Displacement Assay to Monitor Glucose Oxidase Activity in Blood Serum. *Organic Letters* **2007**, *9*, 1627–1629
- (28) Tang, W.; Matyjaszewski, K. Effect of Ligand Structure on Activation Rate Constants in ATRP. *Macromolecules* **2006**, *39*, 4953–4959
- (29) Tang, W.; Tsarevsky, N. V; Matyjaszewski, K. Determination of Equilibrium Constants for Atom Transfer Radical Polymerization. *Journal of the American Chemical Society* **2006**, *128*, 1598–1604
- (30) Matyjaszewski, K.; Jakubowski, W.; Min, K.; Tang, W.; Huang, J.; Braunecker, W. A.; Tsarevsky, N. V Diminishing catalyst concentration in atom transfer radical polymerization with reducing agents. *Proceedings of the National Academy of Sciences* **2006**, *103*, 15309–15314
- (31) Anderegg, G.; Hubmann, E.; Podder, N. G.; Wenk, F. Pyridinderivate als Komplexbildner. XI. Die Thermodynamik der Metallkomplexbildung mit Bis-,



- Tris- und Tetrakis[(2-pyridyl)methyl]-aminen. *Helvetica Chimica Acta* **1977**, *60*, 123–140.
- (32) Wenk, F.; Anderegg, G. Thermodynamic investigations of metal complexes with pyridines ligands. *Chimia* **1970**, *24*, 427–431.
- (33) Rostovtsev, V. V; Green, L. G.; Fokin, V. V; Sharpless, K. B. A Stepwise Huisgen Cycloaddition Process: Copper(I)-Catalyzed Regioselective “Ligation” of Azides and Terminal Alkynes. *Angewandte Chemie International Edition* **2002**, *41*, 2596–2599
- (34) Wang, Q.; Chan, T. R.; Hilgraf, R.; Fokin, V. V; Sharpless, K. B.; Finn, M. G. Bioconjugation by Copper(I)-Catalyzed Azide-Alkyne [3 + 2] Cycloaddition. *Journal of the American Chemical Society* **2003**, *125*, 3192–3193
- (35) Tornøe, C. W.; Christensen, C.; Meldal, M. Peptidotriazoles on Solid Phase: [1,2,3]-Triazoles by Regiospecific Copper(I)-Catalyzed 1,3-Dipolar Cycloadditions of Terminal Alkynes to Azides. *The Journal of Organic Chemistry* **2002**, *67*, 3057–3064
- (36) Kolb, H. C.; Finn, M. G.; Sharpless, K. B. Click Chemistry: Diverse Chemical Function from a Few Good Reactions. *Angewandte Chemie International Edition* **2001**, *40*, 2004–2021
- (37) Chan, T. R.; Hilgraf, R.; Sharpless, K. B.; Fokin, V. V Polytriazoles as Copper(I)-Stabilizing Ligands in Catalysis. *Organic Letters* **2004**, *6*, 2853–2855

## **Chapter 4 – Progress Towards the Development of a Sensing System for Chiral Thiols**

### **4.1 INTRODUCTION**

#### **4.1.1 – Goals and Scientific Questions**

In this chapter, a system using a tripodal ligand system to be determined the chirality of thiols using CD signals. Several different chiral thiols were synthesized and tested with the system. Furthermore, the equivalents of thiol need for the system to reach equilibrium were explored using CD signal as well as the effects of different secondary amines. Generally, this project seeks to answer if the tripodal ligand system explored in the previous chapter can be used to measure *ee* of different thiols.

#### **4.1.2 – Chirality in Biological Systems**

Biological systems are constructed primarily of amino acids, sugars and lipids, many of which contain at least one stereogenic center. A stereogenic center is an atom or point in a molecule in which changing any two groups creates a new stereoisomer.<sup>1</sup> Many stereogenic centers impart chirality to a molecule, where these centers create two nonsuperimposable mirror images known as enantiomers. Enantiomers are stereoisomers which have the same connectivity of atoms but are not superimposable on their mirror image. Each of these structures is chemically identical in an achiral environment except for the spacial orientation of the functional groups around a central point or atom. Amino acids are one of the common examples of a chiral molecule (Figure 4.1).

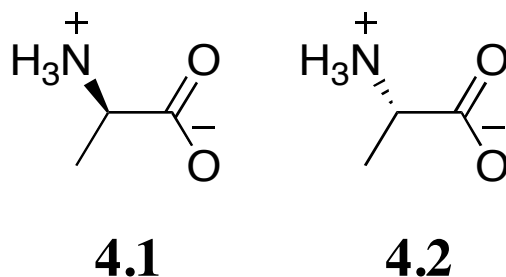


Figure 4.1 – A Pair of Amino Acids Showing Both Enantiomers

Furthermore, diastereomers are stereoisomers that are not enantiomers. Often, diastereomers are thought of as compounds that have different configurations at one or more stereocenters but are also not mirror images of each other. Diastereomers, unlike enantiomers, are different in their physical properties and can be easily distinguished from each other.

#### 4.1.3 – Naming Systems of Chiral Compounds

Several different systems for labeling stereogenic centers have been developed based upon the type of chirality shown by the molecule. The most common form is based upon the direction the enantiomer rotates plane polarized light. Molecules which rotate plane polarized light clockwise are called dextrorotatory and are labeled (+), and conversely those that rotate plane polarized light counterclockwise are called levorotatory and are labeled (-). This description is based upon a physical property of the molecule and cannot be assigned *a priori* without an experiment. Additionally, the description provides no physical information about the location of the groups around the stereogenic center relative to the other groups.

Several methods for describing stereoisomers based upon the orientation of the groups around the stereogenic unit have been developed. The simplest of these describes the relationship between two different units on adjacent atoms in a ring or on a double

bond. A molecule with a cis configuration has the groups in the same orientation while a trans molecule has the groups in the opposite orientation.

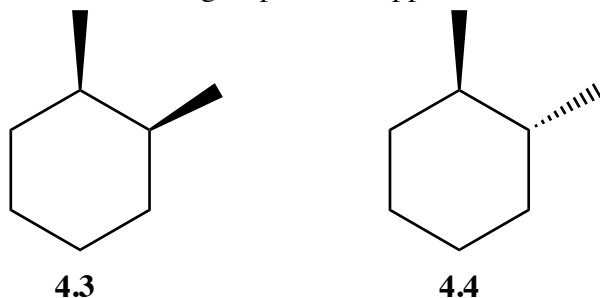


Figure 4.2 – Representation of Both Stereoisomers of 1,2-Methylcyclohexane Which Shows Cis versus Trans Relationship

When looking at a single carbon atom with four different groups attached, the most commonly used naming method is the Cahn, Ingold, Prelog system.<sup>2</sup> Each of the groups is assigned a priority based upon the atomic number. When the groups are arranged based upon priority with the lowest priority group directed into the plane, the molecule is labeled R from the Latin word (rectus) for right if the numbers increase in a clockwise fashion. When the groups increase in a counterclockwise fashion, the molecule is labeled S, again from the Latin (sinister) for left.

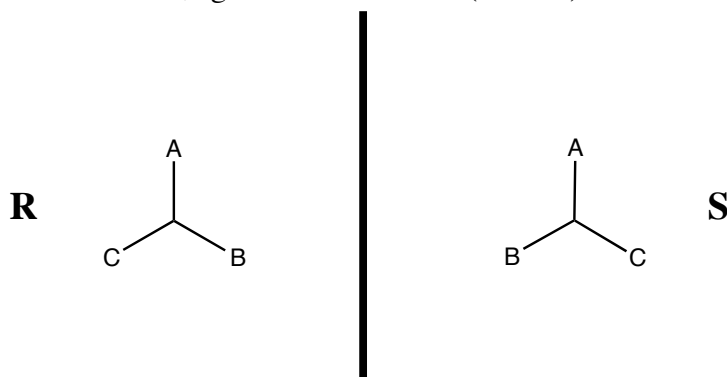


Figure 4.3 – Representation of Two Idealized Molecules Showing R and S Using the Cahn, Ingold, Prelog System (Fourth Group is Behind Central Atom)

There are several other descriptors for chirality, such as the D- or L- system used to describe biological molecules, but the last one that is relevant for our current work describes the twist of molecules. In this case, the molecule itself does not necessarily have a chiral center but rather contains an axis of chirality based upon the twist of groups or helical nature of the molecule. A structure which has a right handed twist is labeled p (for plus), and a left handed twist is labeled m (for minus). This form of chirality becomes important when we look at the orientation of the groups around a central metal ion in our tripodal assembly, because they can adopt either orientation. This alignment will be described later in more detail because it is the basis for the signal generation in our detection system.

#### **4.1.4 Importance of Chirality**

Since many biomolecules are created from amino acids and sugar building blocks, these components create a chiral environment. One of the inherent characteristic of chiral environments is that it interacts differently with other chiral molecules based upon the stereochemical identity of the molecule.<sup>3</sup> In the majority of biological systems, proteins and peptides are created using amino acids that contain a single enantiomer, making the chirality of molecules that interact with the biological matrix important.

Because of the handedness of biological systems, many drugs and drug candidates also contain stereogenic centers, and the differences between enantiomers can be quite dramatic. The most common and oft quoted example is the difference between the enantiomers of thalidomide (Figure 4.4). Thalidomide was a popular antinausea drug

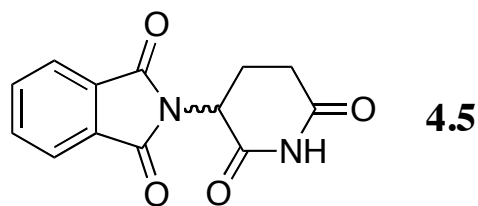


Figure 4.4 – Structure of the Antinausea Medication, Thalidomide

given to pregnant women to help with morning sickness during the mid-20<sup>th</sup> century.<sup>4</sup> The drug was given as a racemate, i.e. a mixture of equal proportions of each enantiomer.<sup>5</sup> Unfortunately, only one of the enantiomers had the desired benefits; the other enantiomer was a powerful teratogen causing numerous and serious birth defects. The teratogenic effects of the drug were enhanced by the fact that the drug was primarily given to pregnant women. Within a few years after landing on the market, the drug was pulled because it was considered too unsafe for continued use.

While the history of thalidomide is more nuanced, the case was a cautionary tale for drug manufacturers who had not considered the impact of having both enantiomers in a medicine. Because of the case of thalidomide, screening of each enantiomer has become the standard practice. Additionally, if only one enantiomer has biological activity synthesizing a single enantiomer is a more cost efficient approach to developing a drug. By creating a single enantiomer, all of the starting material and reagents needed are converted into the final product leading to fewer materials being wasted. Furthermore, a drug created as a single enantiomer does not contain any inactive components making the drug more potent.

#### 4.1.5 – Need for High Throughput Detection Methods for Chirality

The need for compounds of a single enantiomer has dramatically increased research into asymmetric synthesis methodologies.<sup>6</sup> Asymmetric synthesis is a synthetic

protocol that preferentially forms one enantiomer over the other stereoisomer, often utilizing a chiral auxiliary to direct the formation of the desired stereoisomer. As one might imagine, the identification of the chiral auxiliary that gives the highest amount of one stereoisomer without impeding the yield of the reaction is not a trivial task. Modern automation and synthetic methodologies have enhanced the ability to run reactions in parallel producing hundreds of samples in a single day. Each of these

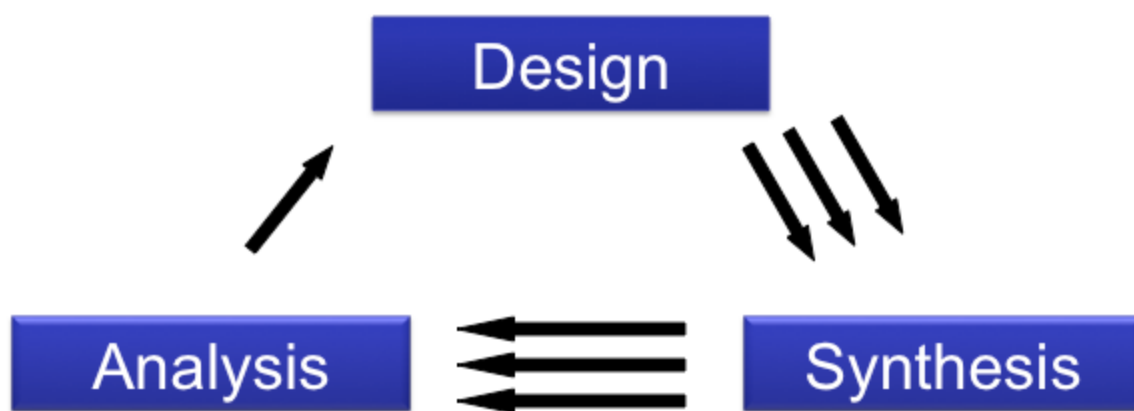


Figure 4.5 – Schematic Showing the Bottleneck in Asymmetric Catalyst Development

reactions must be screened both for overall yield as well as the yield of the desired enantiomer. The most common measurement of how enriched a reaction is in one enantiomer is enantiomeric excess (*ee*), calculated using Equation 4.1.

$$ee = 100\%(|R - S|)/(|R + S|)$$

Equation 4.1 – Equation for calculating enantiomeric excess (*ee*)

The most common way to screen a reaction mixture for enantiomeric excess is through the use of chiral HPLC or GC.<sup>7</sup> Both of these techniques are highly accurate with a relative error of 1-2 % but are slow as they can only screen a few hundred samples each day compared to the thousands that can be generated each day. Furthermore, these

techniques require expensive chiral columns that degrade over time and must be replaced. Additionally, the method requires liters of carrier gas or expensive solvents. The other major technique for *ee* determination is NMR chiral shift reagents.<sup>8</sup> Chiral shift reagents, though, do not always work for all compounds, only have an average error of 5 %, and are not adaptable to running large amounts of samples in a short amount of time. All of these methodologies do not allow access to *ee* determination in a high throughput manner leaving *ee* screening as the bottleneck in the development of asymmetric reactions.

Optical methods are readily amenable to high throughput analysis because wellplate readers are relatively inexpensive and allow for the analysis of nearly 100 or 400 samples at one time. The development of a general optical technique that would allow for the monitoring of *ee* would eliminate the bottleneck and speed the development of asymmetric reaction methodologies. Faster and more efficient asymmetric reactions would lower the cost of pharmaceuticals and other chiral chemical products by making the synthetic scheme shorter and fewer byproducts.

#### **4.1.6 – Optical Methodologies in Chirality Detection**

Several optical techniques can be used for *ee* determination, including fluorescence and UV/Vis spectroscopy. However, one of the most commonly used is circular dichroism (CD) spectroscopy.<sup>9</sup> In CD spectroscopy, the detector measures the difference between the absorbance of right and left circularly polarized light by the sample. The difference between each absorbance is plotted at each wavelength and is read from higher to lower wavelengths. The peaks in the CD spectra are known as Cotton effects. A positive Cotton effect increases above the x-axis, while a negative Cotton effect decreases below the x-axis.



#### 4.1.7 – Supramolecular Chirality Determination

Several different optical methods for enantiomeric excess determination have been developed for a wide range of different functional groups. Several research groups have developed optical detection methodologies for such functional groups as amines and carboxylic acids. In one of the most widely used supramolecular systems for *ee* determination, the James group used enantiopure BINOL, 2-formylphenylboronic acid, and a chiral amine to form a diastereomeric complex which gave a distinct NMR signal for chiral amines. Our group expanded the method to generate a CD signal and created calibration curves to determine *ee* (Figure 4).<sup>10-12</sup> Another noteworthy system is that of Wolf and coworkers, who used a

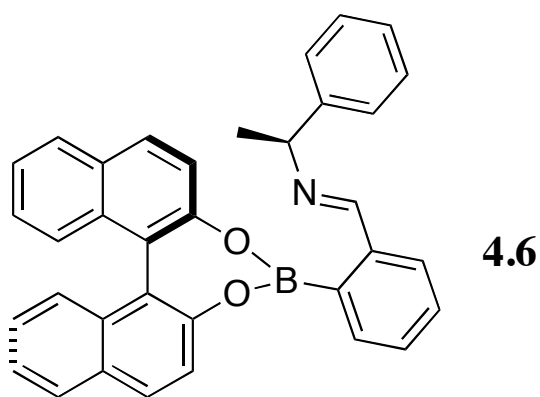


Figure 4.6 – James and Anslyn Supramolecular Assembly for Chiral Amine *ee* Determination

rigid linker with two aldehydes to detect the stereoisomers of an amine or diamine complex.<sup>13-14</sup> In solution, the amines condensed on the aldehydes to form imines creating a rigid cage-like structure that resulted in a different induced CD signal for each enantiomer of the amine added.

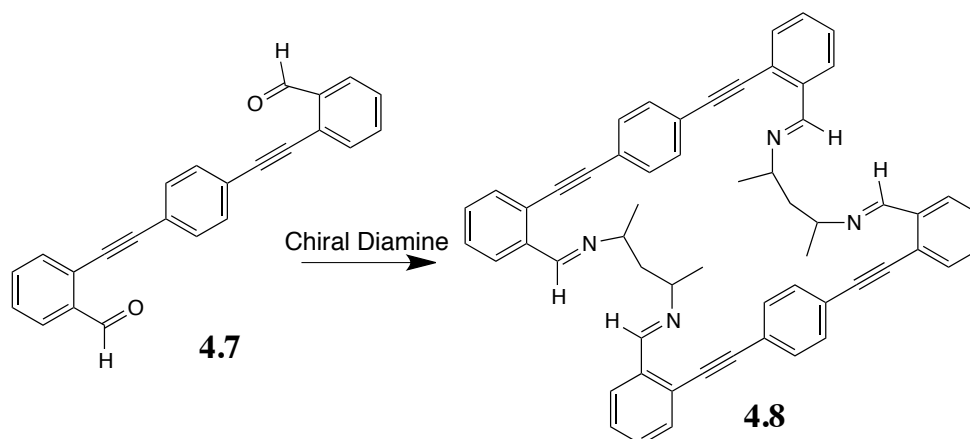


Figure 4.7 – Wolf dialdehyde which forms a rigid imine based structure that can be used for *ee* determination

Determining the *ee* of polyols and diols is easier than monoals since they have two adjacent reactive functional groups, and they have been the topic of several studies. Using a single enantiomer of a boronic acid-based receptor, an enantioselective indicator displacement assay (eIDA) was developed to discriminate chiral diols.<sup>15</sup> Boronic acids are known to bind diols and catechol groups. A catechol-based indicator was bound to

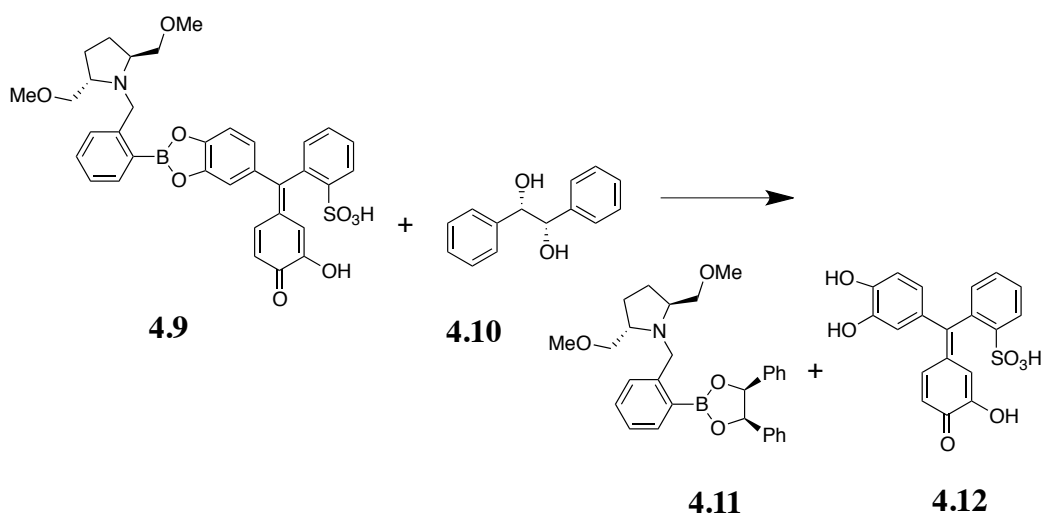


Figure 4.8 – Boronic acid based receptor for *ee* determination of chiral diols using eIDA

the boronic acid through a reversible covalent bond. In an eIDA, the indicator is then displaced in the presence of different target analytes based upon the enantiomeric identity of the host and the analyte, where one enantiomer preferentially binds the enantiomeric boronic acid host. Using multiple boronic acid hosts, an average 3% error in *ee* was obtained for a representative group of polyols.

#### 4.1.8 Chirality Determination Using Tripodal Ligand Systems

The Canary group used the amine group of amino acids to displace halides on quinolylmethyl halides to form a tripodal ligand system that chelates the metal around an apical nitrogen.<sup>16-17</sup> Optical signals in the CD spectra from the metal to ligand charge transfer bands are generated by the system based upon the configuration around the  $\alpha$ -carbon of the amino acids. These ligand systems produce strong CD signals, but

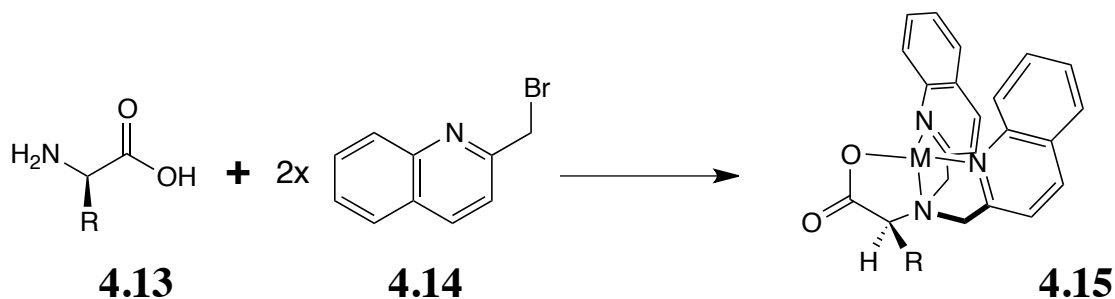
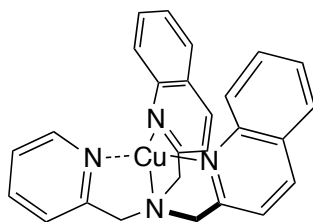


Figure 4.9 – Canary bisquinolylamine system from modified amino acids

modifying the analyte through irreversible covalent bonds makes them impractical for quick screening of reaction mixtures.

Other functional groups have been targeted through supramolecular techniques to determine the *ee* of the produced chiral functional group using similar tripodal ligand structures. Our group has expanded upon the Canary ligand structure to use a

(bisquinyl)pyridyl)amine chelated to a copper ion to detect  $\alpha$ - and  $\beta$ -chiral carboxylates.<sup>18</sup> The anionic carboxylate group binds to a vacant coordination site at the



#### 4.16

Figure 4.10 – Anslyn modified heterocyclic copper complex which can be used to determine the *ee* of chiral carboxylates

copper ion, positioning the stereogenic center between the heterocyclic rings. The rings adopt a twist which gives rise to an exciton coupled circular dichroism signal based on the steric size of the medium and large groups on that carbon. A larger difference in size of the groups around the stereocenter leads to a larger CD signal. Even a  $\beta$ -chiral carboxylate, with a longer distance between the carboxylate and stereocenter leads to an observable signal. In addition to *ee* determination, the system was able to differentiate the identify of the carboxylate through chemometric techniques such as linear discriminate analysis.

#### 4.1.9 – Anslyn Group Work on Alcohol *ee* Determination

Furthermore, our group has developed a dynamic assembly (highlighted in Chapter 3) through the condensation of a heterocyclic aldehyde with the amine of dipicolylamine to create a hemiaminal with pendant heterocyclic arms (Figure 4.7).<sup>19</sup> In solvents such as

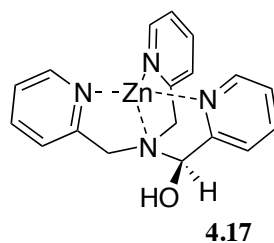


Figure 4.11 – Dynamic Tripodal Assembly Used for Alcohol *ee* Determination

acetonitrile and in the presence of zinc ions, the condensation of 2-pyridinecarboxyaldehyde proceeds with an equilibrium constant of almost  $6,600 \text{ M}^{-1}$  giving primarily the tripodal complex. The dynamics and the range of variability of this system have been studied and was further explored earlier in this dissertation. While tripodal ligand systems have a variety of uses, such as phosphodiesterase and polymerization catalysis, our group has used this dynamically produced tripodal ligand system to determine the *ee* of secondary alcohols, and we are expanding the studies to chiral thiols.

In the tripodal ligand system, the hemiaminal is dehydrated to produce an iminium salt. The dehydration is catalyzed by a Brønsted acid. The iminium ion is trapped by a chiral secondary alcohol producing a hemiaminal ether. The groups around the stereogenic alcohol center cause a perturbation of the twist between the pyridine

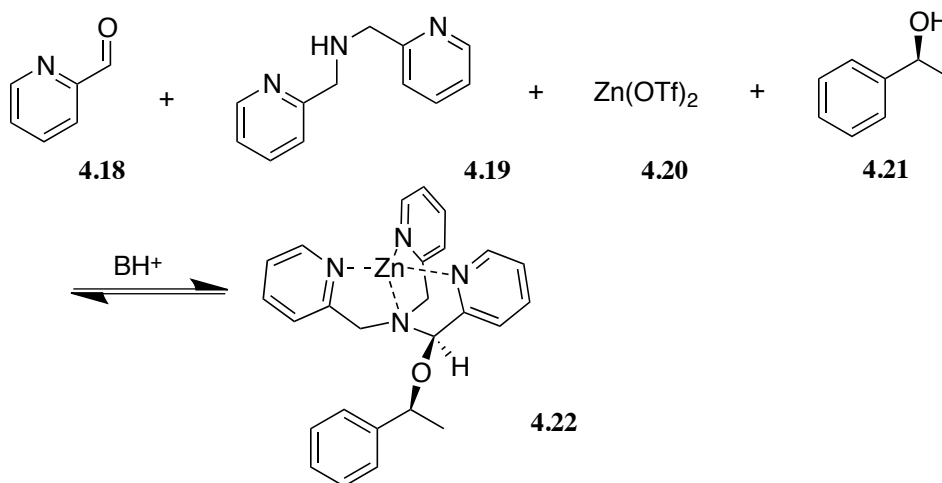


Figure 4.12 – Anslyn system which condenses on a chiral alcohol to give a hemiaminal ether and leads to a CD signal that can be used to quantify the *ee* of a solution

groups amplifying the signal in the CD spectrum.<sup>20-21</sup> A wide variety of secondary alcohols were screened; each alcohol showed a unique CD spectra leading to discrimination of identity as well as *ee* values. A variety of secondary alcohols containing a wide range of other functional groups were screened, showing that the system was compatible with those functional groups and giving an average *ee* error of 3%. The groups on the stereocenter of the alcohol can be correlated to the CD signal through the use of Charton parameters.<sup>22</sup>

#### 4.1.10 Importance of Thiols

Given the structural similarity to alcohols, we planned to expand the substrates that the system can differentiate and hence to determine the *ee* of thiols. While thiols are not as prevalent as alcohols, chiral thiols are present in many natural products and their syntheses are targets of asymmetric catalysis.<sup>23</sup> Similar to the challenges faced by differentiation of alcohols, monothiols have a single reactive functional group with only limited reversible covalent bond forming reactions.

Furthermore, several of the leading drugs contain a chiral sulfur atom, making thiols an important building block for their synthesis. Within the top 25 grossing drugs in the 2000's, two, Nexium® and Singulair®, contain a chiral sulfur atom that can be obtained through the use of a thiol.<sup>24</sup> Furthermore, the formation of carbon-sulfur bonds has increased in popularity in recent years given the functional group's biological properties.<sup>25</sup>

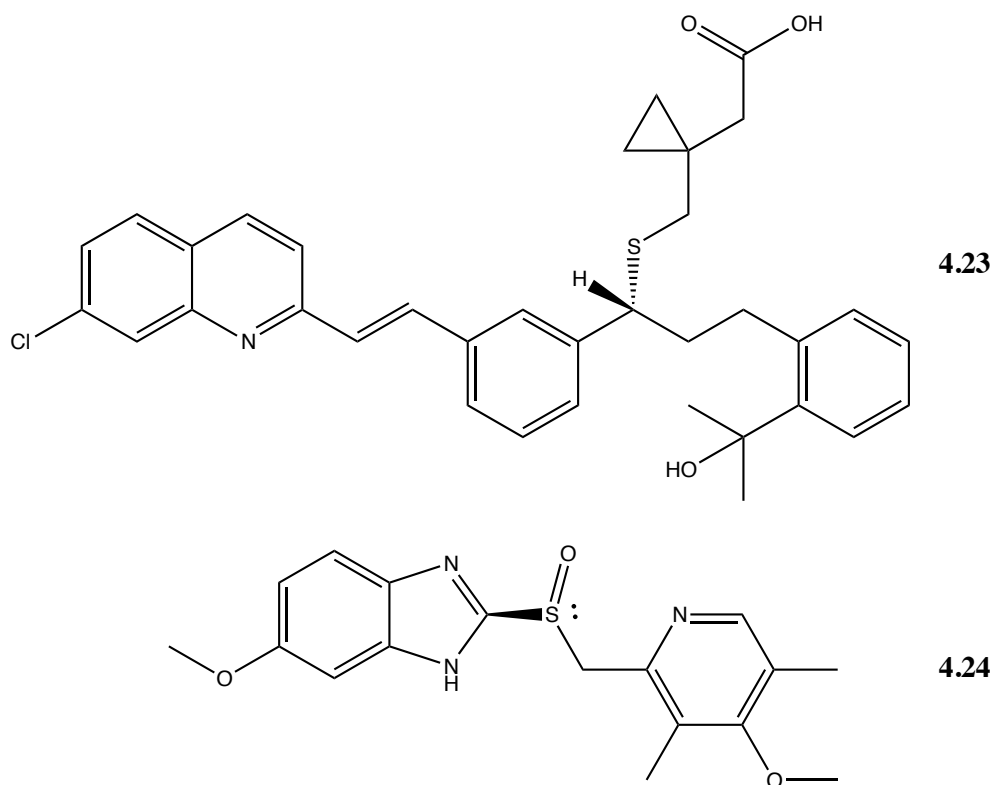


Figure 4.13 – Structure of Two Drugs Containing Chiral Sulfur Atoms From Which Chiral Thiols are Synthetically Important

#### 4.1.11 Previous Work on *ee* Determination of Chiral Thiols

In previous reports, the Riguera group has shown that chiral thiols can be modified with chiral carboxylic acids.<sup>26</sup> In NMR spectroscopy, the final product shows

peaks for each stereoisomer, and the integration of each peak could be used to calculate the *ee* percentage. However the system requires the modification of the thiol and is only

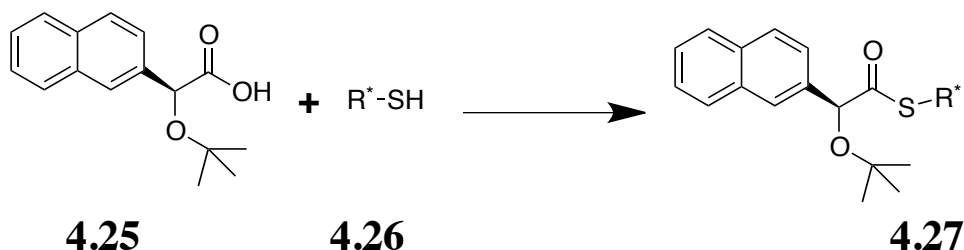


Figure 4.14 – Riguera chiral derivatizing agent for thiols

compatible with NMR spectroscopy, limiting its ability to be adapted to a high throughput use.

Furthermore, the standard methodology for determining the *ee* of thiols is through a diastereomer-forming reaction with Mosher's acid.<sup>27</sup> The acid, which is itself chiral, is used as a chiral derivatizing agent. An enantiopure acid reacts with the thiol to form a thioester and thus creates diastereomers. By measuring the resonance of the



Figure 4.15 – Mosher's acid reaction scheme for *ee* determination

trifluoromethyl group on the acid in <sup>19</sup>F NMR, the amount of each enantiomer of the thiol can be determined. While this method works well, it is not amenable to high throughput screening. Thus, we propose the use of our dynamic tripodal ligand system to measure the *ee* of chiral thiols.



## 4.2 – SYNTHESIS OF CHIRAL THIOLS

### 4.2.1 Representative Chiral Thiols

Because few chiral thiols are commercially available, the thiols to be used in our analysis were synthesized from the corresponding enantiopure alcohol. In reviewing our previous work determining the *ee* of chiral alcohols, seven different starting alcohols were explored as possible starting materials that could be converted to chiral thiols.

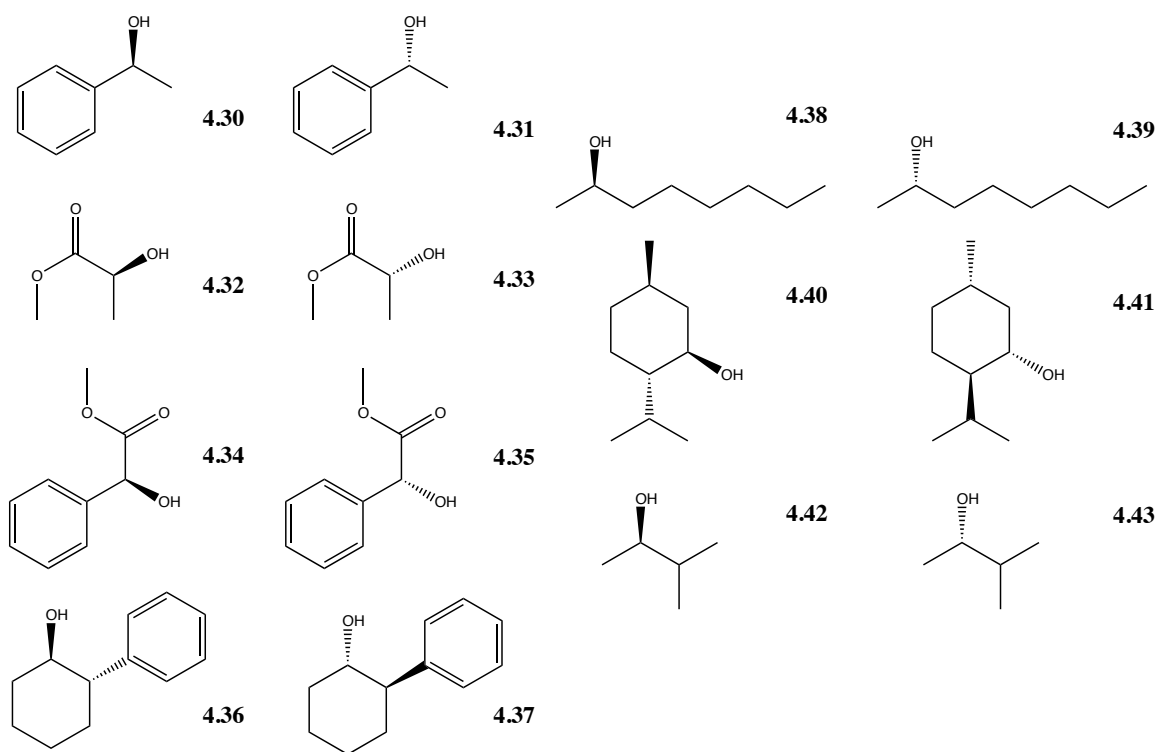


Figure 4.16 – Seven Initial Chiral Alcohols for Conversion to Chiral Thiols

### 4.2.2 Synthesis of Chiral Thiols

Four of the starting alcohols had been previously converted to chiral thiols. Using that methodology, we proposed the other three could be similarly synthesized.<sup>28</sup> Unfortunately, the synthetic workup consists of a number of extractions from ether to

water, and the 3-methyl-2-butanol (4.42 and 4.43) tends to move into the aqueous layer preventing this method from being used. Furthermore, trans-2-phenylcyclohexanol was relatively expensive and thus was excluded from the final suite of chiral thiols.

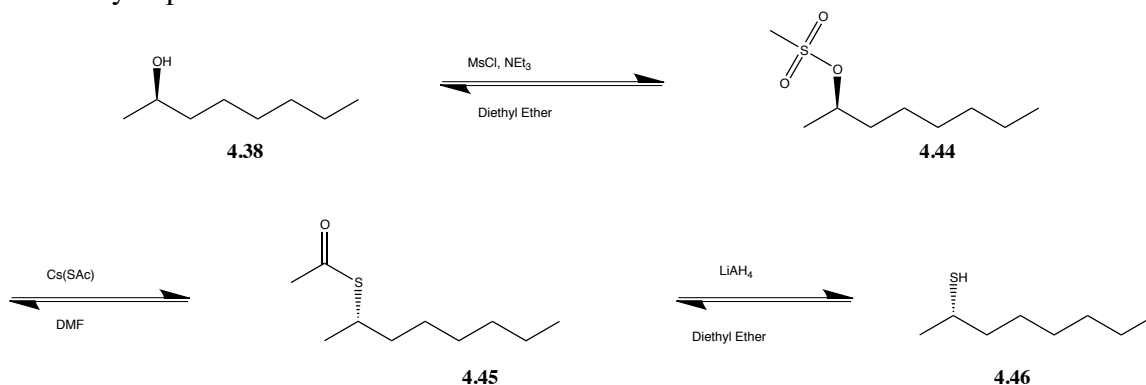


Figure 4.17 – Synthetic Scheme for Thiol Synthesis

Using the procedure developed by Kellogg, the starting alcohol is reacted in diethyl ether with methanesulfonyl chloride and triethylamine to produce the corresponding mesylate. *In situ*, cesium thioacetate was generated by reacting cesium carbonate with thioacetic acid in dry methanol. The mesylate produced earlier was combined with the cesium thioacetate in DMF with moderate heating and stirring. The resultant thioacetate was then deprotected using a variety of methods depending on the other functional groups present in the molecule. The chiral center, in this synthetic protocol, shows overall inversion of the starting stereochemistry.

### 4.2.3 Difficulties with Chiral Thiol Synthesis

One of the alcohols (2-octanol) has currently been converted to thiols. In both cases, the molecule contained no other reactive functional groups leaving open a number of different cleavage methods from the thioacetate to generate the free thiol. The gentlest method suggested by Kellogg and coworkers used 3% HCl in methanol. Unfortunately, this cleavage method afforded no free thiol and only the thioacetate was obtained. Based

upon a literature procedure, cleavage of the acetyl protecting group was attempted using hydrazine monohydrate.<sup>29</sup>

Again, no cleavage of the acetyl group was observed in either <sup>1</sup>H NMR or through LCMS. Thus, we turned our attention to using another method outlined in the report by Kellogg, which used lithium aluminum hydride (LAH) to cleave the acetate group. LiAlH<sub>4</sub> is a strong reducing agent and we felt it was not a good starting point for our cleavage protocol. However, given the lack of success with the other cleavage protocols, we decided to use LiAlH<sub>4</sub> on these thioacetates.

Unfortunately, the octanethiol obtained was not enantioenriched showing only 62% *ee* for the R enantiomer and 78% *ee* for the S enantiomer using Mosher's method to determine the *ee* of the compound.

Furthermore, efforts to synthesize the other thiols have been attempted but have met with limited success. The thiol derivative of methyl lactate has yet to be successfully isolated. The conversion to the mesylate proceeded with near quantitative conversion. The displacement with cesium thioacetate has also been successfully carried out. Unfortunately, the acidic cleavage with 3% HCl in methanol was unsuccessful in cleaving the acetyl group. Given that the other methods using hydrazine or LAH would destroy the methyl ester, a new cleavage method must be developed. Using a more strongly acidic alcohol solution is a logical next step in developing that method.

Other difficulties with the synthesis of 1-phenylethanethiol and ethyl thiomandelate were observed. With 1-phenylethanol, the mesyl activation of the alcohol showed only limited conversion (approximately 40%) to the activated sulfonate. Current efforts are underway to separate the starting material from this activated form before the mesylate is carried on to the displacement step. In the case of ethyl mandelate, the resultant mesylate is not very soluble in ethanol, the reported solvent used, and no

displacement product was isolated. The displacement of the mesylates of ethyl mandelate and crude 1-phenylethanol were carried out in this solvent because literature reports with ethyl mandelate reported racemization in DMF, likely due to the increased stability of the mesylate being in a benzylic position in that solvent. Given the limited solubility, coupled with the fact that no displacement was observed in ethanol, a new solvent system needs to be identified.

#### **4.2.4 Current Status of Thiol Synthesis**

As it currently stands, one thiol has been successfully synthesized; the thiol obtained from 2-Octanol although with low enantiomeric excess. The thioacetate from menthol remains to be cleaved using LAH. Another thioacetate, methyl lactate thioacetate, has also been successfully synthesized and the activated sulfonates for both ethyl mandelate and 1-phenylethanol have been obtained. The mesylate from 1-phenylethanol first needs to be purified before further derivatization can be carried out. Finally, a new solvent needs to be identified for the displacement with cesium thioacetate of the benzylic sulfonates.

### **4.3 ASSEMBLY STUDIES WITH CHIRAL THIOLS**

#### **4.3.1 Studies with a Model Chiral Thiol**

To test if the assembly would incorporate a chiral thiol, a thiol derivative of glucose was explored.  $\beta$ -D-thioglucose tetraacetate was used because it contained a chiral free thiol in the anomeric position.

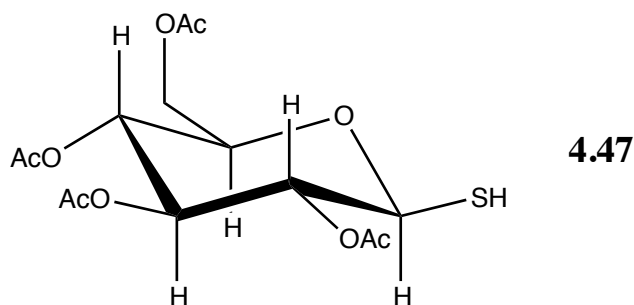


Figure 4.18 – The Model Chiral Thiol -  $\beta$ -D-thioglucose tetraacetate

Because glucose and glucose derivatives are chiral, we expect a CD signal when it is incorporated into the assembly. Because the thiol is in the anomeric position, the thiol can racemize in solution, so a negative result would not be conclusive that the system does not work. Fortunately, a CD signal was obtained of approximately 40 millidegrees using this chiral thiol giving positive proof that the assembly system is responsive to chiral thiols like the system was to chiral alcohols.

### 4.3.2 $^1\text{H}$ NMR Analysis of Assembly Formation

In studying our assembly reaction,  $^1\text{H}$  NMR were used to determine the extent of assembly formation and we turned to a similar procedure to study the formation of a hemiaminal thioether. When comparing the  $^1\text{H}$  NMR spectra relative to the assembly when no thiol is present, the spectrum with thiol showed no remaining aldehyde peak meaning the aldehyde had completely reacted to form the assembly. Furthermore, the peaks at approximately 6 ppm corresponding to the hydroxyl hydrogen atom disappeared. The corresponding hydrogen atom on the aldehyde carbon shifted upfield by approximately one ppm to approximately 4.5 ppm

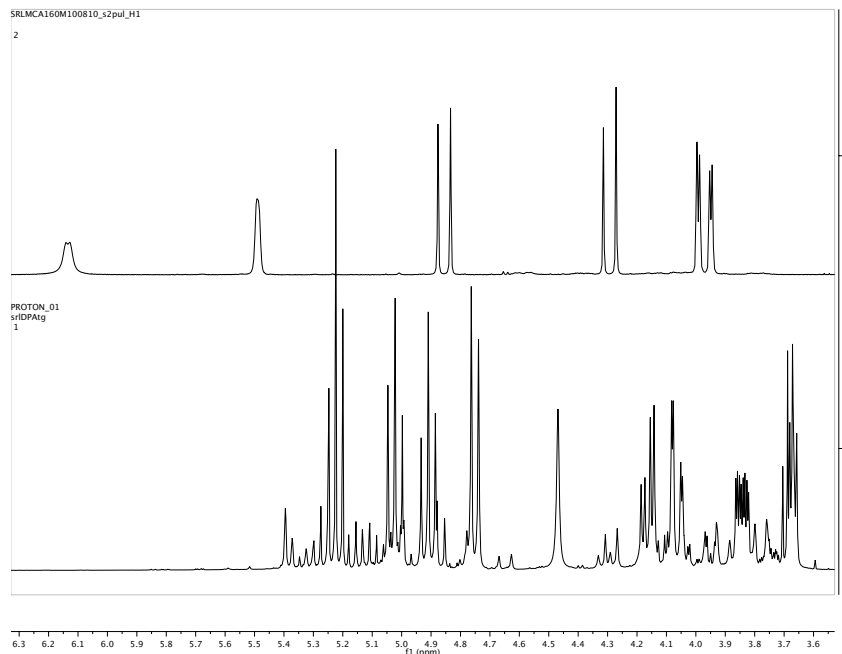


Figure 4.19 -  $^1\text{H}$  NMR spectral overlay from 3.5 to 6.4 ppm of the assembly with no thiol (on top) and the assembly with 5 equivalents of thiol (bottom).

as they hydroxyl group is replaced with a thioether. The methylene peaks also shifted upfield to varying degrees and are split into two sets of doublets. The sets of doublets arise from the formation of a diastereomeric complex and are roughly equal in magnitude. These modulations of the spectrum appear to correlate with the formation of the hemiaminal thioether.

### 4.3.3 Studies of the Equivalents of Thiol Needed to Reach Signal Saturation

Because the system can depend on the concentration of the thiol, a concentration in which there was no signal modulation must be identified. In order to identify that amount of thiol, a titration with increasing amounts of thiol was carried out. By monitoring the CD signal and the number of equivalents, and thus the concentration, that leads to no change in the CD signal can be determined. In Figure 4.13, the CD spectra

were plotted showing how the spectral curve changes as a function of increasing equivalents of thiol. After the signal

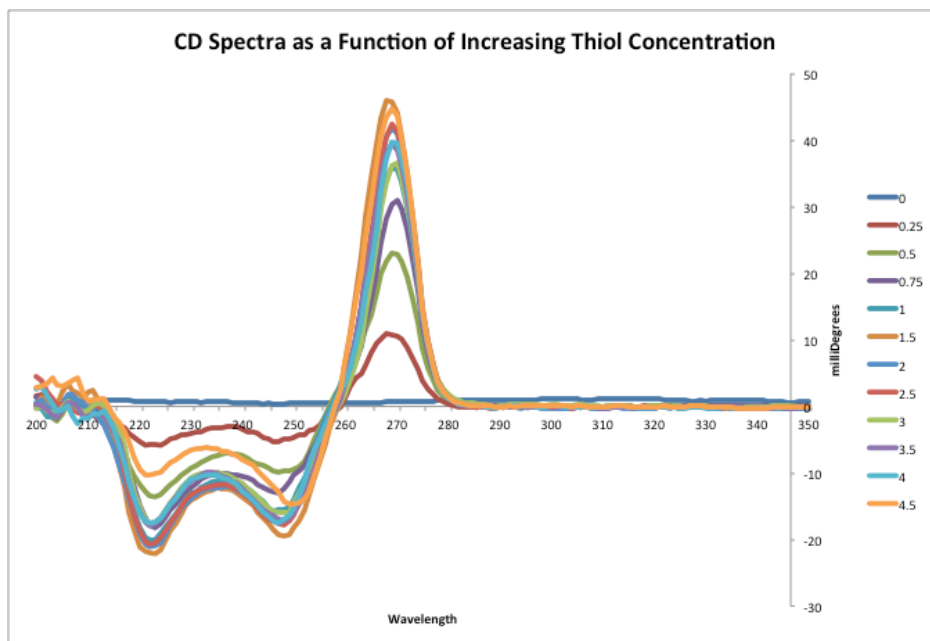


Figure 4.20 – Graph of CD spectra as a Function of Thiol Equivalents

reached saturation at 1.5 equivalents, some variation of the signal was observed. While some instrumental noise is expected, the variance could be explained by the presence of additional thiol that could form disulfides and thus shift the mixture equilibrium. In order to more easily identify the point at which the signal is saturated, the CD signal at the  $\lambda_{\max}$  of 269 nm was plotted against the equivalents of thiol added (Figure 4.14). Based upon

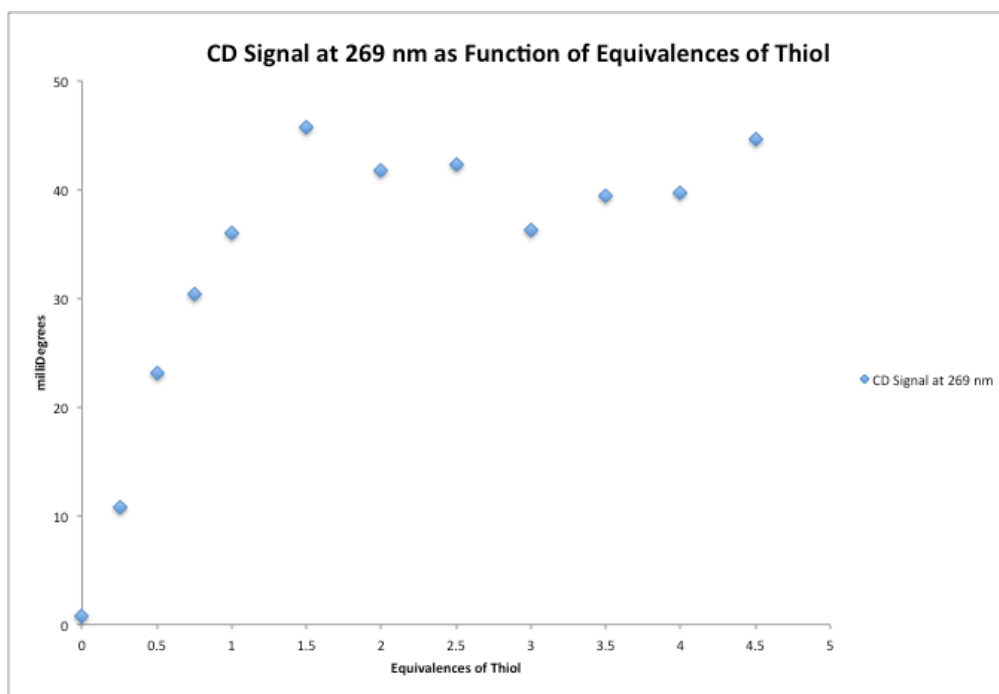


Figure 4.21 – CD Signal at 269 nm as a Function of Thiol Equivalence

this plot, we postulate the CD signal is saturated at 1.5 equivalents, and thus all future assembly processes will be carried out at 2 equivalents of thiol.

#### 4.3.4 Comparison of Secondary Amines Between Dipicolylamine and Bis(triazole)amine through $^1\text{H}$ NMR and CD Spectroscopy

In an effort to determine the optimal system for *ee* determination, a comparison between the two secondary amines used in our previous study – dipicolylamine and bistriazoleamine – was carried. When looking at the  $^1\text{H}$  NMR spectrum of the two different systems, they appear to be very similar. The spectra showed both no remaining aldehyde peak and the disappearance of the peak corresponding to the hydroxyl group, but the peak corresponding to the hydrogen on the hemiaminal thioether did not shift as



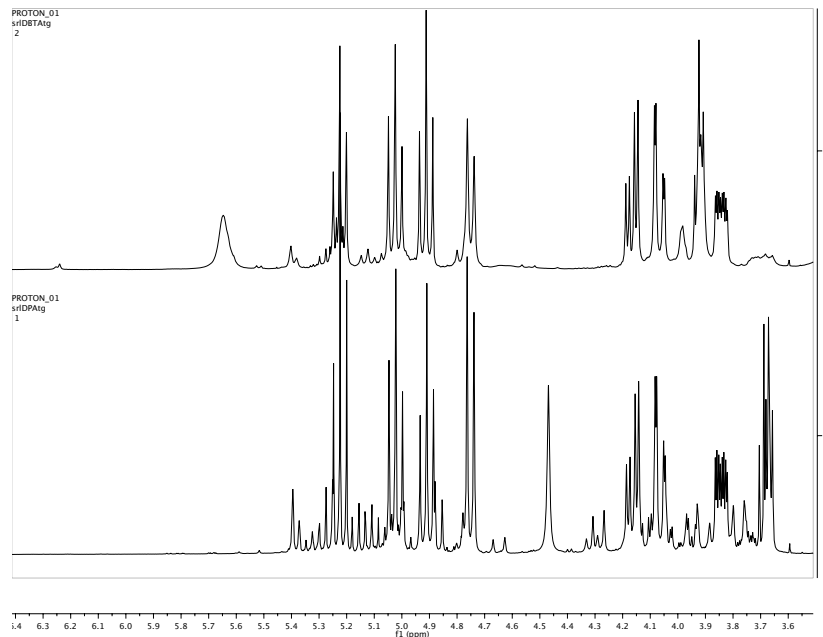


Figure 4.22 -  $^1\text{H}$  NMR Spectral Overlay of the Two Secondary Amine Ligands with Thiols

much as in the case of the dipicolylamine assembly. Similar spectral changes were observed in the bis(triazole)amine spectrum leading to the conclusion that both systems form the thioether with the dipicolylamine assembly forming to a greater extent (Figure 4.15)

At a concentration of thiol when the CD signal is saturated, the dipicolylamine system showed an approximately 40 mDeg signal. The signal obtained using the bis(triazole)amine only showed a signal of 9 mDeg at saturation. The much smaller signal of the bis(triazole)amine likely arises from the fact that triazoles are weaker chromophores. The triazole itself and the attached benzene rings generate a weaker UV signal when coupled together compared to the pyridine rings. As further evidence, the UV spectra obtained for the bis(triazole)amine also showed a much lower absorbance than any of the spectrum obtained using the dipicolylamine. While this system showed

some promise, the conditions need to be optimized to generate a larger CD signal using the triazole based ligand. Finally, a bis(triazole)amine with a better chromophore would also greatly enhance the signal in the CD spectrum.

#### **4.4 *ee* MEASUREMENTS**

##### **4.4.1 Measurement of *ee***

In order to measure the *ee* of a solution, a relationship between *ee* and optical signal must be determined. In order to quantify *ee*, a calibration curve must be generated. By measuring the CD signal as a function of different ratios of enantiomers, a line can be generated. By fitting the line, an equation is generated that relates CD signal to the *ee* of the solution.

##### **4.4.2 *ee* Calibration Curve of 2-Octanethiol**

Unfortunately, given the low *ee* obtained from the recovered 2-octanethiol, a calibration curve proved difficult to obtain. Since both solutions were extremely enantioenriched and the relative signal of the molecule, the CD spectra showed little definitive peak structure and limited the construction of a calibration curve. The alcohol, 2-octanol, showed only a 12 milliDegree signal and a similar signal would be expect with the thiol derivative. With such a low signal and low enantioenrichment, the calibration curve was put on hold until a more enatiomerically pure sample could be obtained.

#### **4.5 CONCLUSIONS**

The tripodal assembly explored in the previous chapter will incorporate thiols to form hemiaminal thioethers. If the thioether is chiral, the assembly gives rise to a CD signal that can be quantified. The number of equivalents of thiol needed to saturate the signal was identified using a model commercially available thiol. Currently, five chiral

thiols are being synthesized and one has been successfully made but with limited enantiopurity.

#### **4.6 FUTURE WORK**

While the current work is promising for the determination of *ee* of different chiral thiols, a larger pool of thiols should be screened to determine the range of the system. To this end, synthetic methods should be improved to allow more effective cleavage of the acetate group. Furthermore, a new solvent system for the synthesis of the benzyl thiols needs to be identified. Finally, continued exploration of the use of the different secondary amines should be explored to determine if a larger signal could be generated with modifications of the heterocycles.

#### **4.7 EXPERIMENTAL METHODS**

All NMR spectra were collected through The University of Texas at Austin NMR facility on a Varian 400 MHz NMR equipped with a robotic arm. A Jasco J-815 CD Spectrometer from the Texas Institute for Drug and Diagnostic Development (TI-3D) at The University of Texas at Austin was used to collect all CD spectra. All mass spectral data were collected through the mass spec facility at The University of Texas at Austin on an Agilent Liquid Chromatography Mass Spectrometer with a 4-minute acetonitrile/water gradient and a coupled electrospray ionization and atmospheric pressure chemical ionization. All starting alcohols were purchased from either Sigma Aldrich or Acros and used as received. All reagents were purchased from Sigma Aldrich and most were used as received. The thioacetic acid was distilled under nitrogen prior to use. All solvents were collected from a solvent delivery system and used as collected.

The mesylation of the alcohols was carried out in dry diethyl ether. The alcohol was added to the solution followed by three equivalents of triethylamine that had been

dried over sieves. After the addition of the amine, a solution of mesyl chloride in ether was prepared. This solution was titrated into the alcohol solution which was cooled to -10°C using a brine ice bath. As the mesyl chloride was added, a solid formed. After an hour, the reaction was quenched using 1M HCl. The ether was washed with 1M HCl, brine and then water. The ether was dried with magnesium sulfate, filtered and removed under reduced pressure to give a clear oil (or in the case of ethyl mandelate, a white solid).

Mesylate of Menthol – <sup>1</sup>H NMR, 400 MHz – 4.77 (1H, multiplet), 2.99 (3H, singlet), 2.25 (1H, multiplet), 2.05 (1H, multiplet), 1.67 (2H, multiplet), 1.40 (2H, multiplet), 1.23 (1H, quartet), 1.04 (1H, multiplet), 0.92 (6H, doublet of doublets), 0.81 (3H, doublet)

Mesylate of Octanol -<sup>1</sup>H NMR, 400 MHz – 4.51 (1H, quintet), 2.99 (3H, singlet), 1.60 (2H, multiplet), 1.27 (12H, multiplet), 1.60 (3H, triplet)

Mesylate of Lactate -<sup>1</sup>H NMR, 400 MHz – 4.51 (1H, triplet of doublets), 3.79 (3H, singlet), 3.11 (3H, singlet), 1.60 (3H, doublet)

The cesium thioacetate was obtained by reacting thioacetic acid with cesium carbonate in dry methanol under a nitrogen atmosphere. The solvent was removed and the resultant compound was washed with acetone and used without further purification.

The thioacetate was prepared by combining the cesium thioacetate immediately after it was prepared with the corresponding mesylate in dry DMF. The thioacetate of octanol was heated to 40°C, and the thioacetate of menthol was heated to 55°C. All others were stirred at room temperature. Each of these reactions were stirred for 18 hours except for menthol which was heated for 40 hours. The cesium salts were precipitated through the addition of ether and the resultant solution was washed with brine and then

water. The resultant ether was dried using magnesium sulfate and removed under reduced pressure.

Menthol Thioacetate –  $^1\text{H}$  NMR, 400 MHz – 3.45 (1H, multiplet), 2.30 (3H, singlet), 2.24 (1H, multiplet), 2.05 (1H, multiplet), 1.65 (2H, multiplet), 1.39 (2H, multiplet), 1.26 (1H, quartet), 1.04 (1H, multiplet), 0.92 (6H, doublet of doublets), 0.81 (3H, doublet),  $\text{M}+\text{H}^+$  215.37

Octane Thioacetate –  $^1\text{H}$  NMR, 400 MHz – 3.50 (1H, multiplet), 2.25 (3H, singlet), 1.48 (2H, multiplet), 1.23 (12H, multiplet), 0.82 (3H, triplet),  $\text{M}+\text{H}^+$  189.12

Methyl Lactate Thioacetate –  $^1\text{H}$  NMR, 400 MHz – 4.25 (1H, quartet), 3.71 (3H, singlet), 2.33 (3H, singlet), 1.48 (3H, doublet),  $\text{M}+\text{H}^+$  163.21

The thioacetate was cleaved using lithium aluminum hydride. The thioacetate was dissolved in dry ether. Using a cannula, an excess of 1M solution of lithium aluminum hydride in ether was added to the thioacetate solution. After 2 hours, the reaction was quenched with water and then 1M HCl. The reaction was extracted with 1M HCl and the ether was removed under reduced pressure.

Octanethiol – Yield ~90% (traces of ether) –  $^1\text{H}$  NMR, 400 MHz – 2.89 (1H, multiplet), 1.51 (2H, multiplet), 1.35 (12H, multiplet), 0.85 (3H, triplet)  $^{13}\text{C}$  NMR, 100 MHz – 40.91, 35.56, 31.71, 28.96, 27.37, 25.57, 22.57, 14.02,  $\text{M}+\text{H}^+$  147.29

#### 4.8 REFERENCES –

1. Anslyn, E. V.; Dougherty, D. A., *Modern Physical Organic Chemistry*. University Science books: Sausalito, California, 2006.
2. Cahn, R. S.; Ingold, C.; Prelog, V. Specification of Molecular Chirality. *Angewandte Chemie International Edition in English* **1966**, 5, 385–415.
3. Finefield, J. M.; Sherman, D. H.; Kreitman, M.; Williams, R. M., Enantiomeric Natural Products: Occurrence and Biogenesis. *Angewandte Chemie International Edition* 2012, n/a-n/a.

4. Franks, M. E.; Macpherson, G. R.; Figg, W. D., Thalidomide. *The Lancet* 2004, 363 (9423), 1802-1811.
5. Agranat, I.; Caner, H.; Caldwell, J., Putting chirality to work: the strategy of chiral switches. *Nat Rev Drug Discov* 2002, 1 (10), 753-768.
6. Maruoka, K.; Ooi, T., Enantioselective Amino Acid Synthesis by Chiral Phase-Transfer Catalysis. *Chemical Reviews* 2003, 103 (8), 3013-3028.
7. Leung, D.; Kang, S. O.; Anslyn, E. V., Rapid determination of enantiomeric excess: a focus on optical approaches. *Chem. Soc. Rev.* 2012, 41, 448-479.
8. Wenzel, T. J.; Wilcox, J. D., Chiral reagents for the determination of enantiomeric excess and absolute configuration using NMR spectroscopy. *Chirality* 2003, 15, 256-270.
9. Gottarelli, G.; Lena, S.; Masiero, S.; Pieraccini, S.; Spada, G. P., The use of circular dichroism spectroscopy for studying the chiral molecular self-assembly: An overview. *Chirality* 2008, 20 (3-4), 471-485.
10. Kelly, A. M.; Perez-Fuertes, Y.; Arimori, S.; Bull, S. D.; James, T. D., Simple protocol for NMR analysis of the enantiomeric purity of diols. *Org. Lett.* 2006, 8, 1971-1974
11. Metola, P.; Anslyn, E. V.; James, T. D.; Bull, S. D., Circular dichroism of multi-component assemblies for chiral amine recognition and rapid ee determination. *Chem. Sci.* 2012, 3, 156-161
12. Perez-Fuertes, Y.; Kelly, A. M.; Johnson, A. L.; Arimori, S.; Bull, S. D.; James, T. D., Simple protocol for NMR analysis of the enantiomeric purity of primary amines. *Org. Lett.* 2006, 8, 609-612.
13. Iwaniuk, D. P.; Wolf, C., Enantioselective Sensing of Amines Based on [1 + 1]-, [2 + 2]-, and [1 + 2]-Condensation with Fluxional Arylacetylene-Derived Dialdehydes. *Organic Letters* 2011, 13 (10), 2602-2605
14. Iwaniuk, D. P.; Wolf, C., A Stereodynamic Probe Providing a Chiroptical Response to Substrate-Controlled Induction of an Axially Chiral Arylacetylene Framework. *Journal of the American Chemical Society* 2011, 133 (8), 2414-2417.
15. Shabbir, S. H.; Regan, C. J.; Anslyn, E. V., A general protocol for creating high-throughput screening assays for reaction yield and enantiomeric excess applied to hydrobenzoin. *Proceedings of the National Academy of Sciences* 2009, 106 (26), 10487-10492.
16. Holmes, A. E.; Zahn, S.; Canary, J. W., Synthesis and circular dichroism studies of N,N-bis(2-quinolylmethyl)amino acid Cu(II) complexes: determination of absolute configuration and enantiomeric excess by the exciton coupling method. *Chirality* 2002, 14, 471-477;

17. Zahn, S.; Canary, J. W., Electron-induced inversion of helical chirality in copper complexes of N,N-dialkylmethionines. *Science* 2000, 288, 1404-1406.
18. Joyce, L. A.; Maynor, M. S.; Dragna, J. M.; da, C. G. M.; Lynch, V. M.; Canary, J. W.; Anslyn, E. V., A Simple Method for the Determination of Enantiomeric Excess and Identity of Chiral Carboxylic Acids. *J. Am. Chem. Soc.* 2011, 133, 13746-13752.
19. You, L.; Long, S. R.; Lynch, V. M.; Anslyn, E. V., Dynamic Multicomponent Hemiaminal Assembly. *Chem.--Eur. J.* 2011, 17, 11017-11023, S11017/1-S11017/14.
20. You, L.; Berman, J. S.; Anslyn, E. V., Dynamic multi-component covalent assembly for the reversible binding of secondary alcohols and chirality sensing. *Nat. Chem.* 2011, 3, 943-948;
21. You, L.; Pescitelli, G.; Anslyn, E. V.; Di, B. L., An Exciton-Coupled Circular Dichroism Protocol for the Determination of Identity, Chirality, and Enantiomeric Excess of Chiral Secondary Alcohols. *J. Am. Chem. Soc.* 2012, 134, 7117-7125.
22. You, L.; Berman, J. S.; Lucksanawichien, A.; Anslyn, E. V., Correlating Sterics Parameters and Diastereomeric Ratio Values for a Multicomponent Assembly To Predict Exciton-Coupled Circular Dichroism Intensity and Thereby Enantiomeric Excess of Chiral Secondary Alcohols. *J. Am. Chem. Soc.* 2012, 134, 7126-7134.
23. Han, X.; Wu, J. Ga(OTf)<sub>3</sub>-Catalyzed Direct Substitution of Alcohols with Sulfur Nucleophiles. *Organic Letters* 2010, 12, 5780-5782.
24. Njardarson, J. Top 2011 Drugs  
<http://cbc.arizona.edu/njardarson/group/news/2011-top-200-drug-posters-are-now-available> (accessed Nov 8, 2012).
25. Robertson, F.; Wu, J. Convenient Synthesis of Allylic Thioethers from Phosphorothioate Esters and Alcohols. *Organic Letters* 2010, 12, 2668-2671.
26. Porto, S.; Seco, J. M.; Ortiz, A.; Quiñoá, E.; Riguera, R., Chiral Thiols: The Assignment of Their Absolute Configuration by <sup>1</sup>H NMR. *Organic Letters* 2007, 9 (24), 5015-5018.
27. Dale, J. A.; Dull, D. L.; Mosher, H. S. alpha-Methoxy-alpha-trifluoromethylphenylacetic acid, a versatile reagent for the determination of enantiomeric composition of alcohols and amines. *The Journal of Organic Chemistry* 1969, 34, 2543-2549.
28. Strijtveen, B.; Kellogg, R. M. Synthesis of (racemization prone) optically active thiols by SN<sub>2</sub> substitution using cesium thiocarboxylates. *The Journal of Organic Chemistry* 1986, 51, 3664-3671.

29. Endo, A.; Yanagisawa, A.; Abe, M.; Tohma, S.; Kan, T.; Fukuyama, T. Total Synthesis of Ecteinascidin 743. *Journal of the American Chemical Society* **2002**, *124*, 6552–6554.



## **Chapter 5: Teaching Through Research: Revolutionizing the Freshman Experience**

### **5.1 INTRODUCTION –**

#### **5.1.1 Overview of Study –**

In this chapter, the use of a novel teaching methodology in freshman laboratory courses was explored. The effects of this teaching methodology is explored through examples of teaching different skill sets through three different chemistry disciplines. Students' performance in courses taught through research oriented teaching methods are compared to traditional laboratory courses to see if the teaching methods are detrimental to student's progress. Finally, the ability to use this teaching methodology at other universities or colleges is explored all in hopes of determining if freshman laboratory courses can be taught through research without affecting students' performance.

#### **5.1.1 Introduction on the Teaching of Science –**

College science education has traditionally focused on classroom instruction coupled with laboratory experiences to teach basic scientific skills. Then, after several semesters of experience advanced students may approach a professor and get involved in research projects within that professor's laboratory. In this traditional model, little opportunity for freshmen students to become involved in research is available.<sup>1</sup> Numerous studies have shown that students who become involved in research report better college experiences, are more likely to succeed, stay interested and continue in science.<sup>2-4</sup> While we teach science through the classroom and in labs designed to teach concepts through prepared experiments, the primary goal of any scientific pursuit is centered around research to create new knowledge, conduct experiments with unknown

answers and work towards solving the problems of society.<sup>3</sup> Yet hands-on, authentic research rarely is incorporated into the curriculum and science is generally taught through a set of skills and techniques students must learn in lectures and routine laboratories.<sup>5</sup>

Efforts have been undertaken to incorporate research into the classroom, but it often takes the form of end-of-term projects in the mandatory laboratories that build upon previous experiments.<sup>5-6</sup> But often, this form of research is removed from the laboratory and does not address a larger scientific question or does not involve the creation of new knowledge. Experiments where students have to identify elements in solution, or a material, or are asked to quantify a material in a common object through major analytical techniques and instrumentation, are often referred to as “research” experiences in these labs. These experiments are designed to mimic research experiences, but have known answers or have established procedures that the students follow, making these unique from traditional research experiences where answers are rarely known and procedures often do not work as reported.

The Freshman Research Initiative (FRI) program at the University of Texas at Austin and its associated curriculum were designed to give students an authentic research experience that also fulfills the general laboratory curriculum for many of the scientific disciplines.<sup>7</sup> At the heart of the FRI program is an effort to couple the twin missions of modern research universities, research and teaching, into a single cogent set of curricula. The program’s classes teach students the skills that they need in order to

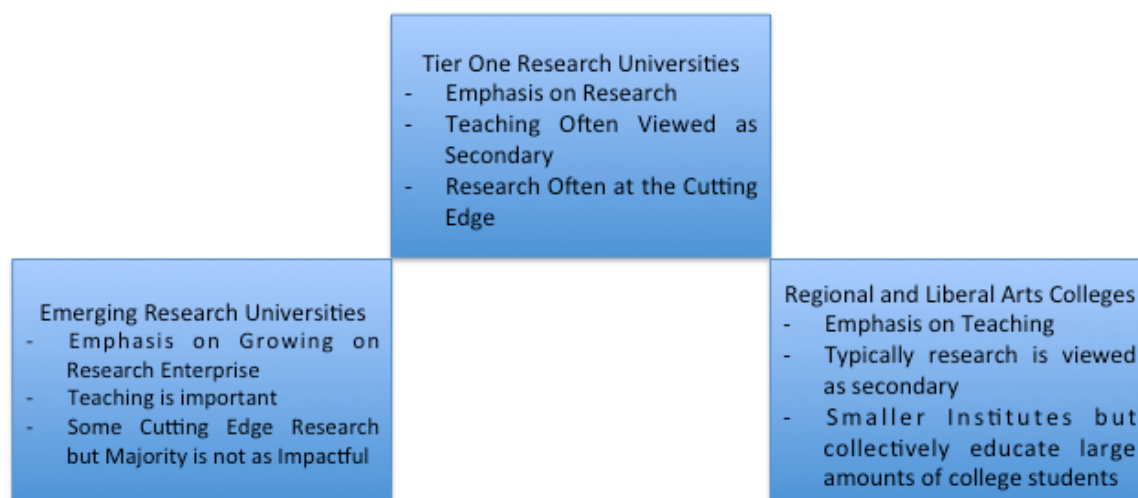


Figure 5.1 – Representation of the three major classifications of universities and how they relate to research and teaching

advance into more senior level laboratory courses while giving them the skills needed in order to carry out research in a particular area of science that attempts to solve some novel problem. These themes manifest themselves in all aspects of a student's experience in an FRI research group known as streams.

In this chapter, I hope to take you on a journey through the FRI program, how it functions and the successes of the program and its model for students at The University of Texas at Austin. First, the FRI model and program including its required curriculum will be explained. Next, three chemistry groups will be highlighted and the main research question that each of those groups is trying to answer will be summarized to provide a background on the experience students will have in those groups. Each of these groups comes from different areas of chemistry – nanomaterials, biochemistry, and analytical organic – to show the applicability of this teaching methodology to the majority of research avenues within chemistry. While this methodology can be applied to any of the scientific disciplines, this chapter will only highlight the chemistry

components of the program. Then, the typical experiences for different techniques of each stream will be highlighted showing how each research group fits within the context of teaching techniques and in ways that allow students to apply that technique to their research project.<sup>8</sup> Finally, we will highlight some data on the success of students who have gone through the program and show ways to incorporate the idea of research into teaching these techniques at other universities and colleges.

## **5.2 FRI SUMMARY –**

The Freshman Research Initiative (FRI) was created to help merge the twin missions of the tier one research university: research and teaching. When comparing the traditional models of teaching and research at a top tier research university, you often see a significant disconnect from the teaching and research missions.

In research labs, a professor runs the laboratory and decides on the major research focus of the lab. The professor has postdoctoral researchers and graduate students who carry out the majority of the experiments and basic research in the laboratory. These researchers may have undergraduate students who work with them, but they often work only under the direction of more senior lab members and on the projects that those lab personnel are working on. Researchers use advanced techniques often beyond those taught in the required laboratory courses. Furthermore, if a lab has undergraduate students, the lab only involves a small number of students, unlike the number of students needed to be served in introductory laboratory courses.

On the other hand, teaching laboratories at such universities often employ a lab coordinator who works with the departmental faculty to develop the laboratory experience. Teaching assistants often do the majority of the individual instruction in the lab sections. Finally, the students enrolled in the course conduct experiments with well-

defined procedures as well as answers that can be completed in short amounts of time. But these lab courses, unlike the research lab, are also designed to meet the needs of large numbers of students teaching basic and fundamental techniques. Often, laboratory courses like these are the only hands-on experience students carrying out experimental bench science require.

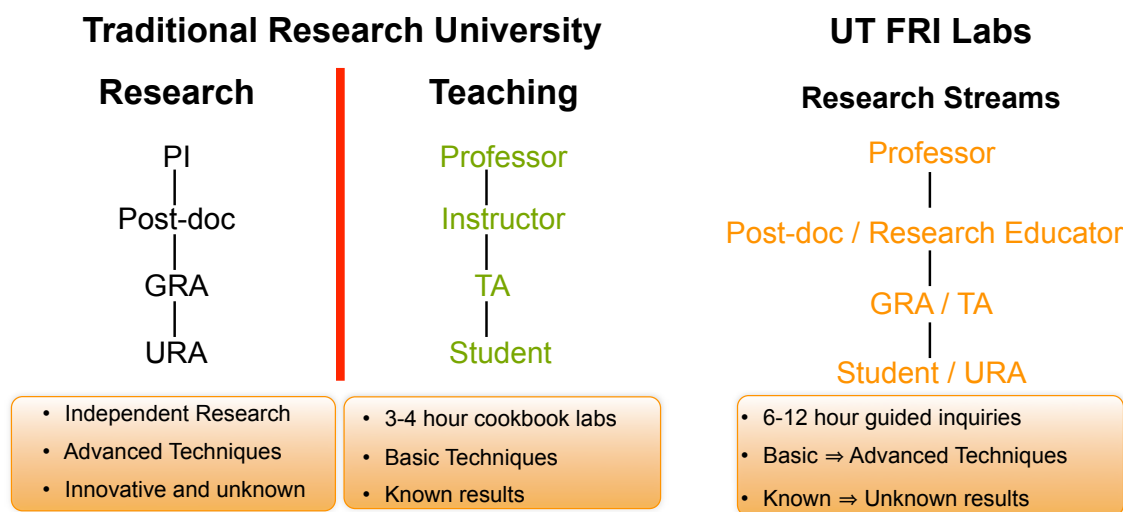


Figure 5.2 – Research Group, Teaching Laboratory and FRI Research Stream Laboratory Traditional Personnel Arrangement

The FRI program combines these two tracks merging the research experience of the research track with the ability of the teaching track to provide laboratory experiences for a large number of students. In the FRI model, a professor designs a research question that they want to see explored, often with the help of a recent PhD student. This person, known in the FRI program as a “research educator” (R.E.), designs the training experiments and curriculum. The curriculum is designed so that students carry out basic experiments that teach the techniques that students will need to conduct the research at the end of the semester. A teaching assistant works with the students as they carry out

the experiments, and helps them become familiar with the techniques. Further, the R.E also conducts research as well as help to facilitate the running of the course. Students also work with peer mentors, previous students in the research stream, who help them understand the techniques and are instrumental in developing a community within the lab beyond the research experience.

Within the FRI program there are currently over 25 different research areas, or “streams”, in which students can become involved. In order to be admitted into the FRI program, students traditionally apply before matriculating to the University, but students can also apply to participate in the program after their first semester at the University. The population of students served by the FRI program is very diverse with over 600 students and 40 percent of those students coming from underrepresented groups.

Once a part of the program, most students take a research methods course in the fall of their freshman year. In this course, students learn about formulating a research question, how to design and conduct a proper scientific experiment, and how to use statistics in data treatment. During this time, students also learn about the different research streams and submit their preferences for which streams they would like to join. After reviewing those preferences, students are selected into streams.

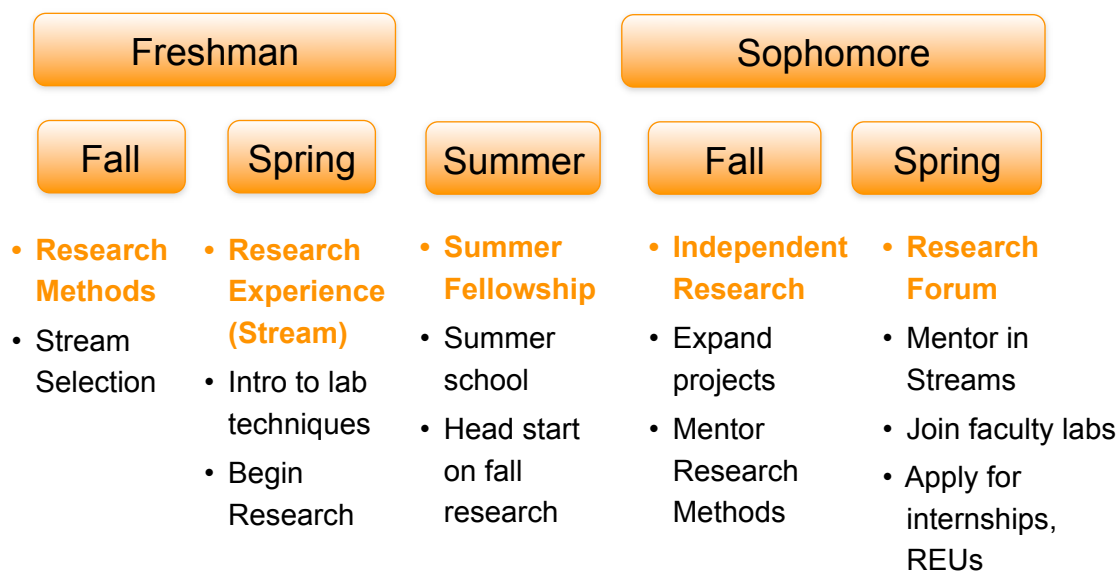


Figure 5.3 – Course Overview and Timeline for Students in the FRI program

In the spring, students take part in the stream lab course, and the students get general laboratory credit for the discipline aligned with the stream. For a chemistry stream, students would most likely get credit for the introductory general chemistry laboratory course. In the FRI course, students go from learning basic techniques to working on preliminary research towards the streams desired research goal during the semester.

After the conclusion of the freshman year, students can continue with their stream in the fall in an upper division independent research course as well as serve as peer mentors for the research methods course. Students who have shown some level of interest and proficiency during the spring semester can apply for a fellowship to conduct research during the summer to get a head start on their fall research experience.

After the completion of the fall semester of their second year, students will present their research at professional science conferences or at a college-wide

undergraduate research symposium. Students who have completed the program can apply to serve as peer mentors for the research stream, continue to conduct research with the stream they were involved in or can seek out other faculty members' labs individually or through a rotation program.

This model has allowed the program to grow to its current size and provides a framework for the streams and laboratory methodologies that are presented in this report.

### **5.3 STREAM SUMMARIES –**

#### **5.3.1 Supramolecular Stream**

The Supramolecular Sensors Stream (PI: Eric Anslyn) develops sensors — components used in arrays to reproducibly differentiate complex solutions of structurally similar compounds, an area of research the Anslyn group has investigated for the last 15 years. Array sensing uses a collection of different sensors that produce a unique pattern of responses for a mixture of compounds. Each sensor is composed of a sensing ensemble that uses a signaling methodology known as *indicator displacement*<sup>9</sup> as a means to detect binding between the target analyte and the receptor part of the sensing ensemble. Each sensing ensemble includes a dye whose optical properties vary dependent on whether it is bound in the sensing ensemble or displaced from the ensemble into the bulk solution. Binding of the target analyte to the receptor displaces the dye, providing a spectroscopically detectable signal (that of free indicator) from the sensing ensemble.



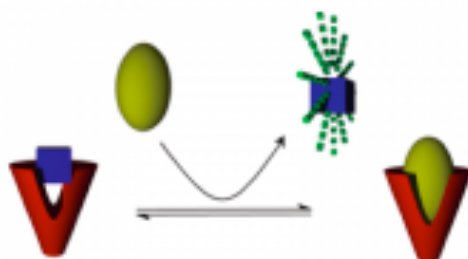


Figure 5.4 – Graphical Representation of the Supramolecular Sensors Stream’s Research

Specifically, this stream works to develop peptidic sensors that can be used to differentiate different types of wine varietals or other liquors via an array of indicator displacement assays. During the first semester in the stream, each student synthesizes a metal chelating peptide employing solid phase synthesis techniques<sup>10</sup>, analyzes their product using HPLC and LCMS, and, if needed, purifies their peptide using SPE. After preparation of their peptide, each student then screens different metals and dyes until an optical sensing ensemble is developed using a unique combination of these three components that shows different optical properties between the bound indicator and the free indicator. Each metal, dye and peptide complex, or ternary sensing ensemble, is then tested for its ability to detect the presence of tannins, first in solution, and then in wines by displacing the dye from the complex into solution, giving a measurable optical change. The ensembles that are most sensitive to tannins, those that show the most optical change, are combined into an array of sensors that is exposed to different wine varietals. Each of the different varietals gives a different level of displacement from the other varietals based upon the amount and type of each tannin present in that varietal. This differential displacement can be used to distinguish each of the varietals, and using mathematical manipulation and statistical methods, a graph can be generated which

clusters similar varieties. The stream recently published some of its initial differentiation of wine varieties.<sup>11-12</sup>

In addition to the basic differentiation of wine varieties, the stream has worked on a number of other related projects, including the comparison of the ability of the optical sensor arrays to the differentiation performed by a human test panel, and further wine differentiation, such as blends of different varieties, different harvest times of the same variety, and measuring the brix number of the wine.

The stream is also diversifying its research efforts to start working on the differentiation of other spirits and liquors, starting with cachaça, a Brazilian rum. These liquors contain tannins from the different types of fermentation casks, making the method of fermentation particularly important for differentiation of the analyte. Additionally, the stream is advancing toward the development of sensors using phage display as a mechanism to predetermine peptides that are more likely to bind tannins.<sup>13</sup> This methodology will provide a larger pool of potential receptors for the stream to utilize, and thereby increasing the efficiency of developing new sensing ensembles. The more the sensor pool is expanded, the greater the potential for the system to be able to differentiate more subtle mixtures or differences in varieties.

### **5.3.2 Nanomaterials for Chemical Catalysis Stream**

Faculty mentors Keith Stevenson, Richard Crooks, and David Vanden Bout lead the Nanomaterials Stream, with the aim to better understand the properties of metals on the nano scale. Nanomaterials range in size from 1 to 100 nanometers and their properties, particularly for catalysis, often differ vastly from their bulk counterparts.<sup>14</sup> One of the greatest challenges in the study of nanomaterials comes from controlling the size and composition of the particles: altering a particle's size or composition by even a

few atoms can change its reactivity. The Nano stream's goal is to synthesize and characterize new chemical catalysts that could be useful in a variety of applications, including industrial chemical synthesis, fuel cells, and pharmaceutical synthesis.<sup>15-18</sup>

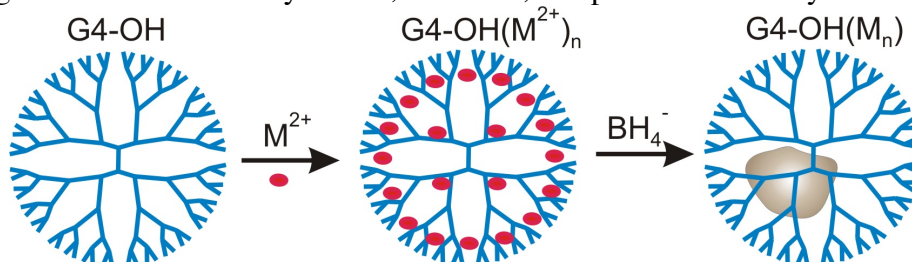


Figure 5.5 – Graphical Representation of the Nanomaterials for Chemical Catalyst Stream's Research

The students in the Nanomaterials stream synthesize nanoparticles made of copper, gold, palladium, and other metals using a dendrimer template method. As was mentioned before in this dissertation, dendrimers are a class of large, branched organic molecules, which are capable of chelating metal ions using their interior amine groups. By controlling the molar ratio of metal ions to dendrimer in aqueous solution, the number of metal ions bound and thus the resultant nanoparticle size and composition can be controlled.<sup>19</sup> With many types of metal ions, the binding of metal ions to dendrimer results in specific UV-Visible absorbance shifts that can be monitored by spectrophotometry during synthesis of the nanoparticle. Hence, students can design various dendrimer-metal complexes and characterize them using UV-Vis spectroscopy. In order to complete the nanoparticle synthesis, a reducing agent is added, which reduces the metal ions complexed within each dendrimer to collapse into a single dendrimer-encapsulated nanoparticle (DEN). A wide variety of DENs containing particles of differing size and composition can be synthesized by simply adjusting the identity and molar ratio of metal ions used in the synthesis procedure.

The catalytic activity of DENs can then be analyzed by studying the catalytic turnover of the nanoparticle catalyst in a variety of model reactions such as the reduction of *p*-nitrophenol to *p*-aminophenol. The stream has recently introduced a larger repertoire of model substrates, so that the substrate specificity of each catalysts generated can be studied. The stream also collaborates with another FRI stream, the Computational Nanoparticles Stream. The stream models the binding of the substrate to the nanoparticle surface and calculates an estimate of the binding energy for this interaction. Graphing the reaction rate constant versus the binding energy reveals the most favorable binding strength for optimal catalytic activity.

### **5.3.3 Mitochondrial Gene Expression Stream**

Students in the Mitochondrial Gene Expression Stream, under the direction of Dr. Dean Appling, utilize both biochemistry and molecular genetics techniques to identify and characterize the proteins involved in the initiation of mitochondrial translation in yeast, *Saccharomyces cerevisiae*. The mitochondria possess independent machinery for DNA replication, transcription, and protein synthesis separate of that used for other cellular processes. All three of these processes are necessary for the biogenesis and proper function of for the organelle. But the current understanding of the mitochondrial protein synthesis machinery lags behind that of the bacterial or the eukaryotic cytoplasmic systems. Some basic components of the yeast mitochondrial protein synthesis system have been identified, but the current understanding highlights the fact that accessory factors still remain to be discovered and characterized. FRI students in the Mitochondrial Gene Expression Stream routinely use a mutant screen, called a synthetic petite screen, to identify these proteins (accessory factors) involved in mitochondrial protein synthesis. The screen is designed to identify genes that interact with a target

gene, known to encode a protein involved in mitochondrial translation. Starting with a yeast strain using a defective copy of the target gene, students mutagenize cells with ultraviolet light and perform several replica-plating steps to select the mutants of interest, and thus obtaining a mutation that in combination with the target gene defect, cause overall respiratory deficiency. The resulting respiration deficient mutants are transformed with a yeast genomic DNA plasmid library to complement the UV-induced mutation, which leads to the eventual identification of genes that interact with the target gene. Genes that have been identified in this screen may be the genes that encode for the accessory factors involved in the process of mitochondrial translation.



Figure 5.6 – Graphical Representation of the Mitochondrial Gene Expression Stream's Research

Following the identification of potential accessory factors, the Mitochondrial Stream students use protein biochemistry techniques to investigate the physical interactions between these proteins and other known mitochondrial translation initiation factors, particularly the mitochondrial initiation factor 2 (IF-2). The availability of yeast strains possessing tandem affinity purification (TAP) tags on target genes has made this procedure readily accessible for experimental use.<sup>20</sup>

In addition to general chemistry laboratory techniques, students in the Mitochondrial Gene Expression research stream learn how to culture, plate and analyze

the growth of various yeast strains. Furthermore, students are taught molecular biology techniques such as PCR, agarose gel electrophoresis, transformation of plasmid DNA and genomic DNA libraries into yeast, DNA sequence analysis, and other basic molecular cloning procedures. When students assay their system for protein-protein interactions, they learn other important biochemistry skills including protein expression and purification, SDS-polyacrylamide gel electrophoresis, and immunoblotting and immunoprecipitation techniques.

#### **5.4 FUNDAMENTAL LABORATORY SKILLS**

The American Chemical Society (ACS) has designed a set of broad concepts which must be taught by institutions who want to receive ACS accreditation. Many of these concepts address such skills, as keeping a laboratory notebook, understanding how to make accurate measurements and communicate effectively through oral and written reports, which are general and useful to all scientific disciplines. The ACS guidelines require institutions, though, to create their own set of important laboratory skills to obtain accreditation. At The University of Texas at Austin, the institution has defined the skills and techniques that students must be taught in their introductory chemistry laboratory course. Within this set of skills, there are eight major categories: General Lab Skills, Measurement Skills, Solutions, Separations/Purifications, Acid/Base Chemistry, Qualitative Analysis, Synthesis, and Advanced Skills. Most of these categories have subcategories and specific skills students must learn. Additionally, the Advanced Skills category contains several additional techniques including UV-Vis spectroscopy, Redox Chemistry, and calorimetry. From this institutional skill inventory, four skills were selected to be the focus of our analysis of the research-oriented teaching of freshman chemistry laboratories taught in the FRI program.

## 5.5 SOLUTIONS AND DILUTIONS –

In each of the next three sections on different scientific techniques, the differences between each stream will be highlighted as a scientific technique is explored. However, with this technique, the similarities between the streams will be emphasized through one of the most basic of chemical laboratory techniques – solution preparation and dilutions. This skill provides the foundation of knowledge upon which each of the other techniques explored in this report are constructed.

Very often, undergraduates have difficulties understanding the concept of solution formulas, or alternatively, they are only able to remember and apply a sequence of mechanical steps to follow, when using solution formulas without a conceptual understanding of why they should use those steps. Thus, students are unable to visualize their meaning or application in the lab environment, unless specifically instructed on how to use the concepts. As an illustration of this point, all three streams represented in this paper have experienced their students adding a measured aliquot of a solution of known concentration into a mixture, and then not understanding that the concentration of that component of the mixture has changed, as well as not being able to calculate the new concentration.

In most undergraduate general chemistry lab courses at the University of Texas at Austin, solutions are prepared for the students to save time and increase efficiency of getting students through the course, given the large number of students enrolled. However, in Freshman Research Initiative labs, students prepare their own solutions and buffers from the beginning of the course. During the first week of class, students are introduced to using volumetric glassware such as volumetric flasks, volumetric pipettes, and the analytical balance. Each student learns to calculate the number of grams of a

solid, or the volume of a pure liquid, needed to prepare a solution of a defined volume and concentration using the molecular weight, or density, of the solute.

In the Supramolecular Sensors Stream, students learn how to express concentration in terms of molarity, normality and molality. The students learn how to dilute a stock concentration of liquid reagent to a fixed volume of a specific concentration using the  $V_1C_1=V_2C_2$  formula. In addition, the students are taught to make dilutions using the dilution factor method to create a new solution. For example, they learn that a 1 to 3 dilution requires combining 1 part volume of the more concentrated stock solution plus 2 parts of the solvent. Therefore, the dilution factor (3 in this case) for that solution is 1+2. While investigating the absorption spectra of different food color additives, students make serial dilutions and observe that the intensity of absorption at the relevant  $\lambda_{\max}$  changes proportionally as a function of the concentration according to the Beer-Lambert law. Students make replicates of each dilution and use UV-Vis spectrometry to determine the precision of their solution making to see how reproducible they can make multiple solutions at a given concentration.

Similarly, students in the Nanomaterials Stream prepare their own solutions and make their own dilutions as necessary to carry out their experiments. In a lab studying iron complexation, students prepare different concentrations of each of the complex and observe the absorbance as  $\lambda_{\max}$  changes, accordingly. When students carry out the DEN synthesis experiment, the students are forced to plan their own experimental protocol and carry out the numerous different dilutions required in the synthesis. This protocol requires students to have a deep understanding of the concept in order to carry out the experiment. They must prepare their own metal and dendrimer stock solutions that are more concentrated than the desired final concentration. The kinetics experiment, another experiment were students design their own protocol, provides students with another



opportunity to think about dilutions. The solutions that students prepare for their experiments are distinct from those in the reference papers that force them to consider how to make the necessary change in the solution to perform the experiment.

Lastly, the Mitochondria Gene Expression Stream also seeks to provide a strong basic knowledge of solution preparation and dilutions. The introductory experiments of the stream require students to prepare solutions for future experiments, using a variety of different types of solution preparation including molarity, percent weight volume (% w/v) and mass/volume (such as micrograms/milliliter) to express the concentration of their solutions. In the process of preparing these solutions, students must learn to work with unit conversions, formula weight calculations and the use of basic laboratory equipment such as top-loading and analytical balances, graduated cylinders or volumetric flasks and pipettes. In addition to standard solution preparation for experiments, students also use Henderson-Hasselbach calculations to prepare their buffer solutions and learn how to estimate the pH of a defined buffer.

The Mitochondrial Gene Expression Stream general chemistry laboratory course has several experiments throughout the semester that require preparation of dilute solutions. For many experiments, yeast cells grown in liquid culture must be diluted through a series of serial dilutions either for plating (on agar plates) or “diluted back” in liquid media for further growth. Typically, serial dilutions are required when plating cells, as students must often dilute cells more than 500- or 1000-fold before they can be plated. Components of growth media typically must be diluted from 100X to 1X in order to grow the yeast cells. Students must routinely prepare stock buffer solutions and then dilute these solutions in order to use them in SDS-polyacrylamide gel electrophoresis or western blots through formula weight calculations and the  $C_1V_1 = C_2V_2$  formula for dilution from a concentrated stock solution. Therefore, students are exposed to a variety

of contexts in which the concentration of a solution must be considered, and perform dilution in order to carry out the experiment properly.

In each of these streams, the preparation of solutions, the types, and amount of dilution may be different, but the pedagogical manner that the skill is taught through repetition and continual reinforcement of the technique throughout the course remains constant. The fact that this skill is fundamental to chemistry and chemical research is illustrated by the fact each of the streams utilizes similar teaching methodologies, especially repetition, to teach it. The emphasis on this technique further highlights the importance of this skill as a chemistry concept.

## **5.6 SYNTHESIS –**

Synthesis is also an important concept in chemistry, which tends to excite students and gives them a sense of accomplishment. Each stream within the FRI program approaches the concept of synthesis very distinctly with unique target molecules and types of synthesis. For the Mitochondrial Gene Expression Stream, students carry out synthesis in a biological context through the polymerase chain reaction. Students in that stream use the polymerase chain reaction (PCR) to synthesize double-stranded DNA from a plasmid DNA or from a yeast genomic DNA template. Using standard PCR protocols for the amplification of DNA, students synthesize the DNA, and then analyze their resulting PCR products using agarose gel electrophoresis. Although the students are not given a complete explanation of the DNA polymerase enzymatic process, they learn the basic catalytic process of the PCR reaction and how each component helps in the synthesis of the new strands of DNA. The students also conduct a negative (no DNA template) control alongside their experimental samples, so they can clearly verify their DNA product formation using agarose gel electrophoresis.

While the other streams do not take a strongly biological approach to synthesis, the Supramolecular Sensors Stream uses biomolecules such as peptides, which are synthesized through organic chemistry techniques using standard solid phase synthesis methodology. Students in the stream learn how to make peptides through the use of an automated solid phase peptide synthesis (SPPS) instrument. While they perform the synthesis, students are introduced to different functional groups and how they react to form a new product and about the possibility of side reactions and the formation of byproducts. They also learn each step of the reaction sequence in the SPPS cycle: de-protection, coupling, and, finally, cleavage of the newly synthesized peptide from the resin.

In the stream, each student is responsible for making a short peptide of 6-10 amino acids, using an automated peptide synthesizer, a Prelude by Protein Technologies, Inc. In this experiment, students use several organic synthesis, characterization, and purification techniques. Students learn how to calculate the starting material they need to use to obtain a yield and use this information to calculate the theoretical yield of the final product before obtaining an overall yield of their peptide. Students learn how to independently operate the Prelude automated synthesizer, including using the software provided with the instrument. In groups, the students each create a peptide sequence file that programs the instrument on each step in the reaction cycle as well as the loading order of the amino acids to produce the desired six peptides in parallel. They learn how to handle organic solvents, inorganic solvents, and various reagents after reading the MSDS for the compounds. They prepare all the necessary solvents, reagents, and amino acid solutions required for the synthesis, load them into the synthesizer and run their program. When the synthesis cycle is complete, students learn to manually wash and cleave the synthesized peptides from the resins. They learn how to use a rotary evaporator in the

workup of their peptides to remove organic solvents, and a lyophilizer to freeze-dry their final products into a powdery solid.

In addition to solid phase organic synthesis, students in the Supramolecular Sensors stream construct peptidic differential array sensors to discriminate wine varieties through supramolecular assembly methodologies. The sensing ensembles, a form of supramolecular synthesis, are based on indicator displacement signaling methodology and are composed of three components: an indicator, a divalent metal and a peptide. Students use UV-Vis spectroscopy to test the binding of the different combinations of these three components and determine the optimal binding ratio at which the assembly is most sensitive to the addition of different target analytes thus characterizing their synthesized ensemble. Through this synthesis, students learn about molecular recognition and the forces involved in the complementary spatial arrangements of the sensing ensemble such as hydrogen bonding, electrostatic interactions, metal coordination and hydrophobic interactions, the hallmark phenomenon of the supramolecular synthesis.

Traditional general chemistry laboratories tend to focus on the formation of inorganic complexes. Analogously, students in the Nanomaterials for Chemical Catalysis Stream also synthesize organometallic materials. In the synthetic reactions, students also rely on some of the same supramolecular techniques that students use in the Supramolecular Sensors Stream to create sensing arrays. Students in the Nanomaterials Stream synthesize DENs using a protocol that they write for themselves, based on the published literature.<sup>21</sup> The laboratory handout guides them through the development of a synthetic protocol through a series of guided questions and suggested calculations so that they are able to develop a working protocol independently<sup>15</sup>. Students are encouraged to use their own data on the loading capacity of the dendrimer and the importance of pH control to direct the size of their synthesized nanoparticle. The general protocol for DEN

synthesis involves the following steps: prepare aqueous solutions of dendrimer and metal salt, adjust pH of dendrimer solution, combine

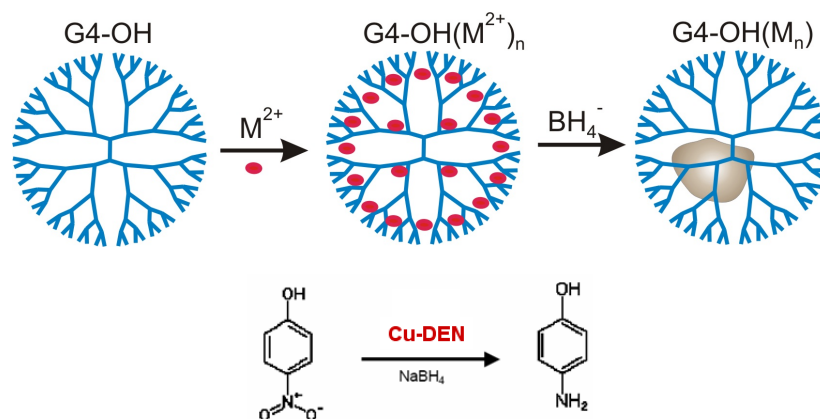
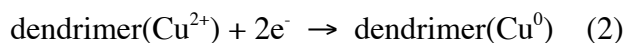
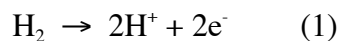


Figure 5.7 – Nanomaterials Stream Synthetic Scheme for the Production of DEN's and Use as a Catalyst in Model Reduction Reaction

dendrimer and metal salt in an appropriate molar ratio, with stirring, until the metal is complexed to the dendrimer, and finally the addition of a reducing agent to form nanoparticles. Each nanoparticle is retained within a dendrimer by steric interactions.<sup>19</sup> Solutions of the dendrimer alone, the dendrimer-metal complex, and the reduced nanoparticles display unique spectral profiles, and hence students follow the progress of their synthesis through UV-Vis spectroscopy. In addition, each step of the synthesis process emphasizes a series of different basic chemistry concepts: dissociation of ionic compounds in solution, hydrogen bonding, metal coordination, oxidation (1), reduction (2), and steric interactions.



In addition to the inorganic synthesis of nanoparticles, students in the Nanomaterials Stream use their DEN's as catalysts in the reaction of organic compounds.

Each student tests the catalytic activity of their nanoparticles through their ability to catalyze the reduction of nitrophenols to aminophenols. The progress of the reaction can be observed by the loss of yellow/orange color as the nitrophenol concentration decreases. The consumption of this compound can be quantitatively monitored as the change in an absorbance peak at ~400nm, which can be recorded over time using an Ocean Optics portable spectrophotometer and LoggerPro software. Through the analysis of reaction kinetics and determination of the reaction order, the students are able to quantitatively characterize their DEN catalyst. Students also measure how the reaction rate constants for nitrophenols change when the substituents on the phenyl ring are altered. Through these experiments we (and the students) are learning how substituents influence the rates of reaction. Some students also use the rate constant data for these substrates to construct a Hammett plot, which may eventually be used to reveal the mechanism of the nitro reduction of the nitrophenols at the surface of various metal nanoparticles.

Each of these streams brings its own twist on synthesis which illustrates the streams' overall research goals. Furthermore, the streams use these methodologies to still satisfy the ACS requirements for freshman chemistry laboratory coursework.

### **5.7 Separations and Purifications –**

Separations and purifications provide students with skills necessary to obtain a single product after synthesizing target complexes. These skills are an advanced technique that is rarely taught in freshman chemistry laboratories, but give students valuable skills for future research endeavors when synthesis rarely proceeds without byproducts and containments. Because like synthesis, separation and purification is

directly related to the streams, the experiments that tend to teach this technique tend to be unique for each of the streams.

Students in the Supramolecular Sensors Stream are introduced to separation and purification techniques in a context of standard organic chemistry techniques built upon column chromatography. When taught these skills, students learn three techniques; high performance liquid chromatography (HPLC), liquid chromatography:mass spectrometry (LCMS), and solid phase extraction (SPE). The purification techniques taught to the students are selected based upon the type of synthesis performed by students within this stream. Each student synthesizes a peptide using Fmoc solid phase peptide synthesis, as described previously. Following the synthesis of their peptide, the target peptide must be isolated and purified. The students' peptides are characterized using an analytical-scale HPLC with a C18 column, using a standard acidic water/acetonitrile gradient to measure the peptide's purity. Each peptide synthesized will ideally show as a single peak in the chromatogram, while multiple peaks can be indicative of an impure peptide. LCMS is used to either confirm the molecular weight of the peptide synthesized, or to identify which of the multiple peaks is attributable to the peptide of interest. Impure peptide mixtures are purified using SPE on a C18 Sep-Pak column via an elution with different ratios of water and acetonitrile. These experiments teach students about the use of columns in the purification of compounds via changing of mobile phase polarity.

While the more traditional column based separation approach suits the Supramolecular Sensors stream, the Mitochondrial Gene Expression Stream takes a biochemical approach to separation. Following the identification of potential accessory factors involved in mitochondrial translation, Mitochondrial Gene Expression students use protein biochemistry techniques to determine whether these putative factors are physically interacting with the mitochondrial translation initiation factor 2 (mtIF-2) or

other proteins involved in mitochondrial protein synthesis. In the undergraduate lab, the students utilize a simple modification of the tandem affinity purification procedure (the TAP method<sup>20</sup>) for partial purification of native protein complexes. A collection of

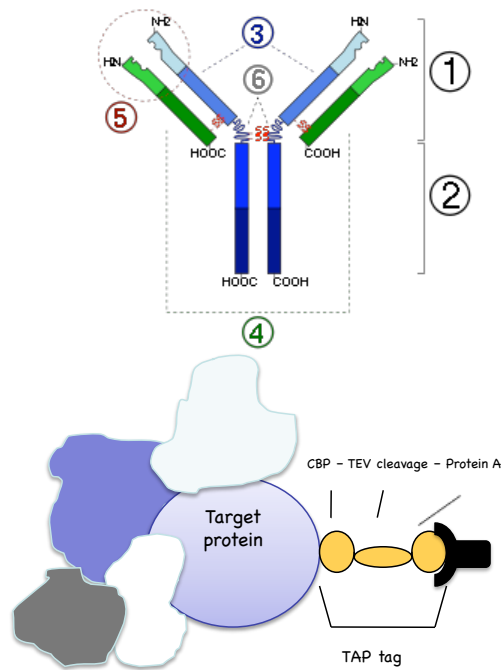


Figure 5.8 – Schematic of Purifications Used by the Mitochondrial Gene Expression Stream. At the Top, a Graphical Representation of the Antibody Which Binds the TAP portion of the Target Protein is Given. At the Bottom, the Binding of the Antibody to the TAP Tag on a Target Protein is Illustrated.

yeast strains is commercially available for the expression of yeast proteins with C-terminal tandem affinity purification (TAP) tags already incorporated (Open Biosystems). The IgG binding domain of *S. aureus* Protein A is engineered into the C-terminal end of these TAP tags and allows for first step affinity purification of TAP-tagged proteins from yeast crude extracts. Using a yeast strain that expresses the TAP-tagged version of the putative accessory factor of interest, students prepare protein extracts and



immunoprecipitate their TAP-tagged protein factors using IgG-sepharose beads. The IgG-sepharose beads are pelleted through low-speed centrifugation and washed repeatedly to remove any unbound proteins, effectively separating the TAP-tagged protein (and any tightly associated proteins) and allowing students to isolate the protein of interest from the remainder of the crude extract. This process trains students in decanting/separation techniques and allows students to partially purify native protein complexes from crude yeast extracts. Students then analyze these protein complexes via SDS-polyacrylamide gel electrophoresis and immunoblotting to determine whether their proteins of interest are interacting with any of the known mitochondrial translation factors. The subsequent steps of the tandem affinity purification method (TEV protease cleavage and a second affinity purification step) can be used to further purify and analyze native protein complexes if needed, but this purification step is often not required in the freshman/sophomore level FRI courses.

Hence, each of these streams teaches the required separation techniques in unique ways that highlight the streams' research focus. In some cases, the students in a stream (Nanomaterials) do not need to learn to do purifications or separations for the stream's research, and thus they do not have any experiments which focus on developing this skill. Beyond just highlighting the research focus, the separations and purification skill set shows us that this teaching methodology can be used to introduce students to advanced chemical research techniques at a very early stage in their careers.

## **5.8 UV-VIS SPECTROSCOPY –**

UV-Vis spectroscopy is one of the hallmark techniques taught in freshman chemistry. As was discussed in the previous two techniques, each of the streams has unique ways to teach many of the basic techniques. UV-Vis spectroscopy is different in

that for most of the streams it is typically taught in a combination of traditional cookbook-like experiments and more advanced research focused methods. As such, a more in-depth discussion of this technique will be presented which highlights both the traditional and the advanced methodologies employed to teach the skill.

For the Supramolecular Sensors Stream, optical spectroscopy plays an extremely important role in the research. Consequently, numerous spectroscopic experiments are performed in the first semester to develop the students' familiarity and understanding of the technique. The first Supramolecular Sensors Stream spectroscopy experiment covers material traditionally taught to freshmen, but in a way that prepares students directly for their research. An absorbance spectrum of a series of food dyes is taken. Additionally, a portion of the experiment teaches students about spectral additivity and saturation is investigated. Furthermore, students explore methodologies to use the spectra as a fingerprint to identify mixture components. Students investigate the use of blanks and test their micropipetting technique by measuring their precision in making multiple solutions of the same concentration. Finally, students construct a calibration curve using FD&C #40 to quantify the dye in cherry juice or soda. Each of these skills is invaluable to teach the basics of the technique that is fundamental to carrying out research that addresses the stream's research goal.

The Nanomaterials for Chemical Catalysis Stream also puts a large emphasis on spectrophotometry for its research goal. Students are first introduced to the concept of Beer's Law in a laboratory module examining iron complex equilibria. In this experiment, UV-visible spectroscopy data is analyzed to determine the molar absorptivity coefficient and the equilibrium constant for the formation of three distinct iron complexes. As in the SMS stream, UV-Vis experiments, the concepts of spectral additivity and saturation are explored. Through the initial experiment students also learn

the importance of the use of appropriate blanks and the need for reproducibility. Students prepare their own solutions of an iron salt and combine it with three different types of ligands: monodentate (thiocyanate  $[\text{SCN}^-]$ ), bidentate (salicylate  $[\text{C}_7\text{H}_4\text{O}_3^{2-}]$ ), and multidentate ( $[\text{EDTA}^{4-}]$ ). Each of these complexes have unique spectral peaks that the students can use to identify each of the complexes, and then the students adjust the concentrations of their complexes so that the peaks' maxima fall within the linear range of the spectrophotometer. This experimental module provides the framework for understanding the complexation of metal ions with dendrimer molecules during nanoparticle synthesis that the students will do later as they begin to carry out research for the stream.

In an attempt to explore metal complexation using UV-Vis spectroscopy, students perform a spectrophotometric titration of a dendrimer solution with copper ions (Feng, 2009). Each incremental addition of copper to dendrimer causes an increase in the 300 nm ligand-to-metal-charge-transfer (LMCT) band<sup>21</sup> from the copper. As the binding of copper to the dendrimer saturates, the increase in the absorbance at 300 nm slows until it no longer changes. Students determine the binding capacity (or "loading

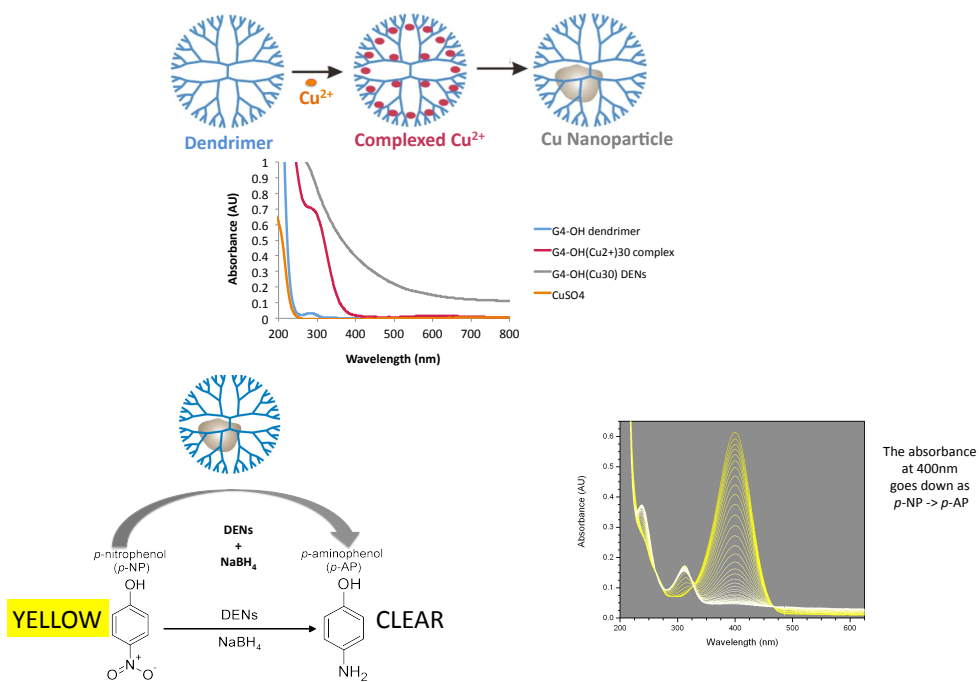


Figure 5.9 – Schematic Showing UV-Vis Spectroscopic Uses by Nanomaterials Stream to Characterize Their Synthesized DEN and the Catalytic Reaction. At the Top, The UV-Vis Spectrum of the Stages of DEN Synthesis is Illustrated. At the Bottom, a Reaction Scheme is Shown for the Catalytic Reaction of the DEN with a UV-Vis Spectra of the Reaction with Increasing Time.

capacity”) of the dendrimer by calculating the inflection point from a plot of the change of absorbance at 300 nm versus the molar excess of copper to dendrimer. They also explore the effect of pH on the loading capacity of the dendrimer by performing the same titration at a variety of pHs.<sup>18,21</sup> Many of the spectroscopic concepts crucial to the Nanomaterials Stream research are emphasized in this titration experiment: spectrophotometric shifts that result from the binding of metal to dendrimer, the saturation of metal binding sites in the dendrimer, and the effect of pH on metal binding.

In the Mitochondrial Gene Expression Stream, as in all biochemistry and molecular biology laboratories, the UV-Vis spectrophotometer is routinely used for the quantification of nucleic acids and proteins in solution. In this stream, the traditional

UV-Vis experiments focus around the use of spectroscopy for quantitation through Beer's Law. Before the students use the spectrophotometer for this purpose, they must learn the basic principles of UV-Vis spectroscopy and the experiment is designed to meet this purpose. Students prepare a 2 mg/ml stock uracil solution, which is used throughout the semester as a yeast media component, and make dilutions of this solution for  $A_{260}$  readings in the UV/Vis spectrophotometer. The students then utilize Beer's Law to determine the molar concentration of the uracil solution and compare the absorbance to the calculated value using the molecular weight of uracil. The UV/Vis

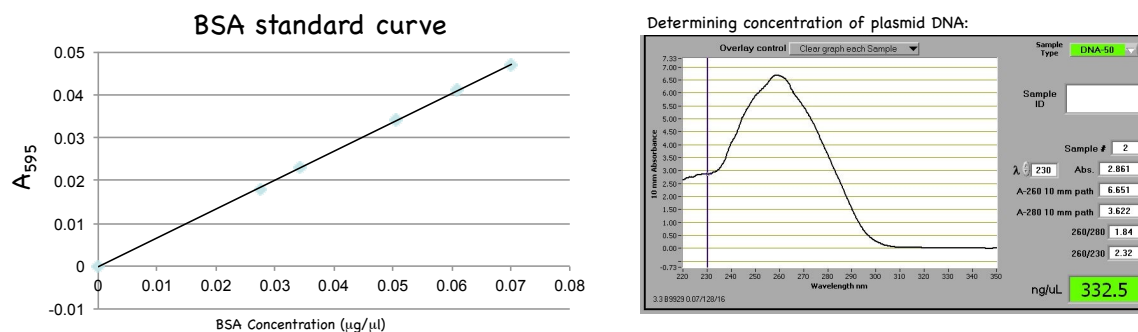


Figure 5.10 – Graphical Representation of UV-Vis Spectroscopy Use in the Mitochondrial Gene Expression Stream

spectrophotometer (or a nano-drop spectrophotometer) is then used to determine the concentration of plasmid DNA and other nucleic acid samples throughout the FRI course series. Students working on protein interaction projects also use the spectrophotometer to complete Bradford assays to measure the amount of protein in yeast crude extracts. A non-traditional use for the UV/Vis spectrophotometer, performed extensively in the Mitochondrial Gene Expression Stream, is the analysis of yeast cell growth in liquid culture. Students take optical density readings at 600nm (OD600) to assess the turbidity of their cultures resulting from the suspension of yeast cells in the media. The students

are clearly taught the difference between using the spectrophotometer to measure the absorbance of light of a particular wavelength and using the instrument for turbidity analysis ( $OD_{600}$ ) which measures the dispersion of light.

While each of these streams uses a basic UV-Vis spectroscopic experiment, the Supramolecular Sensors and the Nanomaterials for Chemical Catalysis Streams make extensive use of the technique in the research the students carry out throughout their experience in the stream. The research in the Supramolecular Sensors stream revolves around the construction of sensors used for the analysis of complex liquid mixtures, in particular wines and other spirits, based on a peptidic sensor using indicator displacement assay as a signal methodology. When constructing sensing ensembles, the optical properties of the dye included in each sensor ensemble are changed by the interactions of the indicator with the metal and peptide, similar to the manner that pH indicators change with different pH values. The indicator displacement assay requires that the indicator bound in the sensing ensemble is spectroscopically discernable from the free indicator in bulk solution. In experiments geared towards teaching the basic concepts and techniques of an indicator displacement assay, students titrate a receptor into a constant indicator solution. By monitoring the absorbance changes between bound and unbound indicators, students are taught to construct a binding isotherm for the interaction between indicator and host.

After the construction of the binding isotherm, students learn how to construct a calibration curve to quantitate an analyte using an indicator displacement assay. While this procedure is similar to the traditional calibration curve experiment performed using a dye, it also illustrates the power and ability of UV-Vis spectroscopy to quantify the presence of an analyte that does not contain a chromophore, something students often are not exposed to in their first year. In the experiment, students displace an indicator from a

sensing ensemble consisting of a synthetic receptor and indicator, using the analyte citric acid, which students had previously quantified in an acid/base titration experiment. Citric acid binds more strongly to the receptor than the indicator, resulting in displacement of the indicator and thus a spectroscopically detectable change. This experiment illustrates the usefulness of sensing ensembles and reinforces the concept of UV-Vis spectroscopy.

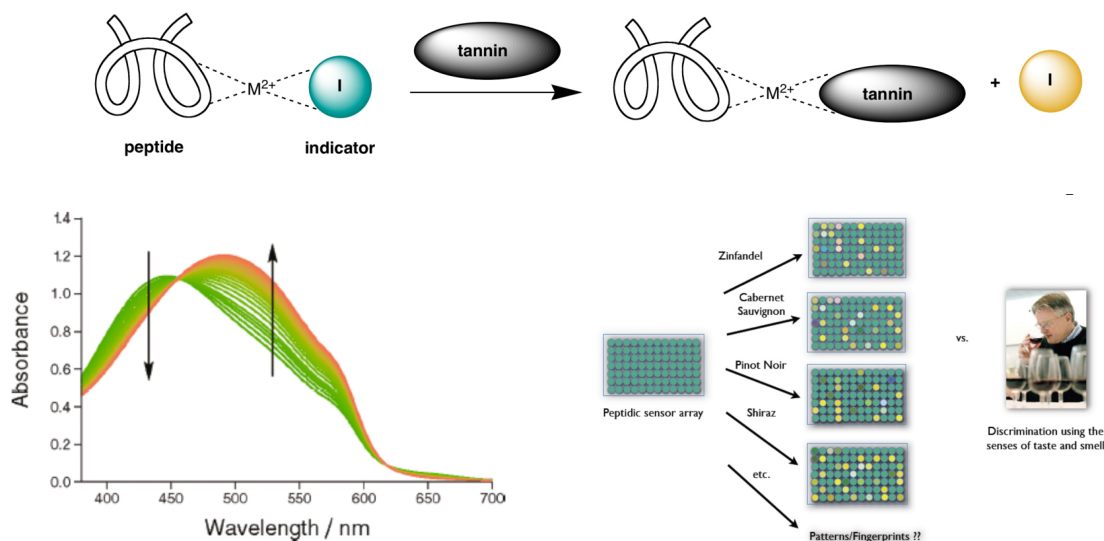


Figure 5.11 – UV-Vis Spectroscopy Techniques Employed by the Supramolecular Sensors Stream. At the Top, a Schematic Representation of the Sensing Ensemble is Shown. At the Bottom Left, an Example Displacement Isotherm is Shown for the Addition of Tannin to the Sensing Ensemble. Finally, on the Bottom Right, an Idealized Representation of the Array When Exposed to Different Wines is Shown

Finally, UV-Vis techniques are also used extensively throughout the students' construction of their individual indicator displacement ensembles using peptidic receptors. Two binding curves must be obtained to optimize the sensing ensemble: one titrating metal and indicator and the other titrating peptide with the metal:indicator complex. Once the optimal ratio of metal:indicator:peptide have been determined,

students construct their calibration curves with a representative tannin to investigate the sensitivity of their sensor to various tannins of interest. Students learn to construct calibration curves and metal:indicator and sensor:analyte binding curves in a high throughput manner, using a UV-Vis micro-well plate reader. Next, the students expose their optimized sensing ensembles to a solution of target analyte tannins, or a mixture of tannins such as wine. They use the resultant UV-Vis data collected to analyze and distinguish amongst the different mixtures of analytes. Using the micro-well plate reader teaches students a different way of obtaining UV-Vis spectral data. Furthermore, students learn to manipulate the large resultant datasets through introduction to several new methods of data analysis, such as pattern recognition and component analysis.

The research in the Nanomaterials Stream also utilizes UV-Vis spectroscopy, as was discussed in the synthesis section, to monitor the production and the catalytic efficiency of the DEN's produced. Monitoring the spectroscopic signature of the metal ions bound to the dendrimer can be used to observe their conversion upon the introduction of a reducing agent to the corresponding DEN. Furthermore, the conversion of *p*-nitrophenol to *p*-aminophenol produces a characteristic color change that can be monitored by the disappearance of the peak to measure the catalytic potential of the DEN synthesized.

Each of these spectroscopy experiments is geared toward teaching techniques in UV-Vis spectroscopy, but each in a different way and for a different ultimate purpose. Each experiment builds upon the previous experiments, teaches skills essential for the stream's research, and shows the power and utility of UV-Vis spectroscopy as a technique. Each stream teaches this technique following its own objectives for furthering the research while still providing students the skills necessary to give students the



experience they need for future classwork and research through both standard and advanced methods.

### **5.9 THE FRI MODEL AND ITS SUCCESS IN STUDENT ACADEMIC PERFORMANCE –**

The Freshman Research Initiative teaches basic laboratory techniques with its introductory course sequence in a unique research oriented manner. As such, data has been collected to measure the program's effectiveness compared to the traditional introductory laboratory experience and to measure any benefits that students in the program might gain through their participation.

When analyzing the data obtained from these studies, a few major trends have been noticed that are important to highlight. The purpose of this report is not to extensively explore each of these observations but to provide a brief overview of the salient highlights.

Students in the program have been shown to have an improved retention within their selected scientific major as well as within the College of Natural Science and the University of Texas. With the current climate of focus on graduation rates and moving students through their higher education experiences, improved retention remains an important step toward increasing those rates shown in Figure 5.12.

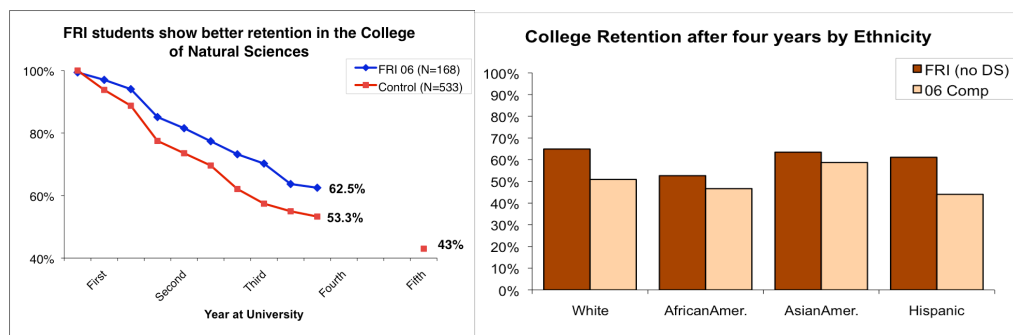


Figure 5.12 – On the Left, the Graph Illustrates the Retention Rates of Students in FRI Compared to a Control Group. On the Right, the Graph Shows Retention Rates of Students in Different Ethnic Groups Between FRI Students and the Control Group

Furthermore, the program has been shown to increase students' interest in science and their propensity to go on to obtain higher degrees in science. These students tend to stay involved with research even after they have left the stream, and are thus more likely to have publications and presentations before finishing their undergraduate career. Additionally, students who have been involved in the FRI program tend to perform better in their coursework compared to their counterparts who have not taken part in the program.

Given these observations, one relationship which had not been previously explored, the correlation between FRI students' later laboratory performance compared to their peers, such a comparison that could support or refute this report's claims about the benefits of a research oriented teaching methodology for an introductory laboratory experience

An analysis of the effects of freshman chemistry lab training provided through an FRI research-based laboratory course was performed to determine if the alternate teaching methods highlighted had any effect on student performance based upon the students' grades in their next chemistry laboratory course. During the year following

their freshman chemistry experience, the majority of students go on to take organic chemistry lab. The laboratory course is a requirement for chemistry and biochemistry majors and any students seeking a career in the health professions, and thus student performance in these courses seemed a suitable way to investigate the effects of our research-based freshman chemistry lab courses on student's future performance in the lab courses.

The Department of Chemistry and Biochemistry at The University of Texas at Austin has several possible organic chemistry course sequences. Both the traditional majors sequence (two semesters of organic chemistry lectures, paired with two semesters of one-credit organic chemistry labs), and the pre-health sequence (two semesters of organic chemistry lectures, paired with one two-credit organic chemistry lab) was examined. The data used in our analysis was collected for each of these lab courses over the last five years (Fall 2008 – Summer 2012).

During the time period included in this study, our University shifted from the standard five letter grade system (A, B, C, D, F) to a system that allows twelve grade levels (A, A-, B+, B, B-, C+, C, C-, D+, D, D-, F). In order to overcome this obstacle, each of the students grades were converted into an equivalent numeric grade point and then grade point distribution histograms were plotted for each of the three organic chemistry lab courses, which is shown in Figure 5.13. Only students who obtained a grade on this scale were included in this study.

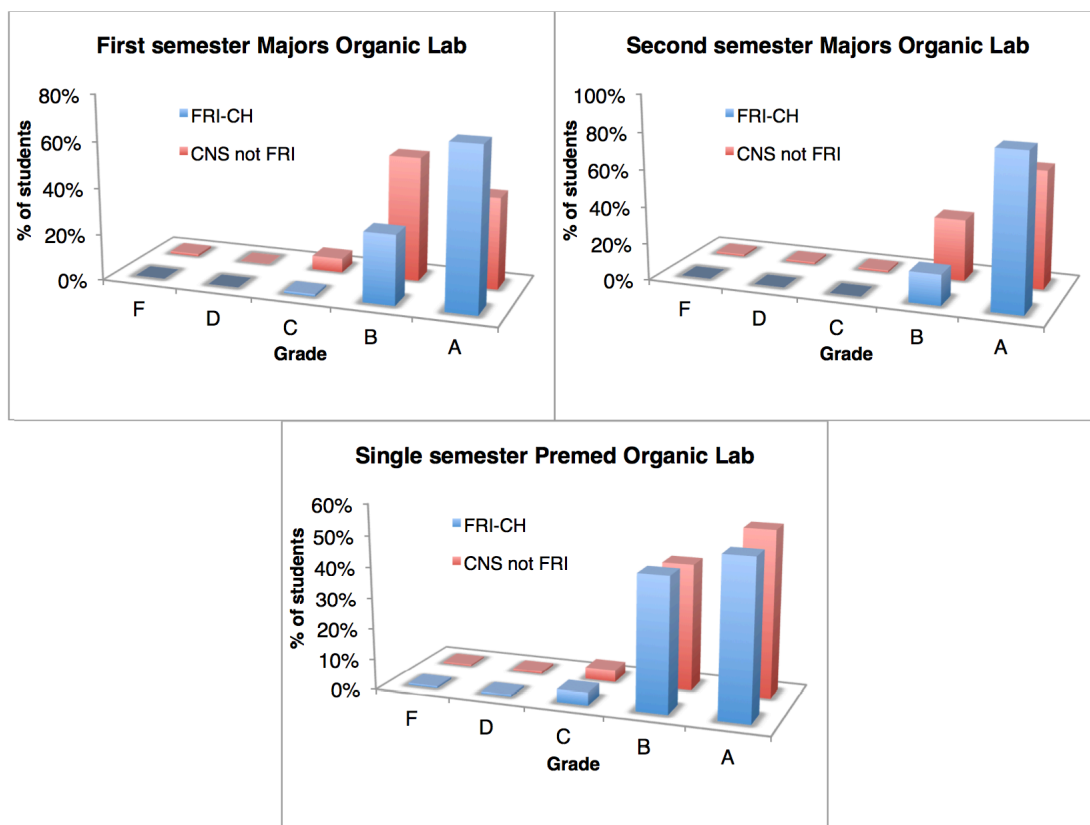


Figure 5.13 – Graphs showing the cumulative grade distributions of students in organic chemistry labs over a five year period, who either received the alternate freshman chemistry lab experience provided through the FRI program (FRI-CH), or who were natural science majors who did not participate in FRI and received the regular freshman chemistry lab training (CNS not FRI).

When looking at the entirety of students, two different populations of these courses were identified and investigated in this study. The first population consists of students who gained freshman chemistry lab credit through one of the many FRI research topic-based alternative lab courses including those highlighted earlier. As a comparison population, all students who were natural science majors, and who did not participate in any of the FRI research topic-based courses, were selected. This selection excludes students who did participate in FRI, but were involved in a research topic that gave

freshman lab credit within a different scientific discipline, because the effects of their lab, although not chemistry focused, could also influence their performance in the organic chemistry lab (e.g., skills in experiment design, scientific understanding, independence, and creative thought).

Almost half of the students taking the two organic chemistry lab courses for chemistry majors were students who gained freshman chemistry lab credit via the alternate FRI program. Typically 60 students took these two courses each year. The pre-medical organic chemistry lab serves a much larger number of students, with typically 1400 students taking this course each year – 1100 of whom are natural science majors, and approximately 18% of whom gained freshman chemistry credit through FRI.

In all three organic chemistry laboratory courses investigated, the grade distribution for students who received their freshman chemistry lab course credit via a FRI research-based alternative course was statistically different from the grade distribution for students who took regular freshman chemistry lab credit, with greater than 99.9% confidence in all three cases (Table 5.1), and in each case, the average grade point average of the FRI students was higher than the non-FRI students.

|                                 | First semester majors organic lab |                  | Second semester majors organic lab |                  | Single semester premed organic lab |                  |
|---------------------------------|-----------------------------------|------------------|------------------------------------|------------------|------------------------------------|------------------|
|                                 | FRI chem                          | nonFRI CNS major | FRI chem                           | nonFRI CNS major | FRI chem                           | nonFRI CNS major |
| <i>Total number of students</i> | 111                               | 225              | 97                                 | 208              | 741                                | 4411             |
| <i>Average grade score</i>      | <b>3.52</b>                       | <b>3.09</b>      | <b>3.68</b>                        | <b>3.37</b>      | <b>3.36</b>                        | <b>3.26</b>      |
| <i>95% confidence interval</i>  | 0.10                              | 0.12             | 0.09                               | 0.12             | 0.05                               | 0.02             |
| <i>t test significance</i>      | 99.99998%                         |                  | 99.995%                            |                  | 99.93%                             |                  |

Table 5.1 - Data comparing performance of students in organic chemistry labs, who either received the alternate freshman chemistry lab experience provided through the FRI program, or who were natural science majors who did not participate in FRI and received the regular freshman chemistry lab training.

Teaching freshman chemistry using our alternative research-based approach not only does not harm the performance of students in consequent courses, but clearly improves student performance.

### **5.9 EXPANDING A RESEARCH ORIENTED MODEL TO OTHER UNIVERSITIES –**

The FRI model has been shown to have great success in future student involvement in science. As discussed above, there are numerous elements that have gone into the success of the program. While each of these elements play a role in development and success, this section will focus on incorporation of research experience into the freshman laboratory experiences at other Universities.

While the FRI program at The University of Texas at Austin has been fortunate to be supported by grants as well as institutional funds, this research model can be extended to other institutions and their freshman laboratories without substantial resources. As has been mentioned, the FRI program employs peer mentors, as well as commits significant research infrastructure to create a research experience for the students. Through a semester long course, the laboratories can be modified so that they create a coherent string of experiment that conclude with students performing original research toward a common research objective in the final weeks of the course.

Numerous researchers have called for the inclusion of some form of research component into laboratories,<sup>1-5</sup> but few have been able to incorporate research as deeply into a course sequence as the FRI program. Often, these efforts involve only projects that are designed to mimic research but are not original research. But any college or university can modify their curriculum to include deep integration of research techniques into laboratories as the FRI program has done at The University of Texas at Austin.

For example, an introductory laboratory course could modify its curriculum so that the lessons are centered around a set of common skills, as is done in the FRI streams, which satisfies the needs to meet a larger research task at the end of the semester. In order to do this, the focus must be changed from teaching a skill to identifying how certain skills are necessary for the overall desired research goal. The experiments should teach those basic skills, or can be modified to give students knowledge of the skills to give students the necessary training to fulfill the research goals and objectives.

By way of an example, we would like to illustrate a laboratory setup can be utilized at other universities from one of the streams we have highlighted. Using a lab that wants to have a final research project to analyze the efficiency of nanoparticles for certain types of catalytic functions, as an example, we will illustrate the modifications necessary for the labs' experiments. Students can learn reduction and oxidation concepts through the reduction of metals into the nanoparticles and learn about quantitation through spectroscopy by quantifying their nanoparticles using UV-Vis spectroscopy in the early experiments of the course. Furthermore, students can learn about synthesis and characterization of nanoparticles, which gives their coursework a consistent theme, prepares them for conducting original research, while teaching the necessary skills that students must learn in an introductory lab in order to succeed in future laboratory courses.

Additionally, students learn more about the techniques if they learn the skill in a larger context. Most labs try to provide that larger context by providing or using real world examples, such as identifying dyes in household products.<sup>22</sup> Yet, to really engage in science, it helps to have the experiments situated in the larger context of a scientific problem that the skill can be used to satisfy. This form of experimentation works by providing a coherent laboratory experiment that teaches students about the importance of research. Modifying the curriculum to include a deeper integration of research gives the

students a much stronger engagement with science and a stronger appreciation of research.

Finally, the modification of the curriculum to include more authentic and substantial research is an important part of the FRI program, but that modification alone is not the only hallmark of the FRI program; it is simply the portion of the program that this chapter is focused on. While it is our belief that this area of the program is an instrumental part, we do not feel that we can claim that any one area of the program, to the exclusion of the others, like the peer mentoring program and the smaller class sizes, has solely achieved the success experienced by the FRI at The University of Texas at Austin.

## **5.9 CONCLUSIONS**

In this chapter, the interworkings of the Freshman Research Initiative and several of its chemical research streams has been covered. Using the research centered model of the FRI program, this chapter has hoped to highlight four different skill sets which are commonly taught in early chemistry laboratory courses. Students learn skills such as UV-Vis spectroscopy, synthesis and purification in each stream through research oriented experiments. The teaching methodology amongst the different streams for techniques could be contrasted and highlighted within the context of the research mission of that stream. Furthermore, one technique, solution preparation, was used to highlight the similarities in teaching methodology rather than the differences, despite the stream's different research missions. Next, the benefits that have been observed from teaching the introductory courses in this research oriented manner, including its impact on student's future performance, was highlighted. Finally, this chapter highlights ways in which this teaching methodology can be incorporated at other institutions of higher learning.



## 5.10 REFERENCES –

1. Hunter, P., Undergraduate research: Winning the battle for students' hearts and minds. *EMBO reports* **2007**, *8* (8), 717-9.
2. Lopatto, D., Undergraduate Research Experiences Support Science Career Decisions and Active Learning. *CBE-Life Sciences Education* **2007**, *6* (4), 297-306;
3. Russell, S. H.; Hancock, M. P.; McCullough, J., Benefits of Undergraduate Research Experiences. *Science* **2007**, *316* (5824), 548-549;
4. Weaver, G. C.; Russell, C. B.; Wink, D. J., Inquiry-based and research-based laboratory pedagogies in undergraduate science. *Nat Chem Biol* **2008**, *4* (10), 577-580.
5. Canaria, J. A.; Schoffstall, A. M.; Weiss, D. J.; Henry, R. M.; Braun-Sand, S. B., A Model for an Introductory Undergraduate Research Experience. *Journal of Chemical Education* **2012**, *89* (11), 1371-1377.
6. Fay, M. E.; Grove, N. P.; Towns, M. H.; Bretz, S. L., A rubric to characterize inquiry in the undergraduate chemistry laboratory. *Chemistry Education Research and Practice* **2007**, *8* (2), 212-219.
7. Freshman Research Initiative. (2012). College of Natural Sciences, The University of Texas at Austin. Retrieved from <http://fri.cns.utexas.edu>
8. ACS Guidelines for Chemistry in Two-Year College Programs. (2009). *ACS Society Committee on Education*. American Chemical Society. Retrieved from [http://portal.acs.org/portal/PublicWebSite/education/policies/twoyearcollege/CST\\_A\\_015380](http://portal.acs.org/portal/PublicWebSite/education/policies/twoyearcollege/CST_A_015380)
9. Kitamura, M.; Shabbir, S. H.; Anslyn, E. V. Guidelines for Pattern Recognition Using Differential Receptors and Indicator Displacement Assays. *The Journal of Organic Chemistry* **2012**, *74*, 4479–4489.
10. Merrifield, R. B. Solid Phase Peptide Synthesis. I. The Synthesis of a Tetrapeptide. *Journal of the American Chemical Society* **1963**, *85*, 2149–2154.
11. Gallagher, L. T.; Heo, J. S.; Lopez, M. A.; Ray, B. M.; Xiao, J.; Umali, A. P.; Zhang, A.; Dharmarajan, S.; Heymann, H.; Anslyn, E. V., Pattern-based discrimination of organic acids and red wine varietals by arrays of synthetic receptors. *Supramolecular Chemistry* **2012**, *24* (2), 143-148;
12. Umali, A. P.; LeBoeuf, S. E.; Newberry, R. W.; Kim, S.; Tran, L.; Rome, W. A.; Tian, T.; Taing, D.; Hong, J.; Kwan, M.; Heymann, H.; Anslyn, E. V., Discrimination of flavonoids and red wine varietals by arrays of differential peptidic sensors. *Chemical Science* **2011**, *2* (3), 439-445.

13. Rozinov, M. N.; Nolan G. P. Evolution of peptide that modulate the spectral qualities of bound, small-molecule fluorophores. *Chemistry & Biology* **1998**, *5*, 713-728.
14. Riedel, R., Nanoscaled inorganic materials by molecular design. *Chemical Society Reviews* **2012**, *41* (15), 5029-5031.
15. Feng, Z. V.; Lyon, J. L.; Croley, J. S.; Crooks, R. M.; Vanden Bout, D. A.; Stevenson, K. J., Synthesis and Catalytic Evaluation of Dendrimer-Encapsulated Cu Nanoparticles. An Undergraduate Experiment Exploring Catalytic Nanomaterials. *Journal of Chemical Education* **2009**, *86* (3), 368;
16. Marvin, K. A.; Johnson, J. A.; Rodenbusch, S. E.; Gong, L.; Vanden Bout, D. A.; Stevenson, K. J., Spectrophotometric Titration of Bimetallic Metal Cation Binding in Polyamido(amine) Dendrimer Templates. *Analytical Chemistry* **2012**, *84* (11), 5154-5158;
17. Marvin, K. A.; Johnson, J. A.; Rodenbusch, S. E.; Gong, L.; Vanden Bout, D. A.; Stevenson, K. J., Spectrophotometric Titration of Bimetallic Metal Cation Binding in Polyamido(amine) Dendrimer Templates. *Analytical Chemistry* **2012**;
18. Marvin, K. A.; Thadani, N. N.; Atkinson, C. A.; Keller, E. L.; Stevenson, K. J., Preparation and catalytic evaluation of ruthenium-nickel dendrimer encapsulated nanoparticles via intradendrimer redox displacement of nickel nanoparticles. *Chemical Communications* **2012**, *48* (50), 6289-6291.
19. Scott, R. W. J.; Wilson, O. M.; Crooks, R. M., Synthesis, Characterization, and Applications of Dendrimer-Encapsulated Nanoparticles. *The Journal of Physical Chemistry B* **2004**, *109* (2), 692-704.
20. Zhao, M.; Sun, L.; Crooks, R. M., Preparation of Cu Nanoclusters within Dendrimer Templates. *Journal of the American Chemical Society* **1998**, *120* (19), 4877-4878.
21. Puig, O.; Caspary, F.; Rigaut, G.; Rutz, B.; Bouveret, E.; Bragado-Nilsson, E.; Wilm, M.; Séraphin, B., The Tandem Affinity Purification (TAP) Method: A General Procedure of Protein Complex Purification. *Methods* **2001**, *24* (3), 218-229.
22. Bosma, W. B. Using Chemistry and Color To Analyze Household Products: A 10-12 Hour Laboratory Project at the General Chemistry Level. *Journal of Chemical Education* **1998**, *75*, 214.

# Appendix 1: Isothermal Titration Calorimetry Traces

## A.1 DENDRIMER COOPERATIVITY ITC TRACES

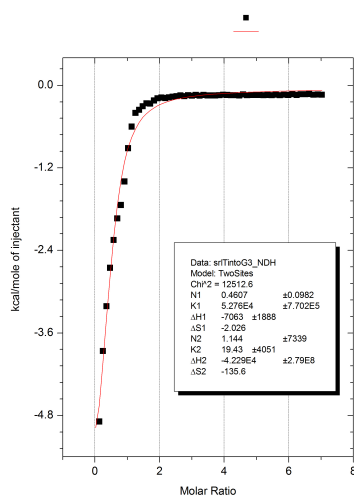


Figure A1.1 – G3 Benzyl Trace

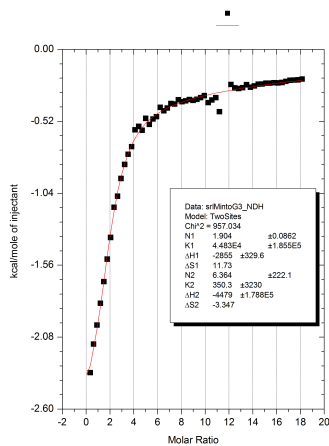


Figure A1.2 – G3 Meta Trace

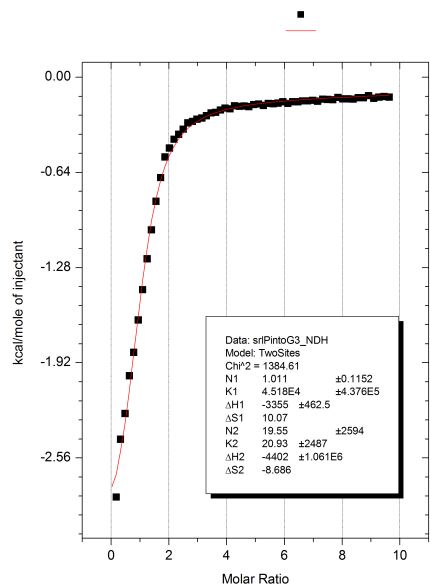


Figure A1.3 – G3 Para Trace

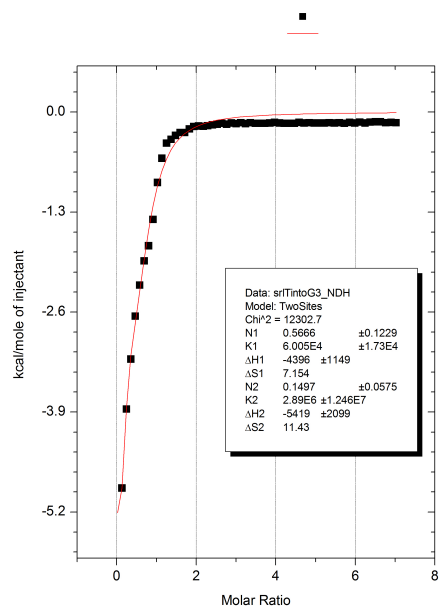


Figure A1.4 – G3 Tris Trace

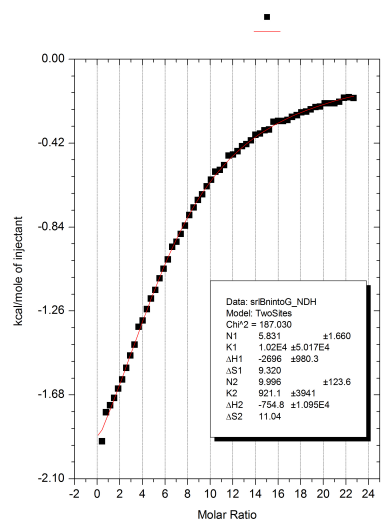


Figure A1.5 – G4 Benzyl Trace

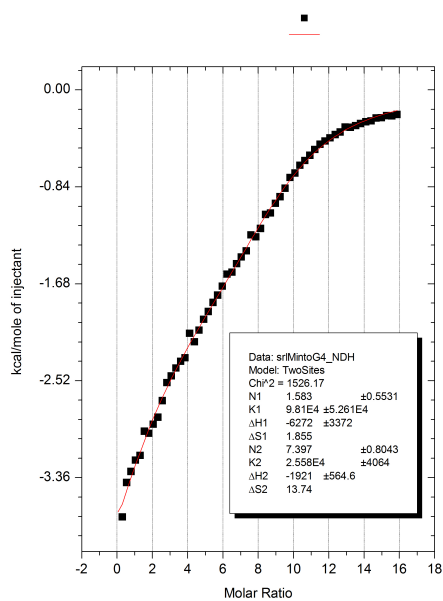


Figure A1.6 – G4 Meta Trace

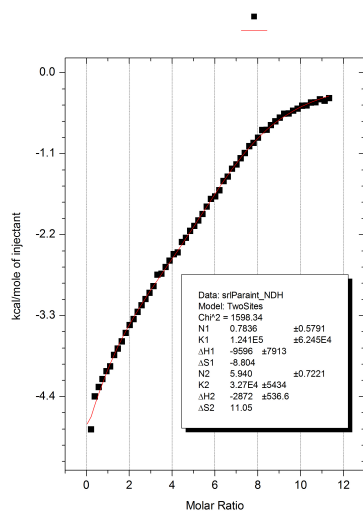


Figure A1.7 – G4 Para Trace

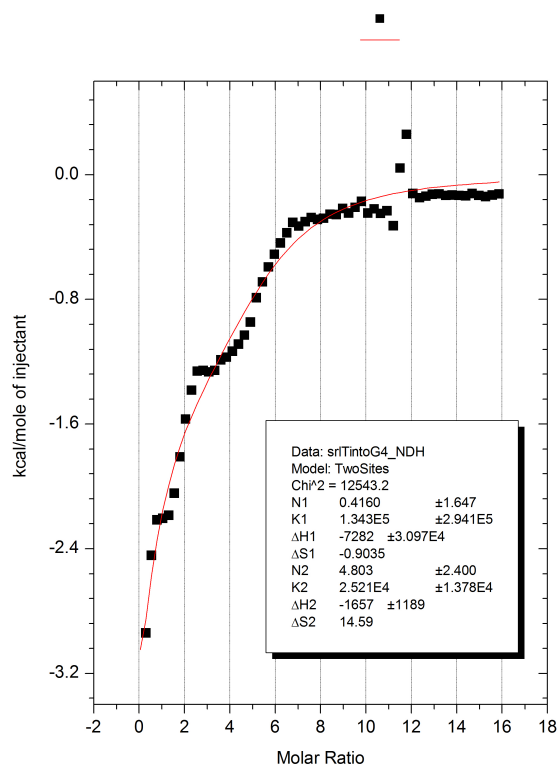


Figure A1.8 – G4 Tris Trace

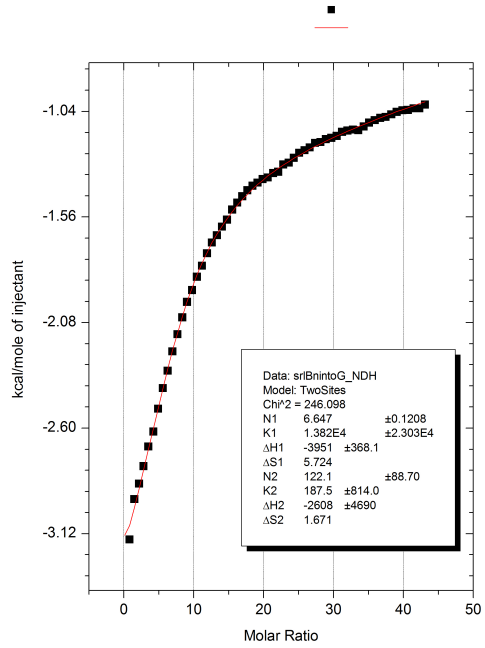


Figure A1.9 – G5 Benzyl Trace

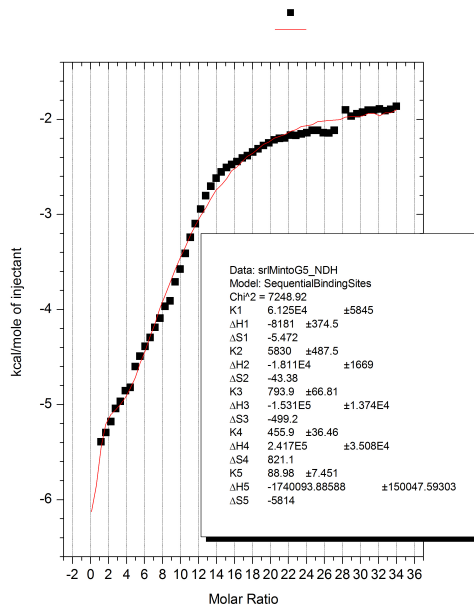


Figure A1.10 – G5 Meta Trace

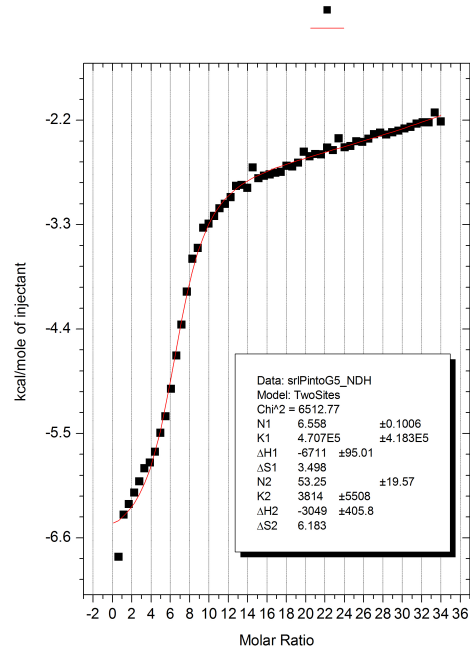


Figure A1.11 – G5 Para Trace

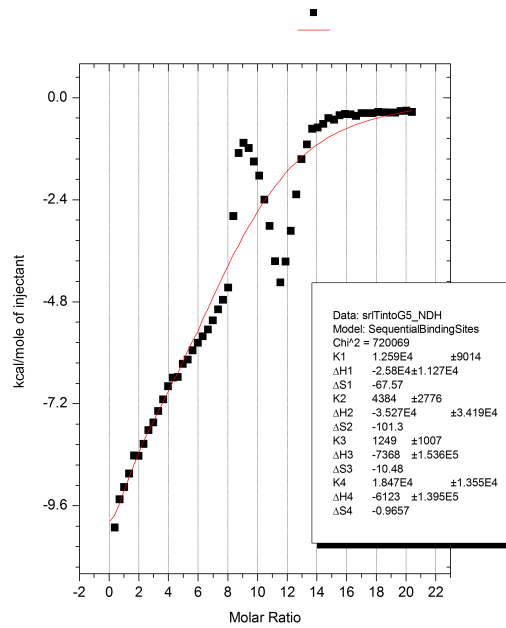


Figure A1.12 – G5 Tris Trace



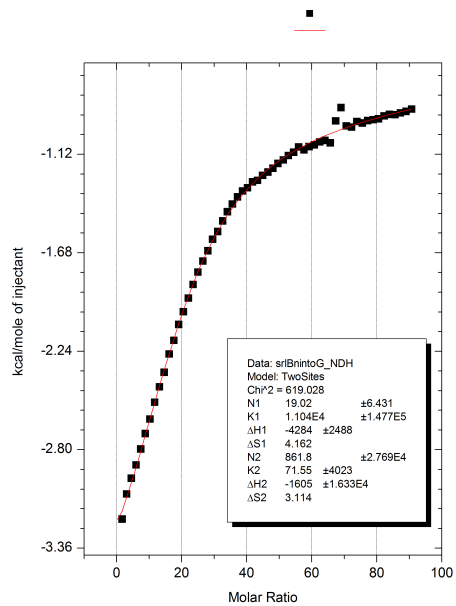


Figure A1.13 – G6 Benzyl Trace

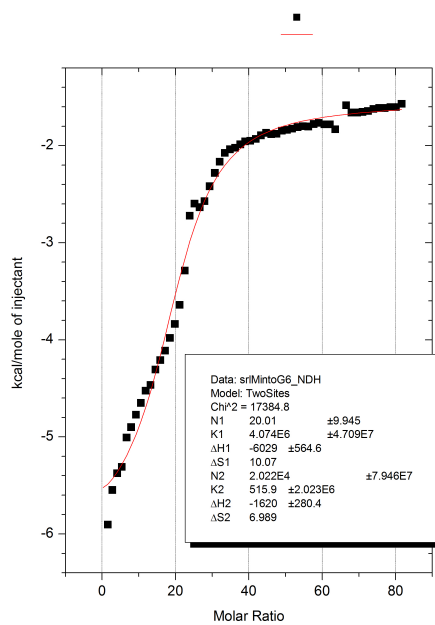


Figure A1.14 – G6 Meta Trace

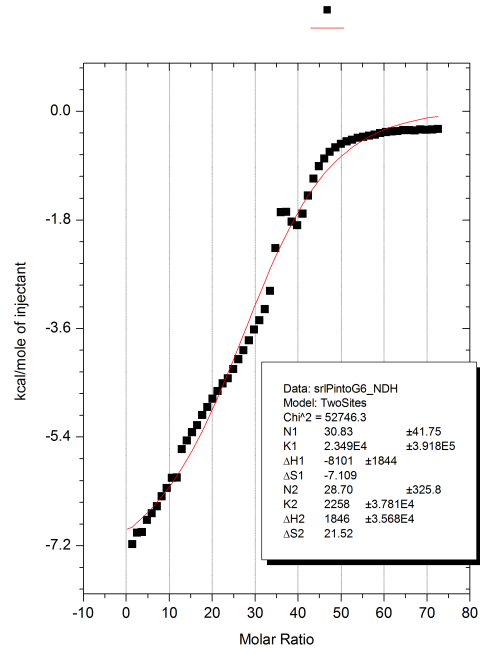


Figure A1.15 – G6 Para Trace

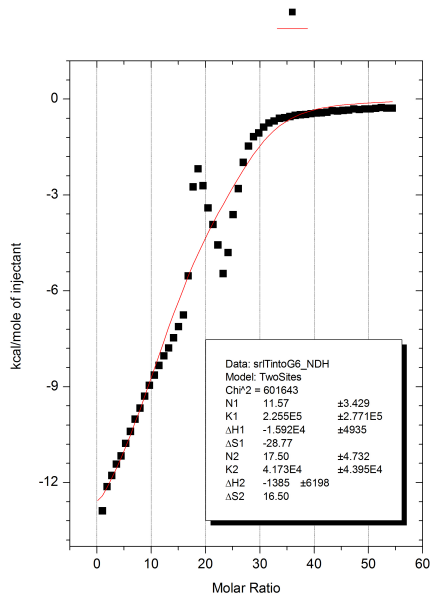


Figure A1.16 – G6 Tris Trace

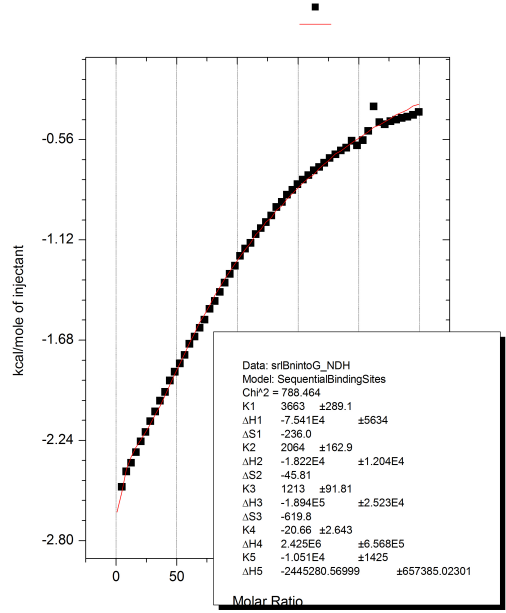


Figure A1.17 – G7 Benzyl Trace

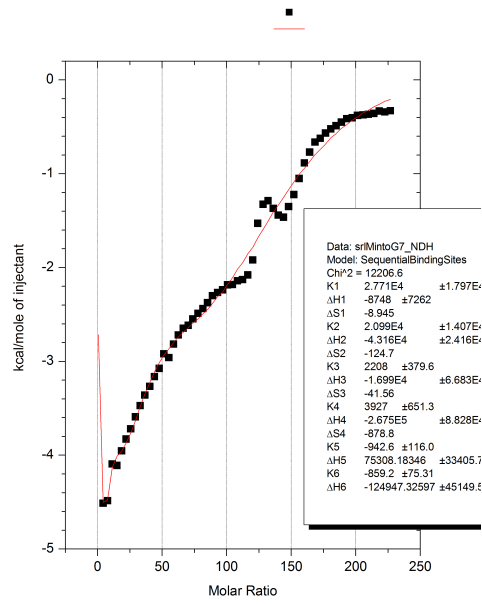


Figure A1.18 – G7 Meta Trace

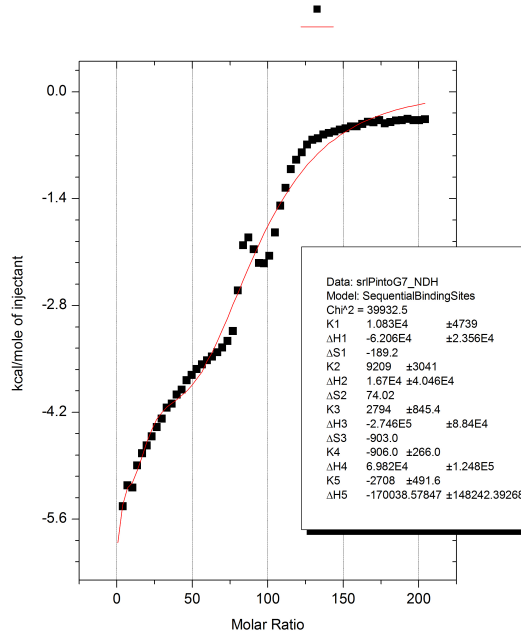


Figure A1.19 – G7 Para Trace

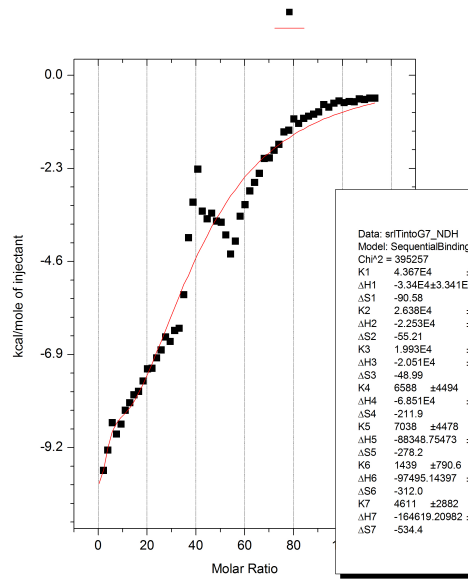


Figure A1.20 – G7 Tris Trace

## A1.2 METAL LIGAND ITC TRACES

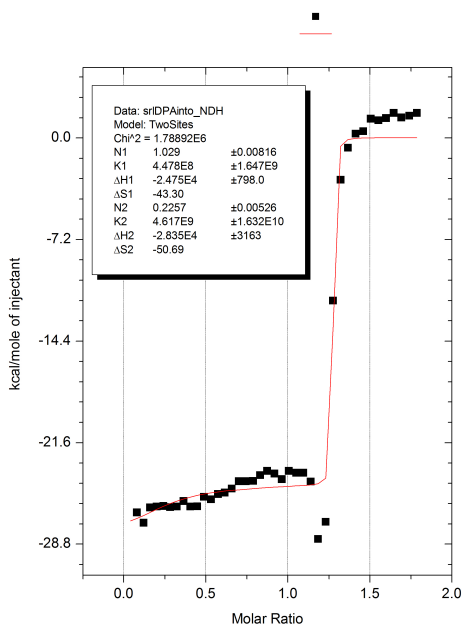


Figure A1.21 – Co DPA Trace

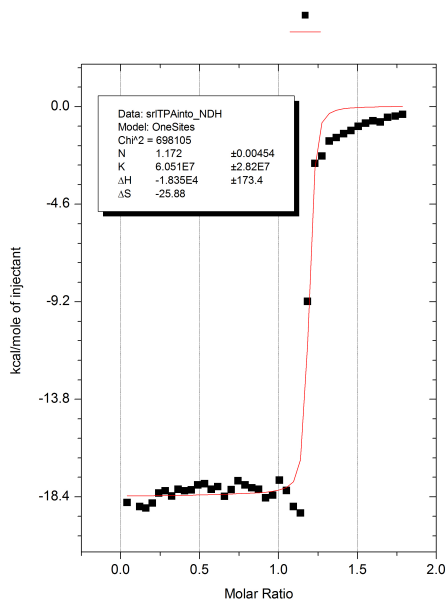


Figure A1.22 – Co TPA Trace

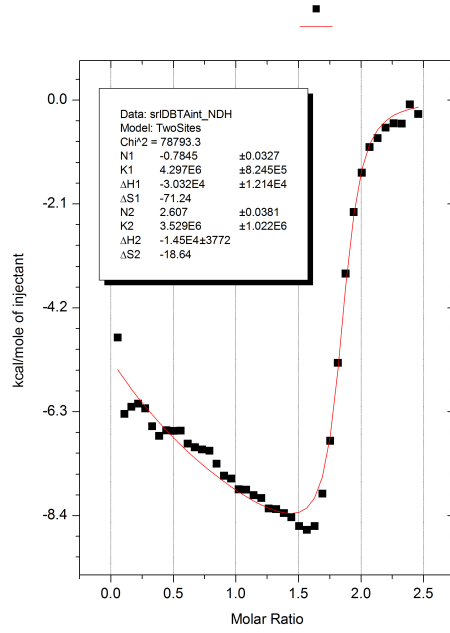


Figure A1.23 – Co DBTA Trace

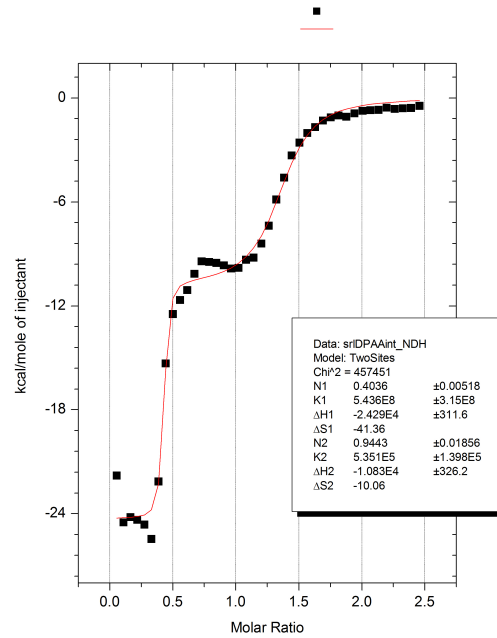


Figure A1.24 – Cu DPA Trace

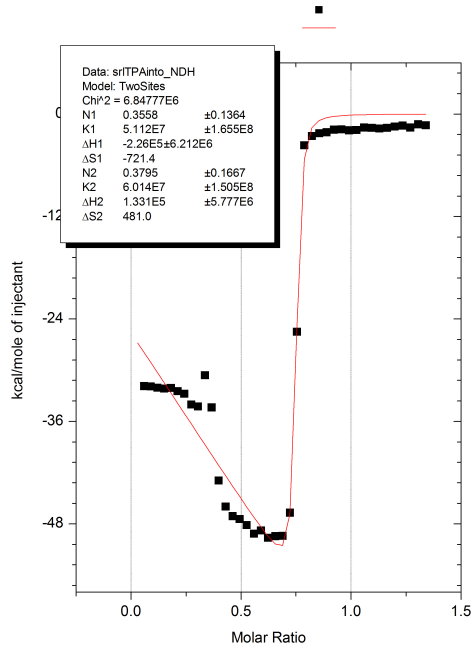


Figure A1.25 – Cu TPA Trace

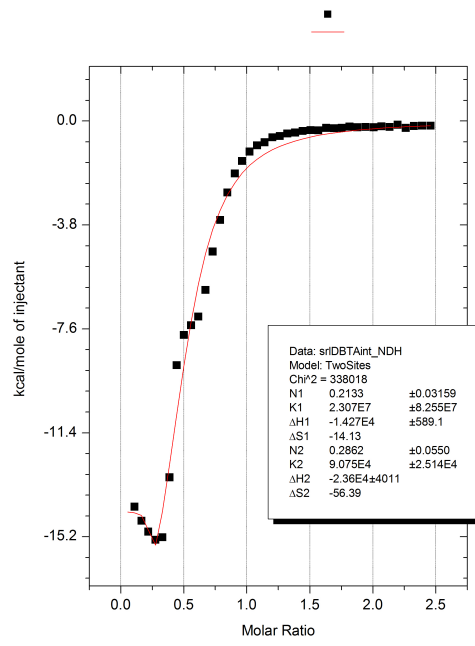


Figure A1.26 – Cu DBTA Trace

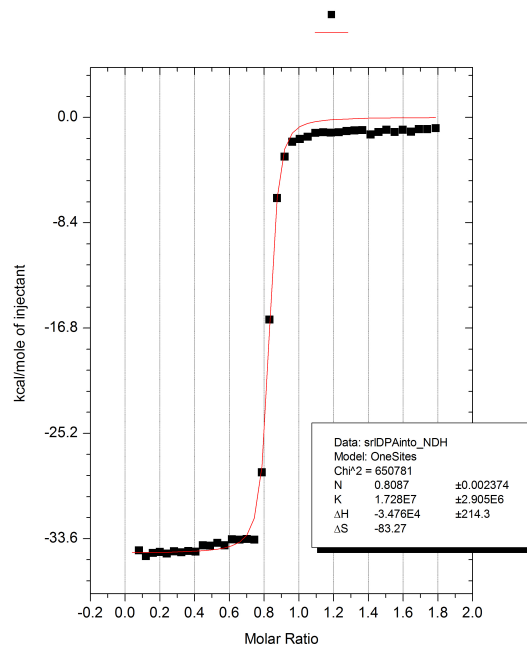


Figure A1.27 – Ni DPA Trace

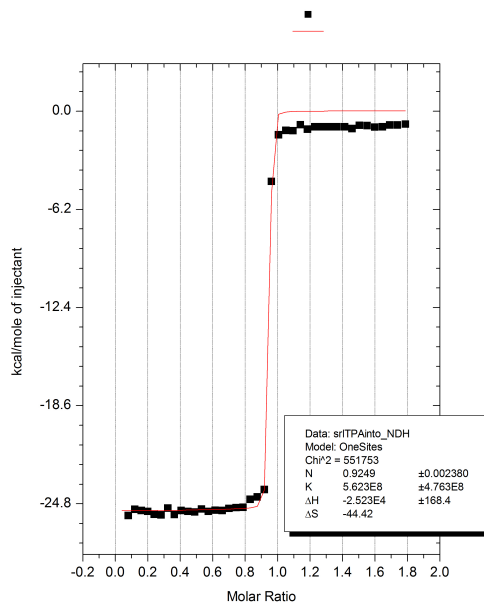


Figure A1.28 – Ni TPA Trace



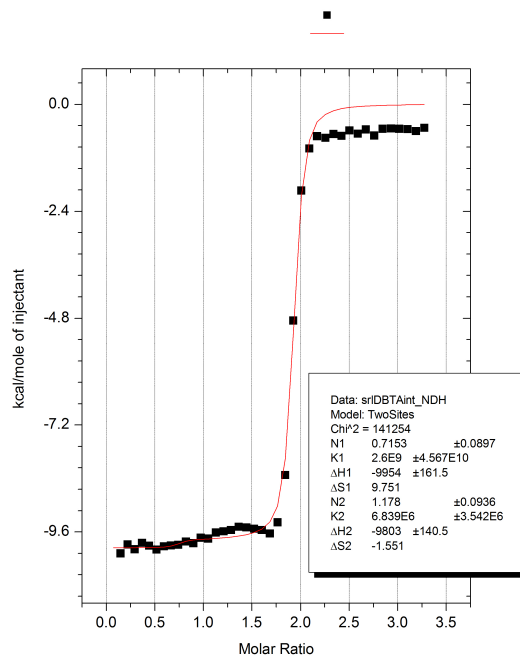


Figure A1.29 – Ni DBTA Trace

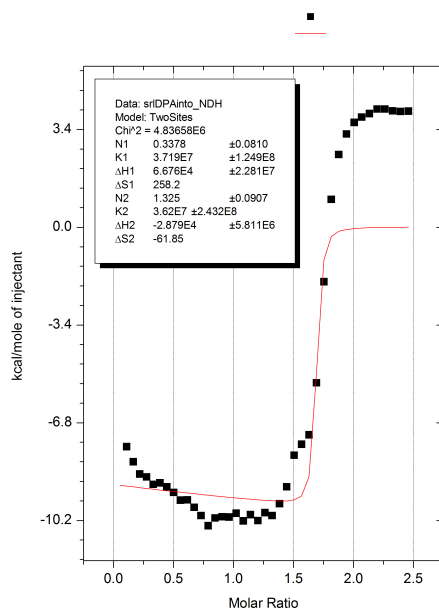


Figure A1.30 – Zn DPA Trace

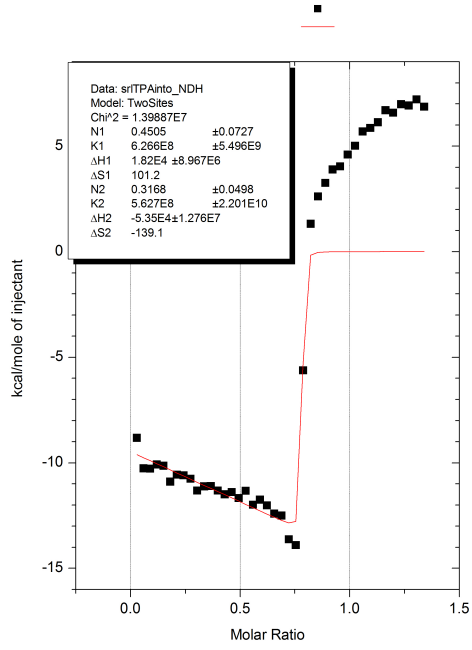


Figure A1.31 – Zn TPA Trace

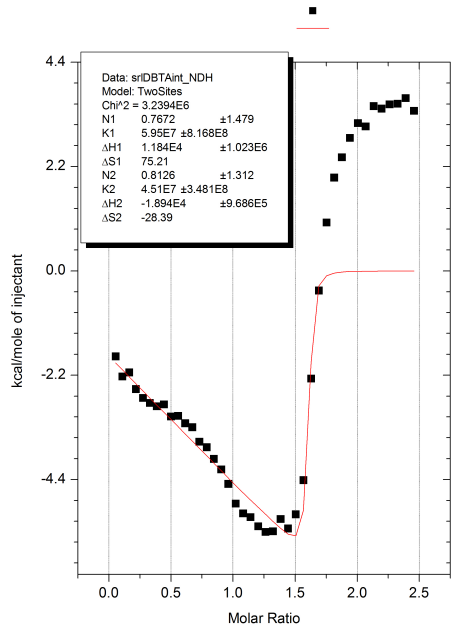


Figure A1.32 – Zn DBTA Trace

## Bibliography

### CHAPTER 1

Buhleier, E.; Wehner, W.; Vogtle, F. "Cascade" and 'Nonskid-Chain-Like; Synthesis of Molecular Cavity Topologies. *Synthesis* **1978**, 155–58.

Newkome, G. R.; Yao, Z.; Baker, G. R.; Gupta, V. K. Micelles. Part 1. Cascade molecules: a new approach to micelles. A [27]-arborol. *The Journal of Organic Chemistry* **1985**, *50*, 2003–2004.

Tomalia, D. A.; Baker, H.; Dewald, J.; Hall, M.; Kallos, G.; Martin, S.; Roeck, J.; Ryder, J.; Smith, P. A New Class of Polymers: Starburst-Dendritic Macromolecules. *Polymer Journal* **1985**, *17*, 117–132.

Hawker, C. J.; Frechet, J. M. J. Preparation of polymers with controlled molecular architecture. A new convergent approach to dendritic macromolecules. *Journal of the American Chemical Society* **1990**, *112*, 7638–7647.

Frechet, J. M.; Tomalia, D. A. *Dendrimer and other Dendritic Polymers*; Wiley, 2001.

Newkome, G. R.; Kotta, K. K.; Moorefield, C. N. Convenient Synthesis of 1 → 3 C-Branched Dendrons. *The Journal of Organic Chemistry* **2005**, *70*, 4893–4896

Inc, D. Dendritech <http://www.dendritech.com/pamam.html> (accessed Nov 9, 2012).

Challa, T.; Goud, B. A.; Baskar, S.; Chandra Mouli, G.; Jukuri, R. DENDRIMERS: A NOVEL POLYMER FOR DRUG DELIVERY. *International Journal of Pharmaceutical Sciences Review & Research* **2011**, *9*, 88–99.

Sun, M.; Fan, A.; Wang, Z.; Zhao, Y. Dendrimer-mediated drug delivery to the skin. *Soft Matter* **2012**, *8*, 4301–4305.

Mullen, D. G.; Fang, M.; Desai, A.; Baker, J. R.; Orr, B. G.; Banaszak Holl, M. M. A Quantitative Assessment of Nanoparticle–Ligand Distributions: Implications for Targeted Drug and Imaging Delivery in Dendrimer Conjugates. *ACS Nano* **2010**, *4*, 657–670

Willerich, I.; Ritter, H.; Gröhn, F. Structure and Thermodynamics of Ionic Dendrimer–Dye Assemblies. *The Journal of Physical Chemistry B* **2009**, *113*, 3339–3354 ST – Structure and Thermodynamics of Io.

Bonizzoni, M.; Long, S. R.; Rainwater, C.; Anslyn, E. V. PAMAM dendrimer-induced aggregation of 5(6)-carboxyfluorescein. *The Journal of organic chemistry* **2012**, *77*, 1258–1266.

Rainwater, J. C.; Anslyn, E. V. Amino-terminated PAMAM dendrimers electrostatically uptake numerous anionic indicators. *Chem. Commun. (Cambridge, U. K.)* **2010**, *46*, 2904–2906

Niu, Y.; Sun, L.; Crooks, R. M. Determination of the Intrinsic Proton Binding Constants for Poly(amidoamine) Dendrimers via Potentiometric pH Titration. *Macromolecules* **2003**, *36*, 5725–5731.

Zeng, F.; Zimmerman, S. C. Dendrimers in Supramolecular Chemistry: From Molecular Recognition to Self-Assembly. *Chemical Reviews* **1997**, *97*, 1681–1712.

Gradinaru, C. C.; Marushchak, D. O.; Samim, M.; Krull, U. J. Fluorescence anisotropy: from single molecules to live cells. *Analyst* **2010**, *135*, 452–459.

Yang, W.; Li, Y.; Cheng, Y.; Wu, Q.; Wen, L.; Xu, T. Evaluation of phenylbutazone and poly(amidoamine) dendrimers interactions by a combination of solubility, 2D-NOESY NMR, and isothermal titration calorimetry studies. *Journal of Pharmaceutical Sciences* **2009**, *98*, 1075–1085.

Voet, D.; Voet, J. G.; Pratt, C. 2006 *Fundamentals of biochemistry : life at the molecular level*; Wiley: Hoboken, N.J. ET - 2nd, 2006.

Channon, K. Tetrahydrobiopterin: Regulator of Endothelial Nitric Oxide Synthase in Vascular Disease. *Trends in Cardiovascular Medicine* **2004**, *14*, 323–327.

Bates, G. W.; Triyanti; Light, M. E.; Albrecht, M.; Gale, P. A. 2,7-Functionalized Indoles as Receptors for Anions. *J. Org. Chem.* **2007**, *72*, 8921–8927 ST - 2,7-Functionalized Indoles as Receptors for Anions.

Ali, H. D. P.; Kruger, P. E.; Gunnlaugsson, T. Colorimetric “naked-eye” and fluorescent sensors for anions based on amidourea functionalised 1,8-naphthalimide structures: anion recognition via either deprotonation or hydrogen bonding in DMSO. *New Journal of Chemistry* **2008**, *32*, 1153–1161

dos Santos, C. M. G.; McCabe, T.; Watson, G. W.; Kruger, P. E.; Gunnlaugsson, T. The Recognition and Sensing of Anions through "Positive Allosteric Effects," Using Simple Urea-Amide Receptors. *The Journal of Organic Chemistry* **2008**, *73*, 9235–9244

Veale, E. B.; Gunnlaugsson, T. Bidirectional Photoinduced Electron-Transfer Quenching Is Observed in 4-Amino-1,8-naphthalimide-Based Fluorescent Anion Sensors. *The Journal of Organic Chemistry* **2008**, *73*, 8073–8076

Sessler, J. L.; Cho, D.-G.; Lynch, V. Diindolylquinoxalines: An Effective Indole-Based Receptors for Phosphate Anion. *Journal of the American Chemical Society* **2006**, *128*, 16518–16519

Gong, H.-Y.; Rambo, B. M.; Karnas, E.; Lynch, V. M.; Keller, K. M.; Sessler, J. L. Environmentally Responsive Threading, Dethreading, and Fixation of Anion-Induced Pseudorotaxanes. *Journal of the American Chemical Society* **2011**, *133*, 1526–1533

Yoo, J.; Kim, M.-S.; Hong, S.-J.; Sessler, J. L.; Lee, C.-H. Selective Sensing of Anions with Calix[4]pyrroles Strapped with Chromogenic Dipyrrolylquinoxalines. *The Journal of Organic Chemistry* **2008**, *74*, 1065–1069

Lee, M. H.; Cao, Q.-Y.; Kim, S. K.; Sessler, J. L.; Kim, J. S. Anion Responsive TTF-Appended Calix[4]arenes. Synthesis and Study of Two Different Conformers. *The Journal of Organic Chemistry* **2010**, *76*, 870–874

Guha, S.; Saha, S. Fluoride Ion Sensing by an Anion- $\pi$  Interaction. *Journal of the American Chemical Society* **2010**, *132*, 17674–17677

Cormode, D. P.; Evans, A. J.; Davis, J. J.; Beer, P. D. Amplification of anion sensing by disulfide functionalized ferrocene and ferrocene-calixarene receptors adsorbed onto gold surfaces. *Dalton Transactions* **2010**, *39*, 6532–6541

Swinburne, A. N.; Paterson, M. J.; Beeby, A.; Steed, J. W. Fluorescent “Twist-on” Sensing by Induced-Fit Anion Stabilisation of a Planar Chromophore. *Chemistry – A European Journal* **2010**, *16*, 2714–2718

Amendola, V.; Fabbrizzi, L.; Mosca, L. Anion recognition by hydrogen bonding: urea-based receptors. *Chemical Society Reviews* **2010**, *39*, 3889–3915.

Schiller, A.; Viložny, B.; Wessling, R. A.; Singaram, B. Recognition of phospho sugars and nucleotides with an array of boronic acid appended bipyridinium salts. *Analytica Chimica Acta* **2008**, *627*, 203–211.

Palacios, M. A.; Nishiyabu, R.; Marquez, M.; Anzenbacher, P. Supramolecular Chemistry Approach to the Design of a High-Resolution Sensor Array for Multianion Detection in Water. *Journal of the American Chemical Society* **2007**, *129*, 7538–7544

Wang, Z.; Palacios, M. A.; Zyryanov, G.; Anzenbacher, P. Harnessing a Ratiometric Fluorescence Output from a Sensor Array. *Chemistry – A European Journal* **2008**, *14*, 8540–8546

Ojida, A.; Nanaka, H.; Miyahara, Y.; Tamaru, S.; Sada, K.; Hamachi, I. Bis(Dpa-ZnII) appended xanthone: excitation ratiometric chemosensor for phosphate anions. *Angew. Chem., Int. Ed.* **2006**, *45*, 5518–5521

Cano, M.; Rodríguez, L.; Lima, J. C.; Pina, F.; Dalla Cort, A.; Pasquini, C.; Schiaffino, L. Specific Supramolecular Interactions between Zn<sup>2+</sup>-Salophen Complexes and Biologically Relevant Anions. *Inorganic Chemistry* **2009**, *48*, 6229–6235.

Schaeferling, M.; Wolfbeis, O. S. Europium tetracycline as a luminescent probe for nucleoside phosphates and its application to the determination of kinase activity. *Chem.--Eur. J.* **2007**, *13*, 4342–4349

McCleskey, S. C.; Griffin, M. J.; Schneider, S. E.; McDevitt, J. T.; Anslyn, E. V. Differential Receptors Create Patterns Diagnostic for ATP and GTP. *Journal of the American Chemical Society* **2003**, *125*, 1114–1115

Hargrove, A. E.; Nieto, S.; Zhang, T.; Sessler, J. L.; Anslyn, E. V. Artificial Receptors for the Recognition of Phosphorylated Molecules. *Chemical Reviews* **2011**, *111*, 6603–6782

Ojida, A.; Mito-oka, Y.; Sada, K.; Hamachi, I. Molecular Recognition and Fluorescence Sensing of Monophosphorylated Peptides in Aqueous Solution by Bis(zinc(II)-dipicolylamine)-Based Artificial Receptors. *Journal of the American Chemical Society* **2004**, *126*, 2454–2463

Ojida, A.; Miyahara, Y.; Wongkongkatep, J.; Tamaru, S.; Sada, K.; Hamachi, I. Design of dual-emission chemosensors for ratiometric detection of ATP derivatives. *Chem.--Asian J.* **2006**, *1*, 555–563

Fenniri, H.; Hosseini, M. W.; Lehn, J.-M. Molecular Recognition of NADP(H) and ATP by Macrocyclic Polyamines Bearing Acridine Groups. *Helvetica Chimica Acta* **1997**, *80*, 786–803

Domenech, A.; Garcia-Espana, E.; A. Ramirez, J.; Celda, B.; Carmen Martinez, M.; Monleon, D.; Tejero, R.; Bencini, A.; Bianchi, A. A thermodynamic, electrochemical and molecular dynamics study on NAD and NADP recognition by 1,4,7,10,13,16,19-heptaazacyclohencosane ([21]aneN7) [dagger]. *Journal of the Chemical Society, Perkin Transactions 2* **1999**, 23–32

- Schmidtchen, F. P. Macrocyclic quaternary ammonium salts. II. Formation of inclusion complexes with anions in solution. *Chem. Ber.* **1981**, *114*, 597–607
- Fokkens, M.; Jasper, C.; Schrader, T.; Koziol, F.; Ochsenfeld, C.; Polkowska, J.; Lobert, M.; Kahlert, B.; Klarner, F.-G. Selective complexation of N-alkylpyridinium salts: binding of NAD<sup>+</sup> in water. *Chemistry* **2005**, *11*, 477–94
- Yano, Y.; Tamura, N.; Mitsui, K.; Nabeshima, T. A flavin receptor. Effect of 2,6-diaminopyridine derivatives on the reduction of benzodipteridine (oxidation-active flavin model). *Chem. Lett.* **1989**, 1655–8
- Ariga, K.; Kamino, A.; Koyano, H.; Kunitake, T. Recognition of aqueous flavin mononucleotide on the surface of binary monolayers of guanidinium and melamine amphiphiles. *Journal of Materials Chemistry* **1997**, *7*, 1155–1161
- Breinlinger, E. C.; Keenan, C. J.; Rotello, V. M. Modulation of Flavin Recognition and Redox Properties through Donor Atom Interactions. *Journal of the American Chemical Society* **1998**, *120*, 8606–8609
- Deans, R.; Niemz, A.; Breinlinger, E. C.; Rotello, V. M. Electrochemical Control of Recognition Processes. A Three-Component Molecular Switch. *Journal of the American Chemical Society* **1997**, *119*, 10863–10864
- Boal, A. K.; Rotello, V. M. Redox-Modulated Recognition of Flavin by Functionalized Gold Nanoparticles. *Journal of the American Chemical Society* **1999**, *121*, 4914–4915
- Breinlinger, E. C.; Rotello, V. M. Model Systems for Flavoenzyme Activity. Modulation of Flavin Redox Potentials through  $\pi$ -Stacking Interactions. *Journal of the American Chemical Society* **1997**, *119*, 1165–1166
- König, B.; Pelka, M.; Zieg, H.; Ritter, T.; Bouas-Laurent, H.; Bonneau, R.; Desvergne, J.-P. Photoinduced Electron Transfer in a Phenothiazine-Riboflavin Dyad Assembled by Zinc-Imide Coordination in Water. *Journal of the American Chemical Society* **1999**, *121*, 1681–1687
- Roychowdhury-Saha, M.; Lato, S. M.; Shank, E. D.; Burke, D. H. Flavin Recognition by an RNA Aptamer Targeted toward FAD. *Biochemistry* **2002**, *41*, 2492–2499
- Rhee, H.-W.; Choi, H.-Y.; Han, K.; Hong, J.-I. Selective Fluorescent Detection of Flavin Adenine Dinucleotide in Human Eosinophils by Using Bis(Zn<sup>2+</sup>-Dipicolylamine) Complex. *Journal of the American Chemical Society* **2007**, *129*, 4524–4525

Giannattasio, S.; Gagliardi, S.; Samaja, M.; Marra, E. Simultaneous determination of purine nucleotides, their metabolites and Beta-nicotinamide adenine dinucleotide in cerebellar granule cells by ion-pair high performance liquid chromatography. *Brain Res. Protoc.* **2003**, *10*, 168–174

Britz-McKibbin, P.; Markuszewski, M. J.; Iyanagi, T.; Matsuda, K.; Nishioka, T.; Terabe, S. Picomolar analysis of flavins in biological samples by dynamic pH junction-sweeping capillary electrophoresis with laser-induced fluorescence detection. *Analytical Biochemistry* **2003**, *313*, 89–96

Mohler, R. E.; Tu, B. P.; Dombek, K. M.; Hoggard, J. C.; Young, E. T.; Synovec, R. E. Identification and evaluation of cycling yeast metabolites in two-dimensional comprehensive gas chromatography-time-of-flight-mass spectrometry data. *J. Chromatogr., A* **2008**, *1186*, 401–411

Cordell, R. L.; Hill, S. J.; Ortori, C. A.; Barrett, D. A. Quantitative profiling of nucleotides and related phosphate-containing metabolites in cultured mammalian cells by liquid chromatography tandem electrospray mass spectrometry. *J. Chromatogr., B: Anal. Technol. Biomed. Life Sci.* **2008**, *871*, 115–124

Yang, S.; Sadilek, M.; Lidstrom, M. E. Streamlined pentafluorophenylpropyl column liquid chromatography-tandem quadrupole mass spectrometry and global <sup>13</sup>C-labeled internal standards improve performance for quantitative metabolomics in bacteria. *J. Chromatogr., A* **2010**, *1217*, 7401–7410

Pabst, M.; Grass, J.; Fischl, R.; Leonard, R.; Jin, C.; Hinterkorn, G.; Borth, N.; Altmann, F. Nucleotide and Nucleotide Sugar Analysis by Liquid Chromatography-Electrospray Ionization-Mass Spectrometry on Surface-Conditioned Porous Graphitic Carbon. *Anal. Chem. (Washington, DC, U. S.)* **2010**, *82*, 9782–9788.

Bolin, C.; Cardozo-Pelaez, F. Assessing biomarkers of oxidative stress: Analysis of guanosine and oxidized guanosine nucleotide triphosphates by high performance liquid chromatography with electrochemical detection. *J. Chromatogr., B: Anal. Technol. Biomed. Life Sci.* **2007**, *856*, 121–130

Edwards, N. Y.; Sager, T. W.; McDevitt, J. T.; Anslyn, E. V. Boronic Acid Based Peptidic Receptors for Pattern-Based Saccharide Sensing in Neutral Aqueous Media, an Application in Real-Life Samples. *Journal of the American Chemical Society* **2007**, *129*, 13575–13583



Wiskur, S. L.; Anslyn, E. V. Using a Synthetic Receptor to Create an Optical-Sensing Ensemble for a Class of Analytes: A Colorimetric Assay for the Aging of Scotch. *Journal of the American Chemical Society* **2001**, *123*, 10109–10110

Zhang, T.; Edwards, N. Y.; Bonizzoni, M.; Anslyn, E. V. The Use of Differential Receptors to Pattern Peptide Phosphorylation. *J. Am. Chem. Soc.* **2009**, *131*, 11976–11984

Umali, A. P.; Anslyn, E. V. A general approach to differential sensing using synthetic molecular receptors. *Curr. Opin. Chem. Biol.* **2010**, *14*, 685–692 ST – A general approach to differential sensing using synthetic molecular receptors.

Gallagher, L. T.; Heo, J. S.; Lopez, M. A.; Ray, B. M.; Xiao, J.; Umali, A. P.; Zhang, A.; Dharmarajan, S.; Heymann, H.; Anslyn, E. V. Pattern-based discrimination of organic acids and red wine varietals by arrays of synthetic receptors. *Supramolecular Chemistry* **2012**, *24*, 143–148

Umali, A. P.; LeBoeuf, S. E.; Newberry, R. W.; Kim, S.; Tran, L.; Rome, W. A.; Tian, T.; Taing, D.; Hong, J.; Kwan, M.; Heymann, H.; Anslyn, E. V. Discrimination of flavonoids and red wine varietals by arrays of differential peptidic sensors. *Chemical Science* **2011**, *2*, 439–445

Kubarych, C. J.; Adams, M. M.; Anslyn, E. V. Serum Albumins as Differential Receptors for the Discrimination of Fatty Acids and Oils. *Org. Lett.* **2010**, *12*, 4780–4783

Adams, M. M.; Anslyn, E. V. Differential Sensing Using Proteins: Exploiting the Cross-Reactivity of Serum Albumin To Pattern Individual Terpenes and Terpenes in Perfume. *J. Am. Chem. Soc.* **2009**, *131*, 17068–17069

Saovapakhiran, A.; D'Emanuele, A.; Attwood, D.; Penny, J. Surface Modification of PAMAM Dendrimers Modulates the Mechanism of Cellular Internalization. *Bioconjugate Chemistry* **2009**, *20*, 693–701.

## Chapter 2

Lundquist, J. J.; Toone, E. J. The Cluster Glycoside Effect. *Chemical Reviews* **2002**, *102*, 555–578

H. Williams, D.; S. Westwell, M. Aspects of weak interactions. *Chemical Society Reviews* **1998**, *27*, 57–64

Cram, D. J. The design of molecular hosts, guests, and their complexes. *Science* **1988**, *240*, 760–767

- Archer, E. A.; Krische, M. J. Duplex Oligomers Defined via Covalent Casting of a One-Dimensional Hydrogen-Bonding Motif. *Journal of the American Chemical Society* **2002**, *124*, 5074–5083
- Wiskur, S. L.; Lavigne, J. J.; Metzger, A.; Tobey, S. L.; Lynch, V.; Anslyn, E. V Thermodynamic Analysis of Receptors Based on Guanidinium/Boronic Acid Groups for the Complexation of Carboxylates,  $\alpha$ -Hydroxycarboxylates, and Diols: Driving Force for Binding and Cooperativity. *Chemistry – A European Journal* **2004**, *10*, 3792–3804
- Mammen, M.; Choi, S.-K.; Whitesides, G. M. Polyvalent Interactions in Biological Systems: Implications for Design and Use of Multivalent Ligands and Inhibitors. *Angewandte Chemie International Edition* **1998**, *37*, 2754–2794
- Johnson, C. R.; Ownby, D. W.; Gill, S. J.; Peters, K. S. Oxygen binding constants and stepwise enthalpies for human and bovine hemoglobin at pH 7.6. *Biochemistry* **1992**, *31*, 10074–10082.
- Philo, J. S.; Lary, J. W. Kinetic investigations of the quaternary enhancement effect and alpha/beta differences in binding the last oxygen to hemoglobin tetramers and dimers. *Journal of Biological Chemistry* **1990**, *265*, 139–143.
- Jencks, W. P. On the attribution and additivity of binding energies. *Proceedings of the National Academy of Sciences* **1981**, *78*, 4046–4050
- Christensen, T.; Gooden, D. M.; Kung, J. E.; Toone, E. J. Additivity and the Physical Basis of Multivalency Effects: A Thermodynamic Investigation of the Calcium EDTA Interaction. *Journal of the American Chemical Society* **2003**, *125*, 7357–7366
- Hughes, A. D.; Anslyn, E. V A cationic host displaying positive cooperativity in water. *Proceedings of the National Academy of Sciences* **2007**, *104*, 6538–6543
- Kitov, P. I.; Bundle, D. R. On the Nature of the Multivalency Effect: A Thermodynamic Model. *Journal of the American Chemical Society* **2003**, *125*, 16271–16284
- Breslow, R.; Greenspoon, N.; Guo, T.; Zarzycki, R. Very strong binding of appropriate substrates by cyclodextrin dimers. *Journal of the American Chemical Society* **1989**, *111*, 8296–8297
- Chekmeneva, E.; Hunter, C. A.; Packer, M. J.; Turega, S. M. Evidence for Partially Bound States in Cooperative Molecular Recognition Interfaces. *Journal of the American Chemical Society* **2008**, *130*, 17718–17725
- Searle, M. S.; Westwell, M. S.; Williams, D. H. Application of a generalised enthalpy-entropy relationship to binding co-operativity and weak associations in solution. *Journal of the Chemical Society, Perkin Transactions 2* **1995**, 141–151
- Rao, J.; Lahiri, J.; Weis, R. M.; Whitesides, G. M. Design, Synthesis, and Characterization of a High-Affinity Trivalent System Derived from Vancomycin and L-Lys-d-Ala-d-Ala. *Journal of the American Chemical Society* **2000**, *122*, 2698–2710

- Lee, Y. C.; Lee, R. T. Carbohydrate-Protein Interactions: Basis of Glycobiology. *Accounts of Chemical Research* **1995**, *28*, 321–327
- Rekharsky, M.; Inoue, Y.; Tobey, S.; Metzger, A.; Anslyn, E. Ion-Pairing Molecular Recognition in Water: Aggregation at Low Concentrations That Is Entropy-Driven. *Journal of the American Chemical Society* **2002**, *124*, 14959–14967
- Tobey, S. L.; Anslyn, E. V Studies into the Thermodynamic Origin of Negative Cooperativity in Ion-Pairing Molecular Recognition. *Journal of the American Chemical Society* **2003**, *125*, 10963–10970
- Linton, B. R.; Goodman, M. S.; Fan, E.; Van Arman, S. A.; Hamilton, A. D. Thermodynamic Aspects of Dicarboxylate Recognition by Simple Artificial Receptors. *The Journal of Organic Chemistry* **2001**, *66*, 7313–7319
- Badjić, J. D.; Nelson, A.; Cantrill, S. J.; Turnbull, W. B.; Stoddart, J. F. Multivalency and Cooperativity in Supramolecular Chemistry. *Accounts of Chemical Research* **2005**, *38*, 723–732
- Yang, R. C. K.; Huang, J. T. B.; Chien, S.-C.; Huang, R.; Jeng, K.-C. G.; Chen, Y.-C.; Liao, M.; Wu, J.-R.; Hung, W.-K.; Hung, C.-C.; Chen, Y.-L.; Waring, M. J.; Sheh, L. Energetic studies on DNA-peptide interaction in relation to the enthalpy-entropy compensation paradox. *Organic & Biomolecular Chemistry* **2013**.
- Starikov, E.; Nordén, B. Entropy-enthalpy compensation may be a useful interpretation tool for complex systems like protein-DNA complexes: An appeal to experimentalists. *Applied Physics Letters* **2012**.
- Sharp, K. Entropy—enthalpy compensation: Fact or artifact? *Protein Science* **2001**, *10*, 661–667.
- Cornish-Bowden, A. Enthalpy-entropy compensation: a phantom phenomenon. *Journal of Biosciences* **2002**, *27*, 121–26.
- Liu, L.; Guo, Q.-X. Isokinetic Relationship, Isoequilibrium Relationship, and Enthalpy–Entropy Compensation. *Chemical Reviews* **2001**, *101*, 673–696.
- Gelb, R. I.; Lee, B. T.; Zompa, L. J. Hexacyclen complexes of inorganic anions. 2. Bonding forces, structures, and selectivity. *Journal of the American Chemical Society* **1985**, *107*, 909–916.
- Nasief, N. N.; Tan, H.; Kong, J.; Hangauer, D. Water Mediated Ligand Functional Group Cooperativity: The Contribution of a Methyl Group to Binding Affinity is Enhanced by a COO– Group Through Changes in the Structure and Thermodynamics of the Hydration Waters of Ligand–Thermolysin Complexes. *Journal of Medicinal Chemistry* **2012**, *55*, 8283–8302.
- Routh, A.; Sandin, S.; Rhodes, D. Nucleosome repeat length and linker histone stoichiometry determine chromatin fiber structure. *Proceedings of the National Academy of Sciences* **2008**, *105*, 8872–8877

Korolev, N.; Allahverdi, A.; Lyubartsev, A. P.; Nordenskiöld, L. The polyelectrolyte properties of chromatin. *Soft Matter* **2012**, *8*, 9322–9333.

Fant, K.; Esbjorner, E. K.; Lincoln, P.; Norden, B. DNA Condensation by PAMAM Dendrimers: Self-Assembly Characteristics and Effect on Transcription†. *Biochemistry* **2008**, *47*, 1732–1740

Pavan, G. M.; Danani, A.; Pricl, S.; Smith, D. K. Modeling the Multivalent Recognition between Dendritic Molecules and DNA: Understanding How Ligand “Sacrifice” and Screening Can Enhance Binding. *Journal of the American Chemical Society* **2009**, *131*, 9686–9694

Pavan, G. M.; Albertazzi, L.; Danani, A. Ability to Adapt: Different Generations of PAMAM Dendrimers Show Different Behaviors in Binding siRNA. *The Journal of Physical Chemistry B* **2010**, *114*, 2667–2675

Örberg, M.-L.; Schillén, K.; Nylander, T. Dynamic Light Scattering and Fluorescence Study of the Interaction between Double-Stranded DNA and Poly(amido amine) Dendrimers. *Biomacromolecules* **2007**, *8*, 1557–1563

Braun, C. S.; Vetro, J. A.; Tomalia, D. A.; Koe, G. S.; Koe, J. G.; Russell Middaugh, C. Structure/function relationships of polyamidoamine/DNA dendrimers as gene delivery vehicles. *Journal of Pharmaceutical Sciences* **2005**, *94*, 423–436

Coles, D. J.; Yang, S.; Minchin, R. F.; Toth, I. The characterization of a novel dendritic system for gene delivery by isothermal titration calorimetry. *Peptide Science* **2008**, *90*, 651–654

Jensen, L. B.; Pavan, G. M.; Kasimova, M. R.; Rutherford, S.; Danani, A.; Nielsen, H. M.; Foged, C. Elucidating the molecular mechanism of PAMAM–siRNA dendriplex self-assembly: Effect of dendrimer charge density. *International Journal of Pharmaceutics* **2011**, *416*, 410–418.

Newkome, G. R.; Kotta, K. K.; Moorefield, C. N. Convenient Synthesis of 1 → 3 C- Branched Dendrons. *The Journal of Organic Chemistry* **2005**, *70*, 4893–4896

### Chapter 3

Collet, J.-F.; Depuydt, M.; Messens, J. How proteins form disulfide bonds. *Antioxidants & Redox Signaling* **2012**, *15*, 49+

Fass, D. Disulfide Bonding in Protein Biophysics. *Annual Review of Biophysics* **2012**, *41*, 63–79

Narayan, M. Disulfide bonds: protein folding and subcellular protein trafficking. *FEBS Journal* **2012**, *279*, 2272–2282

Au-Yeung, H. Y.; Pantos, G. D.; Sanders, J. K. M. Dynamic combinatorial synthesis of a catenane based on donor–acceptor interactions in water. *Proceedings of the National Academy of Sciences* **2009**, *106*, 10466–10470

Au-Yeung, H. Y.; Cougnon, F. B. L.; Otto, S.; Pantos, G. D.; Sanders, J. K. M. Exploiting donor-acceptor interactions in aqueous dynamic combinatorial libraries: exploratory studies of simple systems. *Chemical Science* **2010**, *1*, 567–574

Corbett, P. T.; Sanders, J. K. M.; Otto, S. Competition between Receptors in Dynamic Combinatorial Libraries: Amplification of the Fittest? *Journal of the American Chemical Society* **2005**, *127*, 9390–9392

Au-Yeung, H. Y.; Pengo, P.; Pantos, G. D.; Otto, S.; Sanders, J. K. M. Templated amplification of a naphthalenediimide-based receptor from a donor-acceptor dynamic combinatorial library in water. *Chemical Communications* **2009**, 419–421

Zhang, T.; Anslyn, E. V A Colorimetric Boronic Acid Based Sensing Ensemble for Carboxy and Phospho Sugars. *Organic Letters* **2006**, *8*, 1649–1652

Edwards, N. Y.; Sager, T. W.; McDevitt, J. T.; Anslyn, E. V Boronic Acid Based Peptidic Receptors for Pattern-Based Saccharide Sensing in Neutral Aqueous Media, an Application in Real-Life Samples. *Journal of the American Chemical Society* **2007**, *129*, 13575–13583

Kataoka, K.; James, T. D.; Kubo, Y. Ion Pair-Driven Heterodimeric Capsule Based on Boronate Esterification: Construction and the Dynamic Behavior. *Journal of the American Chemical Society* **2007**, *129*, 15126–15127.

James, T. D.; Sandanayake, K. R. A. S.; Shinkai, S. Novel photoinduced electron-transfer sensor for saccharides based on the interaction of boronic acid and amine. *Journal of the Chemical Society, Chemical Communications* **1994**, 477–478

Shabbir, S. H.; Joyce, L. A.; Da Cruz, G. M.; Lynch, V. M.; Sorey, S.; Anslyn, E. V Pattern-Based Recognition for the Rapid Determination of Identity, Concentration, and Enantiomeric Excess of Subtly Different Threo Diols. *Journal of the American Chemical Society* **2009**, *131*, 13125–13131

Shabbir, S. H.; Regan, C. J.; Anslyn, E. V A general protocol for creating high-throughput screening assays for reaction yield and enantiomeric excess applied to hydrobenzoin. *Proceedings of the National Academy of Sciences* **2009**, *106*, 10487–10492.

Zhu, L.; Zhong, Z.; Anslyn, E. V Guidelines in Implementing Enantioselective Indicator-Displacement Assays for  $\alpha$ -Hydroxycarboxylates and Diols. *Journal of the American Chemical Society* **2005**, *127*, 4260–4269

Wiskur, S. L.; Anslyn, E. V Using a Synthetic Receptor to Create an Optical-Sensing Ensemble for a Class of Analytes: A Colorimetric Assay for the Aging of Scotch. *Journal of the American Chemical Society* **2001**, *123*, 10109–10110

Wiskur, S. L.; Lavigne, J. J.; Metzger, A.; Tobey, S. L.; Lynch, V.; Anslyn, E. V Thermodynamic Analysis of Receptors Based on Guanidinium/Boronic Acid Groups for the Complexation of Carboxylates,  $\alpha$ -Hydroxycarboxylates, and Diols: Driving Force for Binding and Cooperativity. *Chemistry – A European Journal* **2004**, *10*, 3792–3804

Belowich, M. E.; Stoddart, J. F. Dynamic imine chemistry. *Chemical Society Reviews* **2012**, *41*, 2003–2024.

Lao, L. L.; Schmitt, J.-L.; Lehn, J.-M. Evolution of a Constitutional Dynamic Library Driven by Self-Organisation of a Helically Folded Molecular Strand. *Chemistry – A European Journal* **2010**, *16*, 4903–4910

Mastalerz, M. Shape-Persistent Organic Cage Compounds by Dynamic Covalent Bond Formation. *Angewandte Chemie International Edition* **2010**, *49*, 5042–5053

Schneider, M. W.; Oppel, I. M.; Mastalerz, M. Exo-Functionalized Shape-Persistent [2+3] Cage Compounds: Influence of Molecular Rigidity on Formation and Permanent Porosity. *Chemistry – A European Journal* **2012**, *18*, 4156–4160

Hasell, T.; Wu, X.; Jones-James, T. A.; Bacsá, J.; Steiner, A.; Mitra, T.; Trewin, A.; Adams, D. J.; Cooper, A. I. Triply interlocked covalent organic cages. *Nat Chem* **2010**, *2*, 750–755

Von Delius, M.; Geertsema, E. M.; Leigh, D. A.; Tang, D.-T. D. Design, Synthesis, and Operation of Small Molecules That Walk along Tracks. *Journal of the American Chemical Society* **2010**, *132*, 16134–16145

Metola, P.; Anslyn, E. V; James, T. D.; Bull, S. D. Circular dichroism of multi-component assemblies for chiral amine recognition and rapid ee determination. *Chem. Sci.* **2012**, *3*, 156–161.

M. Dragna, J.; Pescitelli, G.; Tran, L.; Lynch, V. M.; Anslyn, E. V; Di Bari, L. In Situ Assembly of Octahedral Fe(II) Complexes for the Enantiomeric Excess

Determination of Chiral Amines Using Circular Dichroism Spectroscopy. *Journal of the American Chemical Society* **2012**, *134*, 4398–4407

Rowan, S. J.; Cantrill, S. J.; Cousins, G. R. L.; Sanders, J. K. M.; Stoddart, J. F. Dynamic Covalent Chemistry. *Angewandte Chemie International Edition* **2002**, *41*, 898–952.

You, L.; Long, S. R.; Lynch, V. M.; Anslyn, E. V Dynamic Multicomponent Hemiaminal Assembly. *Chem.--Eur. J.* **2011**, *17*, 11017–11023, S11017/1–S11017/14.

Zhang, T.; Anslyn, E. V Using an Indicator Displacement Assay to Monitor Glucose Oxidase Activity in Blood Serum. *Organic Letters* **2007**, *9*, 1627–1629

Tang, W.; Matyjaszewski, K. Effect of Ligand Structure on Activation Rate Constants in ATRP. *Macromolecules* **2006**, *39*, 4953–4959

Tang, W.; Tsarevsky, N. V; Matyjaszewski, K. Determination of Equilibrium Constants for Atom Transfer Radical Polymerization. *Journal of the American Chemical Society* **2006**, *128*, 1598–1604

Matyjaszewski, K.; Jakubowski, W.; Min, K.; Tang, W.; Huang, J.; Braunecker, W. A.; Tsarevsky, N. V Diminishing catalyst concentration in atom transfer radical polymerization with reducing agents. *Proceedings of the National Academy of Sciences* **2006**, *103*, 15309–15314

Anderegg, G.; Hubmann, E.; Podder, N. G.; Wenk, F. Pyridinderivate als Komplexbildner. XI. Die Thermodynamik der Metallkomplexbildung mit Bis-, Tris- und Tetrakis[(2-pyridyl)methyl]-aminen. *Helvetica Chimica Acta* **1977**, *60*, 123–140.

Wenk, F.; Anderegg, G. Thermodynamic investigations of metal complexes with pyridines ligands. *Chimia* **1970**, *24*, 427–431.

Rostovtsev, V. V; Green, L. G.; Fokin, V. V; Sharpless, K. B. A Stepwise Huisgen Cycloaddition Process: Copper(I)-Catalyzed Regioselective “Ligation” of Azides and Terminal Alkynes. *Angewandte Chemie International Edition* **2002**, *41*, 2596–2599

Wang, Q.; Chan, T. R.; Hilgraf, R.; Fokin, V. V; Sharpless, K. B.; Finn, M. G. Bioconjugation by Copper(I)-Catalyzed Azide-Alkyne [3 + 2] Cycloaddition. *Journal of the American Chemical Society* **2003**, *125*, 3192–3193

Tornøe, C. W.; Christensen, C.; Meldal, M. Peptidotriazoles on Solid Phase: [1,2,3]-Triazoles by Regiospecific Copper(I)-Catalyzed 1,3-Dipolar Cycloadditions of Terminal Alkynes to Azides. *The Journal of Organic Chemistry* **2002**, *67*, 3057–3064

Kolb, H. C.; Finn, M. G.; Sharpless, K. B. Click Chemistry: Diverse Chemical Function from a Few Good Reactions. *Angewandte Chemie International Edition* **2001**, *40*, 2004–2021

Chan, T. R.; Hilgraf, R.; Sharpless, K. B.; Fokin, V. V Polytriazoles as Copper(I)-Stabilizing Ligands in Catalysis. *Organic Letters* **2004**, *6*, 2853–2855

#### Chapter 4

Anslyn, E. V.; Dougherty, D. A., *Modern Physical Organic Chemistry*. University Science books: Sausalito, California, 2006.

Cahn, R. S.; Ingold, C.; Prelog, V. Specification of Molecular Chirality. *Angewandte Chemie International Edition in English* **1966**, *5*, 385–415.

Finefield, J. M.; Sherman, D. H.; Kreitman, M.; Williams, R. M., Enantiomeric Natural Products: Occurrence and Biogenesis. *Angewandte Chemie International Edition* 2012, n/a-n/a.

Franks, M. E.; Macpherson, G. R.; Figg, W. D., Thalidomide. *The Lancet* 2004, *363* (9423), 1802-1811.

Agranat, I.; Caner, H.; Caldwell, J., Putting chirality to work: the strategy of chiral switches. *Nat Rev Drug Discov* 2002, *1* (10), 753-768.

Maruoka, K.; Ooi, T., Enantioselective Amino Acid Synthesis by Chiral Phase-Transfer Catalysis. *Chemical Reviews* 2003, *103* (8), 3013-3028.

Leung, D.; Kang, S. O.; Anslyn, E. V., Rapid determination of enantiomeric excess: a focus on optical approaches. *Chem. Soc. Rev.* 2012, *41*, 448-479.

Wenzel, T. J.; Wilcox, J. D., Chiral reagents for the determination of enantiomeric excess and absolute configuration using NMR spectroscopy. *Chirality* 2003, *15*, 256-270.

Gottarelli, G.; Lena, S.; Masiero, S.; Pieraccini, S.; Spada, G. P., The use of circular dichroism spectroscopy for studying the chiral molecular self-assembly: An overview. *Chirality* 2008, *20* (3-4), 471-485.

Kelly, A. M.; Perez-Fuertes, Y.; Arimori, S.; Bull, S. D.; James, T. D., Simple protocol for NMR analysis of the enantiomeric purity of diols. *Org. Lett.* 2006, *8*, 1971-1974

Metola, P.; Anslyn, E. V.; James, T. D.; Bull, S. D., Circular dichroism of multi-component assemblies for chiral amine recognition and rapid ee determination. *Chem. Sci.* 2012, *3*, 156-161

Perez-Fuertes, Y.; Kelly, A. M.; Johnson, A. L.; Arimori, S.; Bull, S. D.; James, T. D., Simple protocol for NMR analysis of the enantiomeric purity of primary amines. *Org. Lett.* 2006, *8*, 609-612.



- Iwaniuk, D. P.; Wolf, C., Enantioselective Sensing of Amines Based on [1 + 1]-, [2 + 2]-, and [1 + 2]-Condensation with Fluxional Arylacetylene-Derived Dialdehydes. *Organic Letters* 2011, *13* (10), 2602-2605
- Iwaniuk, D. P.; Wolf, C., A Stereodynamic Probe Providing a Chiroptical Response to Substrate-Controlled Induction of an Axially Chiral Arylacetylene Framework. *Journal of the American Chemical Society* 2011, *133* (8), 2414-2417.
- Shabbir, S. H.; Regan, C. J.; Anslyn, E. V., A general protocol for creating high-throughput screening assays for reaction yield and enantiomeric excess applied to hydrobenzoin. *Proceedings of the National Academy of Sciences* 2009, *106* (26), 10487-10492.
- Holmes, A. E.; Zahn, S.; Canary, J. W., Synthesis and circular dichroism studies of N,N-bis(2-quinolylmethyl)amino acid Cu(II) complexes: determination of absolute configuration and enantiomeric excess by the exciton coupling method. *Chirality* 2002, *14*, 471-477;
- Zahn, S.; Canary, J. W., Electron-induced inversion of helical chirality in copper complexes of N,N-dialkylmethionines. *Science* 2000, *288*, 1404-1406.
- Joyce, L. A.; Maynor, M. S.; Dragna, J. M.; da, C. G. M.; Lynch, V. M.; Canary, J. W.; Anslyn, E. V., A Simple Method for the Determination of Enantiomeric Excess and Identity of Chiral Carboxylic Acids. *J. Am. Chem. Soc.* 2011, *133*, 13746-13752.
- You, L.; Long, S. R.; Lynch, V. M.; Anslyn, E. V., Dynamic Multicomponent Hemiaminal Assembly. *Chem.--Eur. J.* 2011, *17*, 11017-11023, S11017/1-S11017/14.
- You, L.; Berman, J. S.; Anslyn, E. V., Dynamic multi-component covalent assembly for the reversible binding of secondary alcohols and chirality sensing. *Nat. Chem.* 2011, *3*, 943-948;
- You, L.; Pescitelli, G.; Anslyn, E. V.; Di, B. L., An Exciton-Coupled Circular Dichroism Protocol for the Determination of Identity, Chirality, and Enantiomeric Excess of Chiral Secondary Alcohols. *J. Am. Chem. Soc.* 2012, *134*, 7117-7125.
- You, L.; Berman, J. S.; Lucksanawichien, A.; Anslyn, E. V., Correlating Sterics Parameters and Diastereomeric Ratio Values for a Multicomponent Assembly To Predict Exciton-Coupled Circular Dichroism Intensity and Thereby Enantiomeric Excess of Chiral Secondary Alcohols. *J. Am. Chem. Soc.* 2012, *134*, 7126-7134.
- Han, X.; Wu, J. Ga(OTf)<sub>3</sub>-Catalyzed Direct Substitution of Alcohols with Sulfur Nucleophiles. *Organic Letters* **2010**, *12*, 5780-5782.
- Njardarson, J. Top 2011 Drugs <http://cbc.arizona.edu/njardarson/group/news/2011-top-200-drug-posters-are-now-available> (accessed Nov 8, 2012).

Robertson, F.; Wu, J. Convenient Synthesis of Allylic Thioethers from Phosphorothioate Esters and Alcohols. *Organic Letters* **2010**, *12*, 2668–2671.

Porto, S.; Seco, J. M.; Ortiz, A.; Quiñoá, E.; Riguera, R., Chiral Thiols: The Assignment of Their Absolute Configuration by <sup>1</sup>H NMR. *Organic Letters* **2007**, *9* (24), 5015-5018.

Dale, J. A.; Dull, D. L.; Mosher, H. S. alpha.-Methoxy-.alpha.-trifluoromethylphenylacetic acid, a versatile reagent for the determination of enantiomeric composition of alcohols and amines. *The Journal of Organic Chemistry* **1969**, *34*, 2543–2549.

Strijtveen, B.; Kellogg, R. M. Synthesis of (racemization prone) optically active thiols by SN2 substitution using cesium thiocarboxylates. *The Journal of Organic Chemistry* **1986**, *51*, 3664–3671.

Endo, A.; Yanagisawa, A.; Abe, M.; Tohma, S.; Kan, T.; Fukuyama, T. Total Synthesis of Ecteinascidin 743. *Journal of the American Chemical Society* **2002**, *124*, 6552–6554.

## Chapter 5

Hunter, P., Undergraduate research: Winning the battle for students' hearts and minds. *EMBO reports* **2007**, *8* (8), 717-9.

Lopatto, D., Undergraduate Research Experiences Support Science Career Decisions and Active Learning. *CBE-Life Sciences Education* **2007**, *6* (4), 297-306;

Russell, S. H.; Hancock, M. P.; McCullough, J., Benefits of Undergraduate Research Experiences. *Science* **2007**, *316* (5824), 548-549;

Weaver, G. C.; Russell, C. B.; Wink, D. J., Inquiry-based and research-based laboratory pedagogies in undergraduate science. *Nat Chem Biol* **2008**, *4* (10), 577-580.

Canaria, J. A.; Schoffstall, A. M.; Weiss, D. J.; Henry, R. M.; Braun-Sand, S. B., A Model for an Introductory Undergraduate Research Experience. *Journal of Chemical Education* **2012**, *89* (11), 1371-1377.

Fay, M. E.; Grove, N. P.; Towns, M. H.; Bretz, S. L., A rubric to characterize inquiry in the undergraduate chemistry laboratory. *Chemistry Education Research and Practice* **2007**, *8* (2), 212-219.

Freshman Research Initiative. (2012). College of Natural Sciences, The University of Texas at Austin. Retrieved from <http://fri.cns.utexas.edu>

ACS Guidelines for Chemistry in Two-Year College Programs. (2009). *ACS Society Committee on Education*. American Chemical Society. Retrieved from [http://portal.acs.org/portal/PublicWebSite/education/policies/twoyearcollege/CSTA\\_015380](http://portal.acs.org/portal/PublicWebSite/education/policies/twoyearcollege/CSTA_015380)

Kitamura, M.; Shabbir, S. H.; Anslyn, E. V. Guidelines for Pattern Recognition Using Differential Receptors and Indicator Displacement Assays. *The Journal of Organic Chemistry* **2012**, *74*, 4479–4489.

- Merrifield, R. B. Solid Phase Peptide Synthesis. I. The Synthesis of a Tetrapeptide. *Journal of the American Chemical Society* **1963**, *85*, 2149–2154.
- Gallagher, L. T.; Heo, J. S.; Lopez, M. A.; Ray, B. M.; Xiao, J.; Umali, A. P.; Zhang, A.; Dharmarajan, S.; Heymann, H.; Anslyn, E. V., Pattern-based discrimination of organic acids and red wine varieties by arrays of synthetic receptors. *Supramolecular Chemistry* **2012**, *24* (2), 143-148;
- Umali, A. P.; LeBoeuf, S. E.; Newberry, R. W.; Kim, S.; Tran, L.; Rome, W. A.; Tian, T.; Taing, D.; Hong, J.; Kwan, M.; Heymann, H.; Anslyn, E. V., Discrimination of flavonoids and red wine varieties by arrays of differential peptidic sensors. *Chemical Science* **2011**, *2* (3), 439-445.
- Rozinov, M. N.; Nolan G. P. Evolution of peptide that modulate the spectral qualities of bound, small-molecule fluorophores. *Chemistry & Biology* **1998**, *5*, 713-728.
- Riedel, R., Nanoscaled inorganic materials by molecular design. *Chemical Society Reviews* **2012**, *41* (15), 5029-5031.
- Feng, Z. V.; Lyon, J. L.; Croley, J. S.; Crooks, R. M.; Vanden Bout, D. A.; Stevenson, K. J., Synthesis and Catalytic Evaluation of Dendrimer-Encapsulated Cu Nanoparticles. An Undergraduate Experiment Exploring Catalytic Nanomaterials. *Journal of Chemical Education* **2009**, *86* (3), 368;
- Marvin, K. A.; Johnson, J. A.; Rodenbusch, S. E.; Gong, L.; Vanden Bout, D. A.; Stevenson, K. J., Spectrophotometric Titration of Bimetallic Metal Cation Binding in Polyamido(amine) Dendrimer Templates. *Analytical Chemistry* **2012**, *84* (11), 5154-5158;
- Marvin, K. A.; Johnson, J. A.; Rodenbusch, S. E.; Gong, L.; Vanden Bout, D. A.; Stevenson, K. J., Spectrophotometric Titration of Bimetallic Metal Cation Binding in Polyamido(amine) Dendrimer Templates. *Analytical Chemistry* **2012**;
- Marvin, K. A.; Thadani, N. N.; Atkinson, C. A.; Keller, E. L.; Stevenson, K. J., Preparation and catalytic evaluation of ruthenium-nickel dendrimer encapsulated nanoparticles via intradendrimer redox displacement of nickel nanoparticles. *Chemical Communications* **2012**, *48* (50), 6289-6291.
- Scott, R. W. J.; Wilson, O. M.; Crooks, R. M., Synthesis, Characterization, and Applications of Dendrimer-Encapsulated Nanoparticles. *The Journal of Physical Chemistry B* **2004**, *109* (2), 692-704.
- Zhao, M.; Sun, L.; Crooks, R. M., Preparation of Cu Nanoclusters within Dendrimer Templates. *Journal of the American Chemical Society* **1998**, *120* (19), 4877-4878.
- Puig, O.; Caspary, F.; Rigaut, G.; Rutz, B.; Bouveret, E.; Bragado-Nilsson, E.; Wilm, M.; Séraphin, B., The Tandem Affinity Purification (TAP) Method: A General Procedure of Protein Complex Purification. *Methods* **2001**, *24* (3), 218-229.

Bosma, W. B. Using Chemistry and Color To Analyze Household Products: A 10-12 Hour Laboratory Project at the General Chemistry Level. *Journal of Chemical Education* **1998**, 75, 214.

## **Vita**

Samuel Reid Long was born the son of Tommy and Carolyn Long in Greenville, Texas in 1983 and raised outside of Sulphur Springs, Texas. He graduated as the valedictorian from North Hopkins High School in 2002. After high school, he attended The University of Texas at Austin where he obtained a Bachelor of Arts through the Plan II Honors program and a Bachelor of Science in Chemistry in 2007. During his undergraduate years, he conducted research on the synthesis of transition metal complexes through electrochemical methods under Dr. J.J. Lagowski. After graduating, he started the graduate program in organic chemistry at The University of Texas at Austin where he joined the group of Eric V. Anslyn with Brent L. Iverson as a coadvisor. During his graduate career, he served as the Vice President for External Affairs for the Graduate Student Assembly, served as Abbot of the Friar Society and worked as the Research Coordinator for the Welch Summer Scholars Program.

Permanent address (or email): 10745 Texas Highway 19 North Sulphur Springs, Texas  
75482 E-mail – Reid.Long@utexas.edu

This dissertation was typed by Samuel Reid Long.